FLOTATION CHARACTERISTICS OF MINERALS IN FELDSPAR ORES

A THESIS SUBMITTED TO
THE GRADUATE SCHOOL OF NATURAL AND APPLIED SCIENCES
OF
MIDDLE EAST TECHNICAL UNIVERSITY

BY

SAVAŞ ÖZÜN

IN PARTIAL FULFILLMENT OF THE REQUIREMENTS
FOR
THE DEGREE OF DOCTOR OF PHILOSOPHY
IN
MINING ENGINEERING

MARCH 2012

Approval of the thesis:

FLOTATION CHARACTERISTICS OF MINERALS IN FELDSPAR ORES

submitted by **SAVAŞ ÖZÜN** in partial fulfillment of the requirements for the degree of **Doctor of Philosophy in Mining Engineering Department, Middle East Technical University** by,

Prof. Dr. Canan Özgen
Dean, Graduate School of **Natural and Applied Sciences**   _____

Prof. Dr. Ali İhsan Arol
Head of Department, **Mining Engineering**   _____

Prof. Dr. Mustafa Ümit Atalay
Supervisor, **Mining Engineering Dept., METU**   _____

Examining Committee Members:

Prof. Dr. Çetin Hoşten
Mining Engineering Dept., METU   _____

Prof. Dr. Mustafa Ümit Atalay
Mining Engineering Dept., METU   _____

Prof. Dr.Ali İhsan Arol
Mining Engineering Dept., METU   _____

Prof. Dr. Özcan Gülsoy
Mining Engineering Dept., HU   _____

Prof. Dr. Gülsün Gökağaç
Chemistry Dept., METU   _____

Date :   15.03.2012

I hereby declare that all information in this document has been obtained and presented in accordance with academic rules and ethical conduct. I also declare that, as required by these rules and conduct, I have fully cited and referenced all material and results that are not original to this work.

Name, Last name   : Savaş ÖZÜN

Signature   :

ABSTRACT

FLOTATION CHARACTERISTICS OF MINERALS IN FELDSPAR ORES

ÖZÜN, Savaş

PhD., Department of Mining Engineering

Supervisor: Prof. Dr. Mustafa Ümit ATALAY

March 2012, 251 Pages

Albite (Na-feldspar) and orthoclase (K-feldspar) are the major feldspar minerals used in the production of glass and ceramics. They are found together with impurities like biotite, muscovite, quartz and rutile which are not desired for ceramics and glass industries. Therefore, these have to be removed to make the ore available for industrial use. In order to shed light on the actual feldspar ores, in this study; the flotation characteristics of albite, biotite, muscovite, orthoclase, quartz and rutile were investigated separately in their pure forms. In the investigation, the electrokinetic potential measurements and micro-flotation studies have been carried out to get information about their flotation characteristics under the effect of three different collectors, Aero 704, Aero 3000C and Aero 825, and the pH of the medium. The flotation recoveries were found to be pH dependent and the effective between the pH range of 7.0 and 11.5 in the presence of Aero 704. In the case of flotation with Aero 3000C, the recoveries reached up to 95.0% at certain concentrations and pH values and decreased sharply below pH 3.0 and above pH 9.5 for all the minerals tested. In the presence of Aero 825, the flotation recoveries of the minerals except for rutile, were found to be insufficient even with its highest concentration. In order to evaluate the adsorption mechanism of the collectors, Atomic Force Microscopy

(AFM) and Fourier Transform Infrared Spectroscopy (FTIR) analyses were carried out. From the AFM results it might be deduced that the behavior of Aero 3000C and Aero 825 was found to be almost similar for biotite and muscovite as monolayer adsorption and for the remaining minerals, albite, orthoclase, quartz and rutile, as monolayer and bilayer adsorption together. In the case of Aero 704, for albite and orthoclase, the adsorption of the collector might be the reason for monolayer and bilayer formation on their surfaces. The strength of the interaction of the collectors on the mineral surfaces was followed by FTIR analyses before and after acetone washing. The interaction of all the collectors was found to be weak in the case of albite, orthoclase, quartz and rutile whereas the interaction of Aero 704 and Aero 3000C was found to be strong in the case of biotite and muscovite.

ÖZ

FELDSPAT CEVHERLERİNDEKİ MİNERALLERİN FLOTASYON ÖZELLİKLERİ

ÖZÜN, Savaş

Doktora, Maden Mühendisliği Bölümü

Tez Yöneticisi: Prof. Dr. Mustafa Ümit ATALAY

Mart 2012, 251 Sayfa

Albit (Na-feldspat) ve ortoklaz (K-feldspat), seramik ve cam yapımda kullanılan esas feldspat mineralleridir. Bunlar endüstrice istenmeyen; biyotit, muskovit, kuvars ve rutil gibi safsızlıklarla birlikte bulunurlar. Cevheri endüstriyel kullanımlara uygun hale getirmek için bu safsızlıkların uzaklaştırılması gerekmektedir. Bu çalışmada feldspat cevherine ışık tutması amacı ile saf albit, biyotit, muskovit, ortoklaz, kuvars ve rutil minerallerinin flotasyon özellikleri ayrı ayrı incelenmiştir. Araştırmada; üç farklı toplayıcı (Aero 704, Aero 3000C ve Aero 825) ve ortamın pH'sının etkisi altında elektrokinetik potansiyel ölçümleri ve mikro-flotasyon deneyleri ile bu minerallerin flotasyon özellikleri saptanmaya çalışılmıştır. Aero 704 varlığındaki flotasyon verimleri pH'ya bağımlı ve 7.0-11.5 pH aralığında yüksek bulunmuştur. Aero 3000C varlığında ise flotasyon verimleri belirli derişim ve pH değerlerinde %95.0'e kadar yükselmiş ve pH 3.5'in altında ve 9.5'un üstünde hızla düşmüştür. Aero 825 varlığında ise, rutil dışındaki tüm minerallerin flotasyonları yetersiz bulunmuştur. Toplayıcıların adsorplanma mekanizmalarını irdeleyebilmek için AKM (Atomik Kuvvet Mikroskopu) ve FTIR (Fourier Dönüşümlü Kızılötesi Spektrofotometre) analizleri yapılmıştır. AKM sonuçlarına göre, Aero 3000C ve

Aero 825'in biyotit ve muskovit üzerine benzer şekilde tek tabakalı olarak ve diğer minerallere (albit, ortoklaz, kuvars ve rutil) ise tek ve çift tabakalı olarak tutunduğu sonucu çıkarılabilir. Aero 704 durumunda ise toplayıcının albit ve ortoklaz minerallerin üzerine tutunması tek ve çift tabakalı tutunmanın bir arada olması sonucu gerçekleşmiş olabilir. Toplayıcıların mineral yüzeyleri ile etkileşimlerinin gücü asetonla yıkama öncesi ve sonrasında FTIR analizleri ile izlenmiştir. Albit, ortoklaz, kuvars ve rutil minerallerinin kullanılan üç toplayıcı ile olan etkileşimleri zayıf bulunurken Aero 704 ve Aero 3000C'nin biyotit ve muskovit üzerine etkileşimleri ise güçlü bulunmuştur.

Anahtar Kelimeler: Feldspat, biyotit, muskovit, kuvars, rutil, elektrokinetik potansiyel, mikro-flotasyon, AKM, FTIR.

To My Wife, My Son and My Family

ACKNOWLEDGEMENTS

TABLE OF CONTENTS

LIST OF TABLES

TABLES

LIST OF FIGURES

FIGURES

CHAPTER 1

INTRODUCTION

Flotation, or as the common name froth flotation is a physicochemical separation process based on the differences in surface properties of the valuable and gangue minerals. The froth flotation is a complex process which involves three phases (solid, liquid, and gas), many sub-processes and interactions.

As well known, flotation process can only be applied to relatively fine particles. If they are too large the adhesion between the particle and the bubble will be less than the particle weight and the bubble will therefore drop its load. There is an optimum size range for successful flotation of a given system [1].

Froth flotation is used in order to separate minerals from their gangue by taking advantage of differences in their hydrophobicity. Hydrophobicity differences between different substances such as sulfides, carbonates, oxides, coals and silicates are increased by treating them with different surfactants such as collectors and other modifying agents.

In this study, a kind of silicate, the feldspar ores (mainly of albite and orthoclase minerals) with various accompanying minerals including mica (biotite and muscovite), rutile and quartz were intended to study with micro-flotation.

Previously, many studies have been conducted for the application of different collectors in the flotation of feldspars. Particularly, oleates, long-chain

1

alkylammonium salts and sulfonates are the most commonly used flotation collectors for beneficiation of silicates [2, 3].

As an igneous rock feldspar consists of aluminum silicates in combination with an alkaline and alkaline earth ions such as Na^+, K^+ and Ca^{2+} with a general chemical formula of $XAl(Al,Si)_3O_8$. X can be sodium (Na) and/or calcium (Ca) and/or potassium (K). The feldspars may be considered to be solid solutions of three components, orthoclase, $K(AlSi_3O_8)$, albite, $Na(AlSi_3O_8)$ and anorthite, $Ca(Al_2Si_2O_8)$ and can be described with the feldspar triangle whose corners are made up by the K, Na and Ca end-members as shown in Figure 1.1. Any composition on the triangle may be expressed by giving the percentages of three components, often abbreviated Ab (Albite), An (Anortite) and Or (Orthoclase). For example; $Ab_{95}An_2Or_3$ corresponds to nearly pure albite (i.e. 95.0% albite, 2.0% anortite, and 3.0% orthoclase) or $Ab_{20}An_2Or_{78}$ corresponds to soda-rich orthoclase [4].
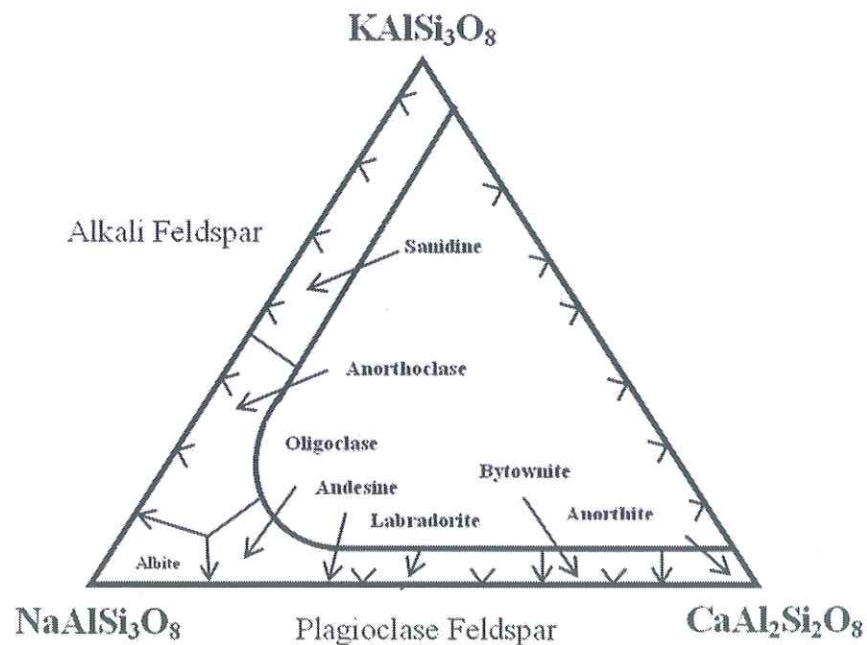
Figure 1. 1   Variation in Composition of Feldspars [5].

Feldspars are found in igneous, metamorphic and sedimentary deposits throughout the world. Even though the most of the reserves are saleable, either directly or after simple processing, as silicates respond poorly to gravity separation technique, it appears that the only successful way to process the feldspar is by flotation. Feldspar is recovered from waste granite fines, pegmatites, nepheline syenites which contain lower amount of biotite, muscovite, rutile, sphene, hornblende, zircon, chlorite, pyroxene and magnetite in addition to other feldspar minerals and quartz [6, 7].

According to the members of Eurofel (European Industrial Minerals Association) which agreed on a standardized definition of the feldspar products placed on the EU market; feldspar products are aluminosilicates with SiO_2 content >58.0%, alkali content (Na_2O+K_2O) > 2.0%, alumina content (Al_2O_3) > 3.0% and loss on ignition < 3.0%. A further distinction can be made between the feldspars (sodium, potassium and mixed) depending on the type of alkali content they have [8].
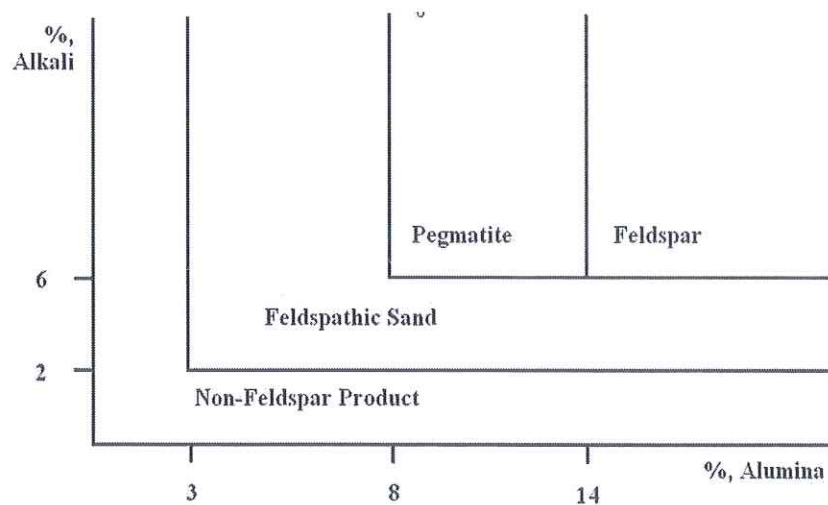
Figure 1. 2   Alumina and Alkali % of Feldspathic and Non-Feldspathic Minerals [8].

3

As Figure 1.2 displays, three distinguished families exist;

- Feldspatic sand; with an alkali content $(Na_2O+K_2O)< 6.0\%$ or alumina content $(Al_2O_3)< 8.0\%$.
- Pegmatite; with an alkali content $(Na_2O+K_2O) >6.0\%$ and alumina content (Al_2O_3) comprised between 8.0 and 14.0%
- Feldspar; with an alkali content $(Na_2O+K_2O) >6.0\%$ and alumina (Al_2O_3) content >14.0%.

Generally, almost 90.0% of feldspar produced in the world is used in the manufacture of ceramic industry (55.0%) and glass industry (35.0%), and the rest, (10.0%) is used in production of enamel frits and glazes, in weld electrode industry and in the paint, plastic, rubber and adhesive industries as fillers [9, 10]. Commercial feldspars, i.e., albite $(NaAlSi_3O_8)$ and orthoclase/microcline $(KAlSi_3O_8)$, are even selectively mined, they are found together with coloring impurities like clay, biotite, muscovite, iron and titanium oxides (hematite, magnetite, rutile, ilmenite, sphene, etc.) and tourmaline. The quality of feldspar has to be increased by removing these coloring impurities from the concentrate for using it in ceramics and glass industries. Although the high intensity permanent magnetic separators are used for the ores having low iron, flotation is inevitable method in order to obtain high quality concentrate from the ores which have high titanium and iron content [11].

Flotation of feldspar is accomplished by three stages [7, 10, 11];

i. Flotation of mica minerals
ii. Flotation of iron and titanium oxide minerals
iii. Feldspar-quartz separation

Unlike conventional feldspar ores, the feldspar deposits in western Turkey are quartz free and contain relatively high titanium compounds as their main impurities. Titanium compounds reduce the quality of feldspars, and hence the revenue, since they produce some adverse effects on their usage in the ceramic industry. The

removal of mica minerals (mostly biotite and muscovite) and iron-titanium oxides from feldspar ores by flotation is illustrated in Figure 1.3.
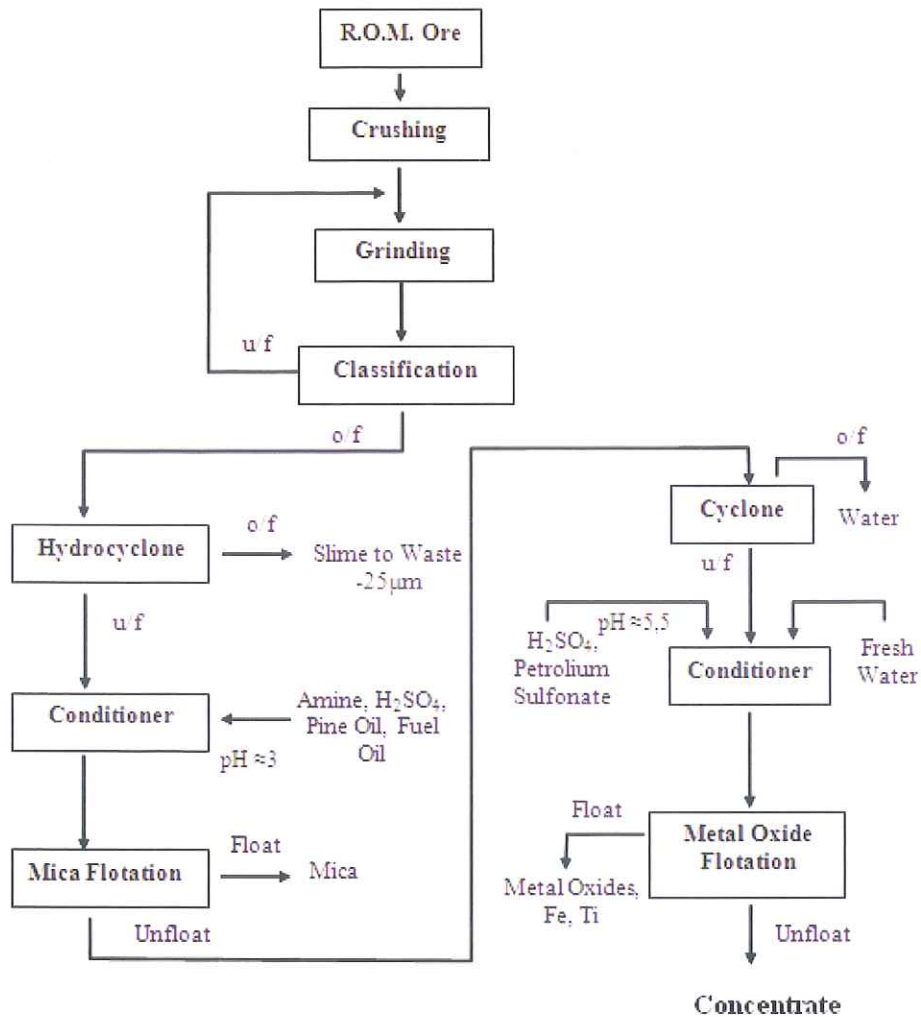
Figure 1. 3   Typical Flowsheet for Separation of Feldspar from Mica and Metal Oxides by Flotation [12].

The separation of feldspars from quartz often fails by applying traditional methods due to fact that they have almost similar densities and magnetic susceptibilities. Thus, beneficiation of feldspars by using froth flotation process has so far proved to be the most suitable method. In conventional flotation processes, feldspars are floated from quartz by using cationic collectors like primary long-chain alkylamine surfactants in the presence of HF or NaF under highly acidic conditions [10].

5

1.1 The Aim of the study

Feldspars are the most abundant mineral group which forms about 60.0% in the Earth's crust. Turkey with its abundant feldspar reserves, mostly in albite form, is emerging as the world leader when its production is taken into consideration [13]. As mentioned above, feldspars, as an important industrial mineral, play an important role as fluxing agents in ceramics and glass with their alumina and alkali content, and are also used in the paint, plastic, rubber and adhesive industries as functional fillers [6-10, 14].

Commercial feldspars are generally found together with other minerals like clay, mica minerals (mostly biotite and muscovite), quartz, tourmaline, iron and titanium oxides (hematite, magnetite, rutile, ilmenite, sphene, etc). These associated minerals have to be removed by applying conventional concentration techniques, such as gravity separation, magnetic separation and flotation, in order to obtain high quality feldspar concentrate for glass and ceramics industries. As silicates respond poorly to gravity separation technique and the concentration scheme is generally dependent upon the quality of the end product, froth flotation is almost constantly the most widely used beneficiation method [13, 15, 16].

Even though certain reagents were tested and reported on the way to achieve better flotation conditions either with pure mineral samples or pre-concentrates, selectivity still is a great problem in the flotation in order to obtain high grade feldspar concentrates for the industrial applications. As well known, flotation of feldspar is accomplished in highly and moderately acidic conditions, by using long-chain amine derivatives and sulfonate as collectors, in two stages for removal of the mica and iron-titanium oxide minerals respectively. Additional flotation circuit, by using long-chain amine derivatives in highly acidic condition with the presence of HF, is also applied for the feldspar ore which contain considerable amount of quartz mineral. In industrial applications, it is known that using large amount of acid for pH adjustment in acidic flotation circuits can cause harmful effect on the flotation

equipment and besides to this, beneficiation of feldspar in two-stage flotation circuits can reduce the capacity. In this respect, there have been produced new collectors which are active in basic conditions and have ability to float mica and iron-titanium oxide minerals in a single stage flotation circuit such as Aero 704. These are mostly oleic acid originated collectors. Their chemical formulas are unknown due to the commercial concerns of the producer [17].

In the present study, the objective was to investigate the flotation characteristics of two different feldspars, albite and orthoclase, and the associated minerals in feldspar ores including biotite, muscovite, quartz and rutile in the presence of varying concentrations of Aero 704, Aero 3000C and Aero 825 flotation collectors. For this purpose the effects of the types and amounts of the collectors were investigated as a function of pH by carrying out laboratory micro-flotation on the highest purity of those minerals (albite, biotite, muscovite, orthoclase, quartz and rutile). The further comparisons were also made on the flotation recoveries of these three collectors with each mineral listed above, depending on the amount and pH values.

As well-known, the relationship established between floatability and the changes in the electrokinetic potential forms the basis for determining the interaction types of the collectors with the surface of the minerals. Therefore, the zeta potential measurements were also conducted to determine the action of collectors on the mineral surfaces.

The interaction of the collectors were followed by AFM and FTIR studies on the mineral samples conditioned with optimum flotation conditions which were determined by micro-flotation studies. Those studies were performed to understand the mechanism of interaction of long-chain alkyl amine (Aero 3000C), petroleum sulfonate (Aero 825) and oleic acid originated collector (Aero 704).

Throughout the study, besides FTIR and AFM, various other analytical techniques, such as XRD and XRF have been used.

The thesis contains six chapters. Besides this first introduction chapter, Chapter 2 contains previous studies on flotation, FTIR and AFM, the Chapter 3 contains materials used in the analyses and the methods applied, the Chapter 4 contains experimental results namely; electrokinetic potential measurement, flotation, AFM and FTIR studies in alphabetically ordered mineral based sub sections; albite, biotite, muscovite, orthoclase, quartz and rutile samples. In the Chapter 5, the discussions of the results of electrokinetic potential measurements, flotation, AFM and FTIR studies on the mineral samples in the presence of the collectors used in addition to the overall interpretation. As the last chapter, Chapter 6 contains the conclusions.

CHAPTER 2

PREVIOUS STUDIES

Up to now, many researchers have been focused on the removal of coloring impurities and quartz from feldspar and published many papers about the application of different collectors in feldspar flotation. Recently, a few researchers have been published papers focused on both the separation of feldspar from quartz in the absence of HF media and the removal of mica and iron-titanium oxides in basic conditions by single stage flotation [2,7, 9-13, 15-27]. Some of the important researches have been summarized below in three heads, namely flotation studies (2.1), adsorption of surfactants on minerals using infrared spectroscopy (2.2) and adsorption of surfactants on minerals using atomic force microscopy (2.3).

2.1 Flotation Studies

In worldwide practice, the removal of -25μm fraction as slimes bearing clay minerals which have adverse effect on mica flotation by amines is the first stage. The next step is the mica flotation about pH 3.0 [11, 13, 15, 28-31] where mica minerals are floated mostly by using long chain aliphatic amines [32]. After the removal of mica minerals, metal oxides containing Fe and/or Ti are floated either by oleate about pH 5.0 or by sulphonates about pH 3.0. Succinamates (salt of succinamic acid $(H_2NCOCH_2CH_2CO_2H)$), soaps of various vegetable oils [13], sarcosine $(CH_3NHCH_2CO_2H)$ and hydroxamate type collectors (RCO_2NH) [16, 23] can also be used for the flotation of minerals having metal oxides.

9

The pulp is dewatered by using a hydrocyclone or spiral classifier etc. between the stages of mica and metal-oxide flotation. This stage is generally consisted of the removal of water that contains residual reagents, namely amines [15].

Bayraktar et al., 1997, carried out flotation test work to find out the optimum conditions for effective separation of titanium bearing minerals from two different feldspars which had low titanium (<0.2% as TiO_2) and high titanium (<0.3% as TiO_2) from Cine province, Aydin, Turkey. They performed flotation experiments in the presence of three different collectors namely, Na-oleate, petroleum sulphonate (R825 and R840) and alkyl succinamate (R845), between the pH range of 3.0 to 7.0 to compare the separation characteristics of rutile and sphene. They also used carboxylates prepared from sunflower, cotton seed oils and local vegetable oils to compare the results with the flotation efficiency of Na-oleate on removal of titanium bearing minerals from feldspar keeping the pH (3.0 to 7.0) and collector amount constant at 3000g/t. The flotation concentrates obtained from all collectors were then subjected to whiteness test of firing button. They found that the flotation results gained by using oleate were superior compared to those of sulphonates (R825 and R840) and succinamate (R845). According to their results; "tests with carboxylates prepared from local oils showed that equivalent concentrate quality could be obtained by sunflower and cotton seed oils. Although the other oils tested i.e. olive, corn seed and soy bean, also had some success in separating titanium bearing minerals, their efficiency was slightly lower" [13].

Celik et al., 1998, studied on the comparison of the effect of potassium oleate with oleoyl sarcosine and hydroxamate on removal of titanium minerals from feldspar ores obtained from Cine, Aydin, Turkey. According to their findings, oleoyl sarcosine required only 200 g/t collector whereas potassium oleate and hydroxamate required 1000 g/t with yielding optimum grades and recoveries at natural pH of 7.7. The quality of the feldspar concentrate was improved by applying stage-wise collector addition for all collectors. The hydroxamate was found to respond better TiO_2 recovery considering the increase in the value from 68.8% to 81.0%. Under the optimum conditions, oleoyl sarcosine produced a feldspar concentrate having

0.039% TiO_2 with 84.2% TiO_2 recovery in a single stage using 42.0% solids by weight and 200 g/t collector concentration. Hydroxamate produced a feldspar concentrate assaying 0.037% TiO_2 with 86.5% TiO_2 recovery in four-stage collector addition using 28.0% solids by weight and 1000 g/t collector. They also investigated the flotation responds of the collectors and found that flotation rates were considerably different. Oleoyl sarcosine required only 30 seconds whereas potassium oleate and hydroxamate required 1 and 2 minutes respectively [16].

Seyrankaya, 2003, studied on the removal of mica and heavy minerals from albite, obtained from Milas province, Mugla, by flotation. Two consecutive stepped schema were applied for the beneficiation of albite; the cationic flotation of mica in an acidic circuit by using amines and the anionic flotation of heavy minerals in an acidic circuit by petroleum sulfonates. Armac T as tallow amine acetate and ArmoFlote-21 as alkyl amine acetate with the amounts in the range of 100-250 g/t at about pH 3.0 were used to remove the mica minerals. As petroleum sulfonate, Aero 801, Aero 825 and Aero 840 were used in the combination of 1:2 with the amount of 200 g/t, 400 g/t of Aero 801 and Aero 825 respectively for the removal of heavy minerals in the rougher flotation stage. Then in order to improve the removal of heavy minerals from albite, Aero 840 with the amount of 200 g/t was used in the scavenger flotation stage. The results showed that Armac T was found more selective compared to ArmoFlote-21 with the amount of 200 g/t considering the minimal loss of albite in the mica flotation stage. Total petroleum sulfonate usage, 1000g/t of Aero 801, Aero 840 and Aero 825 was found effective on the removal of heavy minerals. The resultant concentrate with 77.0% albite recovery had 0.025% TiO_2 with 92.71% removal recovery, 0.029% Fe_2O_3 with 90.68% removal recovery and 11.72% Na_2O with 83.63% obtaining recovery [24].

Sekulic et al. 2004, studied on the usage of different collectors in the beneficiation of mica and feldspars by flotation from the white granite raw material and the reverse flotation of quartz sand from the raw material by using different collectors mainly Aero 3000C, Flotigam Dat, Armoflot, Armac C and R 825. They used the pegmatite ore containing ~60.0% Na-K feldspar, ~25.0% quartz and ~10.0% muscovite and

11

5.0% impurities and the quartz sand containing quartz, feldspar, mica and heavy minerals in the flotation experiments. The results for white granite showed that in mica flotation, Armoflot 64 and Aero 3030C were found satisfactory both in quality and recovery. In feldspar flotation, the quality of feldspar and quartz sand were found to be acceptable however; the obtained results of Aero 3000C with 19.58% recovery was found better than those of Flotigam DAT. In the flotation of impurities from quartz sand, R825 and Armac C combination gave better results when compared to those of Aero 3000C [25].

Bayat et al., 2005, studied on the application of different cationic collectors, Aero 3030C and Aero 801+Aero 825 in the flotation concentration of feldspar from Cine, Aydin, Turkey. They compared the flotation results of Aero 3000C with the amount of 300 g/t in first flotation stage and 100 g/t in second flotation stage and mixture of Aero 801+Aero 825 with the amount of 150 g/t each in first flotation stage and 50 g/t each in second flotation stage keeping the solids by weight ratio and pH (2.5–3.5) constant in the all experiments. According to the results for flotation of feldspars, the combined application of Aero 3000C, Aero 801 and Aero 825 mixture with the quantities of 150 g/t each in first flotation stage and 50 g/t each in second flotation stage performed better than the application of these collectors alone [7].

Gulsoy et al., 2005, studied the possibility of producing various grade feldspar concentrates from a low-grade pegmatitic ore containing 5.94% K_2O, 3.14% Na_2O, 0.61% CaO, 0.41% MgO, 0.11% TiO_2, 0.65% Fe_2O_3, 15.7% Al_2O_3 and 73.08% SiO_2 from Demirci province, Manisa, Turkey by magnetic separation and flotation. They performed magnetic separation on the ore with the size range of -1.0 mm, -0.5 mm and -0.3 mm by high intensity dry magnetic separator and obtained a concentrate containing 5.86% K_2O, 2.96% Na_2O, 0.04% TiO_2, 0.20% Fe_2O_3, 13.6% Al_2O_3 and 76.4% SiO_2 with 72.0% recovery. They concluded that the decrease in $K_2O+Na_2O\%$ and increase in $SiO_2\%$ was due to the fact that grindability of feldspar is much easier than that of quartz because of its hardness. The decrease in $TiO_2\%$ was due to substitution of Ti^{4+} with ions in mica lattices although sphene and rutile are regarded as non-magnetic minerals. They also carried out flotation experiments in -300μm +

12

25μm fraction size. First the flotation experiments were performed to remove of mica minerals in the presence of 200 g/t of tallow amine acetate (Armac TD) at pH range of 2.5-3.0, and then heavy mineral flotation was carried out in the presence of 2500 g/t of Na-oleate at pH range of 5.5-6.0. Having removed all the coloring impurities, in the orthoclase/albite flotation, NaCl was used as depressant for albite and HF as activator for orthoclase at pH range of 2.5-3.0 by tallow amine acetate with the amount of 100 g/t. They used NaCl to compare the effectiveness on the feldspar/quartz flotation as well. The results showed that separation of orthoclase from albite was successful and a concentrate with high alkali content, >15.0% K_2O+Na_2O, having a $K_2O:Na_2O$ of 4 could be obtained. In the flotation of feldspar and quartz, the feldspar and quartz concentrates was acceptable for the industrial use with over 13.0% K_2O+Na_2O and 98.0% SiO_2 respectively [26].

The study concerning flotation of mica and metal oxides from albite of Cine-Milas province, Mugla, Turkey and interaction of sodium oleate and tallow amine acetate (TAA) on the removal of coloring impurities were carried out by Orhan and Bayraktar (2005). They aimed to determine the interaction of residual amine after mica flotation with oleate used in the flotation of metal oxide minerals during two stage feldspar flotation. They considered the fact that the residual amine in the pulp after mica flotation in the presence of an anionic collector may cause flotation of feldspar together with metal oxide minerals. According to the XRD patterns, the albite ore was composed of 84.0–86.0% albite, 5.0–8.0% mica (biotite and muscovite), 4.0–6.0% anorthite, 2.0–3.0% fluoroapatite, 1.0–2.0% quartz and 1.0–2.0% rutile and sphene. They concluded that when compared to zeta potential of albite in the presence of TAA, the presence of TAA together with sodium oleate importantly decreases the zeta potential to more negative values. This suggested that sodium oleate was adsorbed on to albite surface only if TAA is present in the medium. They concluded that in the presence of residual amine during flotation of metal oxide minerals did not have a substantial effect on the feldspar concentrate quality. However, when feldspar loss is taken into consideration, following result can be obtained; while feldspar loss was 1.3% when there was no amine in the system, the loss increased up to 13.4% in the presence of 7.35×10^{-5} M amine. Excess feldspar (loss) in the froth was "obviously due to adsorption of oleate with amine onto

feldspar surfaces since oleate molecules" were not adsorbed onto "feldspar in the absence of the aminium ions in the pulp". They also concluded that the concentration of aminium ion in the pulp was the major factor which determines the feldspar loss to the tailings. "The increase in the oleate dosage at constant amine concentration did not influence the feldspar loss in the froth". Removing the residual TAA from the pulp between mica and metal oxides flotation stages by dewatering/washing increased the feldspar recovery from 86.67% (without dewatering/washing) up to 92.13% with two stages of dewatering/washing and 94.58% with three stages of dewatering/washing. The use of bentonite was found to be satisfactory due to the fact that 97.7% of the residual amine was adsorbed by bentonite as it has high cation exchange capacity [15].

Kurcan et. al., 2007, investigated the removal of mica and iron-titanium oxide minerals from feldspar ores in basic condition at one stage in the presence of a new collector, Aero 704 by Cytec Ind., by flotation and they also aimed the comparison of one stage flotation by new collector with three stage conventional flotation, by using amine and sodium oleate to remove coloring impurities from feldspar ores. According to their findings, Aero 704 collector successfully removed the coloring impurities from feldspar ore in a single stage and the concentrate produced had acceptable specifications for the industrial demand. As the ore used in experiments contained little amount of quartz mineral, they omitted the quartz flotation and obtained a sellable concentrate from a single stage flotation in basic conditions with 75.0% recovery [27].

Ozun et.al., 2009, investigated the possibility of opaque minerals removal from foid bearing rock by flotation. They performed the flotation studies on the removal of mica and iron titanium oxides by using a new collector, Aero 704 by Cytec Ind., in alkali conditions followed by high intensity wet magnetic separation for the purpose of getting feldspar to be used of ceramic industry. According to the results of XRD trace and the mineralogical analyses including microscopic examination of thin sections, the representative ore sample contained 45.0% feldspathoid (tectosilicate mineral), 22.0% orthoclase, 20.0% plagioclase, 7.0% amphibole, 4.0% biotite. In

addition to this respectively smaller quantities of ilmenite, magnetite, hematite minerals were also present in the nepheline syenite. They conducted flotation experiments as a function of pH and collector amounts. They concluded that increasing the amount of collector did not have any significant effect on the quality of feldspar concentrates, but reduced their recovery in -150+38 micron size range. The promising quality concentrate was obtained with consumption of higher than 2000 g/t Aero 704 amount at pH 10. The recovery sharply decreased above and below the given pH. They also performed multi stage flotation experiments performed with different collector amounts followed by high intensity wet magnetic separation (HIWMS) in order to decrease the amount of contaminants in the concentrate. The microscopic analyses of the best concentrate showed that there were still unliberated particles. Then the ore was ground to -106+38 micron size. The three stage flotation of these sized ore with the amount of 1500 g/t Aero 704 followed by HIWMS resulted in a promising concentrate with 0.01% TiO_2 and 0.22% Fe_2O_3 with 62.5% recovery [17].

2.2   The Studies on Adsorption of Surfactants on Minerals using FTIR

Surface chemistry plays an crucial role in many aspects of mineral processing. In particular, an understanding of the interaction of different reagents with the mineral surface in an aqueous medium is of crucial importance in accomplishing the desired beneficiation by flotation [33, 34].

Infrared spectroscopy has found wide acceptance for characterizing adsorption on mineral surfaces. "An infrared spectrum represents a fingerprint of a sample with absorption peaks that correspond to the frequencies of vibrations between the bonds of the atoms making up the material. Because each different material is a unique combination of atoms, no two compounds produce the same infrared spectra". Thus, "infrared spectroscopy can result in positive identification of every different kind of materials" [35, 36].

Fourier Transform Infrared (FTIR) spectrometry measures all of the infrared frequencies simultaneously by interferometer which is a very simple optical device producing a unique type of signal having all of the infrared frequencies encoded into it. Because the analyst needs a frequency spectrum in order to make identification, the measured interferogram signal cannot be interpreted directly. Decoding the individual frequencies is needed and this can be achieved via a well-known mathematical technique, Frourier Transformation. In order to perform this transformation, a computer was used and then presented to user with desired spectral information for analysis [35, 37].

Different experimental techniques are used in the infrared spectroscopy of adsorbed species. The simplest is transmission infrared spectroscopy, KBr disc technique that does not require a separate accessory. In this technique, the solid, which contains adsorbent (mineral sample) and adsorbate (collector or other reagent), is dried first. Then having mixed with KBr it is pressed into a disc which is mounted in the sample beam of spectrometer. As the surfaces of minerals recovered by flotation are relatively small, the mineral particles are is ground into finer size in order to increase the amount of reagent adsorbed [33, 34].

The adsorption of collectors on mineral surfaces has been studied extensively, mostly by indirect methods, such as; contact angle measurement, zeta-potential measurement, surface forces and recovery responses [36-40].

Ince et.al., 1991, investigated the nature of oleic acid species adsorbed on apatite and dolomite minerals in the absence and presence of NaCl at pH 4.0 and pH 10.0 by FTIR analyses. They found that more oleate is adsorbed on apatite at pH 10 than that of at pH 4.0. The amount of oleate adsorbed at pH 4.0 in the presence of NaCl decreased slightly compared to the pH 4 system without NaCl. On the other hand for dolomite, a relatively small amount of oleate is adsorbed at pH 10.0 compared to the amount adsorbed at pH 4 with or without NaCl present. According to their findings, in the case of apatite at pH 10.0, absence of the carboxyl ($-COOH^+$) stretching band

at 1735 cm^{-1} and a moderate intensity of asymmetric carboxylate (-COO$^-$) stretching band at 1560 cm^{-1} indicated that the predominant surface species was oleate. At pH 4.0, the intensity of the two bands reversed indicating oleic acid as the major adsorbed species. Intensity of the carbonyl (>C=O)stretching band increased in the presence of NaCl at pH 4.0 which was attributed to a shift in equilibrium toward oleic acid in the presence of sodium ions. In the case of dolomite at pH 10.0, none of the above bands were detected, presumably due to the small amounts of oleate present at this pH value. At pH 4.0, although there was masking of the carboxylate band at 1560 cm^{-1} by the strong dolomite band in the 1350-1575 cm^{-1} region, based on the intensity of the carboxyl stretching band at 1735 cm^{-1}. It was indicated that the nature of the adsorbed species is similar to the apatite-oleate system [41].

According to Mielczarsk et.al, 1993, interfacial structures formed by adsorption of oleate on hydroxyapatite were characterized by adsorption isotherms, electrokinetic and hydrophobicity measurements, and FTIR reflection techniques. Two different samples of oleate with different amounts of isomers and homologues ("impurities") were used. The attenuated total reflection (ATR) and the diffuse reflectance infrared fourier transform spectroscopy (DRIFT) studies showed that the observation of a doublet or singlet positioned about 1560 cm^{-1}, due to the asymmetric stretching vibration of the carboxyl group, depends on organization of the adsorbed molecules rather than, as was suggested previously, on the mechanism of the adsorption of oleate. It was found that there were close relationships among the adsorption, spectroscopic, electrokinetic, and hydrophobicity data. The chemisorbed oleate molecules form a well-organized close-packed structure (strong lateral interaction) probably of two distinguished structural forms at submonolayer coverage. These structural forms (shown by doublet with maxima at 1572 and 1640 cm^{-1}) are responsible for the hydrophobic properties of the sample. The presence of impurities causes a perturbation of the chemisorbed layer structure (broad band about 1550 cm^{-1}) and, in this case (perturbated lateral interaction), the formation of a more organized structure was observed at higher coverage, close to monolayer, at which maximum hydrophobicity was also found. They concluded that higher than monolayer coverage is formed by the three-dimensional condensation of calcium oleate on apatite (surface precipitation mechanism) which forms a poorly organized

structure that does not produce high hydrophobicity. The adsorption of oleate on hydroxyapatite takes place by the two-dimensional (chemisorption) and/or three-dimensional (surface precipitation) condensation mechanisms. The chemisorption dominates at a lower concentration region, and a well-organized close-packed structure (strong lateral interaction), with likely two different structural domains, is formed at submonolayer coverage. These well-organized structures, shown clearly by a doublet with maxima at 1572 cm^{-1} and 1640 cm^{-1}, were responsible for the hydrophobic properties of the sample. They also concluded that at higher concentration the oleate is adsorbed by the three-dimensional condensation mechanism. The adsorbed molecules form a poorly organized structure which does not produce a high hydrophobicity of apatite. The coverage produced by this mechanism is strongly dependent on the amount of calcium ions present in the solution, therefore the equilibration of apatite in water has a strong influence on the amount of oleate adsorbed. Surface precipitation of calcium oleate was observed only when a part of the apatite surface is covered by oleate chemisorbed. Close relationships between the structures of the adsorption layers and the changes in infrared spectra were remarkable [42].

Vidyadhar et.al. 2002, studied on the mechanisms of amine–quartz interaction in the absence/presence of alcohols and long-chain alkylamines with their acetate salts on quartz by conducting Hallimond flotation, zeta potential, FTIR and X-ray photoelectron spectroscopy (XPS) at neutral pH 6.0–7.0. They also investigated the effect of long-chain alcohols on the adsorption of amines in mixed amine/alcohol on quartz. According to the results they mentioned that "It is shown by infrared spectroscopy that in differentiation to the electrostatic adsorption model of Gaudin–Fuerstenau–Somasundaran, amine cations form strong hydrogen bonds with the surface silanol groups. The XPS spectra revealed the presence of neutral amine molecules together with protonated ammonium ions at and above the critical hemimicelle concentration. The acetate counterions were found to influence the amine adsorption". They also proved spectroscopically that "co-adsorption of long-chain alcohols along with amine cations leads to formation of a closely packed surface layer, as compared to the case of adsorption of pure amine alone at the same concentration. The highest order and packing at the surface were observed when the

alkyl chain length of mixed amine and alcohol were the same". According to their findings; "the FTIR spectra revealed that at low bulk amine concentrations, the surface silanol groups interact with ammonium groups through hydrogen bonds. After hemimicelle concentration, the XPS spectra showed neutral amine molecules along with the protonated ammonium ions coordinated to deprotonated silanol oxygen anions on the surface. Because of this, adsorption steeply increases. At higher concentrations, the molecular amine precipitates onto the surface, which is characterized by the typical absorption band at 3330 cm^{-1}. The presence of alcohol enhanced the two-dimensional precipitation of amine at the same total concentration. The precipitating species is deduced to be the soluble associate of the protonated amine and alcohol. When the alkyl chain lengths are the same, the adsorbed layer is closely packed, leading to increasing hydrophobicity and thus maximum floatability. The total concentration in mixed composition is reduced to one order of magnitude when compared to the amine concentration alone for achieving the same flotation response" [43].

Vidyadhar et.al, 2003, investigated the mechanisms of amine/feldspar interaction in the absence and presence of alcohols by using Hallimond flotation, zeta-potential, FTIR and XPS studies. They also investigated the effect of long-chain alcohols on the adsorption of amines in mixed amine/alcohol on feldspars, i.e. albite and microcline. The results showed that co-adsorption of "the counterion was not revealed, but the counterion was found to affect indirectly the adsorption at concentrations above the concentration of the bulk amine precipitation. It was proved spectroscopically that co-adsorption of long-chain alcohols along with amine cations leads to formation of a closed packed surface layer as compared to the case of adsorption of pure amine alone at the same concentration. The highest order and packing at the surface were observed when the alkyl chain length of mixed amine and alcohol were the same. The condition of same chain length of amines and alcohols adsorbing at the surface corresponded to maximum flotation recovery". They concluded that the results obtained from Hallimond flotation, zeta-potential, FTIR and XPS studies showing the mechanism of adsorption of long-chain primary amines at pH 6.0-7.0 onto albite and quartz was the successive two dimension/three dimension (2D/3D) precipitation" and "the presence of alcohol enhanced the 2D

19

precipitation of amine at the same total concentration. The precipitating species was deduced to be the soluble associate of the protonated amine and alcohol. When the alkyl chain lengths were the same, the adsorbed layer was closely packed leading to increasing hydrophobicity and thus maximum floatability. The total concentration in mixed composition is reduced to one order magnitude when compared to the amine concentration alone for achieving the same flotation response" [44].

Vidyadhar and Rao, 2007, investigated the adsorption mechanism of mixed cationic alkyl diamine and anionic sulfonate/oleate collectors on microcline and quartz mineral samples. They were performed the experiments at acidic pH values by using Hallimond flotation, electrokinetic and diffuse reflectance FTIR studies. According to the results; neither microcline nor quartz responded to flotation in the presence of anionic collectors. However, the flotation of both minerals in the presence of diamine was found to be pH and concentration dependent. "The presence of sulfonate enhanced the diamine flotation of the minerals by its co-adsorption" and "the difference in surface charge between the minerals at pH 2.0 was found to be the basis for preferential feldspar flotation from quartz in mixed diamine/sulfonate collectors". They found that quartz displayed an iep at pH 2.0 and microcline charged negatively down to pH 1.5. The charge difference between microcline and quartz at pH $\leq$ 2.0 was found to be the key factor for the preferential microcline flotation in mixed collector system. Thus, diamine did adsorb on microcline at pH $\leq$ 2.0 but not on quartz. This happened due to quartz's near-zero charge. The concluded that "the infrared spectra revealed no adsorption of sulfonate collector when used alone but displayed its co-adsorption as diamine–sulfonate complex when used with diamine. The presence of sulfonate increased the diamine adsorption due to a decrease in the electrostatic head–head repulsion between the adjacent surface ammonium ions and thereby increasing the lateral tail–tail hydrophobic bonds. The mole ratio of diamine/sulfonate was found to be an important factor in the orientation of alkyl chains and thus the flotation response of minerals. The increase in sulfonate concentration beyond diamine concentration leads to the formation of soluble 1:2 diamine–sulfonate complex or precipitate and the adsorption of these species decreased the flotation since the alkyl chains are in chaotical orientation with a conceivable number of head groups directing towards the solution phase". They also

concluded that "although the flotation results demonstrate the feasibility of selective microcline flotation from quartz at pH 2.0 with mixed diamine/sulfonate collectors, the zeta-potential and FTIR studies at the same pH illustrate similar adsorption behavior on both minerals. This discrepancy in the results is caused by the nature of the coarse and fine particles employed in flotation and adsorption studies, respectively. The similar adsorption behavior of either diamine or mixed diamine/sulfonate collectors on very fine quartz and microcline particles at pH 2.0 is attributed to the increase in the density of the silanol groups on the surface because of several broken bonds when compared to coarse particles. The adsorption of ammonium ions increases with increasing silanol groups as they can bind to silanol groups through hydrogen bonding besides electrostatic interactions" [45].

According to Labidi et.al., 2007, the influence of adsorption of surfactants on solids in contact with aqueous solutions is crucial for controlling a variety of interfacial processes. They aimed to study the adsorption of oleic acid on the surface of quartz particles by the combination of the chemical treatments with the analytic and spectroscopic techniques (x-ray diffraction, FTIR spectroscopy, UV-visible spectrophotometry). The results showed that the oleic acid is adsorbed physically on the surface of quartz. The quantities adsorbed in the distilled water at pH 9.5 prove to be less important in relation to the quantities adsorbed in water doped by calcium and magnesium cations. They concluded that the oleic acid adsorption on quartz at pH 9.5 revealed that in both distilled and lab water oleic acid was adsorbed on the quartz surface since the bands at 2925 cm^{-1} and 2856 cm^{-1} are present and are recognized to represent carbon-hydrogen vibrations. It was difficult to obtain consistent data in the region of between 1500 cm^{-1} and 1600 cm^{-1} because that the species adsorbed on quartz in the same region was frequently masking by substrate. The adsorption isotherm in Lab water is consistently above that of in distilled water. The higher adsorption of oleic acid in Lab water is proposed to be due to the presence of significant amount of dissolved calcium and magnesium in Lab water. Calcium and magnesium can be adsorbed on quartz, reverse its charge and make it suitable for oleate adsorption [46].

2.3   The Studies on Adsorption of Surfactants on Minerals using AFM

Chennakesavulu et.al, 2009, examined the adsorption of oleate on fluorite surface by tapping mode atomic force microscopy. The tapping mode AFM can be utilized to see the topography of surfaces with adsorbed surfactant molecules. The natural fluorite crystals were equilibrated with 1.0×10^{-3} M to 1.0×10^{-7} M oleate solutions. They recorded the AFM images of the system at each concentration together with height profiles and observed concomitant monolayer and bilayer structures even at low oleate concentration of 1.0×10^{-7} M. This "suggests that normal–normal bonding of hydrocarbon chains takes place before the surface is completely covered by the monolayer. Multi-layer adsorption of oleate was observed at oleate concentrations of above 1.0×10^{-4} M". They stated that "the height profiles of the fluorite sample equilibrated $\leq 1 \times 10^{-5}$ M oleate were observed to be 2.98nm, 2.91nm, 2.92nm, 5.59nm, 5.60nm and 5.59nm. Considering the theoretically calculated length of oleate molecule as 2.60nm and the surface unevenness, these height profiles coincide with monolayer and bilayer heights. The concurrent monolayer and bilayer on the same surface clearly shows that normal–normal bonding of hydrocarbon chains takes place before the surface is completely covered with monolayer. This indicates that the oleate adsorption on fluorite crystals proceeds by admicelle hypothesis i.e. patches of bilayer could be seen even before the completion of monolayer coverage". They concluded that instead of indirect evidence of the adsorption isotherms, "this method can be adopted to visualize the adsorption behavior of oleate on mineral surface" [47].

In another AFM study, Paiva et.al, 2011, investigated effect of ionic strength on the adsorption of potassium oleate in apatite surfaces by in-situ AFM analyses. They equilibrated natural apatite crystals with calcium nitrate solutions in the presence and absence of potassium oleate (4.0×10^{-3} M) and they recorded the AFM images of each experiment together with their histograms. According to the results; "the contact AFM mode allowed visualizing the topography of the surfaces with the formation of adsorbed layers and calcium dioleate colloids. The presence of calcium ions in aqueous solution (2.0×10^{-4} M) led to the formation of precipitated calcium

carbonate/hydroxide, as evidenced in the histogram given. In the presence of high ionic strength, oleate adsorption occurs through the formation of clusters of calcium dioleate, observed in both 2D and 3D micro-topographies". They concluded that "from the AFM images obtained, along with the corresponding histograms, it was possible to visualize the behavior of potassium oleate adsorption and the precipitation of Ca^{2+} ions on the surface of the apatite crystal. Under the experimental conditions used in the study, the formation and precipitation of calcium dioleate occurred in the form of agglomerates on the apatite surface. The presence of agglomerates clearly made the apatite surface rougher and heterogeneous. The heterogeneous chemistry that occurs at the surface as well as surface roughness are key factors in apatite floatability". It is also conceived that "calcium oleate precipitation on the apatite surface plays a determining role in the nature of the interactions between the collectors and the interfacial region of the particles, interfering in the selectivity and efficiency of flotation". They also stated that "AFM is an extremely useful tool to examine and elucidate the behavior of the apatite surface during the flotation stage" [48].

CHAPTER 3

MATERIALS AND METHODS

This chapter will be presented in two sub sections namely the materials and the methods used.

3.1 Materials

3.1.1 Minerals

This study focused on the micro-flotation characteristics of minerals in feldspar ores. The minerals in alphabetical order are albite, biotite, muscovite, orthoclase, quartz and rutile. The crystal structures of the minerals are given in Figure 3.1, Figure 3.4, Figure 3.7, Figure 3.10, Figure 3.13 and Figure 3.16.

The high purity albite from Cine region-Aydin deposit, Turkey was obtained from Akmaden Mining Company. The high purity biotite, muscovite and quartz again from Cine region-Aydin, Turkey were obtained from Kaltun Mining Company. The high purity orthoclase was obtained from India by Kaltun Mining Company. The rutile was provided by Dupont Inc., Florida, USA.

3.1.1.1 Albite

"Albite by definition must contain no less than 90.0% sodium and no more than 10.0% of either potassium and/or calcium in the cation position in the crystal

24

structure". Albite crystallizes with triclinic pinacoidal forms. Figure 3.1 shows the crystal structure of albite mineral. "It occurs in granitic and pegmatite masses, in some hydrothermal vein deposits and forms part of the typical greenschist metamorphic facies for rocks of originally basaltic composition" [49].
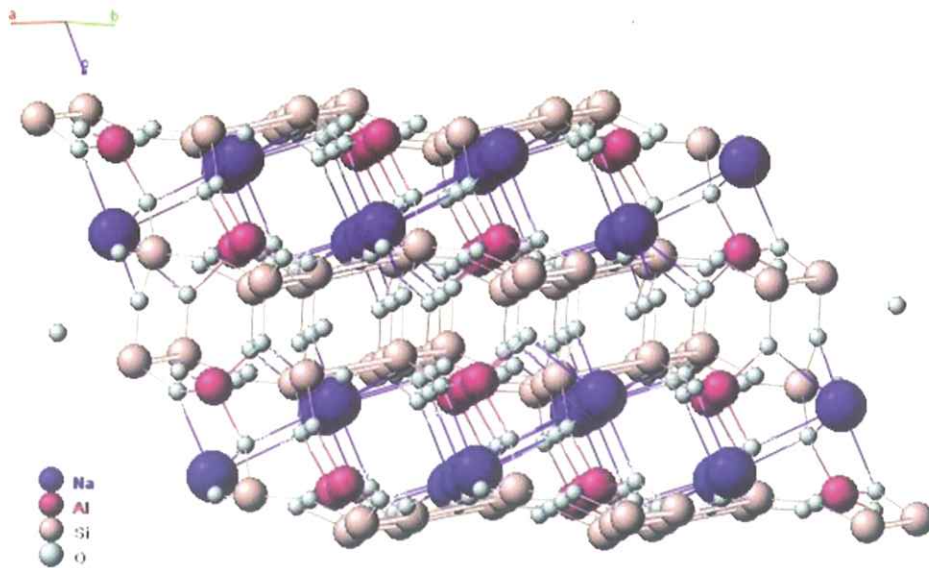
Figure 3. 1   Crystal Structure of Albite Mineral [49].

The crystal structure of albite was investigated by means of its x-ray trace (Figure 3.2). The structural investigation of albite was also carried out by using FTIR analysis. The FTIR analysis results were given in Figure 3.3.
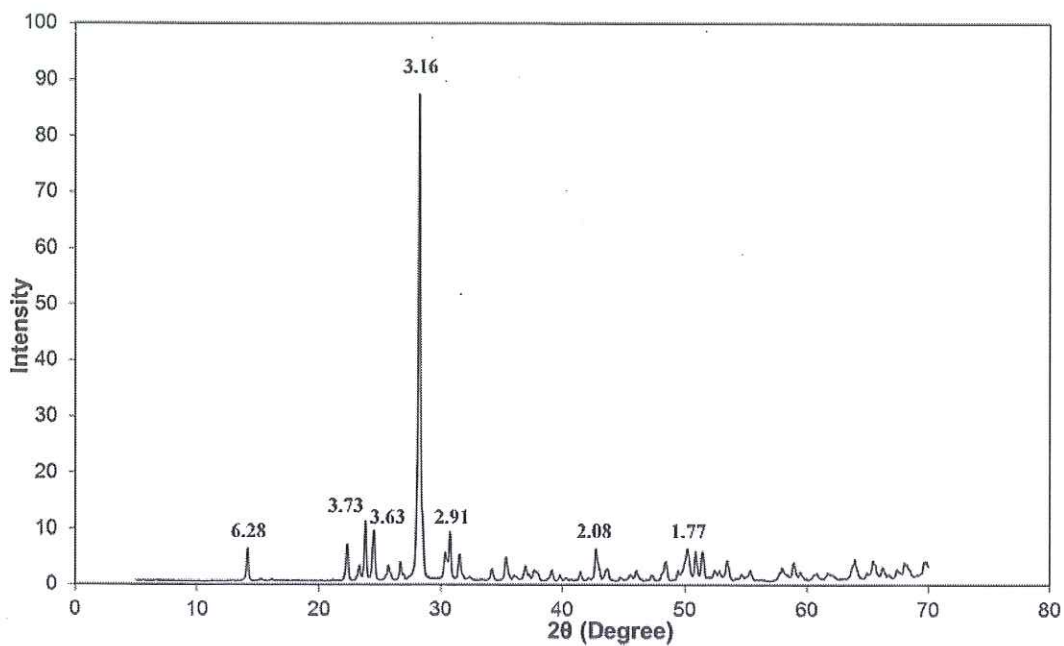
Figure 3. 2   X-Ray Diffraction Trace of Albite. Main Peaks are Listed on the Figure; 3.16 Å, 2.95 Å, 2.91 Å, 3.73 Å, 3.63 Å, 2.99 Å, 6.28 Å.
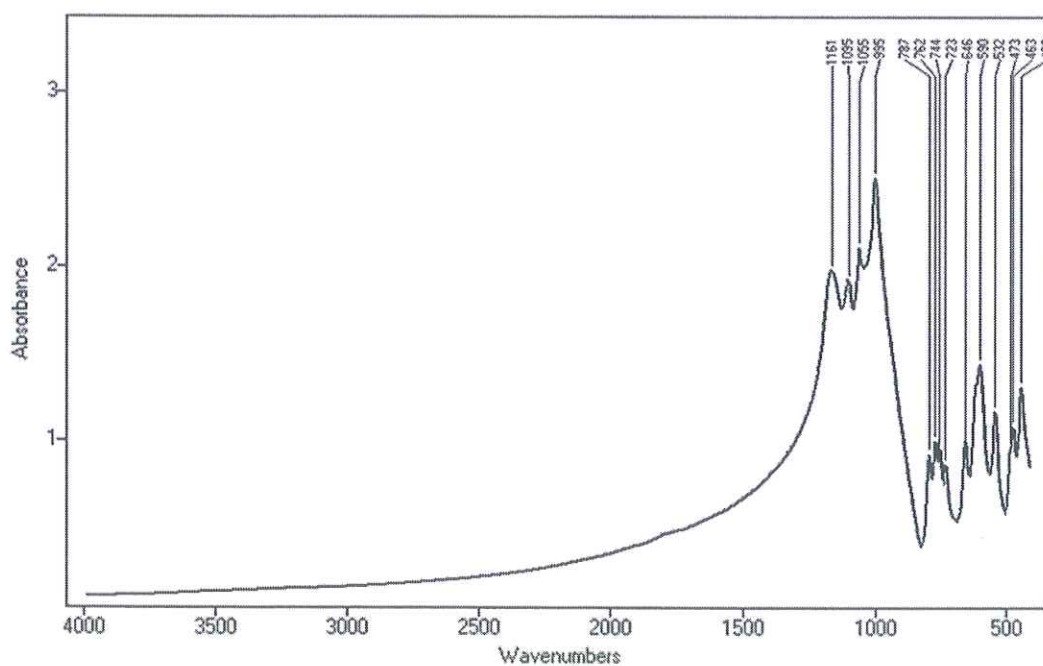
Figure 3. 3   The FTIR Spectrum of Albite. Some of the Characteristic Peaks are Indicated on the Figure.

26

The x-ray trace analysis results showed that albite used was almost pure. All peaks were consisted with the literature data (10-393) published by the International Center for Diffraction Data (ICDD) [50]. The minerals corresponding to a few very weak peaks were not identified.

The FTIR peak positions of albite were similar to that of asserted by Iiishi et al. and County et al. [51, 52].

The peaks of 1161 cm^{-1}, 1095 cm^{-1} corresponds to Si-O cm^{-1} stretching vibrations, 1055 cm^{-1}, 995 cm^{-1} corresponds to Si(Al)-O vibrations, the peaks of 787 cm^{-1}, 762 cm^{-1} correspond to Si-Si vibrations, the peaks of 744 cm^{-1}, 723 cm^{-1} are related with Si(Al)-Si vibrations, the peak of 646 cm^{-1} Si-O vibrations. The band at 433 cm^{-1} corresponds to Si-O-Si deformation vibration [53].

The element composition of albite was obtained by XRF analysis, the results were given in the Table 3.1. The XRF analysis showed presence of considerable amount of CaO which may come from anortite. The calculation have been carried out considering this fact and about 5.0% anortite was found in the sample .

Table 3.1   Element Composition of Albite Sample (Elements are expressed in oxide form).

Element	%	Element	%
Na_2O	10.76	K_2O	0.3425
MgO	< 0.023	CaO	1.155
Al_2O_3	21.19	TiO_2	0.1163
SiO_2	65.31	MnO	0.0403
P_2O_5	0.183	Fe_2O_3	0.0397

3.1.1.2 Biotite

Biotite is a sheet silicate which consists of iron, magnesium, aluminum, silicon, oxygen and hydrogen. They form sheets that are weakly bond together by potassium ions. "It is a common phyllosilicate mineral within the mica group, with the approximate chemical formula of $K(Mg,Fe)_3AlSi_3O_{10}(F,OH)_2$. More generally, it refers to the dark mica series, It is sometimes called iron mica and sometimes called black mica as opposed to white mica (muscovite). Like other mica minerals, biotite has a highly perfect basal cleavage, and consists of flexible sheets, or lamellae, which easily flake off. It has a monoclinic crystal system, with tabular to prismatic crystals with an obvious pinacoid termination. It has four prism faces and two pinacoid faces to form a pseudohexagonal crystal". Figure 3.4 shows the crystal structure of biotite mineral. It is found in a wide variety of igneous and metamorphic rocks [49].
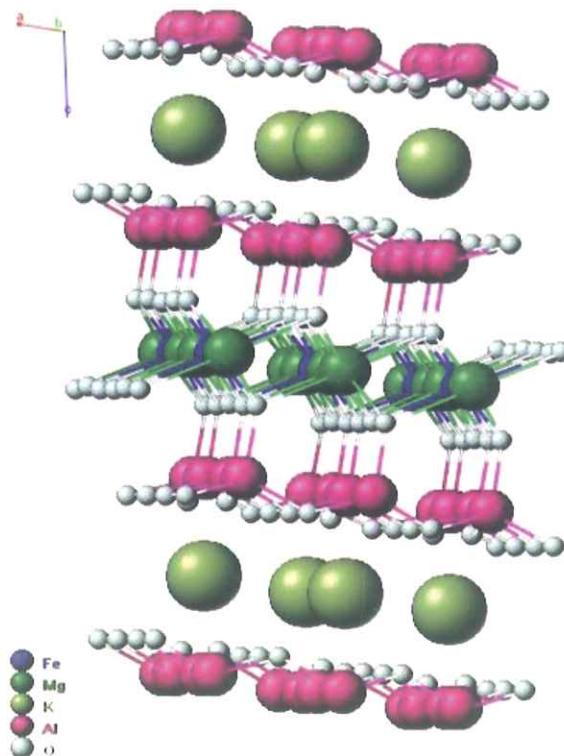
Figure 3. 4   Crystal Structure of Biotite Mineral [49].

28

The crystal structure of biotite was investigated by means of its x-ray trace (Figure 3.5).
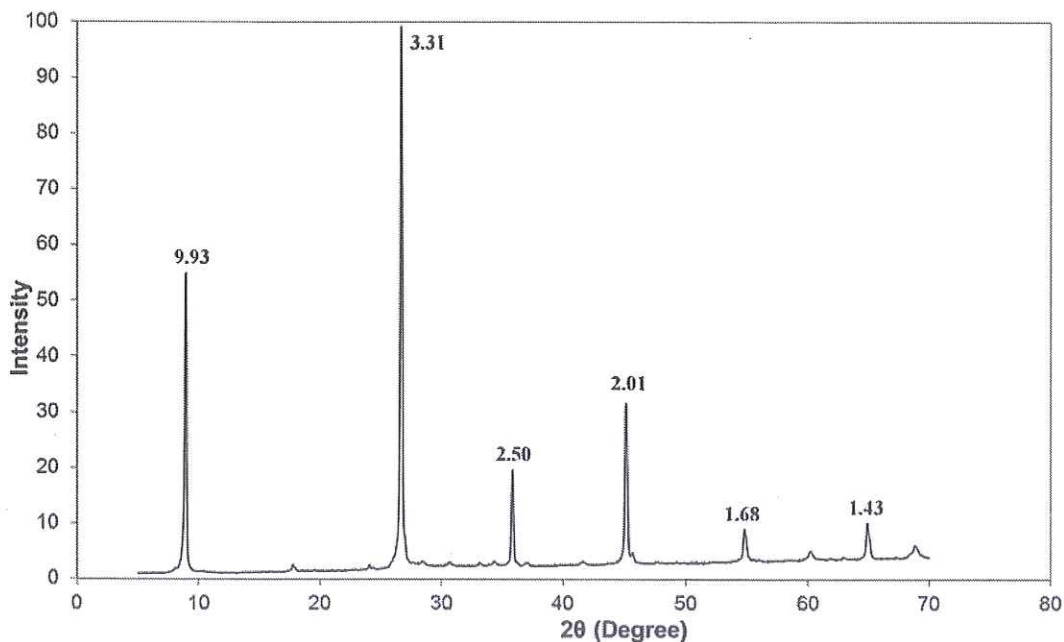
Figure 3. 5   X-Ray Diffraction Trace of Biotite. Main Peaks are Listed on the Figure; 9.93 Å, 3.31 Å, 2.50 Å, 2.01 Å, 1.68 Å, 1.43 Å.
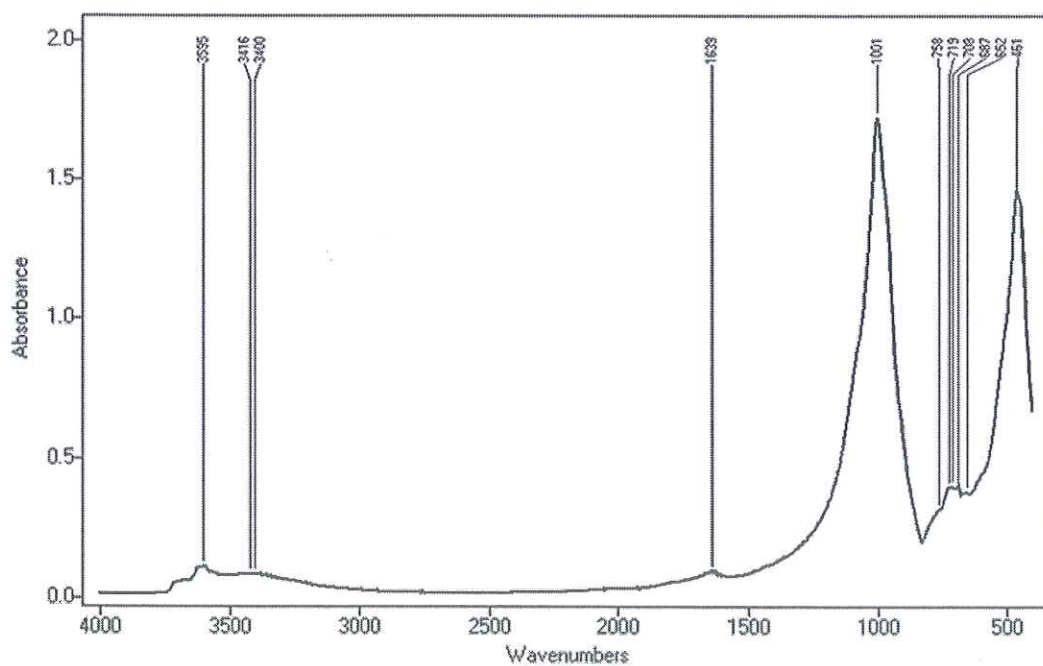
Figure 3. 6   The FTIR Spectrum of Biotite. Some of the Characteristic Peaks are Indicated on the Figure.

29

According to the XRD result, the biotite used was almost pure. All peaks were consisted with the literature data (42-1437) [50]. The minerals corresponding to a few very weak peaks were not identified.

The structural investigation of biotite was also carried out by using FTIR analysis (Figure 3.6). In biotite, stretching band of structural hydroxyl groups has been observed at 3595 cm^{-1} and 3416 cm^{-1}, the peak at 1639 cm^{-1} corresponds to bending of water, the peak of 1001 cm^{-1} and 708 cm^{-1} are related with Si(Al)-Si stretching vibrations, the peak of 652 cm^{-1} corresponds to O-Si(Al)-O bending vibration, finally the peak at 461 cm^{-1} corresponds to bending vibration of O-Si-O [53].

The element composition of biotite was obtained by XRF analysis, the results were given in the Table 3.2. The results showed that the biotite under study has the formula $K(Mg, Fe^{2+})_3(Al, Fe^{3+})Si_3O_{10}(OH, F)_2$. The elemental composition of the biotite was found to be similar with the previous studies [49] and (42-1437) [50]. The absence of fluorine may be due to the sensitivity of XRF instrument used. The sensitivity of the instrument starts from the elements with atomic number eleven or more.

Table 3. 2   Element Composition of Biotite Sample (Elements are expressed in oxide form)

Element	%	Element	%
Na_2O	< 0.067	CaO	0.484
MgO	15.44	TiO_2	1.665
Al_2O_3	13.63	V_2O_5	0.0522
SiO_2	38.73	Cr_2O_3	0.0394
P_2O_5	0.0228	MnO	0.149
Cl	0.0225	Fe_2O_3	11.86
K_2O	8.31		

3.1.1.3 Muscovite

Muscovite, also known as common mica, muscovy glass (isinglass) or potash mica, is the most common member of the mica group. "It is a phyllosilicate mineral of aluminium and potassium with formula $KAl_2(AlSi_3O_{10})(F,OH)_2$, or $(KF)_2(Al_2O_3)_3(SiO_2)_6(H_2O)$" and has a layered structure of aluminum silicate sheets weakly bonded together by potassium ion layers. These potassium ion layers produce the highly perfect basal cleavage yielding remarkably-thin lamellae (sheets) which are often highly elastic. It is a monoclinic mineral found in granites, pegmatites, gneisses, and schists. It is also found as a contact metamorphic rock or as a secondary mineral which result from the alteration of feldspar, kyanite, etc. The crystal structure of muscovite mineral is illustrated in Figure 3.7 [49]. The structural investigation of muscovite was investigated by means of its x-ray trace (Figure 3.8) and FTIR analyses (Figure 3.9).
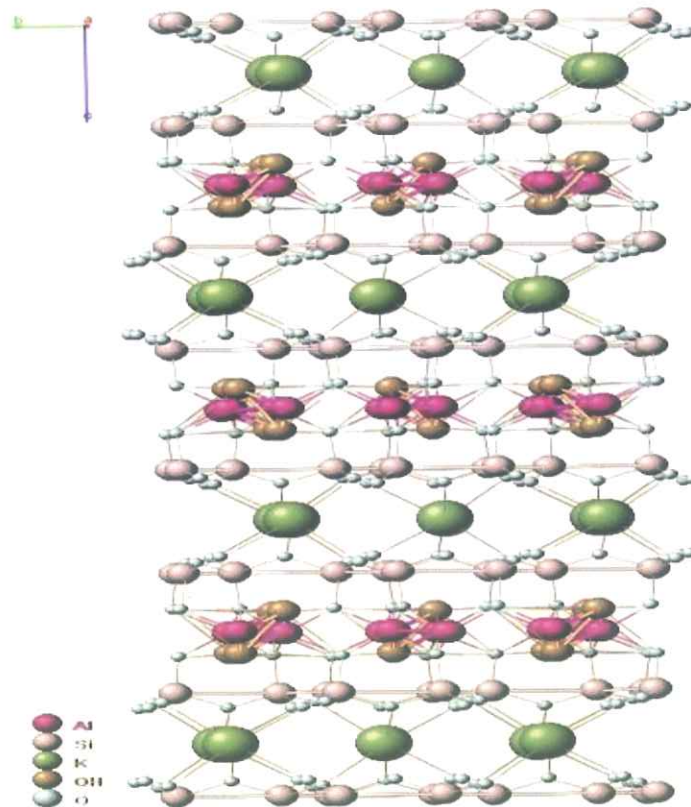
Figure 3. 7   Crystal Structure of Muscovite Mineral [49].
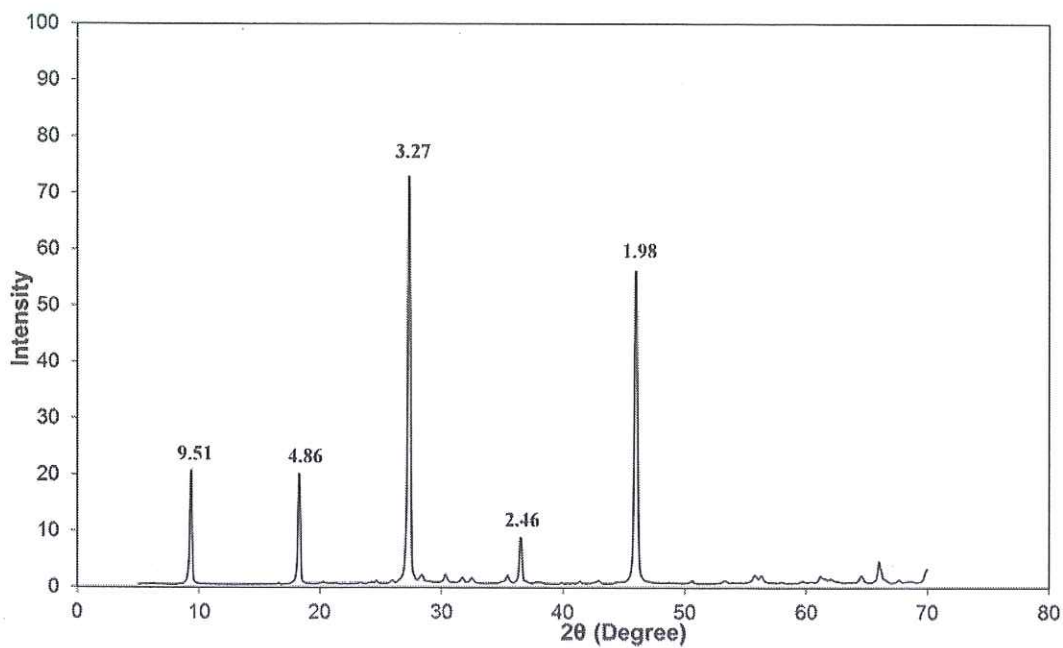
Figure 3. 8   X-Ray Diffraction Trace of Muscovite. Main peaks are listed on Figure; 9.51 Å, 4.86 Å, 3.27 Å, 2.46 Å, 1.98 Å.
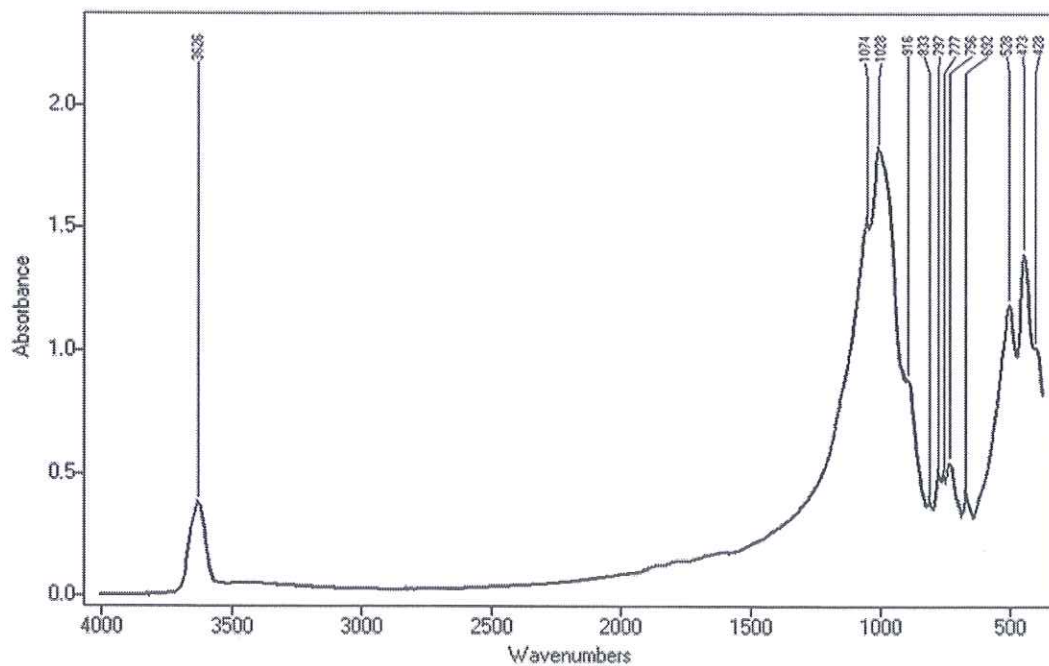
Figure 3. 9   The FTIR Spectrum of Muscovite. Some of the Characteristic Peaks are Indicated on the Figure.

The result showed that muscovite used was almost pure. All peaks were consisted with the literature data (21-993) [50].

According to the FTIR analysis results given in Figure 3.9, in muscovite, the peak at 3526 cm^{-1} corresponds to stretching vibration of OH group. The peaks of 1074 cm^{-1}, 1028 cm^{-1} correspond to Si-O stretching vibration, the peak at 833 cm^{-1} corresponds to Al-O stretching vibration, the peak at 797 cm^{-1} corresponds to Si-O vibration of quartz, 756 cm^{-1} is related with Al-O-Si in-plane vibration, the peak at 473 cm^{-1} corresponds to Si-O-Si bending vibration [53].

The element composition of muscovite was obtained by XRF analysis, the results were given in the Table 3.3. The elemental composition of the muscovite was consisted with the previous results [49] and (21-993) [50].

Table 3. 3   Element Composition of Muscovite Sample (Elements are expressed in oxide form).

Element	%	Element	%
Na$_2$O	0.58	K$_2$O	9.498
MgO	1.714	CaO	0.0773
Al$_2$O$_3$	29.31	TiO$_2$	0.478
SiO$_2$	49.99	V$_2$O$_5$	0.0165
P$_2$O$_5$	0.0348	Cr$_2$O$_3$	0.00303
SO$_3$	0.0063	MnO	0.00593
Cl	0.01781	Fe$_2$O$_3$	1.125

3.1.1.4 Orthoclase

Orthoclase (KAlSi$_3$O$_8$) is an important tectoslilicate mineral which forms igneous rock. "It is a common constituent of most granites and other felsic igneous rocks and

often forms huge crystals and masses in pegmatite. Typically, the pure orthoclase forms a solid solution with albite ($NaAlSi_3O_8$). While slowly cooling within the earth, sodium-rich albite lamellae form by exsolution, enriching the remaining orthoclase with potassium. The resulting intergrowth of the two feldspars is called perthite. Orthoclase and albite form the alkali feldspars, a series in which sodium-bearing and potassium-bearing species intermingle; thus, there is a continuous chemical variation between the two end-members" (Figure 1.1). The crystal structure of orthoclase is given in Figure 3.10. "It is polymorphous with the minerals microcline and sanidine. These three minerals form the potassium feldspar group. They are almost identical in physical properties, and it is sometimes impossible to distinguish one another without x-ray analysis. The only difference between them is their crystal structure. Microcline crystallizes in the triclinic system, and orthoclase and sanidine crystallize in the monoclinic system. Sanidine forms at high temperatures and has a disordered monoclinic symmetry, whereas orthoclase forms at low temperatures and cools slowly, forming more ordered monoclinic crystals" [49].
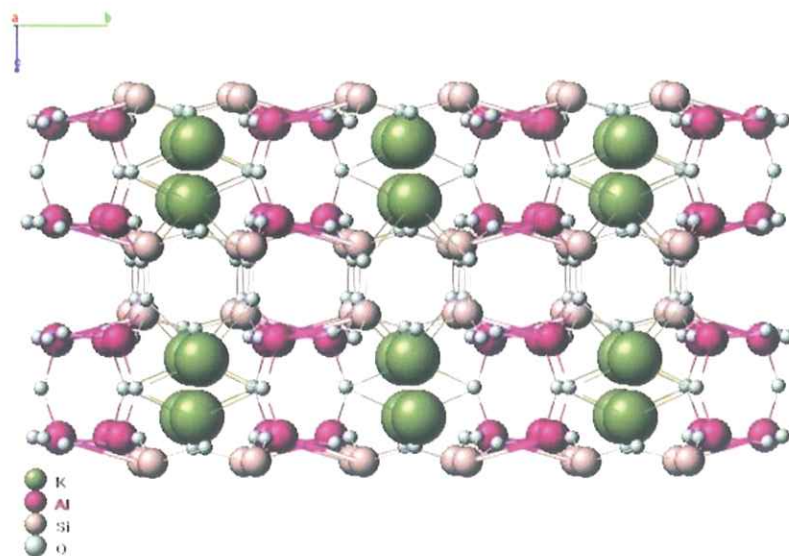
Figure 3. 10   Crystal Structure of Orthoclase Mineral [49].

For orthoclase, the XRD, XRF and FTIR results are given in Figure 3.11, Figure 3.12 and Table 3.4 respectively.
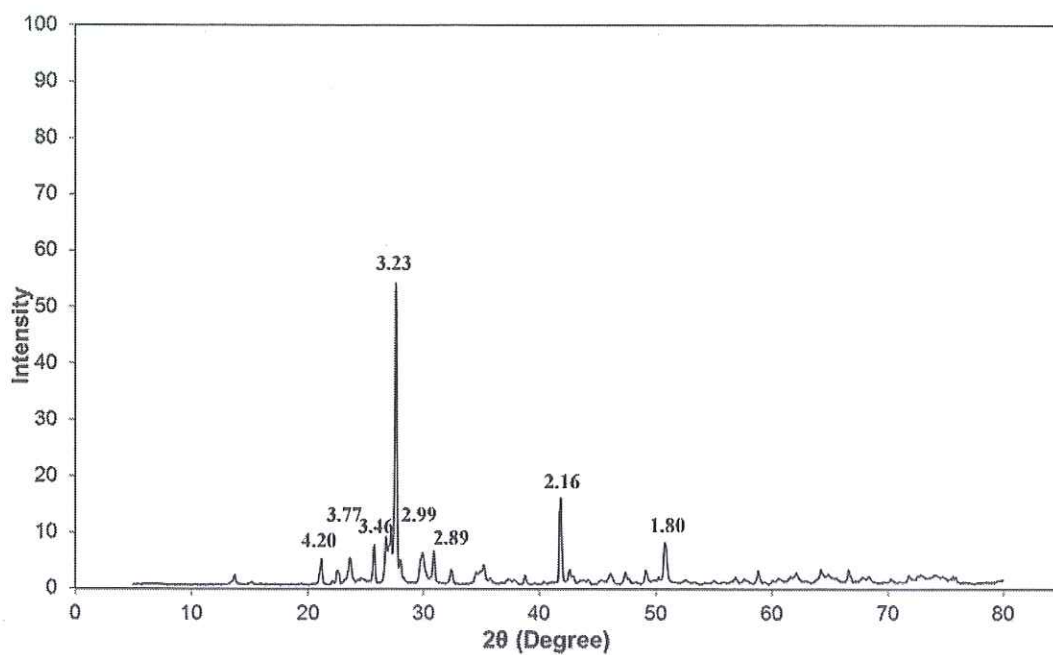
Figure 3. 11   X-Ray Diffraction Trace of Orthoclase. Main peaks are listed on Figure 3.11; 4.20 Å, 3.77 Å, 3.46 Å, 3.23 Å, 2.99 Å, 2.89 Å, 2.16 Å.
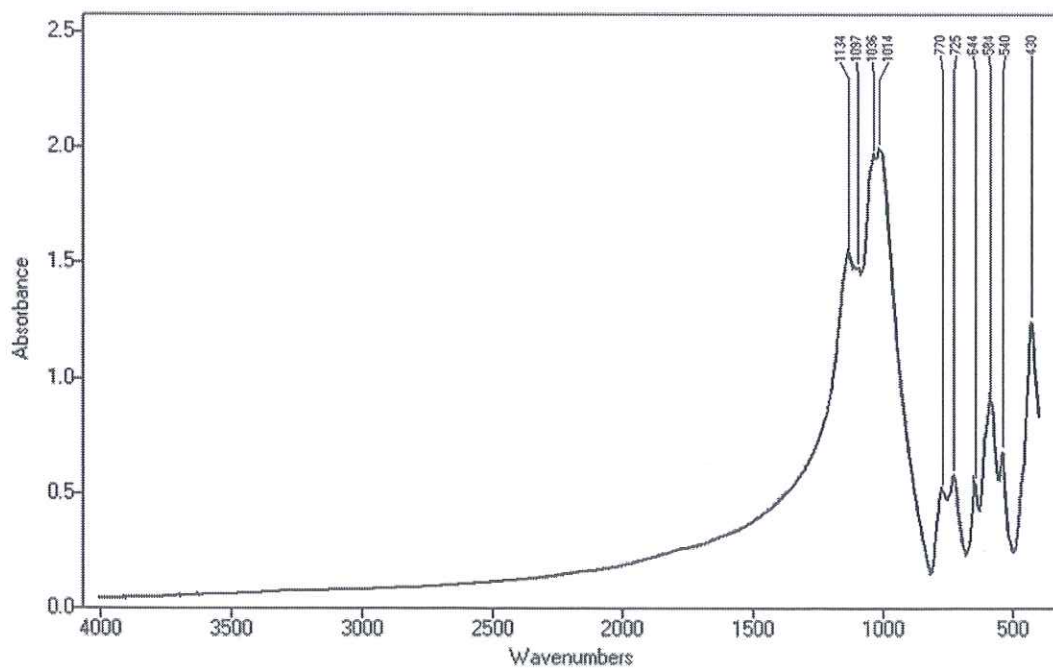
Figure 3. 12   The FTIR Spectrum of Orthoclase. Some of the Characteristic Peaks are Indicated on the Figure.

According to the XRD pattern of orthoclase, all peaks were consisted with the literature data (31-966) [50]. The element composition of orthoclase was consisted with the previous results [49] and (31-966) [50]. The purity of the orthoclase was approved by XRD, XRF and FTIR analyses results. The low value of sodium oxide showed that orthoclase is in pure form and not accompanied by albite.

In orthoclase, the peak at 1134 cm^{-1} corresponds to Si-O stretching vibration, 1014 cm^{-1} is related with Si(Al)-O stretching vibration, the peak at 770 cm^{-1} corresponds to Si-Si stretching vibration, 725 cm^{-1} is related with Si-(Al)Si stretching vibration, 644 cm^{-1} and 584 cm^{-1} peaks are related with O-Si(Al)-O bending vibrations, 540 cm^{-1} is related with O-Si-O bending vibration, finally the peak at 430 cm^{-1} corresponds to Si-O-Si deformation vibration [53].

Table 3. 4   Element Composition of Orthoclase Sample (Elements are expressed in oxide form).

Element	%	Element	%
Na_2O	1.8	K_2O	12.71
MgO	< 0.024	CaO	0.052
Al_2O_3	17.02	TiO_2	< 0.0077
SiO_2	68.56	V_2O_5	0.0039
P_2O_5	0.043	Cr_2O_3	0.0042
SO_3	0.03404	MnO	0.00798
Cl	0.00305	Fe_2O_3	0.063

3.1.1.5 Quartz

Quartz is the second most abundant mineral, after feldspar, in the Earth's crust. It is made up of a continuous framework of silicon–oxygen tetrahedra (SiO_4). In this framework each oxygen is shared between two tetrahedra giving an overall

formula SiO_2. "Pure quartz, traditionally called rock crystal (sometimes called clear quartz), is colorless and transparent (clear)" [49].

"Quartz belongs to the trigonal crystal system. The ideal crystal shape is a six-sided prism terminating with six-sided pyramids at each end". Figure 3.10 represents the crystal structure of quartz. "It is an essential constituent of granite and other felsic igneous rocks. It is very common in sedimentary rocks such as sandstone and shale and is also present in variable amounts as an accessory mineral in most carbonate rocks. It is also a common constituent of schist, gneiss, quartzite and other metamorphic rocks. Because of its resistance to weathering, It is very common in stream sediments and in residual soils" [49].
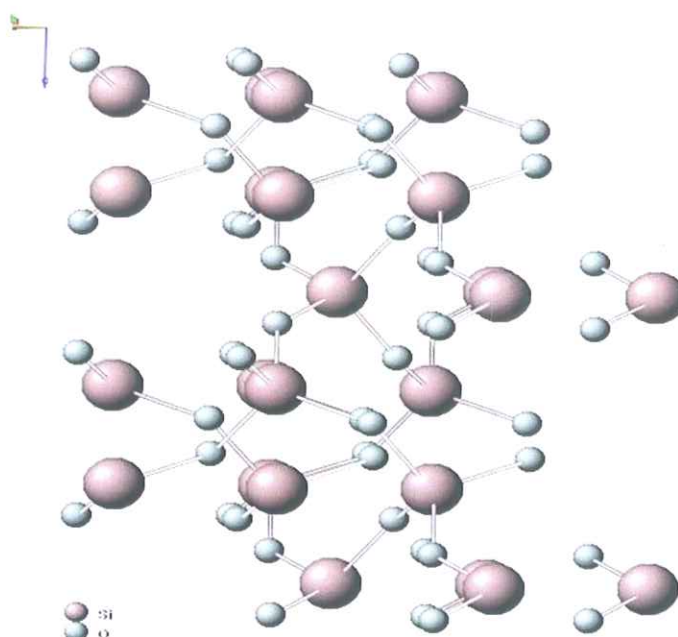
Figure 3. 13   Crystal Structure of Quartz Mineral [49].

For quartz, the XRD, XRF and FTIR results are given in Figure 3.14, Figure 3.15 and Table 3.5. According to the results, the elemental composition and all peaks in the XRD pattern of quartz were consisted with the literature data [49] and (33-1161) [50]. The purity of the quartz was approved by XRD, XRF and FTIR analyses results.
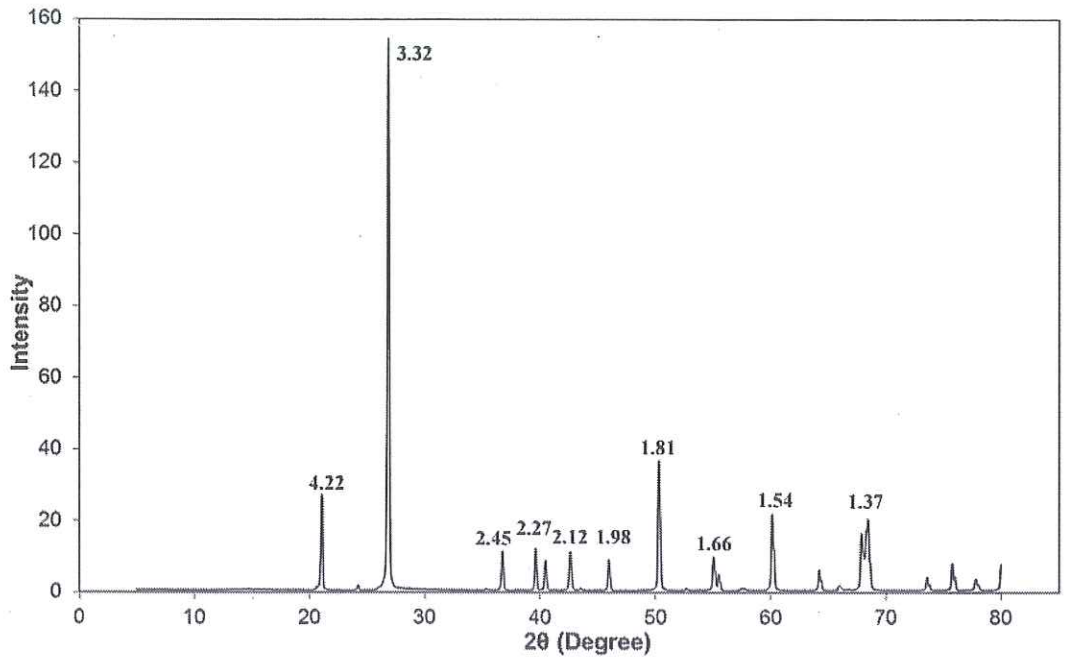
Figure 3. 14   X-Ray Diffraction Trace of Quartz. Main peaks are Listed on Figure; 4.22 Å, 3.32 Å, 2.45 Å, 2.27 Å, 2.12 Å, 1.98 Å, 1.81 Å, 1.66 Å, 1.54 Å and 1.37 Å.

Figure 3. 15   The FTIR Spectrum of Quartz. Some of the Characteristic Peaks are Indicated on the Figure.

In quartz, the peak at 1171 cm^{-1} corresponds to Si-O stretching vibration, 1080 cm^{-1} is related with asymmetric Si-O-Si stretching vibration, 797 cm^{-1} corresponds to Si-O vibration of quartz, the peaks at 779 cm^{-1} and 694 cm^{-1} are related with Si-O-Si bending vibrations, finally the peak 457 cm^{-1} is related with Si-O bending vibration [53].

Table 3. 5   Element Composition of Quartz Sample (Elements are expressed in oxide form).

Element	%	Element	%
Na$_2$O	< 0.063	Cl	< 0.00020
MgO	< 0.11	K$_2$O	0.1239
Al$_2$O$_3$	< 0.019	CaO	0.0337
SiO$_2$	98.49	TiO$_2$	< 0.0013
P$_2$O$_5$	< 0.0026	V$_2$O$_5$	< 0.00094
SO$_3$	< 0.00075		

3.1.1.6 Rutile

Rutile is a mineral which is composed primarily of titanium dioxide, TiO$_2$. It is a major titanium ore used for high tech alloys due to its light weight, high strength and resistance to corrosion. "It has among the highest refractive indices of any known mineral and also exhibits high dispersion. Natural rutiles may contain up to 10.0% iron and significant amounts of niobium and tantalum". They are found in the igneous rocks, especially as autogenic alteration products which are formed during the cooling of plutonic rocks.

"Rutile has a primitive tetragonal unit cell. The titanium cations have a co-ordination number of 6 meaning they are surrounded by an octahedron of 6 oxygen atoms. The oxygen anions have a co-ordination number of 3 resulting in a trigonal planar co-ordination". The structure of rutile is given in Figure 3.16. [49].
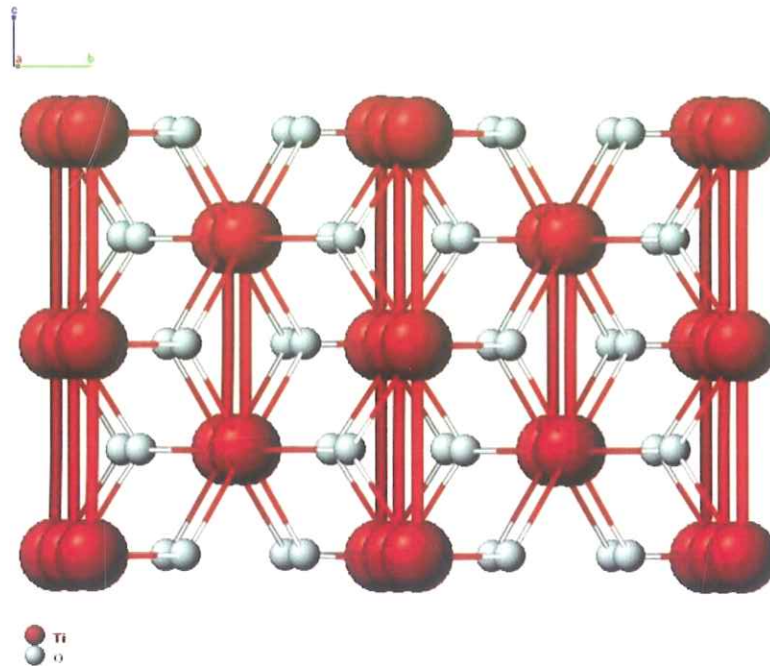
Figure 3. 16   Crystal Structure of Rutile Mineral [49].

For rutile, the XRD, XRF and FTIR results are given in Figure 3.17, Figure 3.18 and Table 3.6. According to the XRD pattern of rutile, all peaks were consisted with the literature data (21-1276) [50]. In addition, the peak at 1.89 Å showed the presence of ilmenorutile (31-646) whose some other peaks such as 2.47 Å, 2.29 Å, 2.18 Å and 2.05 Å were overlapped with the rutile peaks. The presence of ilmenorutile was also supported by the XRF results. The presence of iron with 1.29% (as Fe_2O_3) approved accompanied mineral of ilmenorutile beside rutile.
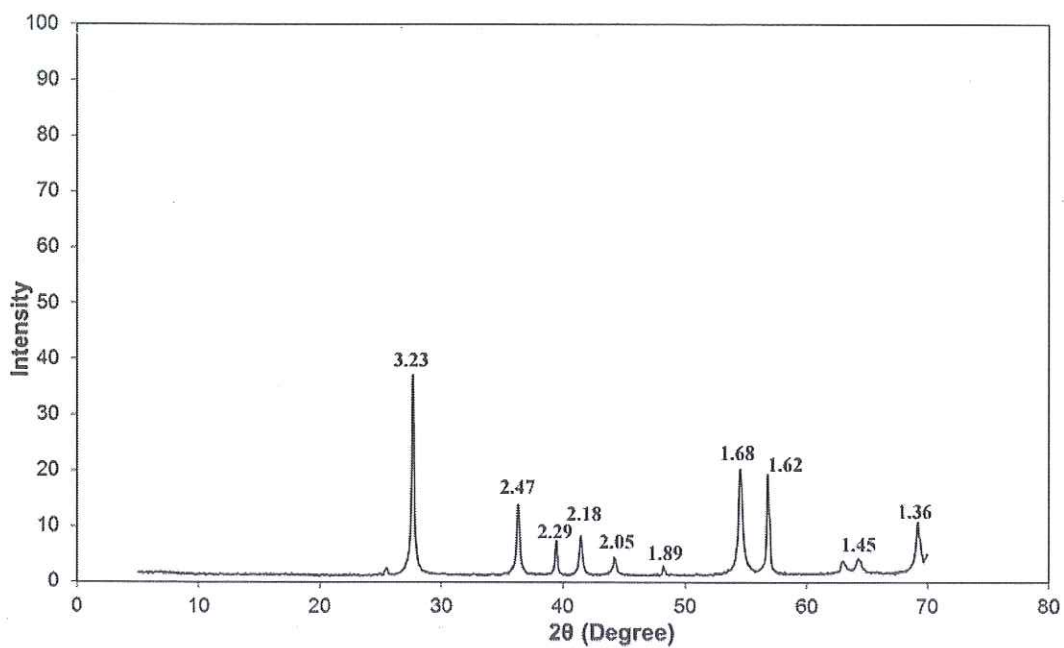
Figure 3. 17   X-Ray Diffraction Trace of Rutile. Main peaks are Listed on Figure;
3.23 Å, 2.47 Å, 2.29 Å, 2.18 Å, 2.05 Å, 1.68 Å, 1.62 Å, 1.45 Å and
1.36 Å.
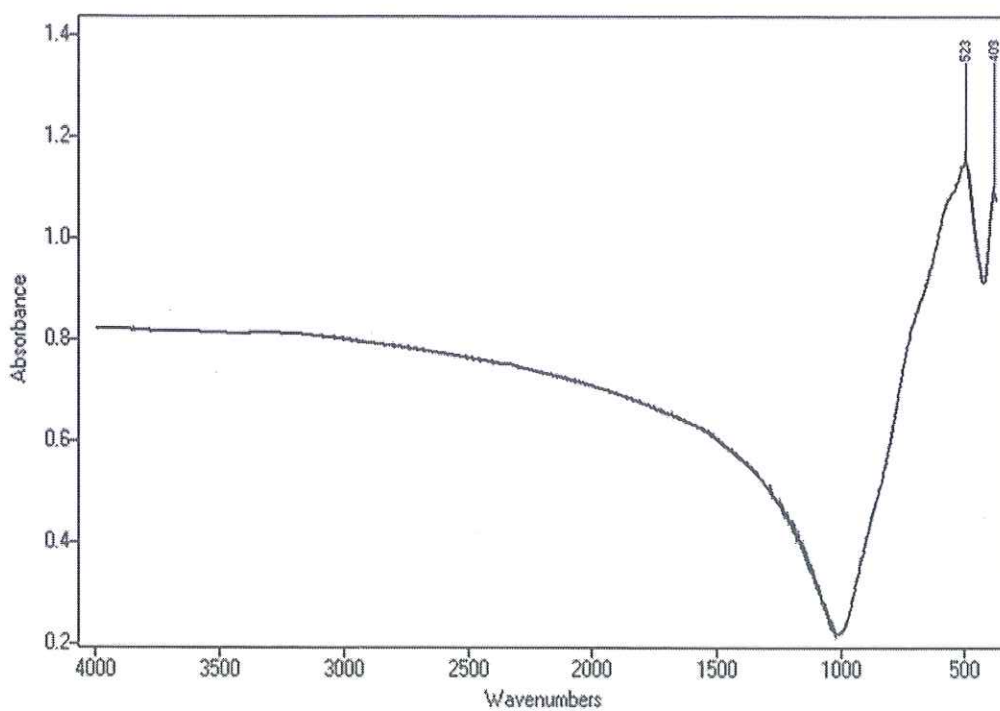
Figure 3. 18   The FTIR Spectrum of Rutile. Some of the Characteristic Peaks are
Indicated on the Figure.

In rutile, the peak at 523 cm^{-1} and 409 cm^{-1} correspond to Ti-O bending vibrations [54, 55].

Table 3. 6   Element Composition of Rutile Sample (Elements are expressed in oxide form).

Element	%	Element	%
TiO_2	93.75	Nb_2O_5	0.31
Fe_2O_3	1.29	MgO	< 0.04
Al_2O_3	0.76	CaO	0.06
SiO_2	0.87	V_2O_5	< 0.05
Cr_2O_3	0.33	P_2O_5	< 0.01
MnO	0.14	Th (ppm)	< 12.5

3.1.2   Collectors

In this study, the other important materials are the collectors. Collectors can be defined as organic substances which can be divided into a non-polar and a polar group. "The non-polar portion of the collector molecule is a hydrocarbon radical, which does not react with water and is therefore water-repellent". On the other hand, the polar part can react with water. When collector molecules interact with the mineral surfaces, "non-polar group of the collector is oriented toward the water phase and the polar parts toward the mineral surfaces. With this orientation, the mineral surface is rendered water-repellent (hydrophobic)".

There are also chemical substances which are apolar hydrocarbon liquids. They do not have a heteropolar structure. These substances do not dissociate in water and can also be used as collectors (non-ionizing collectors, i.e. kerosene).

As the aim of using collectors is to make the mineral surfaces water-repellent, "these reagents are usually classified according to their ability to dissociate into ions in aqueous solution and having regard to which type of ions (anion or cation) gives the water-repelling effect. The basic purpose of the collector is to selectively form a hydrophobic layer on a given mineral surface in the flotation pulp and thus provides conditions for attachment of the hydrophobic particles to air bubbles and recovery of such particles in the froth product" [56].

Bulatovic, 2007 stated that "when a collector dissociates into cation and anion, the one that is the direct cause of the water-repellent action, may be called the active repellent ion, and the other the non-active (non-repellent) ion. The repellent ion structure always includes a hydrocarbon radical, the presence of which ensures that the mineral is rendered water-repellent. The repellent radical includes another group of atoms attached to the carbon radical, which forms a connection between the radical and the mineral surface. This connector group is called a solidophilic group. The water-repellent effect of the collector is directly related to the length and structure of the hydrocarbon radical, whereas the effect of the solidophil group depends on three factors;

a) The nature of the reaction with the mineral surface,
b) The strength of the collector attachment, and
c) Selectivity,

all factors are dependent on the solidophilic group's composition and structure" [56].

Ionizing collectors are the larger group of the collectors. They are divided into two subgroups;

i. Anionic collector, where the anion renders the mineral water-repellent, for example: carboxyl solidophil group (a) and sulfuric acid based solidophil group (b).
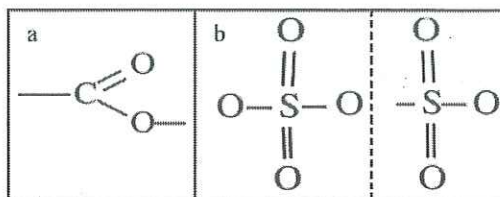
ii.   Cationic collector, where the cation renders the mineral surface water-repellent through pentavalent nitrogen based solidophil group [56]. The pentavalent nitrogen corresponds to 5 valence electrons of nitrogen ($2s^2 2p^3$). In compounds of nitrogen, 3 of valence electrons ($2p^3$) form three covalent bonds like in NH_3, RNH_2, R_2NH, R_3N. In addition, two of the valence electrons ($2s^2$) form coordinate covalent bond, this means that two electrons of the bond come from one atom, here from nitrogen. Examples for this type of combination are NH_4^+, R_4N^+. "The common element shared by all cationic collectors is a nitrogen group with unpaired electrons present, with a structure shown below" [56]:

The flotation collectors used in this study were Aero 704, Aero 3000C and Aero 825, obtained from Cytec Industries Inc.

In the experiments, 1.0×10^{-1} M stock solutions of Aero 3000C and Aero 825 were prepared by dissolving calculated amount of each in distilled water. The solubility Aero 704 was very low; a certain volume of Aero 704 was mixed with the same volume of etil alcohol. Then the mixture was treated with calculated amount of NaOH solution. It this way, oleic acid originated Aero 704 was converted to oleate form and 1.0×10^{-1} M stock solution was prepared in the same with Aero 3000C and Aero 825. The flotation recoveries of both Aero 704 and oleate form of Aero 704 were compared with no difference and the rest of the experiments were carried out by using oleate form of Aero 704 [57]. Then the stock solutions of three different collectors were diluted to the desired molarities with distilled water freshly before use.

It is necessary to give sufficient information about the collectors used, namely Aero 704, Aero 3000C and Aero 825.

3.1.2.1 Aero 704

Aero 704 is a anionic, tall oil fatty acid based collector with varying acid values, rosin acid content, and per cent fatty acid, most widely used for basic circuit flotation of iron ores and iron-bearing mineral impurities from glass making materials like feldspar and quartz. General formula of oleic acid is; $CH_3(CH_2)_7CH=CH(CH_2)_7COOH$. The molecular structure is represented in Figure 3.19.
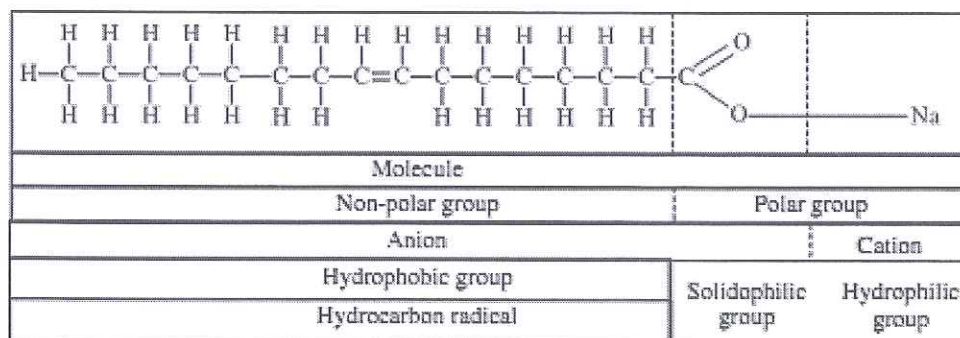
Figure 3. 19   Molecular Structure of Sodium Oleate [57] (here Aero 704).

The molecular structure of Aero 704 was obtained by conducting FTIR analysis and the FTIR spectrum is given in Figure 3.20.

45
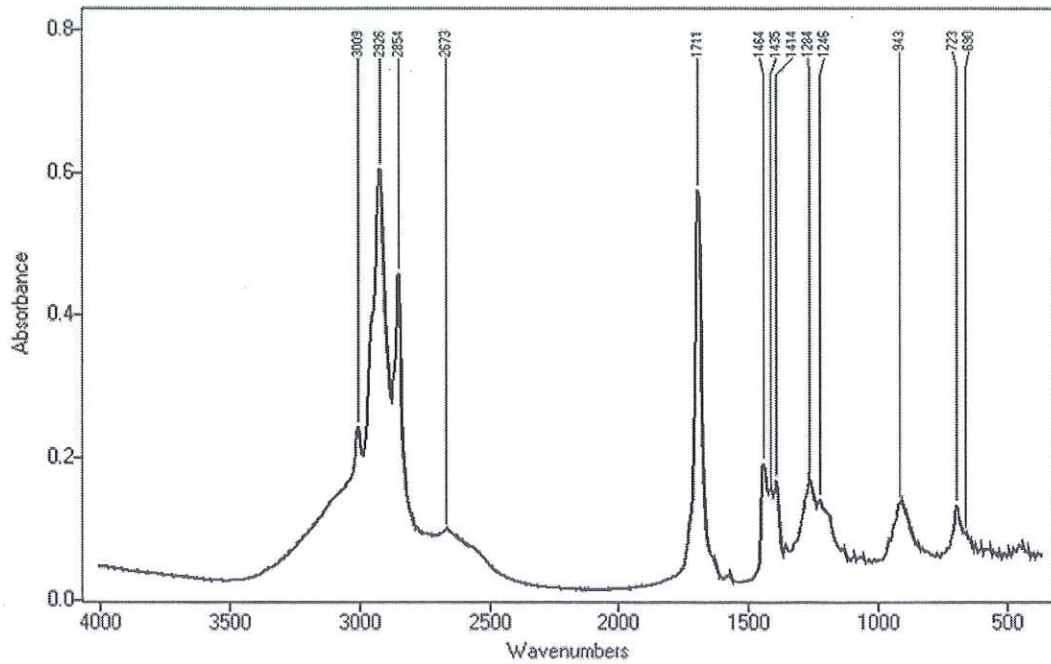
Figure 3. 20   The FTIR Spectrum of Aero 704. Some of the Characteristic Peaks are Indicated on the Figure.

In Aero 704, the peak at 3009 cm^{-1} corresponds to OH stretching vibration, the peaks at 2961 cm^{-1}, 2926 cm^{-1} and 2854 cm^{-1} CH$_2$ stretching vibrations, the peak at 1711 cm^{-1} may correspond to H-OH bending vibration and C=O stretching vibration, 1464 cm^{-1} is related with CH$_2$ bending vibration, the peak at 1414 cm^{-1} is related angular deformation of C-O-H bond, the peak 1378 cm^{-1} is related with CH$_2$ bending vibration, the peak at 1284 cm^{-1} is related with C-O elongation vibration, the peak at 943 cm^{-1} corresponds to angular deformation outside the plane of OH bond, the peak at 723 cm^{-1} is related with out of plane OH bending vibration [10, 58, 59].

3.1.2.2   Aero 3000C

It is an cationic collector that is used in acid or basic circuits for the flotation of mica minerals. It is also used with the addition of HF acid for the flotation of feldspar. Cationic collectors are organic compounds. They have a positive charge when in an aqueous environment.

46

"The covalent connection to nitrogen is usually by a hydrogen atom and hydrocarbon group. A change in the number of hydrocarbon radicals connected to the nitrogen determines flotation characteristics of amines in general. Depending on the number of hydrocarbon radicals attached to the nitrogen bond, amines can be divided into primary (I), secondary (II) and tertiary (III) [56].

(I)	(II)	(III)
$R-N{}^{+}H$ with H above and H below	R, R' attached to N with H^+ and H	R, R attached to $R-N-H^+$ with R below
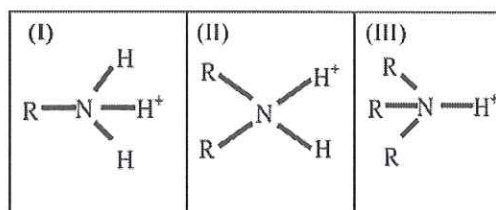
The fourth hydrogen can also be replaced by a hydrocarbon group, giving a quaternary ammonium base compound with the following structure:

$$\left[\begin{array}{c} R_1 \quad R_3 \\ N \\ R_2 \quad R_4 \end{array} \right]^{+} \bar{A}$$
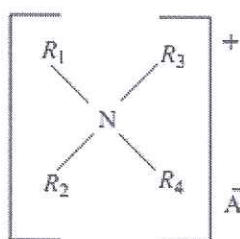
A is an anion, usually chloride or sulfate" [56].

The molecular structure of Aero 3000C was obtained by conducting FTIR analysis and the FTIR spectrum is given in Figure 3.21.
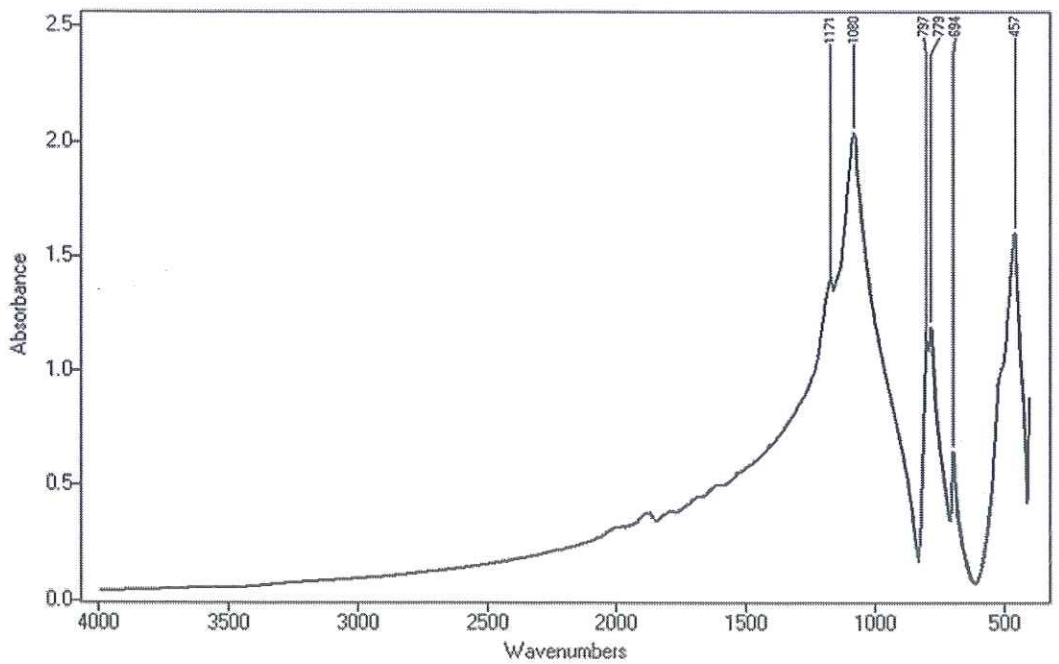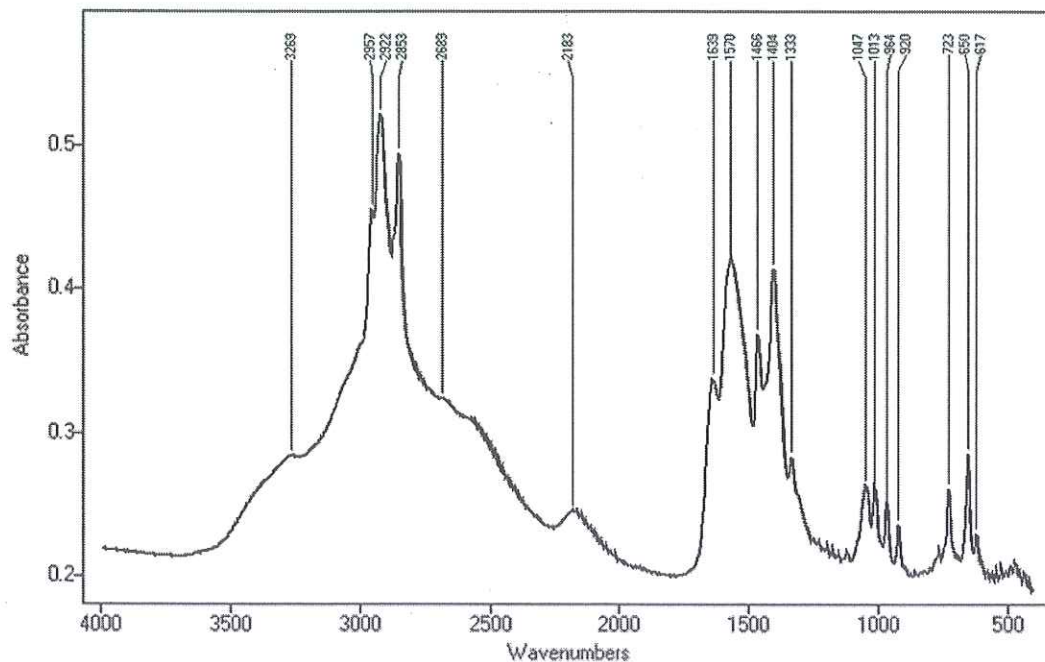
Figure 3. 21   The FTIR Spectrum of Aero 3000C. Some of the Characteristic Peaks are Indicated on the Figure.

In 3000C, the peak at 3269 cm^{-1} correspond to N-H stretching vibrations, the peaks at 2957 cm^{-1}, 2922 cm^{-1}, 2853 cm^{-1} correspond to C-H stretching vibrations, the peaks at 2183 cm^{-1}, 1639 cm^{-1}, 1570 cm^{-1} and 1513 cm^{-1} correspond to N-H bending vibrations, the peak at 1466 cm^{-1} is related with CH$_2$ bending vibration, the peak at 1333 cm^{-1} corresponds to C-N stretching vibration in aromatic amine, the bands at 1176 cm^{-1}, 1116 cm^{-1}, 1047 cm^{-1} and 1013 cm^{-1} correspond to C-N stretching vibration, the peaks at 765 cm^{-1}, 723 cm^{-1}, 650 cm^{-1} and 617 cm^{-1} correspond to C-H bending vibrations, the peaks between 910-665 cm^{-1} (919 cm^{-1}, 765 cm^{-1} and 723 cm^{-1}) are also related with N-H wagging vibrations [10, 58, 59].

3.1.2.3   Aero 825

Aero 825 is anionic, petroleum based sulfonate collector most widely used for the acid circuit flotation of iron ores and iron-bearing mineral impurities from glass making minerals like quartz and feldspar. These type collectors have a similar solidophilic group as alkyl sulfates. The difference is that the hydrocarbon radical is

48

directly connected to sulfur instead of connecting through the oxygen bridge. Structural general formula of sulfonate is as follows;

$$R - \overset{\overset{\displaystyle S}{\|}}{\underset{\underset{\displaystyle O}{\|}}{S}} - O^-$$
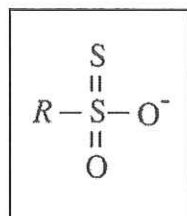
"In practice, sulfonates are produced by treating petroleum fractions with sulfuric acid and removing the acid sludge formed during the reaction, followed by extraction of sulfonate and purification. Purification consists of removing inorganic salts. Petroleum fractions, however, are not the only raw material, unsaturated alcohols, unsaturated fatty acids and their esters are also used as starting material. The products obtained are known as sulfonates. The most widely used reagents of sulfonate type are the Cytec 800 series promoters" [56].

The molecular structure of Aero 825 was obtained by conducting FTIR analysis and the FTIR spectrum is given in Figure 3.22.
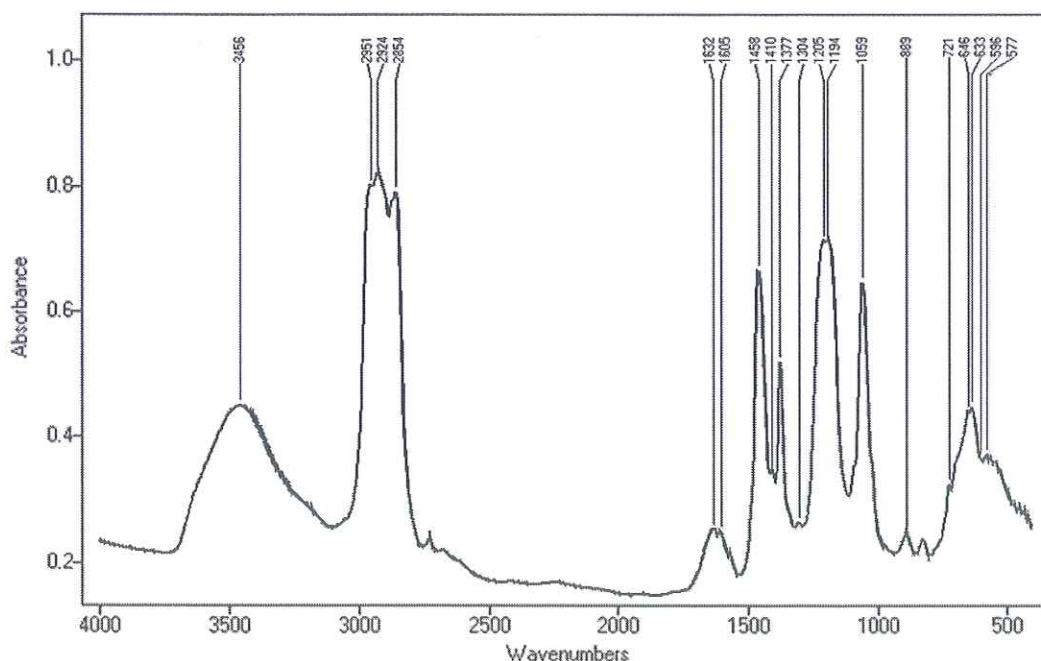
Figure 3. 22   The FTIR Spectrum of Aero 825. Some of the Characteristic Peaks are Indicated on the Figure.

49

In aero 825, the peak at 3456 cm^{-1} corresponds to OH stretching, 2951 cm^{-1}, 2924 cm^{-1} and 2854 cm^{-1} correspond to CH$_2$ stretching, the peaks at 1632 cm^{-1} and 1605 cm^{-1} correspond to OH bending vibrations, the peak at 1458 cm^{-1} and 1377 cm^{-1} correspond to CH$_2$ bending, the peaks at 1377 cm^{-1} and 1194 cm^{-1} are related with S=O stretching vibrations, the peak at 1059 cm^{-1} corresponds to SO$_3^-$ stretching vibration, the peak at 889 cm^{-1} corresponds to vinyl C-H bending vibration, the peak at 721 cm^{-1} corresponds to CH$_2$S stretching vibration, the peak 576 cm^{-1} corresponds to S-S stretching vibration [10, 58, 59].

3.1.3   Material Preparation

In the study, electrokinetic potential measurements, micro-flotation recovery responses and the interaction characteristics of the three different collectors and the six different surfaces of the minerals were investigated. For each study, the materials used were prepared in different ways and now it is necessary to give information about the material preparations.

The as received albite, biotite, muscovite, orthoclase and quartz samples were ground to finer sizes by using agate mortar in order to minimize the effect of grinding media to purity of the samples and sized in -212+38μm range. The rutile was sized in the same size range. Then sized samples were purified from its contaminated gangues to get highest purity by using high intensity dry magnetic separator (HIDMS) and high intensity wet magnetic separator (HIWMS) respectively which are shown in Figure 3.23. The as received rutile had small amount of leucoxene and ilmenite, this sample was also conducted to both magnetic separation steps. Then, all purified samples were washed with distilled water several times and dried at 100ºC ±5ºC in an oven.
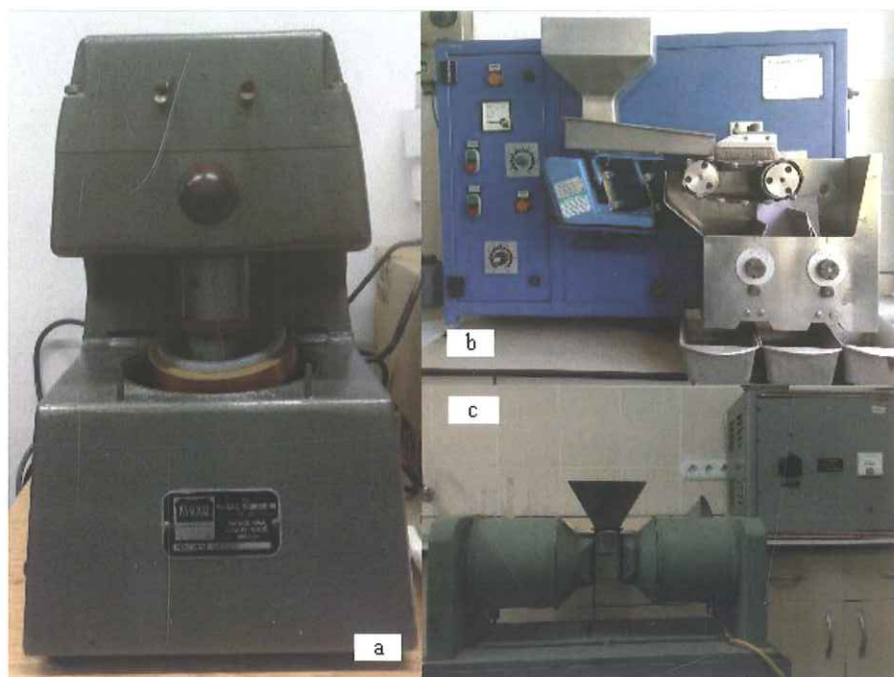
Figure 3. 23   a) Pascall Eng., Agate Mortar, b) Permroll, High Intensity Dry
Magnetic Separator, c) Carpco Inc., High Intensity Wet Magnetic
Separator.

3.1.3.1   Preparation of the Samples for Electrokinetic Potential Measurements

The purified and sized minerals samples studied were ground well by agate mortar
then 10 mg sample was put into a 100 mL of distilled water, conditioned 5 minutes
and 1 minute after conditioning step the pulp was pulled into an injector and
transferred to zeta meter sample cell for the analysis. pH calibration of pH meter was
done by using buffer solutions with pH 4.0-7.0 for acidic condition and pH 7.0-10.0
for basic condition prior to experiments. pH adjustments were done by diluting 0.1
M NaOH solution ten times and fifty times for basic condition and diluting 0.1 M
HCl solution ten times and more for acidic condition.

The same procedure repeated for the electrokinetic potential measurements of the
mineral samples in varying concentrations of the collectors used in the range;
1.0×10^{-4} M, 5.0×10^{-4} M and 1.0×10^{-3}M of Aero 704; 5.0×10^{-5} M, 1.0×10^{-4} M and

5.0x10^{-4}M of Aero 3000C; and 1.0x10^{-4}M, 5.0x10^{-4}M and 1.0x10^{-3}M of Aero 825 respectively.

3.1.3.2 Preparation of the Samples for Micro-Flotation Experiments

For the micro-flotation tests 0.5 gr sized mineral samples were used. The pulp, constituted from the mineral sample, chemical compounds and distilled water, had a total volume of 65 ml and was conditioned in the 100 ml beaker for 5 minutes by a stirrer with adjustable speed to prevent the interaction of pulp with air. 1 minute after the conditioning step, the pulp was sucked in to the test tube and placed into the EMDEE Microflot Agitator. After adjusting the air pressure to 250 kPa, test tube was agitated for 30 cycles. pH calibration of pH meter was done by using buffer solutions with pH 4.0-7.0 for acidic condition and pH 7.0-10.0 for basic condition prior to experiments. pH adjustments were done by diluting 0.1 M NaOH solution ten times and fifty times for basic condition and diluting 0.1 M HCl solution ten times and more for acidic condition.

The concentrations used in the flotation experiments were respectively; 2.0x10^{-4} M, 2.75x10^{-4} M, 3.5x10^{-4} M and 5.0x10^{-4} M of Aero 704; 2.0x10^{-5} M, 5.0x10^{-5} M, 7.5x10^{-5} M and 1.0x10^{-4} M of Aero 3000C and 1.5x10^{-5} M, 2.0x10^{-4} M, 5.0x10^{-4} M and 1.0x10^{-3} M of Aero 825.

3.1.3.3 Preparation of the Samples for FTIR Analysis

For the FTIR analyses, sample preparation was simple, approximately 0.01 g of mineral sample powder was mixed with 0.1 g of pure and dry potassium bromide (KBr) powder by using agate mortar. Then the mixture was put into disk holder to form pellet of 10 mm in diameter by applying pressure of 7 tones.

3.1.3.4   Preparation of the Samples for AFM Analysis

The sample preparation for AFM analysis was rather complicated including several steps which are given below; for the sheet like minerals, biotite and muscovite, they were cut into rectangles of approximately 10 mm and freshly cleaved with an adhesive tape to obtain a smooth, clean surface. For other minerals (albite, quartz, orthoclase and rutile), they were cut into 10 mm in diameter by crusher. Then the mineral samples were mechanically polished with 25 μm, 15 μm, 8 μm sandpapers for 20 minutes each prior to fine polishing. The samples were polished finely to get smoothest surface by applying 1 μm, 0.50 μm, 0.25 μm and 0.05 μm grit size using diamond suspension (Metadi Supreme Diamond Suspension, Buehler) and velvet cloths respectively (Figure 3.24). The sized pure mineral samples were rinsed with Millipore water (Milli-Q UV plus, Millipore Inc., 18.2 MΩcm), and sonicated for 10 minutes in each polishing step to remove the residue of the previous polishing stage.
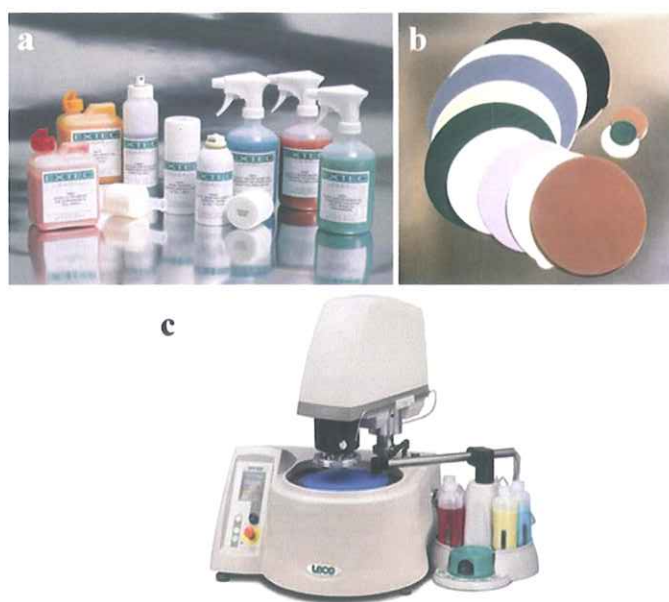
Figure 3. 24   Equipment of Sample Preparation for AFM a) Diamond Suspensions b) Sandpapers and Velvet Cloths (for a and b, different colors show different grit size) c) Polishing Set-up.

It has been found by Chudacek, 1991, that "during intensive agitation of a test-tube, an equilibrium is quickly established between mineral contained in the pulp and in the froth which forms. Once established, this equilibrium is not influenced by prolonged agitation" [60].

After agitation, a few seconds was allowed prior to froth removal as a froth drainage time. After drainage, the froth concentrate was removed using vacuum suction. Then all the floated material was removed and collected in a beaker, the non-float particles were collected in another beaker by rinsing the test tube with distilled water. Then, the float and sink fractions were filtered on tared filter paper. After drying the filter papers at 40°C ± 2°C for 24 hours, they were weighed to determine the recovery.

3.2.3 FTIR Analysis

The FTIR analyses were performed in ambient temperature as KBr disc technique by Bruker 66 vs^{-1} FTIR Instrument, in the Dr. Gülsün Gökağaç's Surface and Nanoscience Research Laboratory, Chemistry Department, METU (Figure 3.27) and then the results were further analyzed by using Opus Version 5.0 software.

Infrared spectroscopy has found wide acceptance for characterizing adsorption on mineral surfaces. An infrared spectrum represents a fingerprint of a sample with absorption peaks corresponding to the frequencies of vibrations between the bonds of the atoms which comprise the material. As each different material has a unique combination of atoms, no two compounds produce the exact same infrared spectrum. Thus, infrared spectroscopy provides a positive identification for every different kind of material [35, 36]. However, this technique is not sufficiently sensitive in the case of that adsorption is low and water interferes seriously with the analysis. It is usually difficult to interpret the spectra when adsorbate orientation effects are involved.

3.2   Methods

3.2.1   Electrokinetic Potential Measurement

The zeta potentials (ζ) of the mineral particles were measured with Malvern Zetasizer Nano-Z meter in the Research Laboratory, Mining Engineering Department, METU (Figure 3.25). Malvern Nano Zetasizer uses laser doppler velocimetry (LDV) for measuring charge of particles. It can measure the charge of particles in a size range 5 nm – 10 μm. The Zetasizer takes a series of measurements (here 3 measurements) and gives an average potential.

Figure 3. 25   Malvern Zetasizer Nano Series Z .

3.2.2   Micro-Flotation Experiment

Micro-flotation experiments in all collector concentrations for all minerals were performed by using EMDEE Microflot Agitator system consist of an Agitator Assembly and a Timer/Counter in the Research Laboratory of Mining Engineering Department of METU, shown in Figure 3.26. The EMDEE Microflot Agitator produces a linear motion by using a rodless pneumatic cylinder and this generates high accelerative field to subject the test-tube contents to high intensity agitation.

Figure 3. 26   EMDEE Microflot Agitator.

The EMDEE Microflot Flotation Recovery Test was "developed to yield information about mineral flotation behaviour on very small samples by exposing the tested system to environmental conditions simulating those prevalent in industrial flotation cells. The main advantages of the EMDEE Microflot Method are its small sample requirement and its high reproducibility through precise control of experimental conditions. This precise control is achieved for two reasons;

a) Use a small volume of pulp in a fully closed system for the flotation step.
b) A highly reproducible agitation performance of the EMDEE Microfloat Agitator" [60].

For the flotation tests 0.5 g mineral sample was used. The pulp, constituted from the mineral sample, reagents and distilled water, had a total volume of 65 ml and was conditioned for 5 minutes in the 100 ml beaker by an adjustable speed stirrer to prevent the interaction of pulp with air. After conditioning, the pulp was sucked in to the test-tube and placed into the EMDEE Microflot Agitator. After adjusting the air pressure to 250 kPa, test-tube was agitated for 30 cycles.

Figure 3. 27   Bruker 66 v s^{-1} FTIR Instrument.

Frouier Transform Infrared (FTIR) spectrometry was developed in order to overcome all limitations like slow scanning process encountered with previous infrared instruments. "A method for measuring all of the infrared frequencies simultaneously, rather than individually, was needed. A solution was developed which employed a very simple optical device called an interferometer. The interferometer produces a unique type of signal which has all of the infrared frequencies encoded into it. The signal can be measured very quickly, usually on the order of one second or so. Thus, the time element per sample is reduced to a matter of a few seconds rather than several minutes. Because the analyst requires a frequency spectrum in order to make identification, the measured interferogram signal can not be interpreted directly. A means of decoding the individual frequencies is required. This can be accomplished via a well-known mathematical technique called the Frouier Transformation. This transformation is performed by the computer, which then presents the user with desired spectral information for analysis" [34, 35].

3.2.4 AFM Analysis

The AFM samples were imaged at ambient temperature tapping mode in air using a Pico SPM 300 (Molecular Imaging) device controlled with a Nano Scope E controller (Digital Instruments) (Figure 3.28) in the Dr. Gewirth Research Laboratory, Chemistry Department of University of Illinois at Urbana-Champaign. The AFM images were recorded by tapping mode in air, as it is possible that under the collector solution the collector is less stable; therefore in contact mode the force of the tip removed the collector on the surface. The cantilever had a resonance frequency of 140–160 kHz. Images were collected in air using Phosphorus (n) doped silicon cantilever Probe at a constant scan rate of 2 Hz and 256 lines per sample. Scanning parameters were kept constant depending on the mineral type and scanning size to provide easy comparison for the effect of collector on mineral surface. AFM scanning parameters are given Table 3.7. Images were flattened with Nano Scope E version 4.23 (Digital Instruments) and further analyzed by WSxM version 5.0 Develop 3.1 (Nanotec Electronica).

Figure 3. 28   Pico SPM 300 (Molecular Imaging) Device with a Nano Scope E Controller.

Table 3. 7   AFM Scanning Parameters

Parameters	Scan Size	
	100nm	1 μm
Scan Rate	2 Hz	2 Hz
Integral Gain	0.05	0.05
Proportional Gain	0.05	0.05
Z Range	35-50nm	75-100nm

"In the past few years, the atomic force microscopy (AFM) has been used directly to image the adsorbed surfactant at the solid–liquid interface. In general, AFM has been used with contact mode (where the tip will touch the substrate) for the imaging of hard surfaces but inappropriate for the imaging of the adsorbed surfactant layers. Surfactant aggregates are fragile, so hard contact measurements will destroy the adsorbed morphology" (Figure 3.29) [61]. There is possibility that the collector becomes less stable under the collector solution, so; in contact mode, the force of the tip may cause removal of the collector from the mineral surface. In order to minimize this effect of tip on adsorbed layer of the collector, during the imaging of each collector-treated mineral surface by AFM, it was operated in tapping mode.
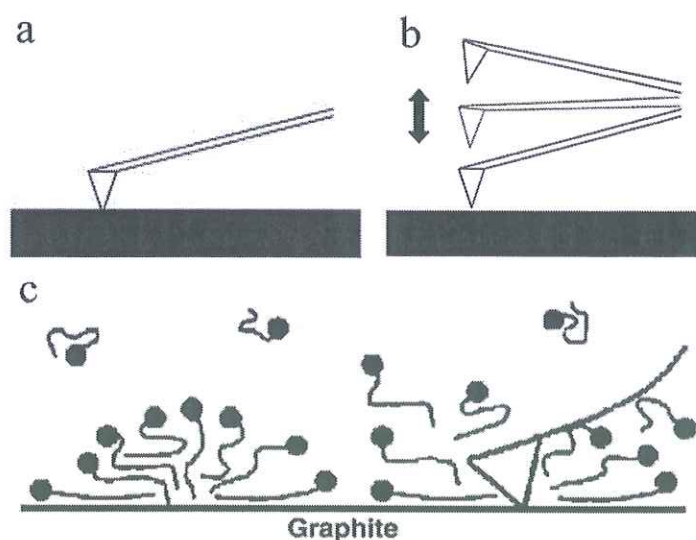
Figure 3. 29   a) Contact Mode AFM Imaging, b) Tapping Mode AFM Imaging and c) Contact Mode Imaging of Graphite in Cationic Surfactant Solution [61].

The minerals studied were also analyzed by using XRD and XRF methods. The mineral structures of the samples were determined by XRD method and chemical composition of the samples were determined by XRF method. For both methods, the mineral samples were ground into finer sizes by using agate mortar. The XRD analyses were conducted using Cu Kα (30kV, 10mA, λ=1.54050 Å) radiation and unoriented mount by Rigaku Miniflex Diffractometer in Chemistry Department, METU. Scanning was done between 5°<2θ<70°. The measurements were performed with 0.01 and 0.05 degree steps and 1 degree/minute rate. The divergence slit was variable and receiving slit scattering was 0.30 mm and 4.20 degree, respectively. The XRF analyses were performed by using Benchtop X-Ray Florescence Spectrometer in Mining Engineering Department, METU and Spectro X-Lab 2000 PED-XRF spectrometer in Geological Engineering Department, Ankara University. For the XRF analyses, 6.25 g of mineral powder samples were mixed with 1.4 g of wax (used as binder) and then pressed (at 15 tons for 1 min) to form discs (40 mm diameter and ~3 mm thickness) for the former spectrometer. In the case of latter spectrometer, discs (32 mm in diameter) were prepared by pressing (at 15 tons for 1 min) the mixture of 4.0 g of mineral powder samples and 0.9 g of wax. The XRF results which were obtained from Spectro X-Lab 2000 PED-XRF were similar to those obtained from Benchtop X-Ray Florescence Spectrometer. Because of that the former results were taken into account.

CHAPTER 4

EXPERIMENTAL RESULTS

In this chapter, experimental results of four groups of studies, namely electrokinetic potential measurements, micro-flotation experiments, infrared spectroscopic analyses and atomic force microscopy analyses conducted on the samples of albite, biotite, muscovite, orthoclase, quartz and rutile minerals were presented. During the electrokinetic potential measurements and micro-flotation studies varying concentrations of two anionic collectors, namely Aero 704, Aero 825 and one cationic collector Aero 3000C were used as a function of pH. In AFM and FTIR studies, these collectors were used in optimum conditions determined by micro-flotation studies.

Experimental results of each mineral will be explained in the following;

4.1 Albite Sample

4.1.1 Electrokinetic Potential Studies on Albite

The results of electrokinetic measurement of albite in distilled water and in 1.0×10^{-3} M of indifferent electrolyte (KCl) are given in Figure 4.1. The isoelectric point (i.e.p.) was found to be below pH 1.5 in distilled water and in 1.0×10^{-3} M of indifferent electrolyte (KCl). The zeta potential values decreased with increasing pH and became more negative towards the more basic region. The zeta potential values of albite in distilled water through the pH range of 1.0-12.5 are in agreement with the results of study published by Vidyadhar et al., 2003 [44].
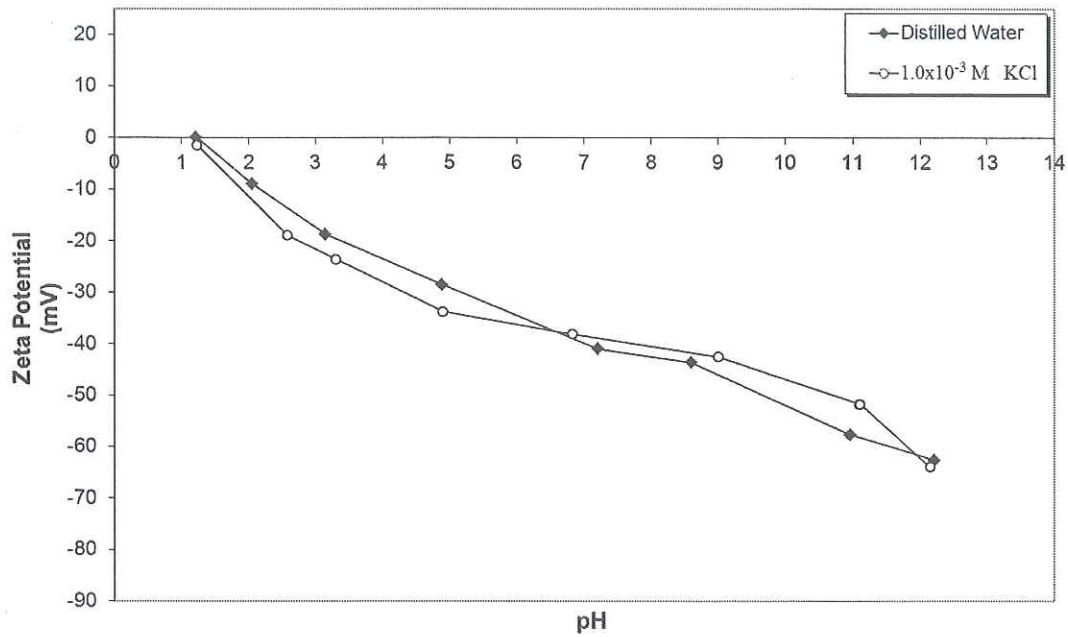
Figure 4. 1   Zeta Potential of Albite as a Function of pH.

Figure 4.2 shows the effect of 1.0×10^{-4} M, 5.0×10^{-4} M and 1.0×10^{-3} M of Aero 704 as a function of pH on the electrokinetic potential values of albite. Albite surface is negatively charged except for the pH value close to i.e.p. It is seen that the zeta potential values of Aero 704-treated albite decreased slightly with increasing Aero 704 concentration at all pH values tested.

Figure 4.3 illustrates the effect of 5.0×10^{-5} M, 1.0×10^{-4} M and 5.0×10^{-4} M of Aero 3000C on the electrokinetic potential values of albite. The isoelectric point (i.e.p.) was shifted from below pH 1.5 to pH values of about 11.0. The zeta potential values increased proportionally to Aero 3000C concentration and pH compared to the zeta potential values in distilled water. The albite surface was positively charged up to about pH 11.0 in all Aero 3000C concentrations.

The electrokinetic potential values in the presence of varying Aero 704 (as oleate) and Aero 3000C (as amine) concentrations are confirming the electrokinetic potential

62

values of albite in the presence of oleate and amine type collectors by Vidyadhar et al., 2002 [10].

In Figure 4.4, the effect of 1.0×10^{-4} M, 5.0×10^{-4} M and 1.0×10^{-3} M Aero 825 on the electrokinetic potential values of albite was displayed as a function of pH. The zeta potential values decreased with increasing Aero 825 concentration and became more negative towards the more basic region. There were no i.e.p. of the albite through all examined Aero 825 concentrations.
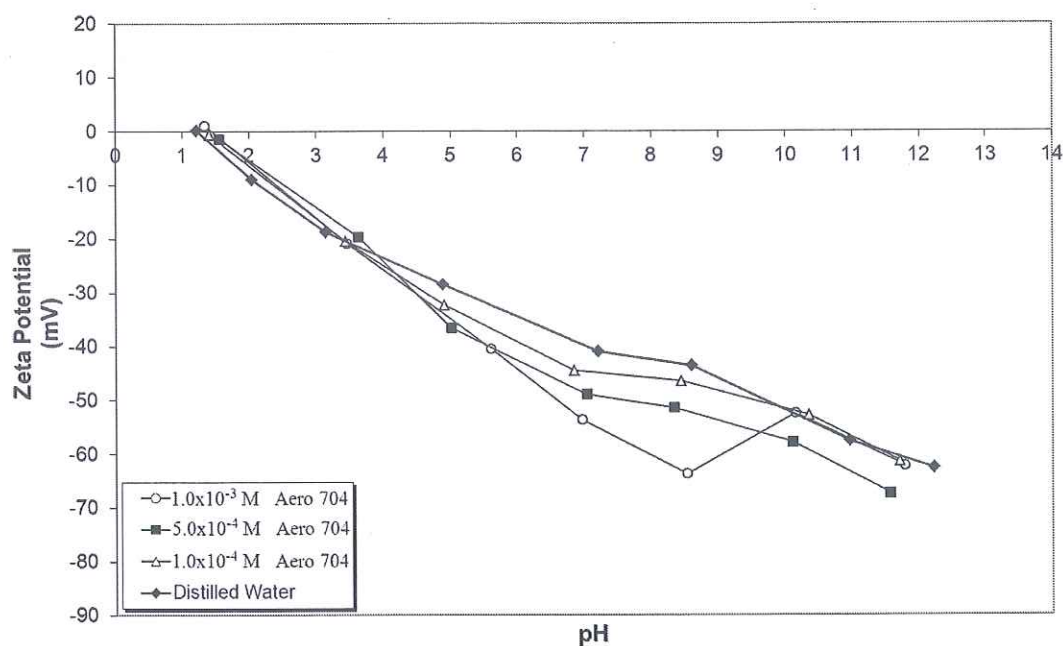
Figure 4. 2   Zeta Potential of   Albite as a Function of pH and Aero 704 Concentration.
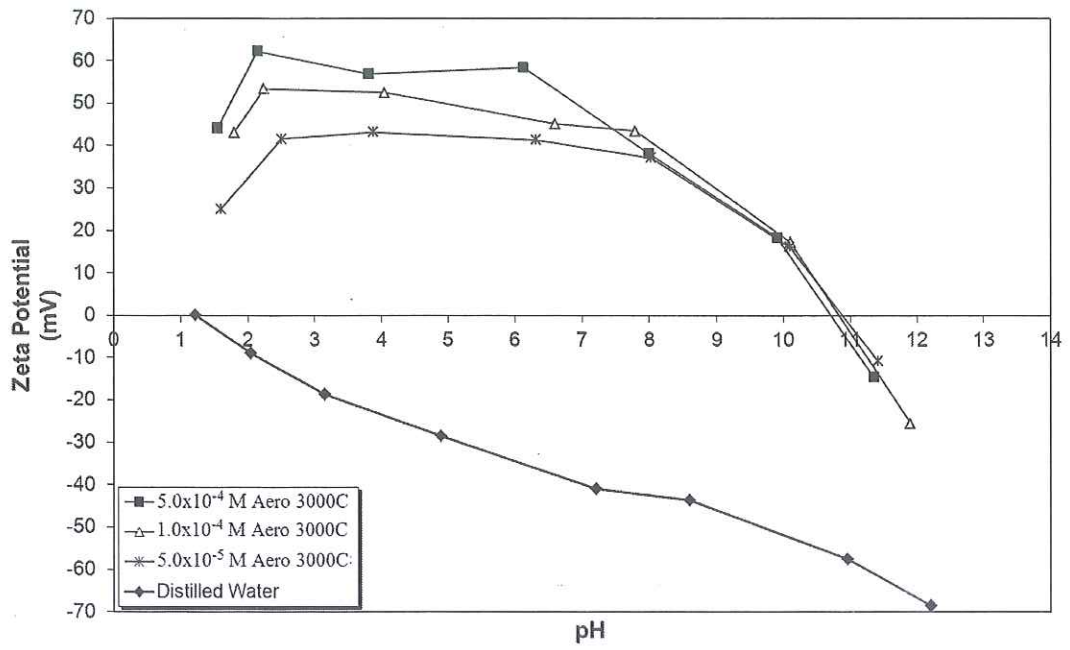
Figure 4. 3   Zeta Potential of Albite as a Function of pH and Aero 3000C
                Concentration.
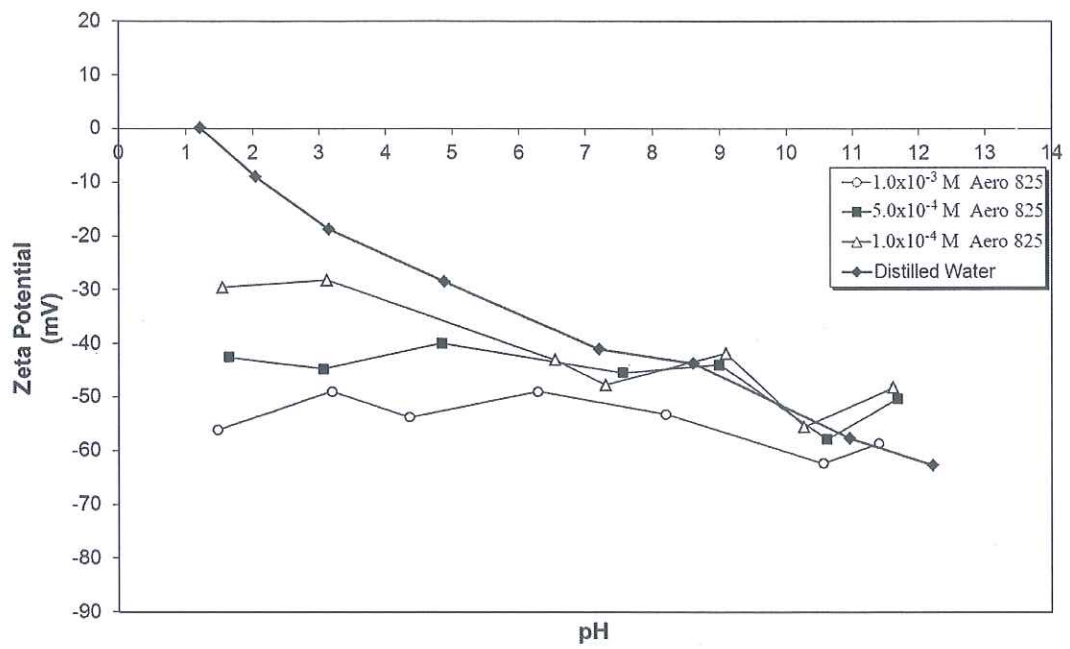
Figure 4. 4   Zeta Potential of Albite as a Function of pH and Aero 825
                Concentration.

The results of previous studies showed that acetone is the solvent to be used to determine the strength of the interaction layer of the adsorbate on various types of adsorbant. If the adsorbate is washed away easily, it is said that adsorption is weak interaction. On the other hand if the adsorbate is not removed by acetone washing it is assumed that interaction is strong [62, 63].

Additional electrokinetic potential measurements were carried out in order to investigate the effect of acetone washing on albite samples which were conditioned with optimum amount of collectors tested. The samples were first conditioned with optimum amount of each collector at optimum pH values which were determined through micro-flotation studies, 3.5×10^{-4} M of Aero 704 about pH 9.5, 5.0×10^{-5} M of Aero 3000C about pH 3.0, 2.0×10^{-4} M of Aero 825 about pH 5.0, and then collector-treated minerals were washed with acetone several times prior to the electrokinetic potential measurements. According to the results, shown in Figure 4.5, the zeta potential values of acetone-washed albite samples displayed similarities compared to those of albite in distilled water.
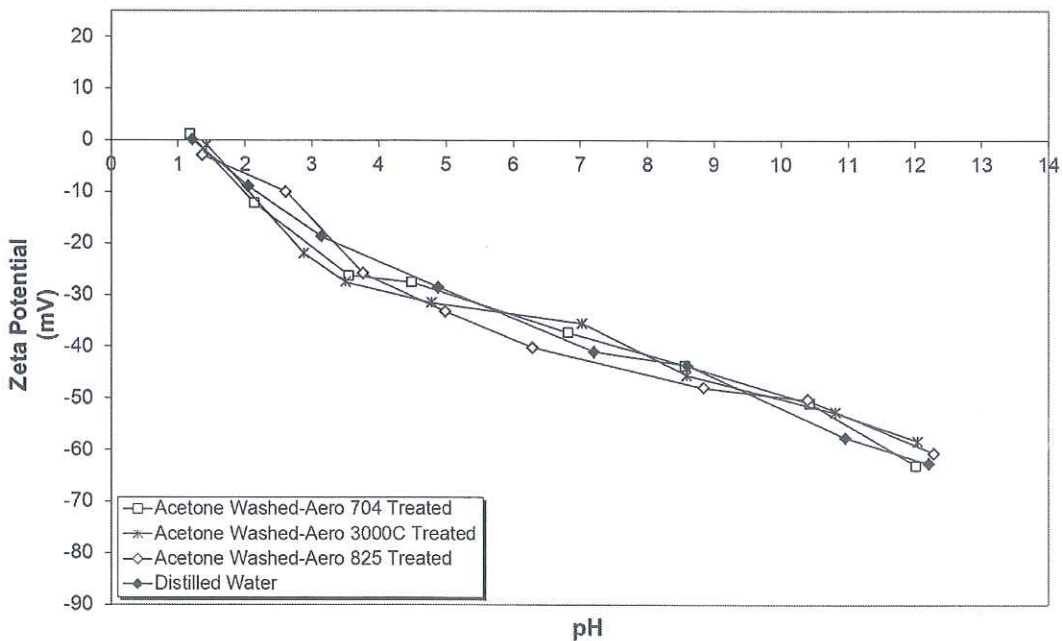
Figure 4. 5   Zeta Potentials of Aero 704, Aero 3000C and Aero 825-Treated Albite Samples After Acetone Washing.

4.1.2 Flotation Studies on Albite

The flotation recoveries of albite as a function of pH and Aero 704 concentration were shown in Figure 4.6. As the flotation recovery of albite was null below pH 7.0, the micro-flotation experiments were performed from this pH on with all Aero 704 concentrations. It is seen that the flotation recovery of the albite increased proportionally to Aero 704 concentration. The maximum flotation recoveries were obtained as 15.5% with 2.0×10^{-4} M, 59.0% with 2.75×10^{-4} M, 85.0% with 3.5×10^{-4} M and 88.5% with 5.0×10^{-4} M of Aero 704 in the pH range of 9.0-10.5.

The flotation recoveries of the albite were maximum between pH 3.5 and 10.5 with the values of 50.0%, 90.0%, 93.0% and 92.8% in the presence of 2.0×10^{-5} M, 5.0×10^{-5} M, 7.5×10^{-5} M and 1.0×10^{-4} M of Aero 3000C respectively (Figure 4.7). The flotation recoveries decreased sharply above pH 10.5 and below pH 3.5 in all Aero 3000C concentrations except for the lowest concentration, 2.0×10^{-5} M. In the latter case, the flotation recovery gradually increased and decreased above/below the neutral pH condition where the maximum flotation recovery obtained was about 50.0%.

For Aero 825, the flotation recoveries of albite increased with increasing concentration. The flotation recoveries were maximum between the pH range of 3.5 and 6.0 with the values of 4.5%, 12.0%, 18.0% and 19.5% in the presence of 1.5×10^{-4} M, 2.0×10^{-4} M, 5.0×10^{-4} M and 1.0×10^{-3} M of Aero 825 respectively (Figure 4.8).
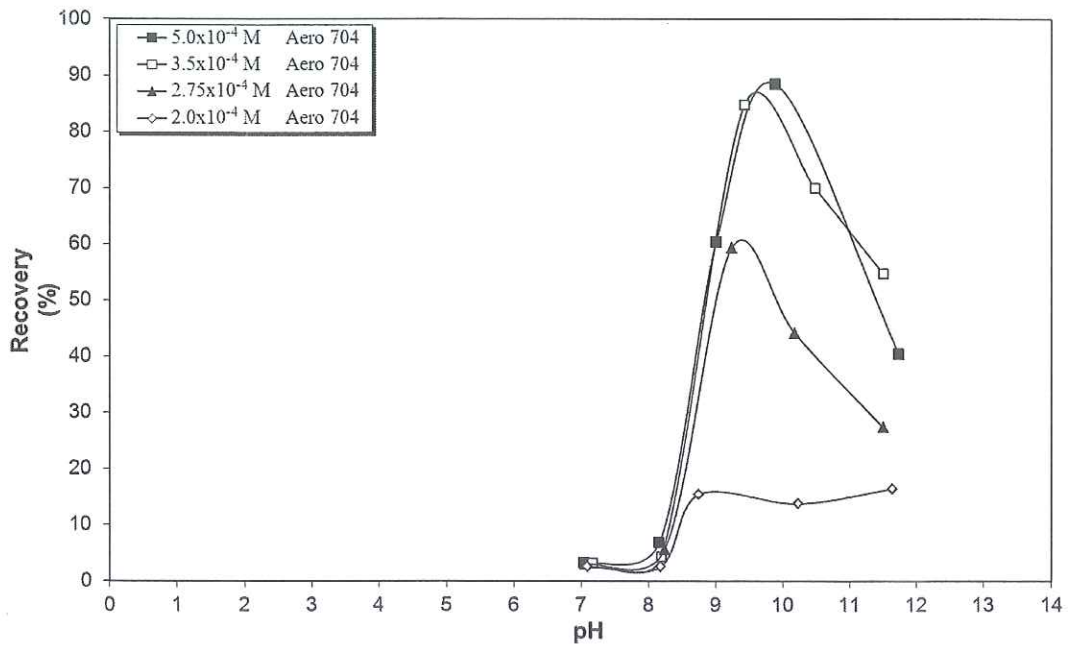
Figure 4. 6   Flotation Recovery of Albite as a Function of pH and Aero 704 Concentration.
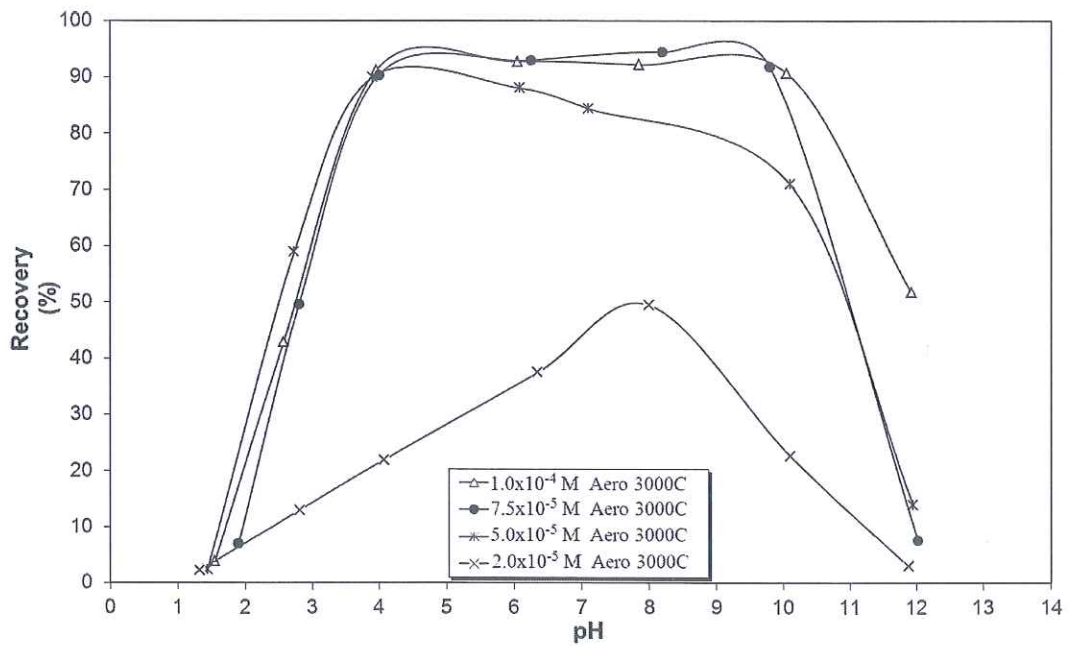
Figure 4. 7   Flotation Recovery of Albite as a Function of pH and Aero 3000C Concentration.
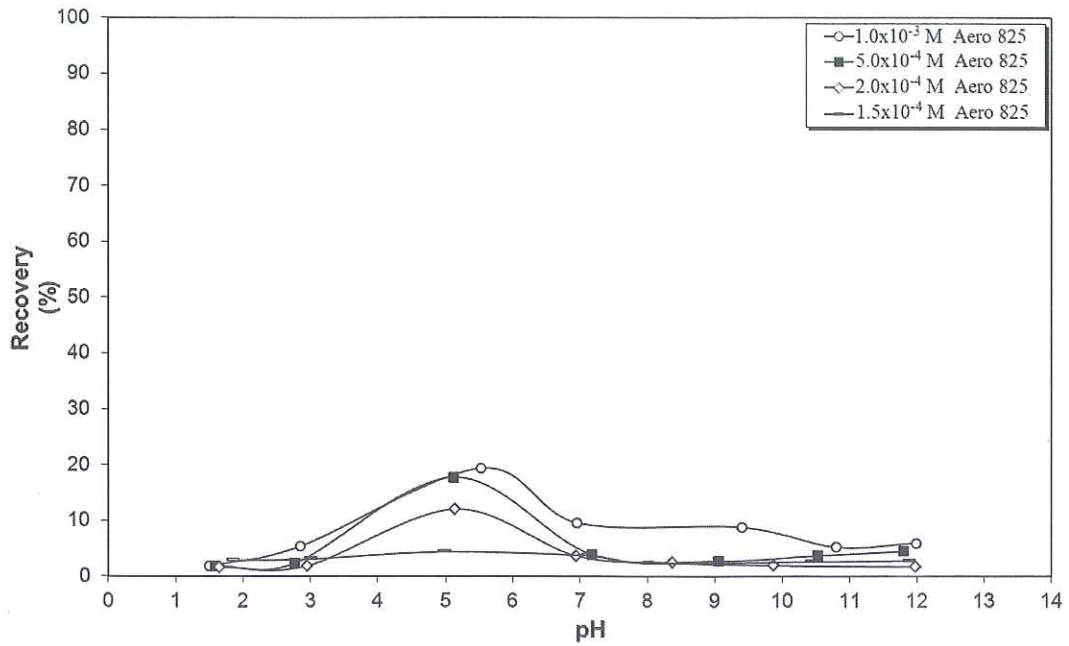
Figure 4. 8   Flotation Recovery of Albite as a Function of pH and Aero 825 Concentration.

4.1.3   AFM Studies on Albite

AFM studies were performed in order to investigate the interaction of the collectors with the mineral surfaces.

For the analyses, the mineral samples were conditioned in optimum flotation conditions which were 3.5×10^{-4} M of Aero 704 about pH 9.5, 5.0×10^{-5} M of Aero 3000C about pH 3.0 and 2.0×10^{-4} M of Aero 825 about pH 5.0.

Firstly, AFM analyses were conducted on the mineral surfaces before treatment with the collectors.

The tapping mode AFM 3D (three dimensional) micro topographies of albite in 100nm (Figure 4.9a) and 1µm (Figure 4.9c) sizes and their corresponding histograms

68

and roughness analyses (Figure 4.9b and 4.9d) were given in Figure 4.9. The resulting histogram provides information about the surface roughness, the maximum peak value and the average height values of albite for 100nm x 100nm and 1μm x 1μm scanning size ranges. The corresponding histograms revealed the roughness average as 0.2077nm, the maximum peak value as 2.2775nm and the average height value as 1.0476nm for 100nm x 100nm scanning size range and as 1.5902nm, 13.104nm and 5.5239nm for 1μm x 1μm scanning size range respectively.
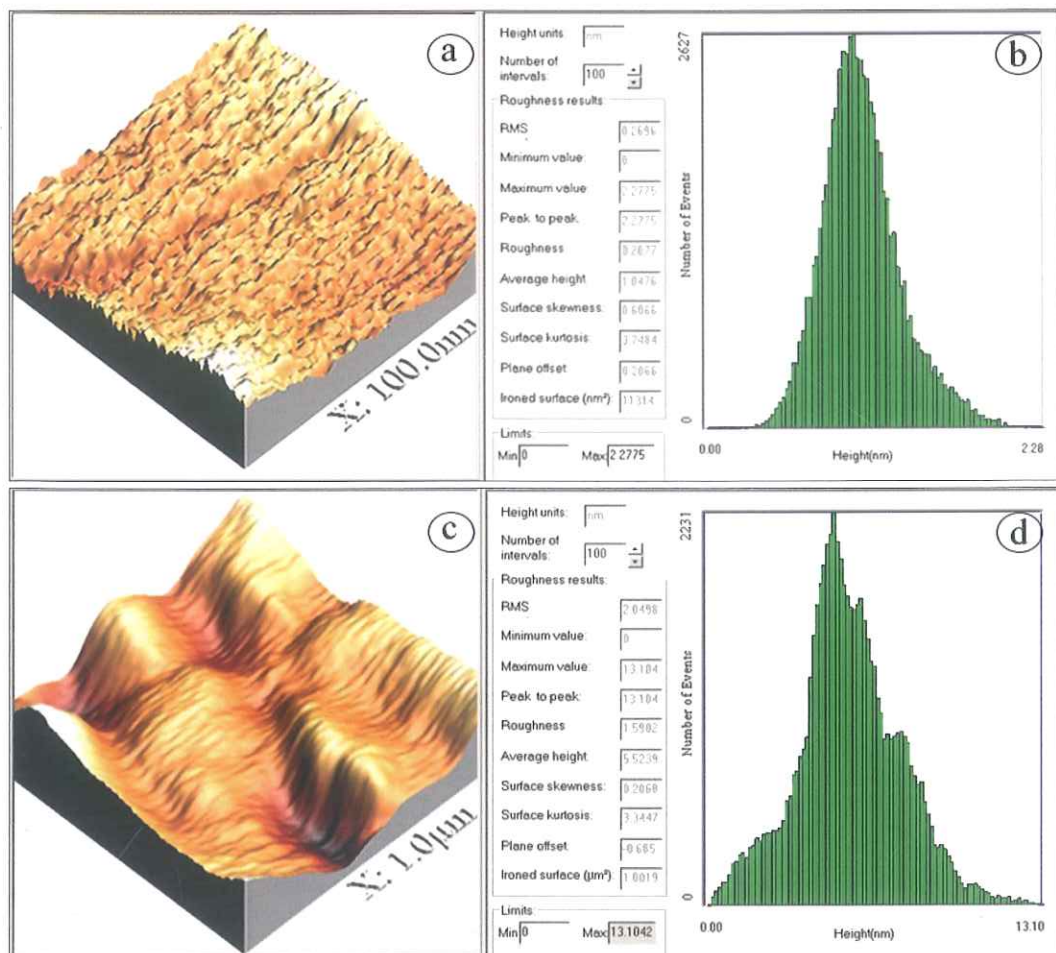
Figure 4. 9   3D Micro Topographies, Corresponding Histograms and Roughness Analyses of Albite.

The tapping mode AFM 3D micro topographies (Figure 4.10a and 4.10c) and the corresponding histograms (Figure 4.10b and 4.10d) of the Aero 704-treated albite revealed the roughness average, the maximum peak value and the average height

value as 0.2482nm, 2.4737nm and 1.0281nm for 100nm x 100nm and as 2.6522nm, 37.6450nm and 16.9820nm for 1μm x 1μm size scanning size ranges respectively (Figure 4.10).

The tapping mode AFM image analysis of albite and Aero 704-treated albite based on their height profiles in 1μm were shown in Figure 4.11 for the scanned area. The albite, shown in green, displayed height profiles less than 6nm while the height profiles of Aero 704-treated albite reached up to 12.50nm.
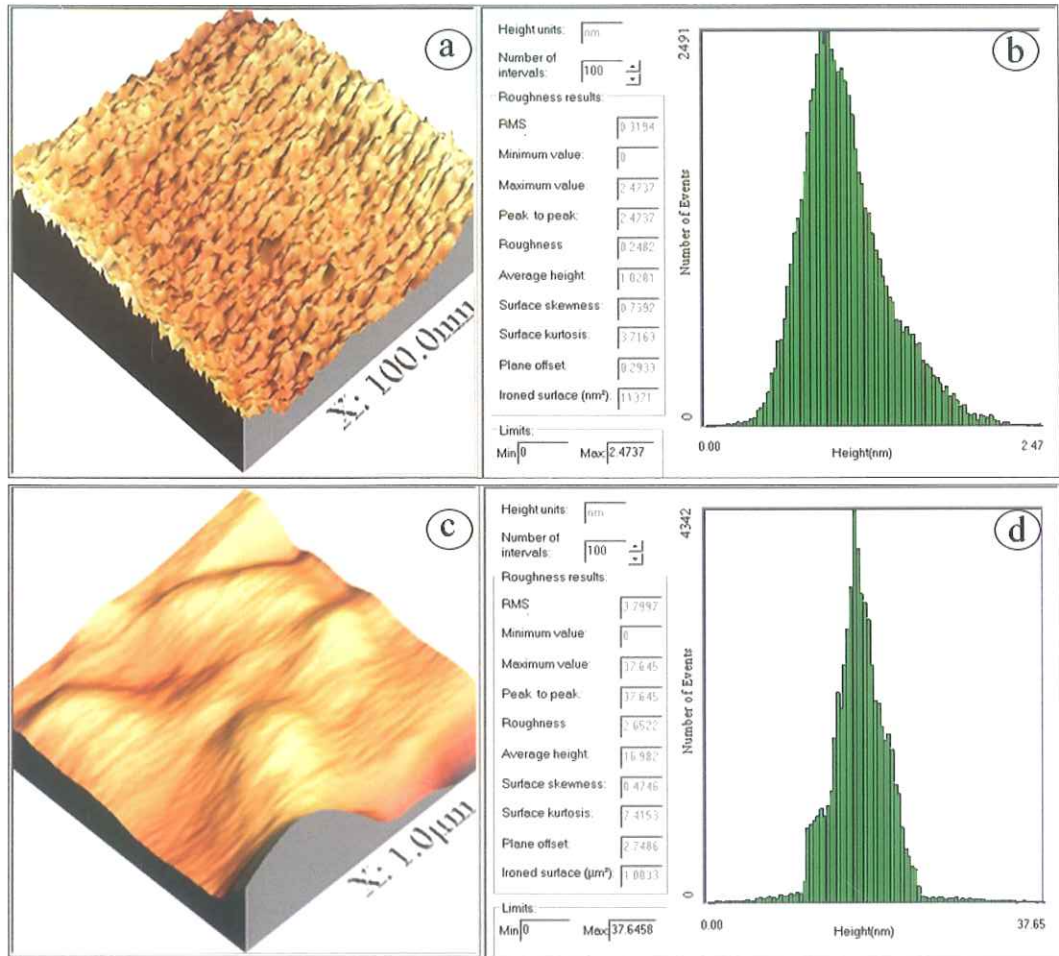
Figure 4. 10   3D Micro Topographies, Corresponding Histograms and Roughness Analyses of Aero 704-Treated Albite.
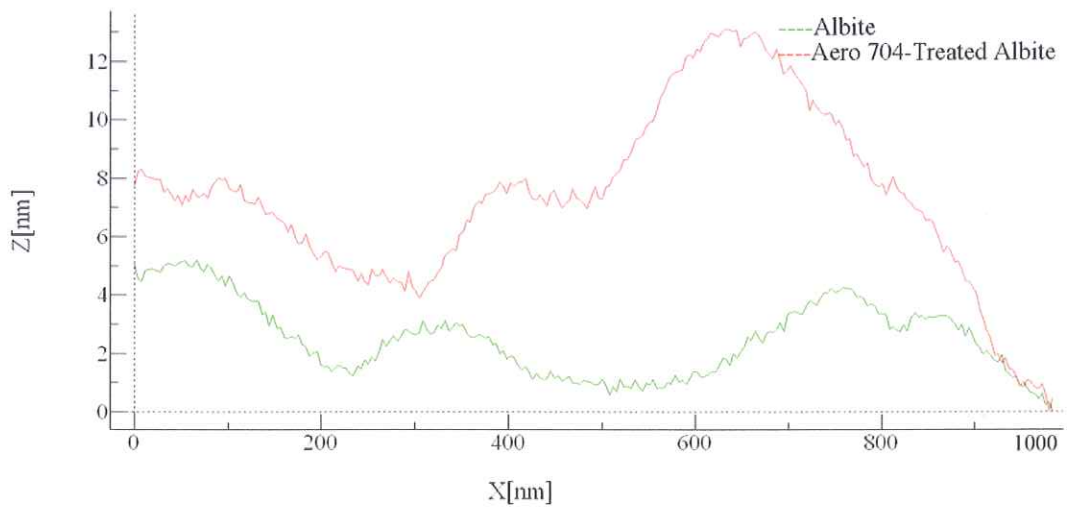
Figure 4. 11   Height Profiles of Albite and Aero 704-Treated Albite in 1μm Size.

71

The tapping mode AFM 3D micro topographies and the corresponding histograms of Aero 3000C-treated and Aero 825-treated albite in 100nm x 100nm (Figure 4.12a-b for Aero 3000C-treated and Figure 4.14a-b for Aero 825-treated albite) and 1μm x 1μm (Figure 4.12c-d for Aero 3000C-treated and Figure 4.14c-d for Aero 825-treated albite) scanning size ranges were given in Figure 4.12 and Figure 4.14 respectively.

For Aero 3000C-treated albite, the histograms revealed that the roughness averages, maximum peak values and average height values as 0.5050nm, 6.1703nm and 2.3055nm for 100nm x 100nm scanning size and 2.1322nm, 11.1460nm and 6.6633nm for 1μm x 1μm scanning size range respectively. In the case of Aero 825-treated albite, the roughness averages, maximum peak values and average height values were obtained as 0.7384nm, 8.2959nm and 4.4704nm for 100nm x 100nm scanning size range and 2.8692nm, 23.9470nm and 8.8211nm for 1μm x 1μm scanning size range respectively.

The tapping mode AFM image analysis of albite and Aero 3000C-treated albite based on their height profiles in 1μm was shown in Figure 4.13 for the scanned area. Similarly, the tapping mode AFM image analysis of albite and Aero 825-treated albite was shown in Figure 4.15. The height profiles of Aero 3000C-treated albite reached to 8.0nm and Aero 825-treated albite reached to 10.0nm while the albite, shown in green in the figures, displayed height profiles less than 6.0nm for the scanned area.
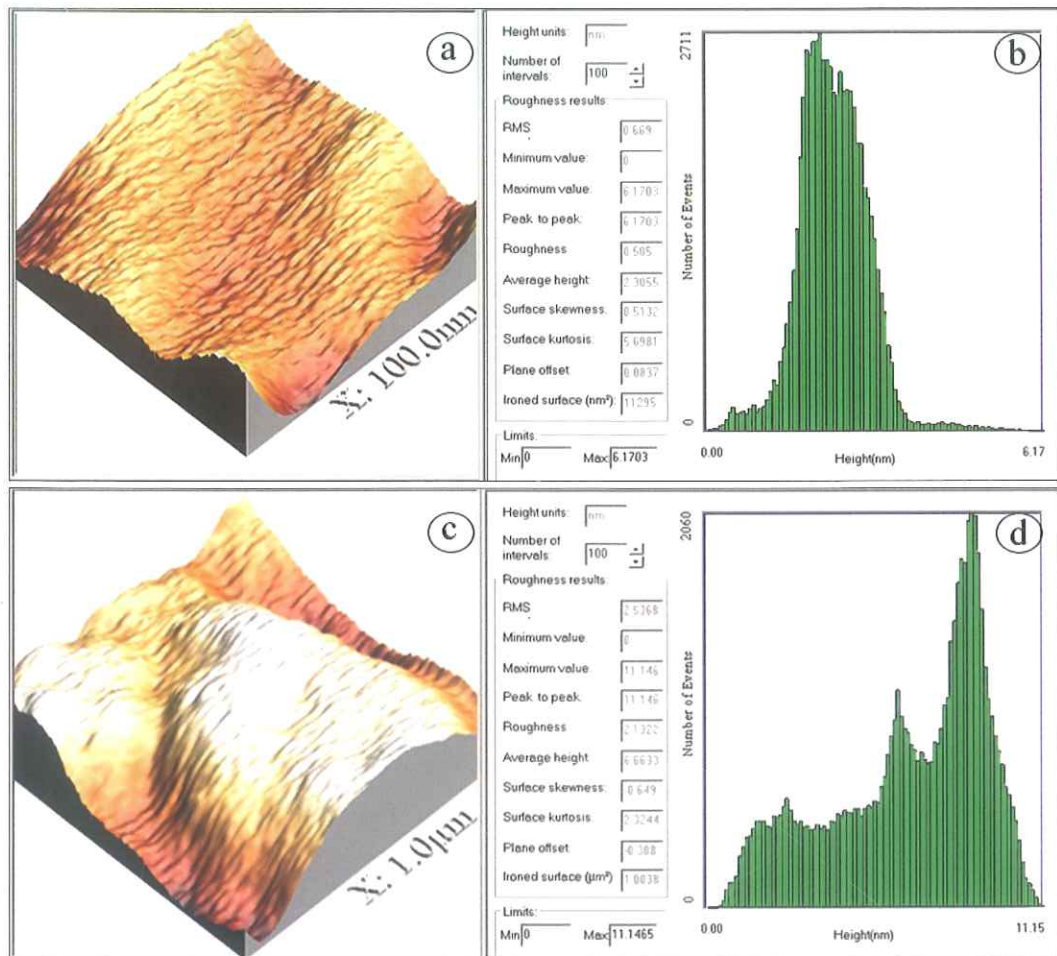
Figure 4. 12   3D Micro Topographies, Corresponding Histograms and Roughness Analyses of Aero 3000C-Treated Albite.
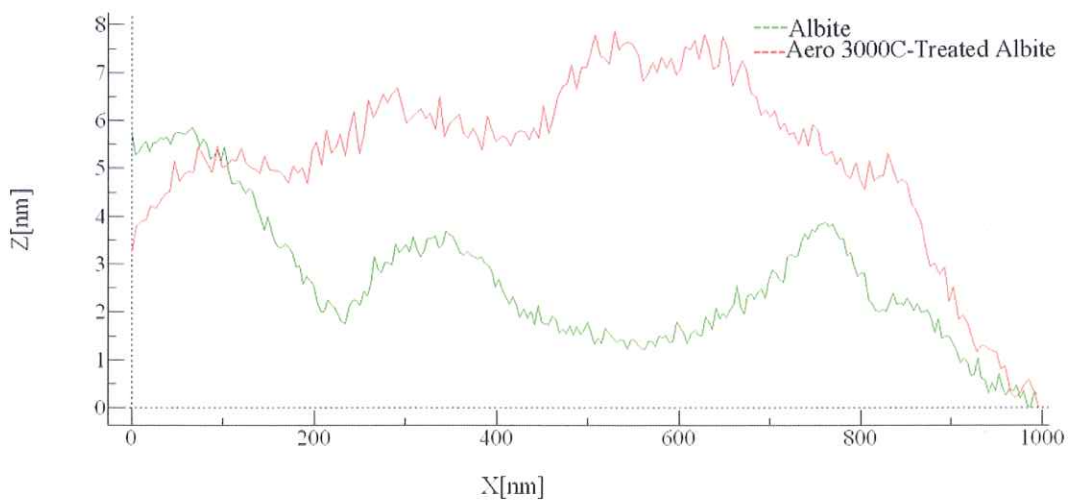
Figure 4. 13   Height Profiles of Albite and Aero 3000C-Treated Albite in 1μm Size.
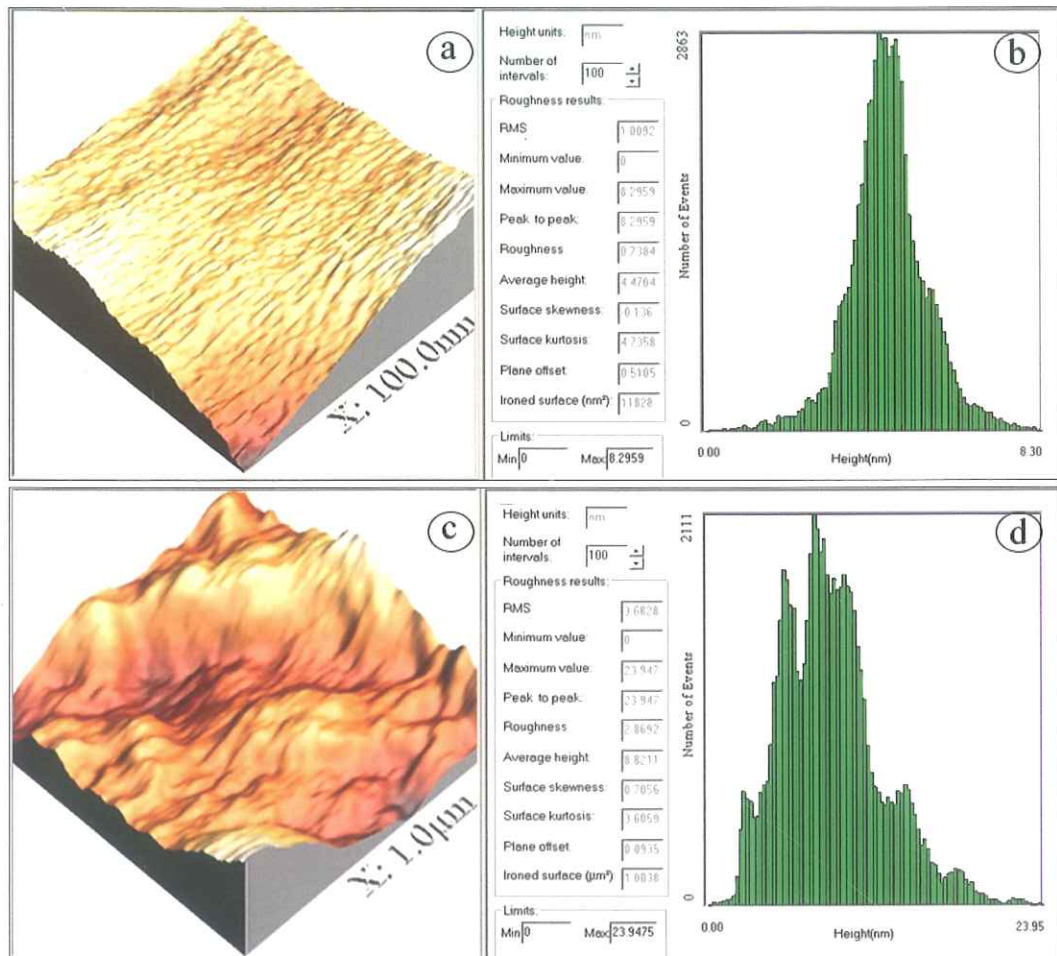
Figure 4. 14   3D Micro Topographies, Corresponding Histograms and Roughness Analyses of Aero 825-Treated Albite.
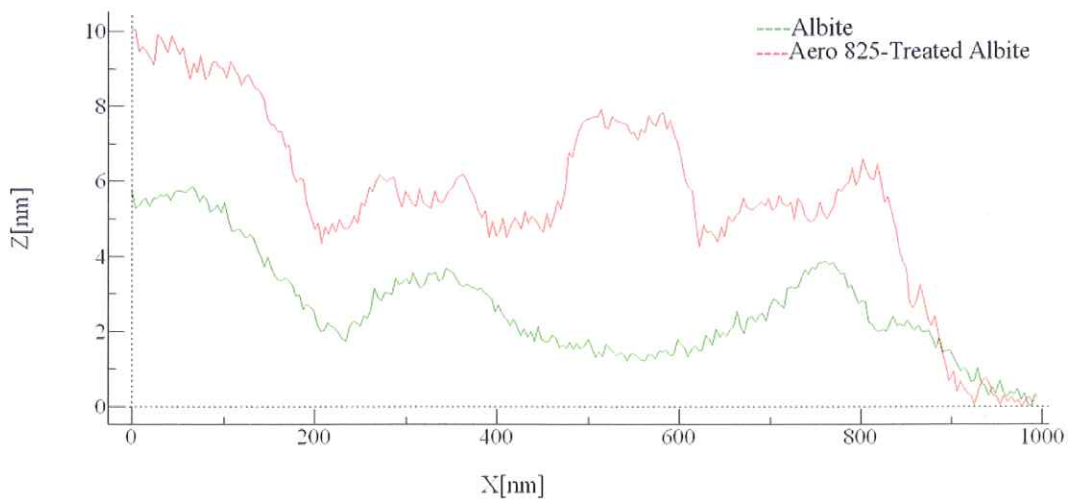
Figure 4. 15   Height Profiles of Albite and Aero 825-Treated Albite in 1µm Size.

74

4.1.4 FTIR Spectroscopy Studies on Albite

FTIR analyses were conducted in order to examine the presence of interaction of three different collectors with the mineral surfaces. For the analyses, the mineral samples were conditioned in optimum flotation conditions which were 3.5×10^{-4} M Aero 704 about pH 9.5, 5.0×10^{-5} M Aero 3000C about pH 3.0 and 2.0×10^{-4} M Aero 825 about pH 5.0.

In the study, albite, collector-treated albite and acetone-washed albite samples were analyzed by FTIR. The characteristic bands of the spectra were compared with each other to determine the existence of additional bands due to interaction of Aero 704, Aero 3000C and Aero 825 on the albite surface. The collector-treated albite samples were prepared in the optimum flotation conditions.

The collector-treated albite samples were washed with distilled water several times before FTIR analysis. In order to investigate the strength of interaction, the collector-treated albite sample was washed with acetone several times. The FTIR spectra of collector, albite, collector-treated albite and acetone-washed albite are shown in Figure 4.16, Figure 4.21 and Figure 4.26 for Aero 704, Aero 3000C and Aero 825 respectively.

In order to obtain more detailed FTIR spectra, the full scale FTIR spectra (4000-400 cm^{-1}) of collector, non-treated, collector-treated and acetone-washed albite samples were analyzed in four major zones depending on the collector's IR peaks. Figures 4.17-4.20 show the FTIR ranges of albite sample in the presence of Aero 704 as 3500-2750 cm^{-1}, 2750-1750 cm^{-1}, 1750-1250 cm^{-1} and 1250-400 cm^{-1} major wavelength's zones respectively.

The spectra obtained for Aero 704-treated albite were given in Figures 4.16- 4.20. The FTIR spectrum of Aero 704 (Figure 4.17) shows that it had bands at 2961 cm^{-1}, 2926 cm^{-1} and 2854 cm^{-1} assigned as CH_2 stretching vibrations. The Aero 704-treated albite has additional weak bands at 2961 cm^{-1}, 2926 cm^{-1} and 2854 cm^{-1} corresponding to Aero 704, since albite itself has not bands at those wavenumbers (Figure 4.17). However, upon washing with acetone, the bands at 2961 cm^{-1}, 2926 cm^{-1} and 2854 cm^{-1} disappeared.
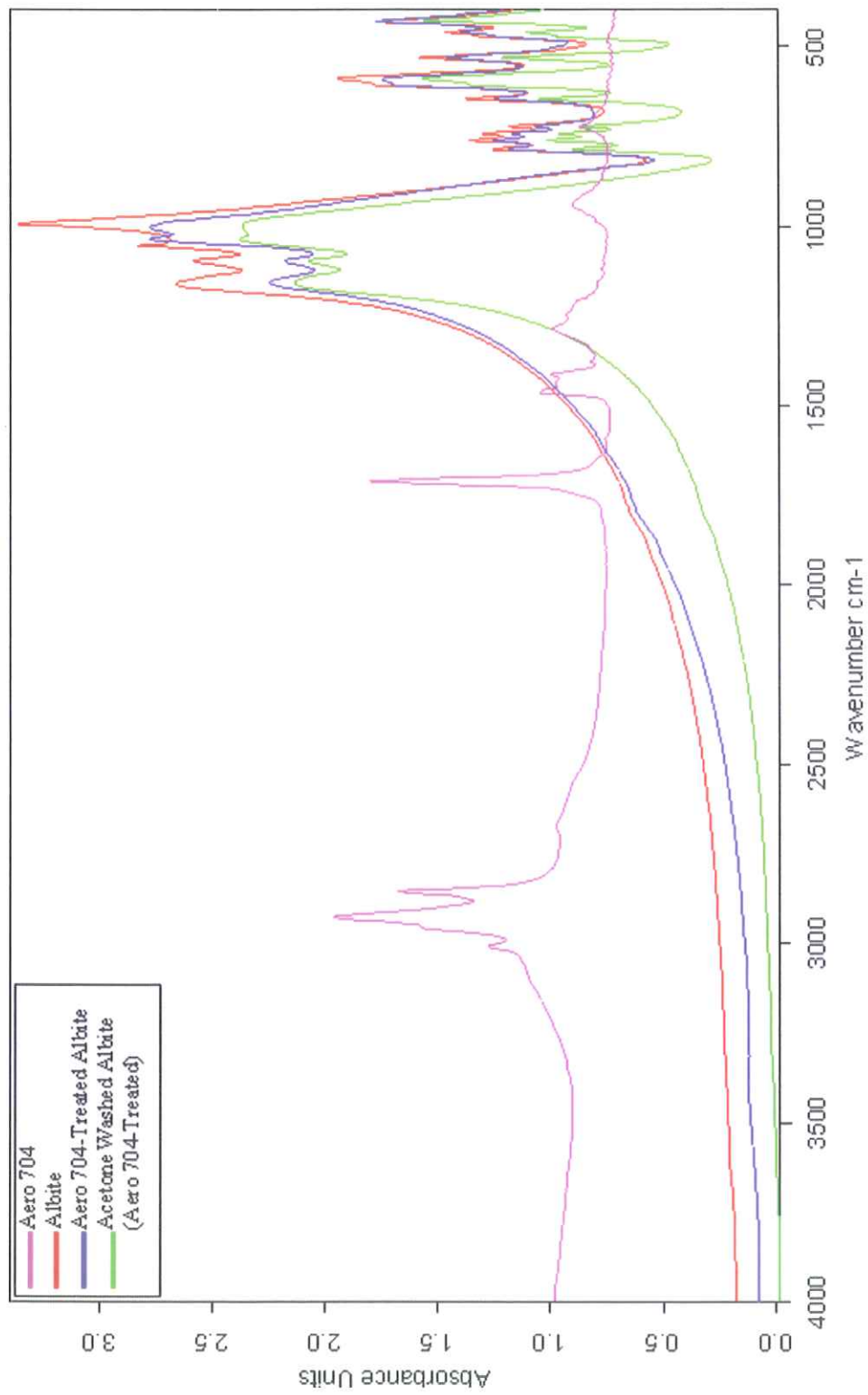
Figure 4. 16   FTIR Spectrum of Albite in the Presence of Aero 704 in 4000–400 cm^{-1} Wavelength Range.

77
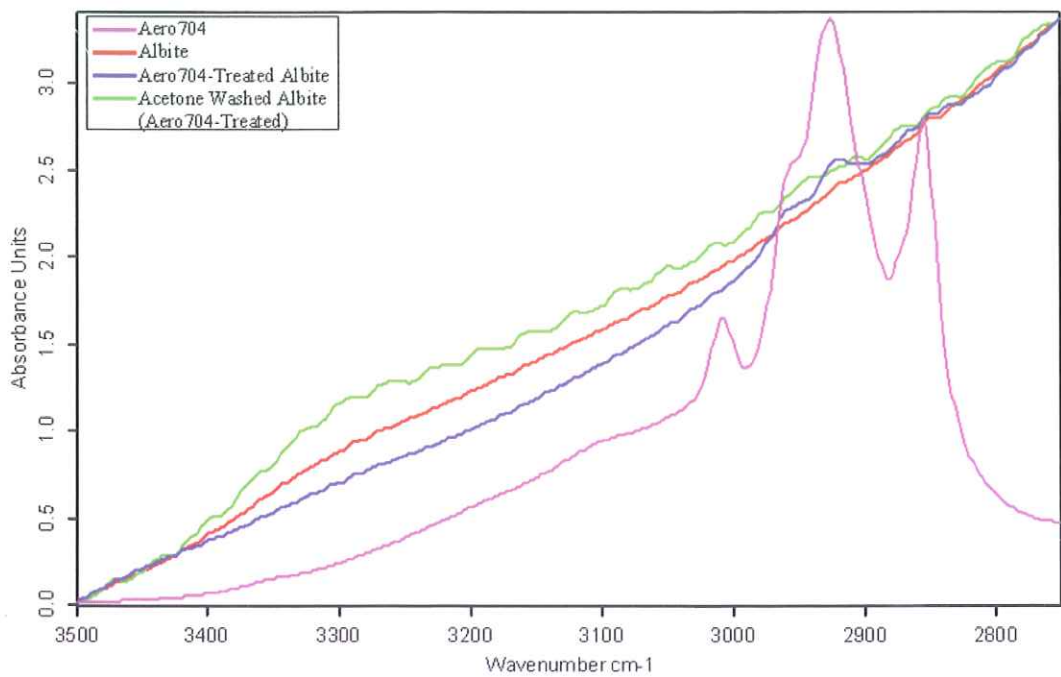
Figure 4. 17   FTIR Spectrum of Albite Sample in the Presence of Aero 704 in 3500–2750 cm^{-1} Wavelength Range.
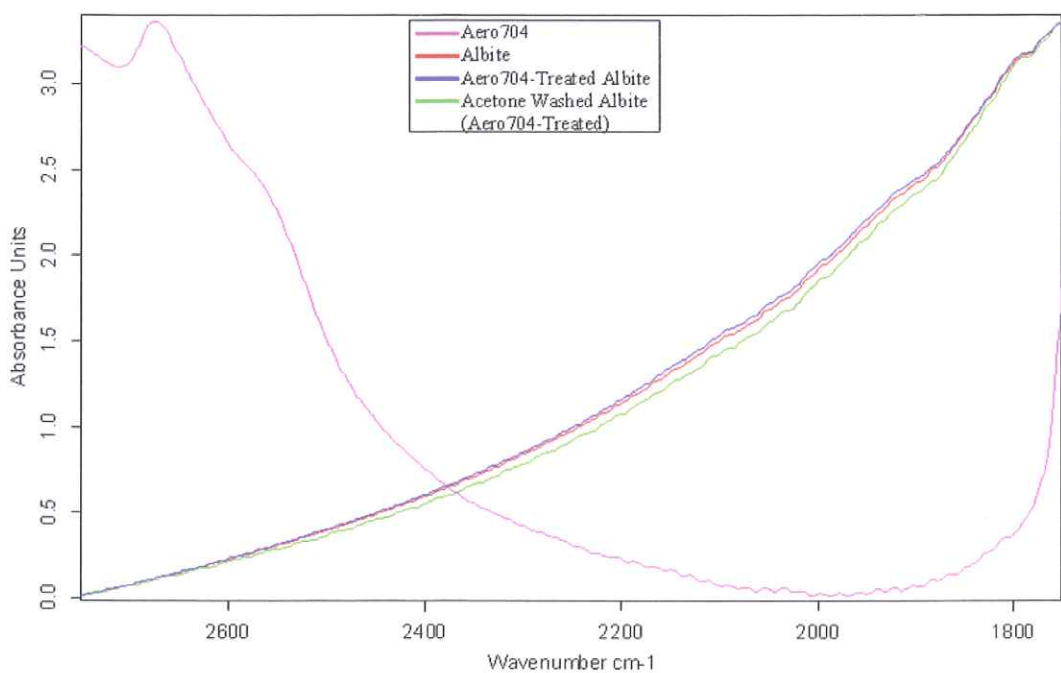
Figure 4. 18   FTIR Spectrum of Albite in the Presence of Aero 704 in 2750–1750 cm^{-1} Wavelength Range.
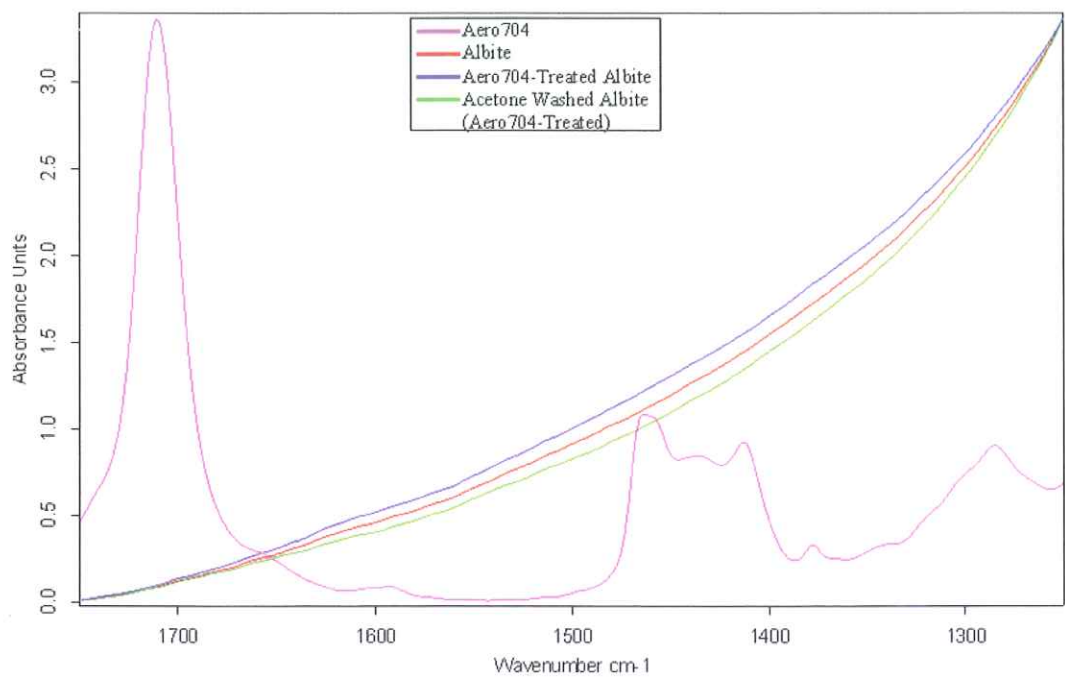
Figure 4. 19   FTIR Spectrum of Albite in the Presence of Aero 704 in 1750–1250 cm^{-1} Wavelength Range.
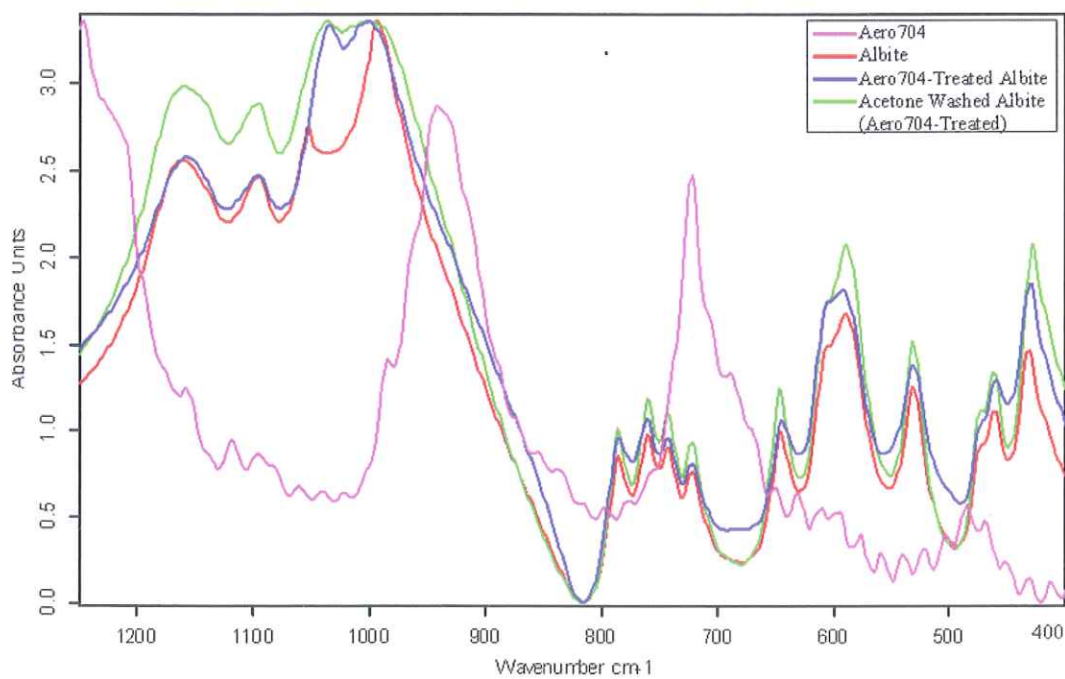
Figure 4. 20   FTIR Spectrum of Albite in the Presence of Aero 704 in 1250–400 cm^{-1} Wavelength Range.

79

The spectra obtained with Aero 3000C, albite, Aero 3000C-treated albite and acetone-washed albite were given in Figures 4.21-4.25. The major zones for the albite in the presence of Aero 3000C were shown as 3250-2750 cm^{-1}, 2750-1750 cm^{-1}, 1750-1250 cm^{-1} and 1250-400 cm^{-1} wavelengths in Figures 4.22-4.25 respectively.

In Figure 4.22; Aero 3000C-treated albite showed additional bands at 2957 cm^{-1}, 2922 cm^{-1} and 2853 cm^{-1} with low intensities assigned as C-H stretching vibrations of Aero 3000C (Figure 4.22). However, upon washing with acetone, the bands at 2953 cm^{-1} and 2916 cm^{-1} disappeared.
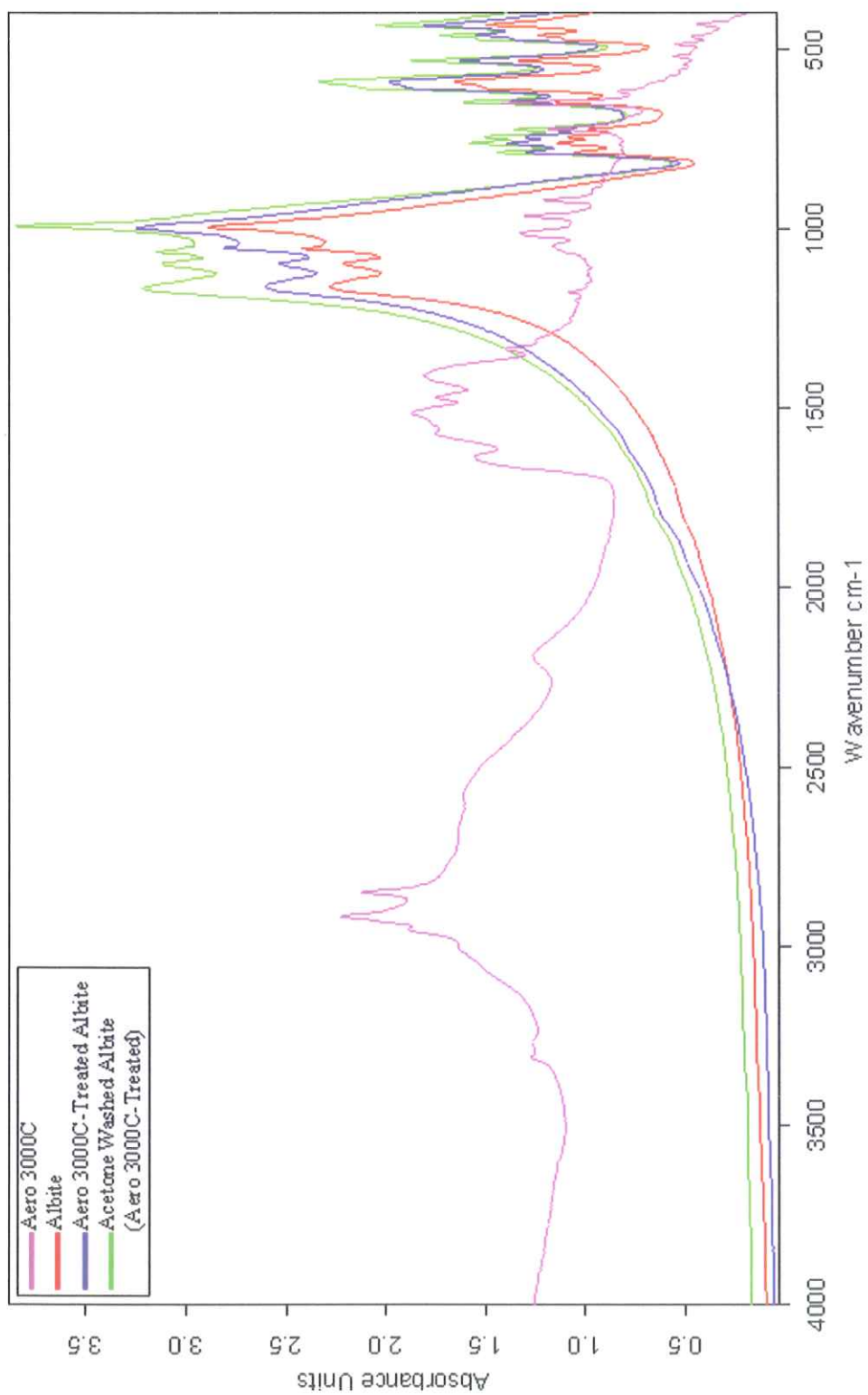
Figure 4. 21   FTIR Spectrum of Albite in the Presence of Aero 3000C in 4000–400 cm^{-1} Wavelength Range.

81
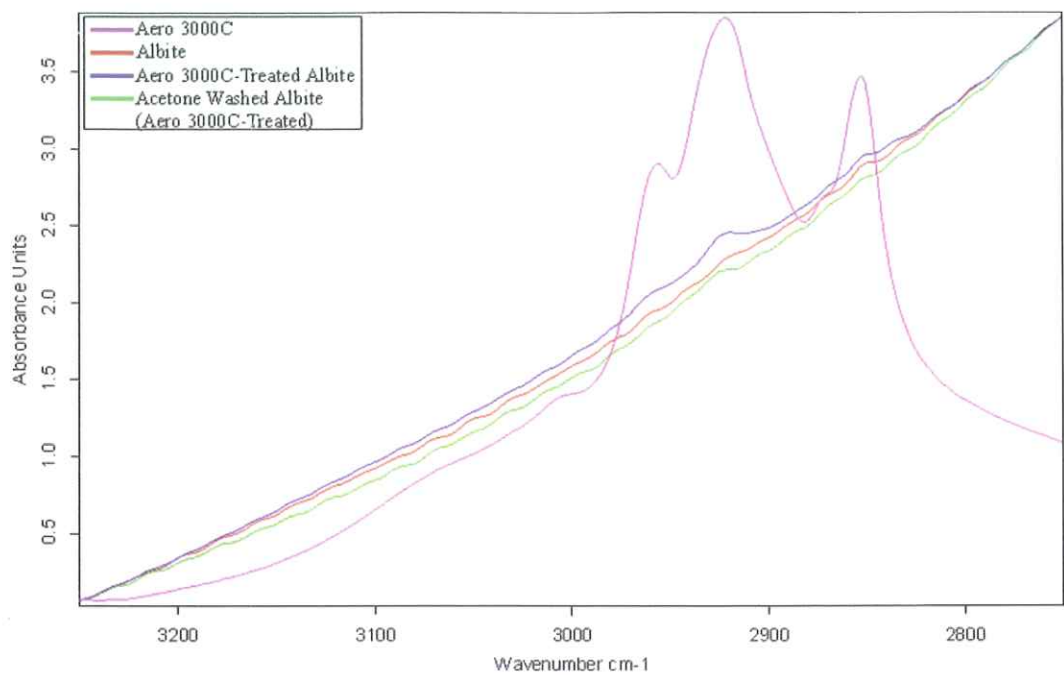
Figure 4. 22   FTIR Spectrum of Albite in the Presence of Aero 3000C in 3250–2750 cm^{-1} Wavelength Range.
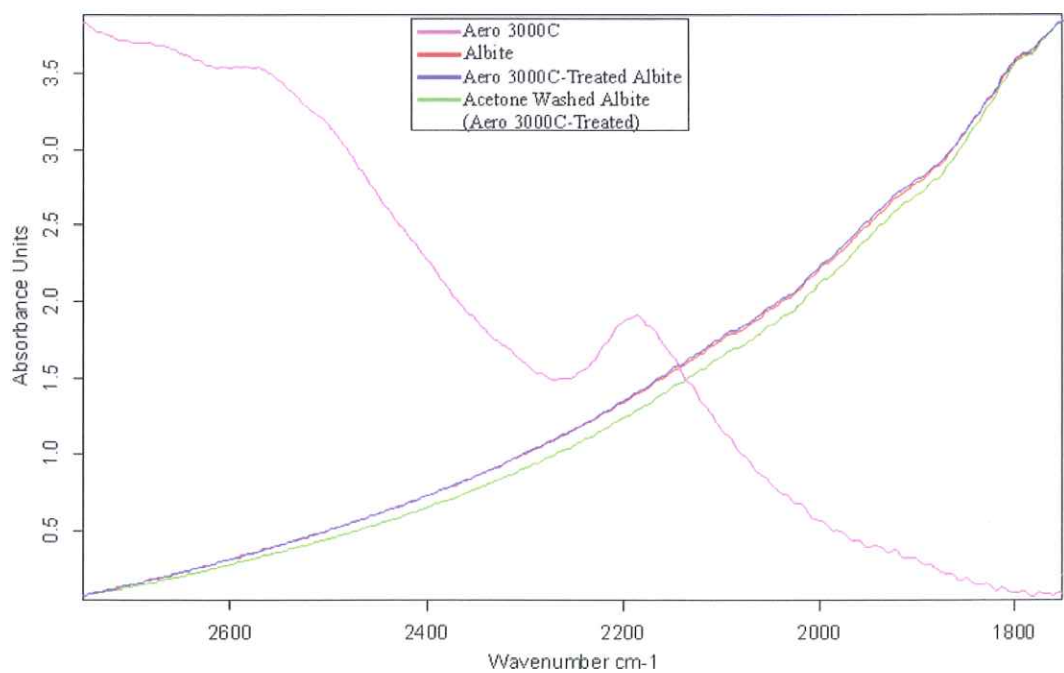
Figure 4. 23   FTIR Spectrum of Albite in the Presence of Aero 3000C in 2750–1750 cm^{-1} Wavelength Range.
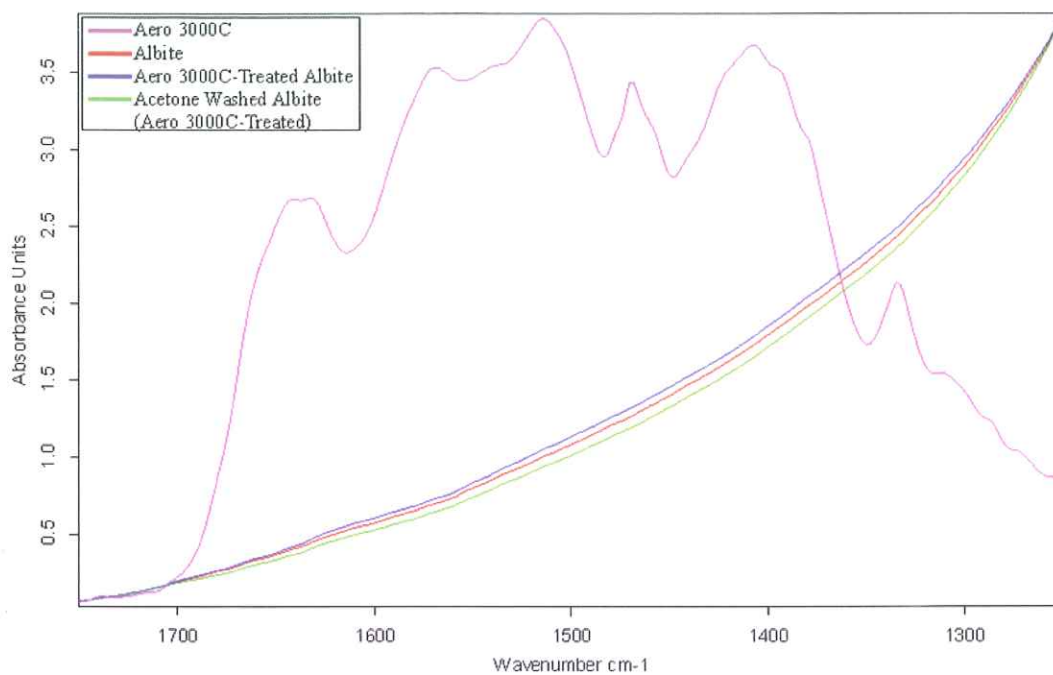
Figure 4. 24   FTIR Spectrum of Albite in the Presence of Aero 3000C in 1750–1250 cm^{-1} Wavelength Range.
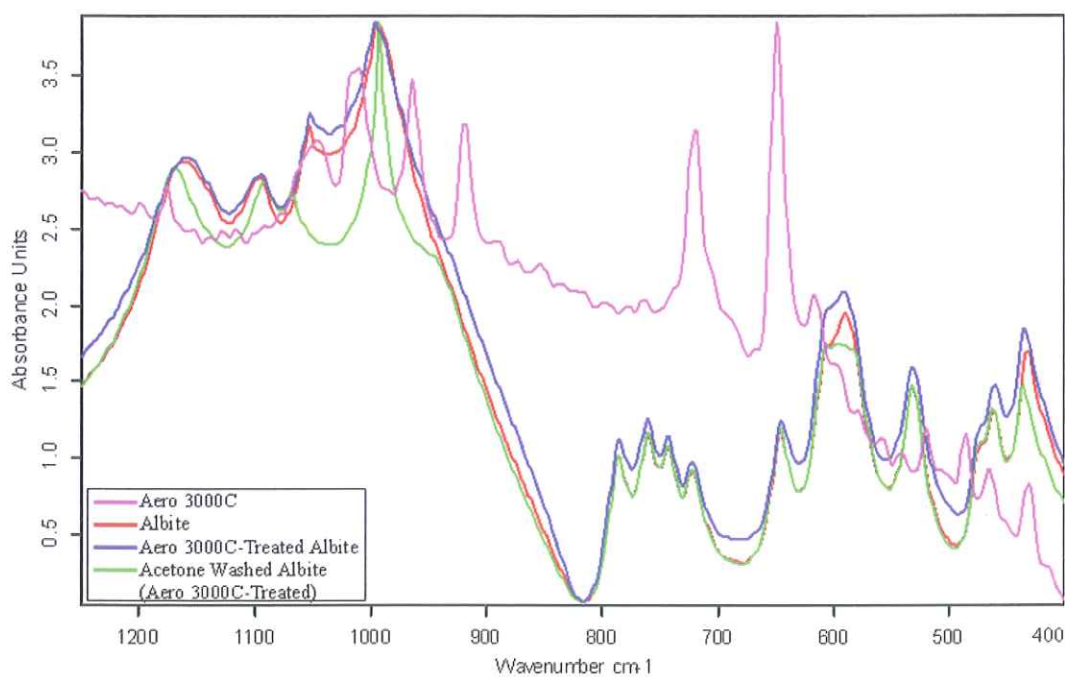
Figure 4. 25   FTIR Spectrum of Albite in the Presence of Aero 3000C in 1250–400 cm^{-1} Wavelength Range.

The spectra obtained for Aero 825, albite, Aero 825-treated albite and acetone-washed albite are given in Figures 4.26-4.30. In order to provide more detailed spectra, the major zones for the albite in the presence of Aero 825 were displayed in Figures 4.27-4.30 as 3750-2750 cm^{-1}, 2750-1500 cm^{-1}, 1500-1000 cm^{-1} and 1000-400 cm^{-1} wavelengths depending on the Aero 825's FTIR peaks.

In Figure 4.27, Aero 825-treated albite had additional bands at 2924 cm^{-1} and 2854 cm^{-1} with very low intensities assigned as CH_2 stretching vibrations of Aero 825. However, upon washing with acetone, the bands at 2924 cm^{-1} and 2854 cm^{-1} disappeared.
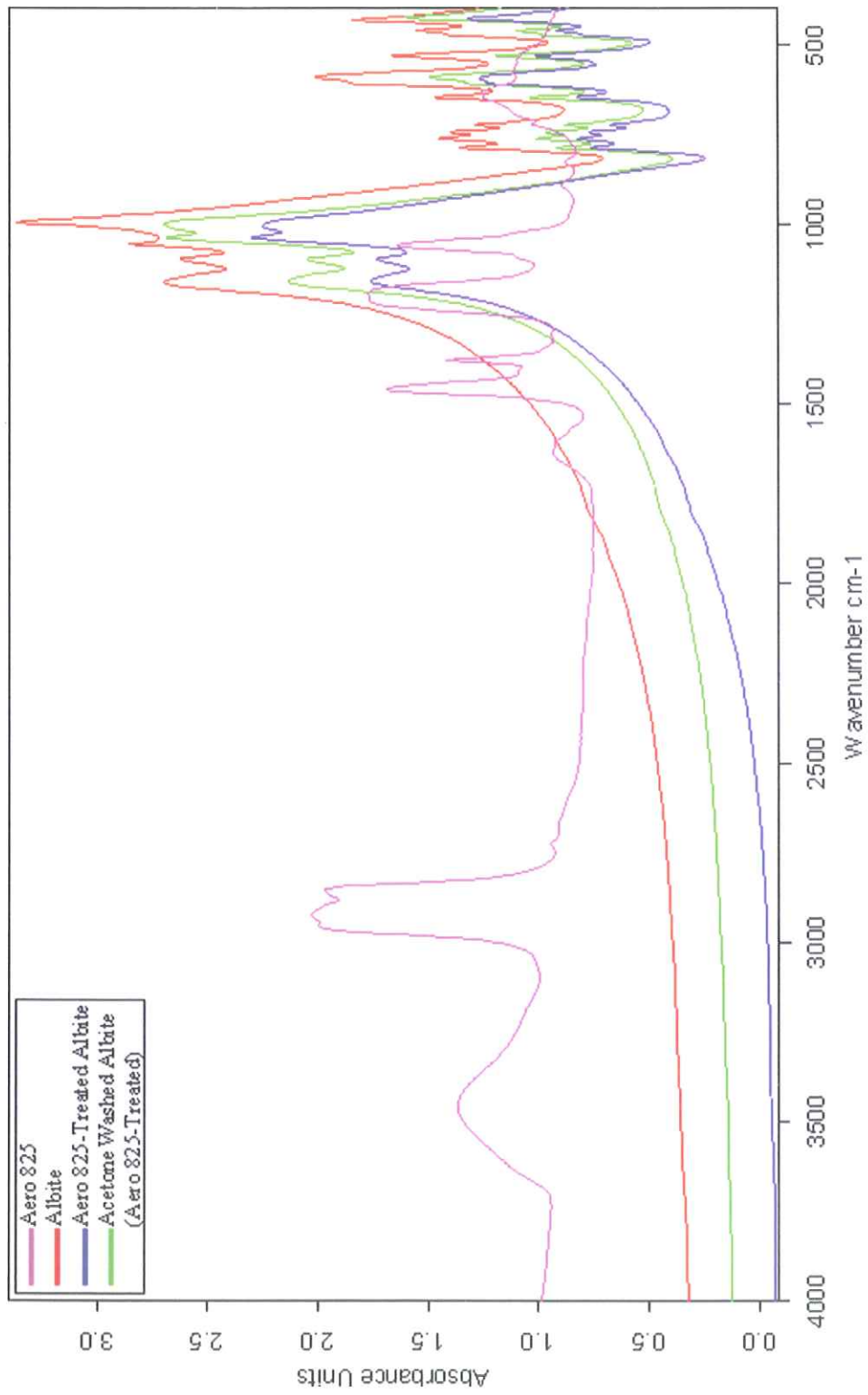
Figure 4. 26   FTIR Spectrum of Albite in the Presence of Aero 825 in 4000–400 cm⁻¹ Wavelength Range.
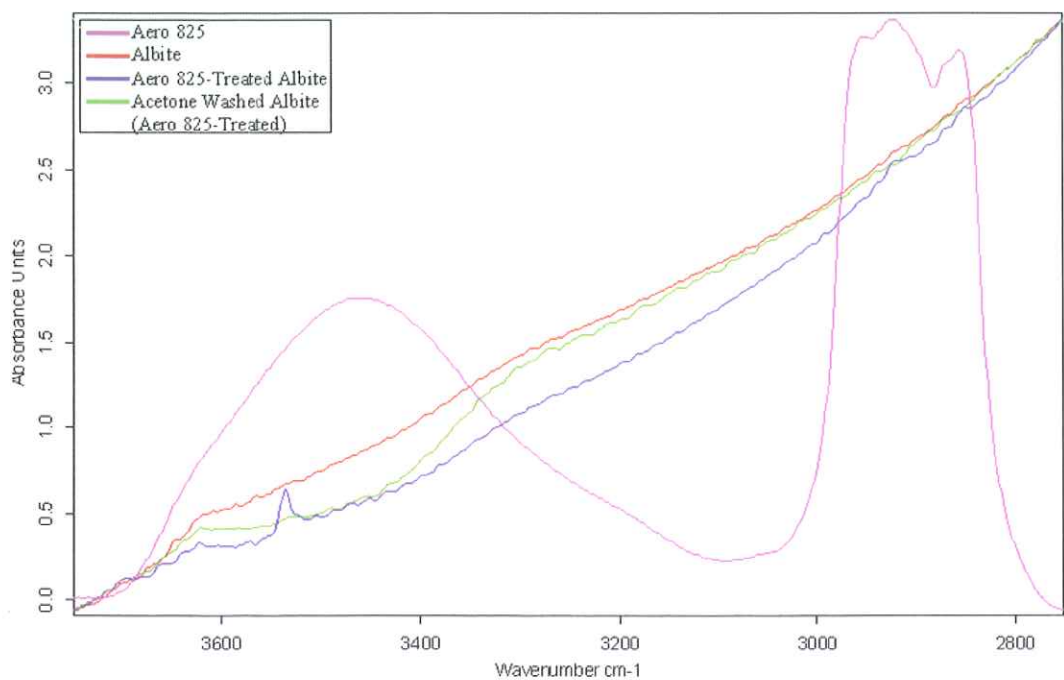
Figure 4. 27   FTIR Spectrum of Albite in the Presence of Aero 825 in 3750–2750 cm^{-1} Wavelength Range.
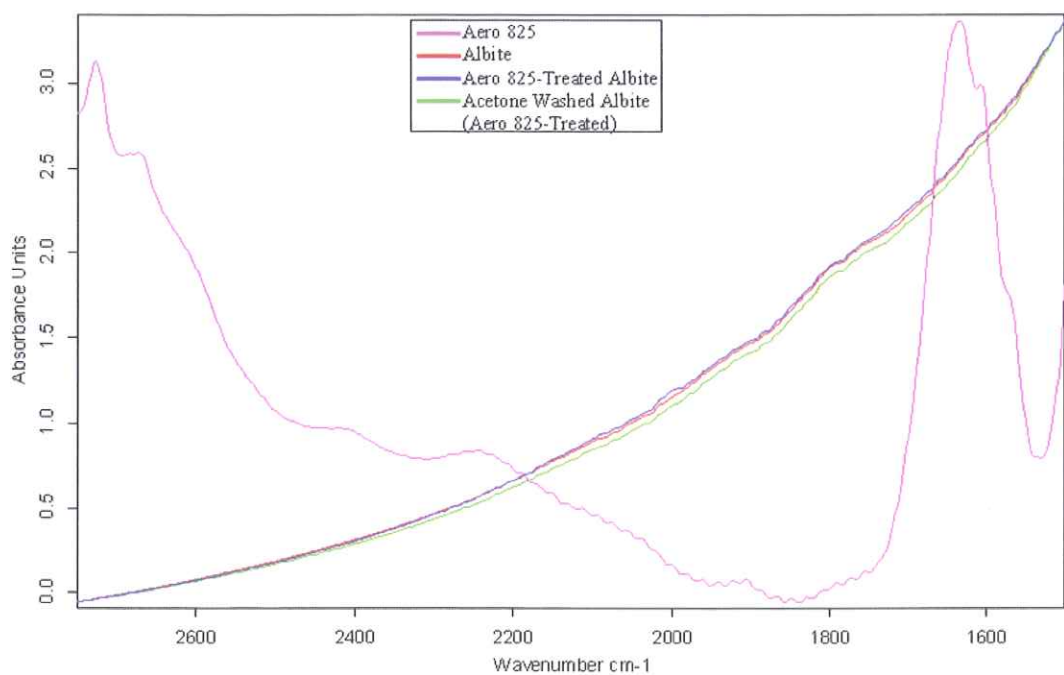
Figure 4. 28   FTIR Spectrum of Albite in the Presence of Aero 825 in 2750–1500 cm^{-1} Wavelength Range.
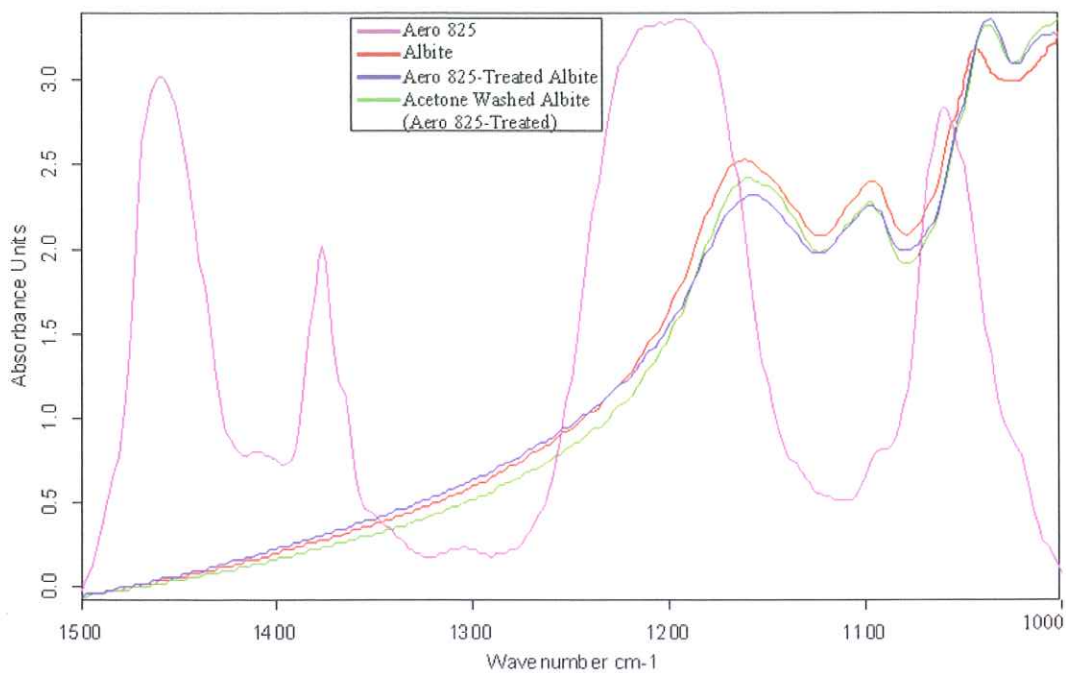
Figure 4. 29   FTIR Spectrum of Albite in the Presence of Aero 825 in 1500–1000 cm^{-1} Wavelength Range.
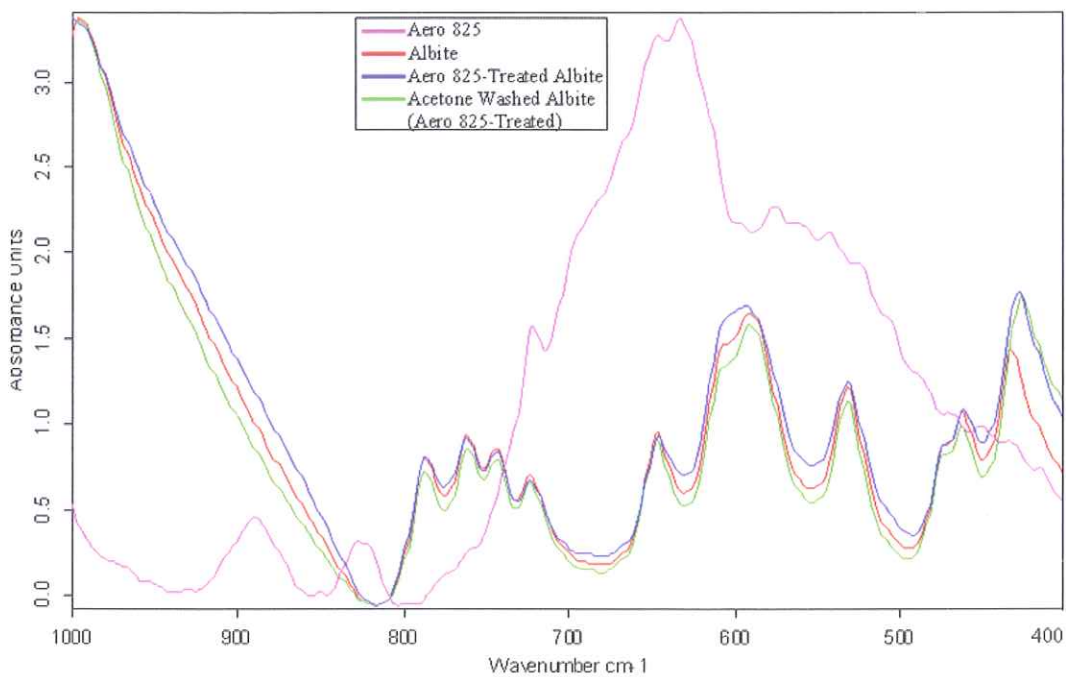
Figure 4. 30   FTIR Spectrum of Albite in the Presence of Aero 825 in 1000–400 cm^{-1} Wavelength Range.

4.2 Biotite Sample

4.2.1 Electrokinetic Potential Measurements on Biotite

When the similar procedure was applied in order to obtain zeta potential values of biotite, the i.e.p. was found to be below pH 1.5 in distilled water and in 1.0×10^{-3} M KCl. The results are given in Figure 4.31. Above the i.e.p. the zeta potential values became more negative towards the more basic region. The results are consisted with the results obtained by Riberio R.C. et al., 2009 [64].
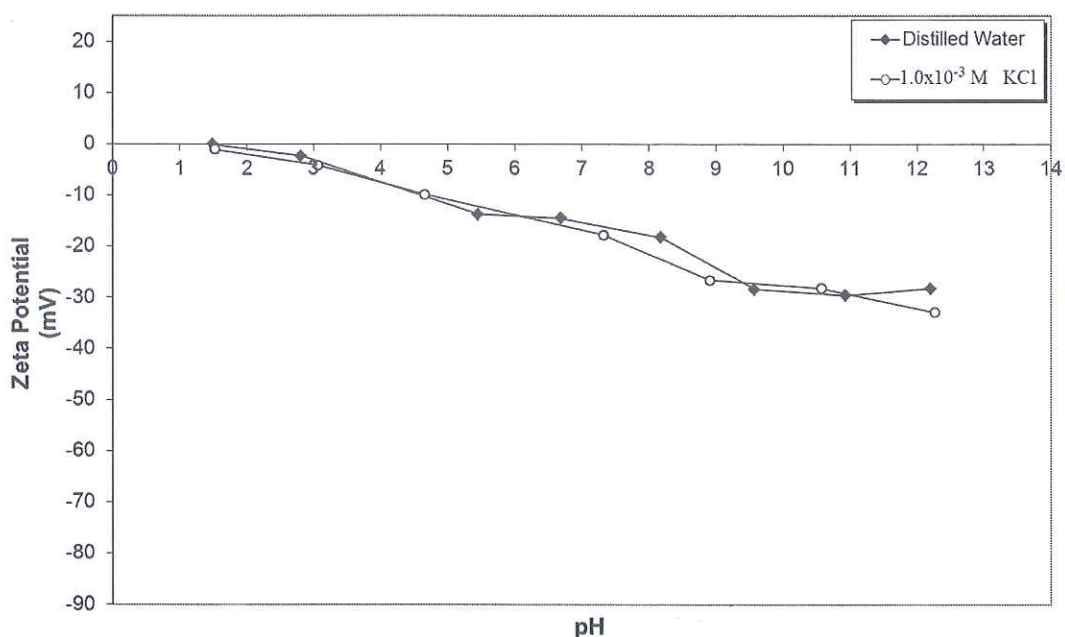
Figure 4. 31   Zeta Potential of Biotite as a Function of pH.

Figure 4.32 shows the effect of 1.0×10^{-4} M, 5.0×10^{-4} M and 1.0×10^{-3} M of Aero 704 on the electrokinetic potential of biotite. The zeta potential values of biotite decreased with increasing Aero 704 concentration and pH.

The zeta potential values of biotite in the presence of 5.0×10^{-5} M, 1.0×10^{-4} M and 5.0×10^{-4} M of Aero 3000C as a function of pH were shown in Figure 4.33. The zeta

potential values increased proportionally to Aero 3000C concentration and pH. The i.e.p. was shifted from below pH 1.5 to highly alkali conditions, about pH 10.8 and the surface of the sample was positively charged up to given pH.

Figure 4.34 displays the zeta potential values of biotite in the presence of 1.0×10^{-4} M, 5.0×10^{-4} M and 1.0×10^{-3} M of Aero 825 as a function of pH. The zeta potential values of biotite decreased with increasing Aero 825 concentration.
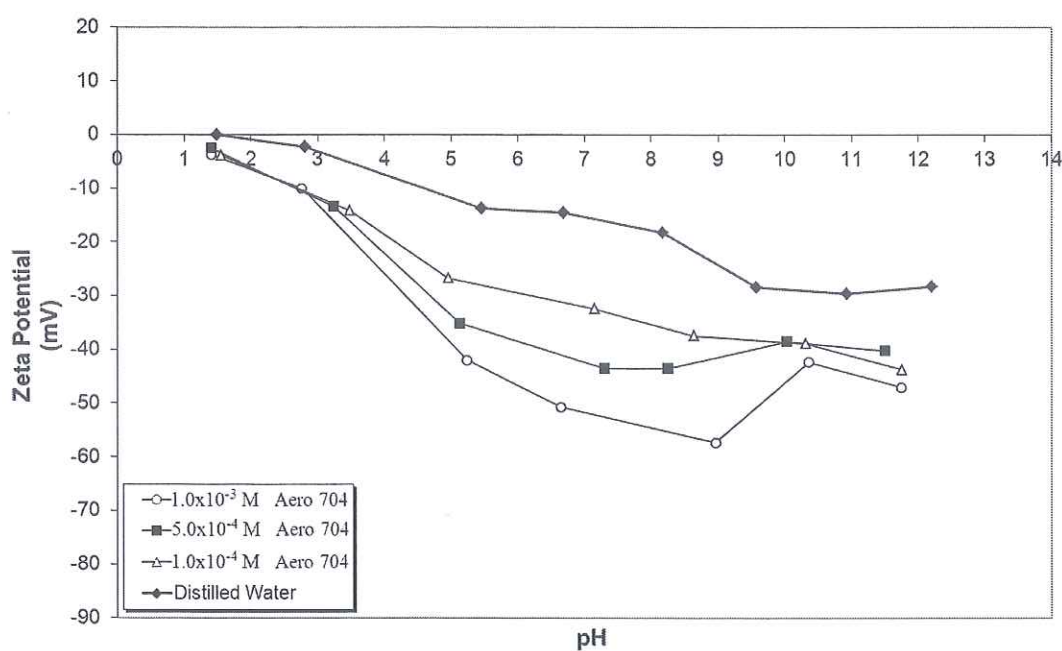
Figure 4. 32   Zeta Potential of Biotite as a Function of pH and Aero 704 Concentration.
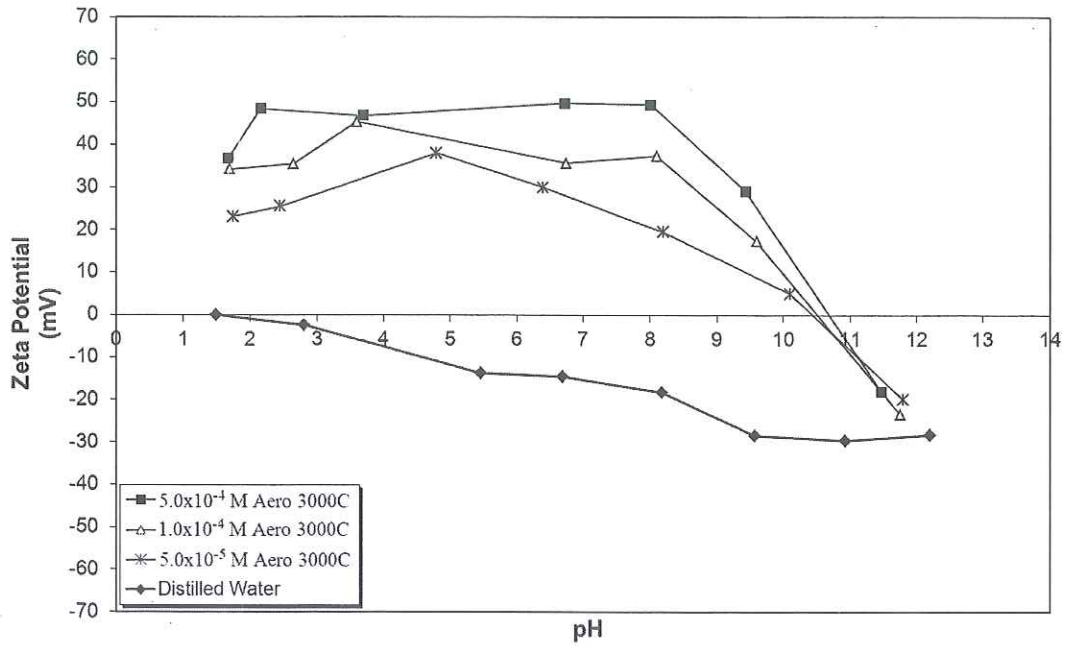
Figure 4. 33   Zeta Potential of Biotite as a Function of pH and Aero 3000C Concentration.
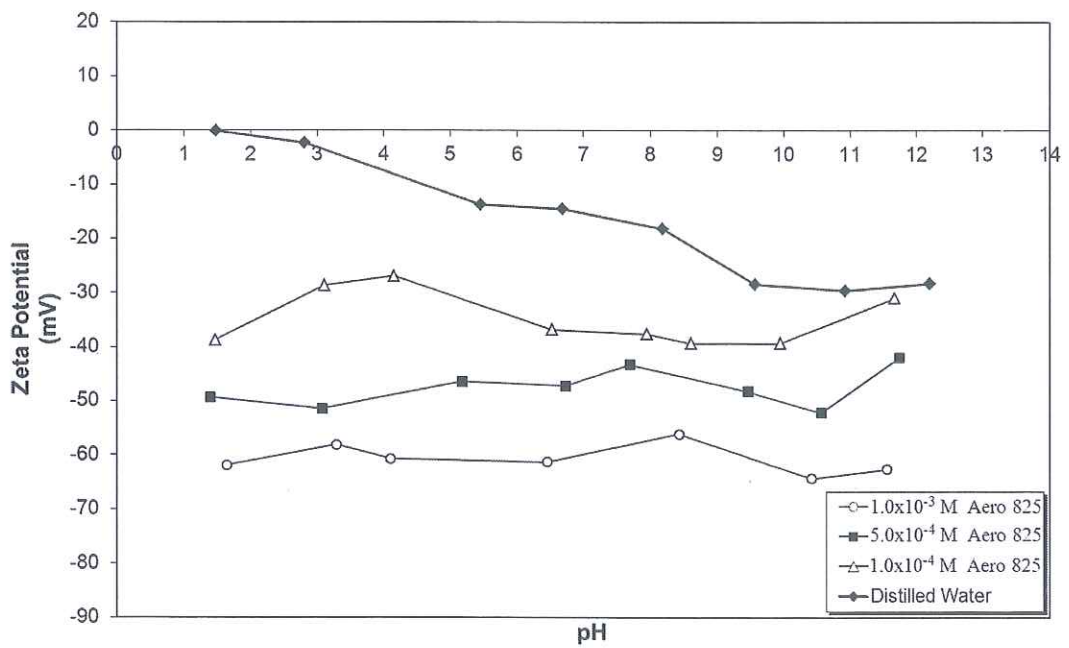
Figure 4. 34   Zeta Potential of Biotite as a Function of pH and Aero 825 Concentration.

Additional electrokinetic potential measurements were carried out on acetone-washed biotite samples which were conditioned with 3.5×10^{-4} M of Aero 704 about pH 9.5, 5.0×10^{-5} M of Aero 3000C about pH 3.0, 2.0×10^{-4} M of Aero 825 about pH 5.0. The samples were first conditioned with each collector and then washed with acetone several times prior to electrokinetic potential measurements.

The effects of acetone washing on the electrokinetic potential values of collector-treated biotite samples were shown in Figure 4.35 as a function of pH. The zeta potential values were found to be very similar to each other for all pH ranges.
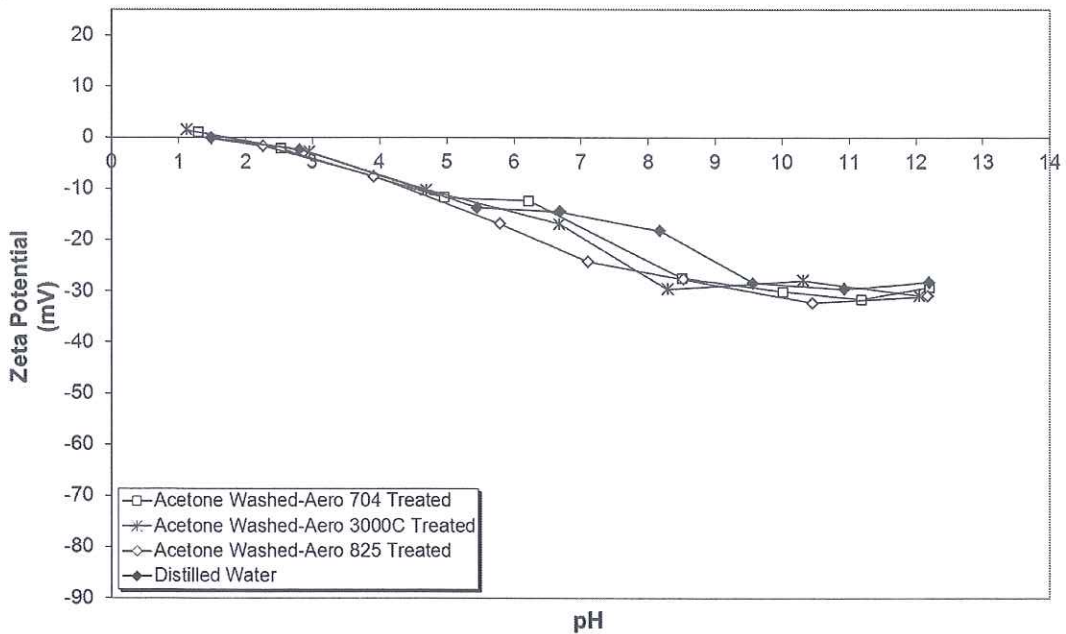
Figure 4. 35   Zeta Potential of Aero 704, Aero 3000C and Aero 825 Treated Biotite Samples After Acetone Washing.

4.2.2   Flotation Studies on Biotite

The flotation recoveries of biotite as a function of pH and Aero 704 concentration were shown in Figure 4.36. As the flotation recovery of biotite was null below pH 7.0, the micro-flotation experiments were performed from this pH on with all Aero 704 concentrations. It is seen that the flotation recovery of the biotite increased

91

proportionally to Aero 704 concentration. The maximum flotation recoveries were obtained as 46.0% with 2.0×10^{-4} M, 67.5% with 2.75×10^{-4} M, 92.5% with 3.5×10^{-4} M and 93.0% with 5.0×10^{-4} M of Aero 704 in the pH range of 9.0-10.5.

The flotation recoveries of the biotite were maximum between the pH 3.5 and 10.5 with the values of 14.0%, 69.0%, 95.0% and 96.5% in the presence of 2.0×10^{-5} M, 5.0×10^{-5} M, 7.5×10^{-5} M and 1.0×10^{-4} M of Aero 3000C respectively (Figure 4.37). The flotation recoveries decreased sharply above pH 10.5 and below pH 3.5 in all Aero 3000C concentrations except for the lowest concentration, 2.0×10^{-5} M. In the latter case, the flotation recoveries were very similar in all pH with the values below 15.0%.

In the case of Aero 825, the flotation recoveries of biotite were shown in Figure 4.38 as function of pH and concentration. As illustrated in the figure, the flotation recoveries were almost null in all Aero 825 concentrations, 1.5×10^{-4} M, 2.0×10^{-4} M, 5.0×10^{-4} M and 1.0×10^{-3} M and pH.
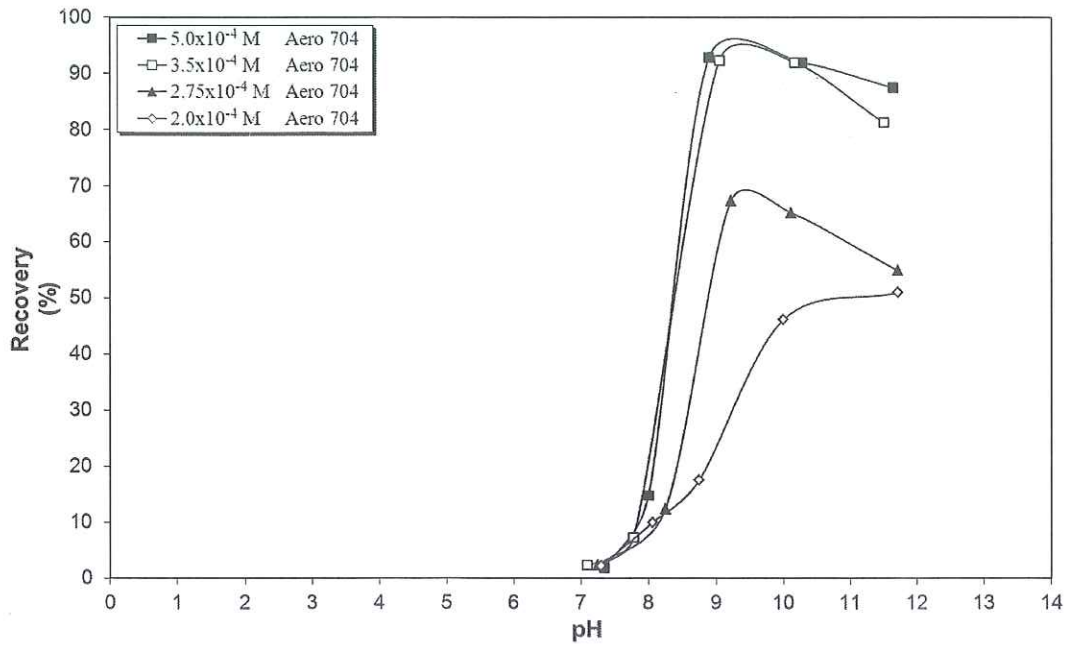
Figure 4. 36   Flotation Recovery of Biotite as a Function of pH and Aero 704
Concentration.
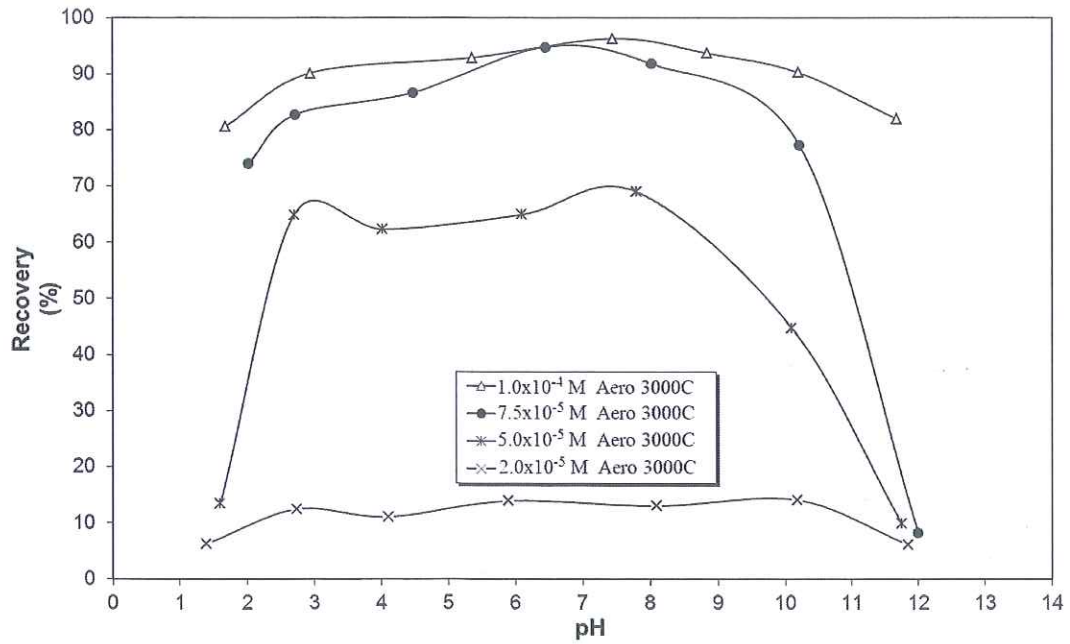
Figure 4. 37   Flotation Recovery of Biotite as a Function of pH and Aero 3000C
Concentration.

93
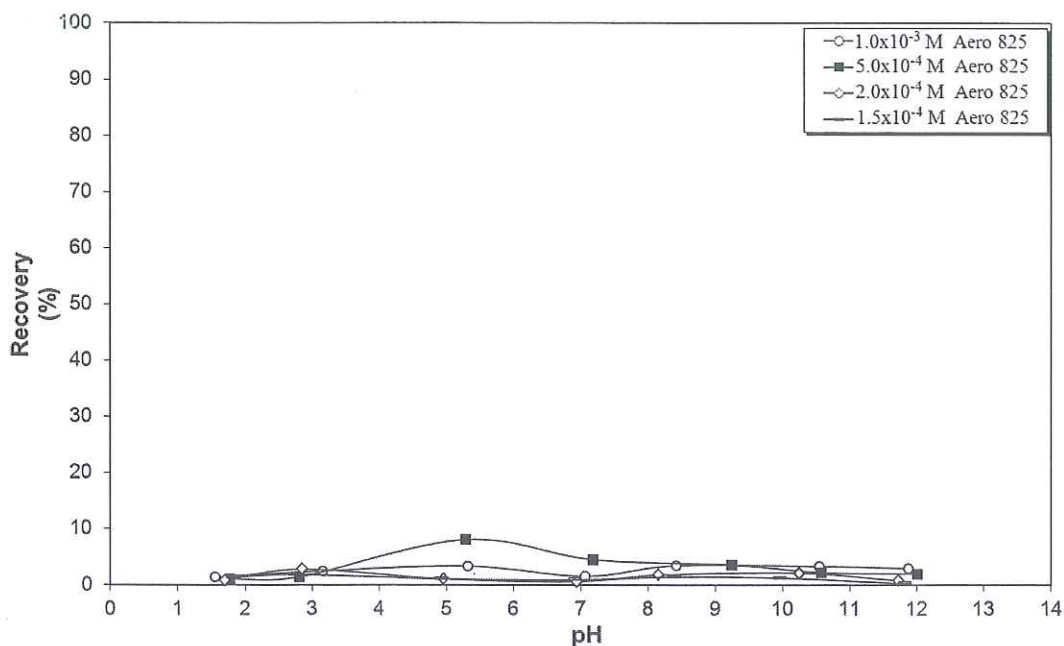
Figure 4. 38   Flotation Recovery of Biotite as a Function of pH and Aero 825 Concentration.

4.2.3   AFM Studies on Biotite

The tapping mode AFM 3D micro topographies of biotite in 100nm (Figure 4.39a) and 1μm (Figure 4.39c) sizes and their corresponding histograms and roughness analyses (Figure 4.39b and Figure 4.39d) were given in Figure 4.39. The resulting histogram provides information about the surface roughness, the maximum peak value and the average height values of biotite for 100nm x 100nm and 1μm x 1μm scanning size ranges. The corresponding histograms revealed the roughness average as 0.1199nm, the maximum peak value as 1.2904nm and the average height value as 1.4745nm for 100nm x 100nm scanning size range and as 0.1406nm, 1.4745nm and 0.7018nm for 1μm x 1μm scanning size range respectively.
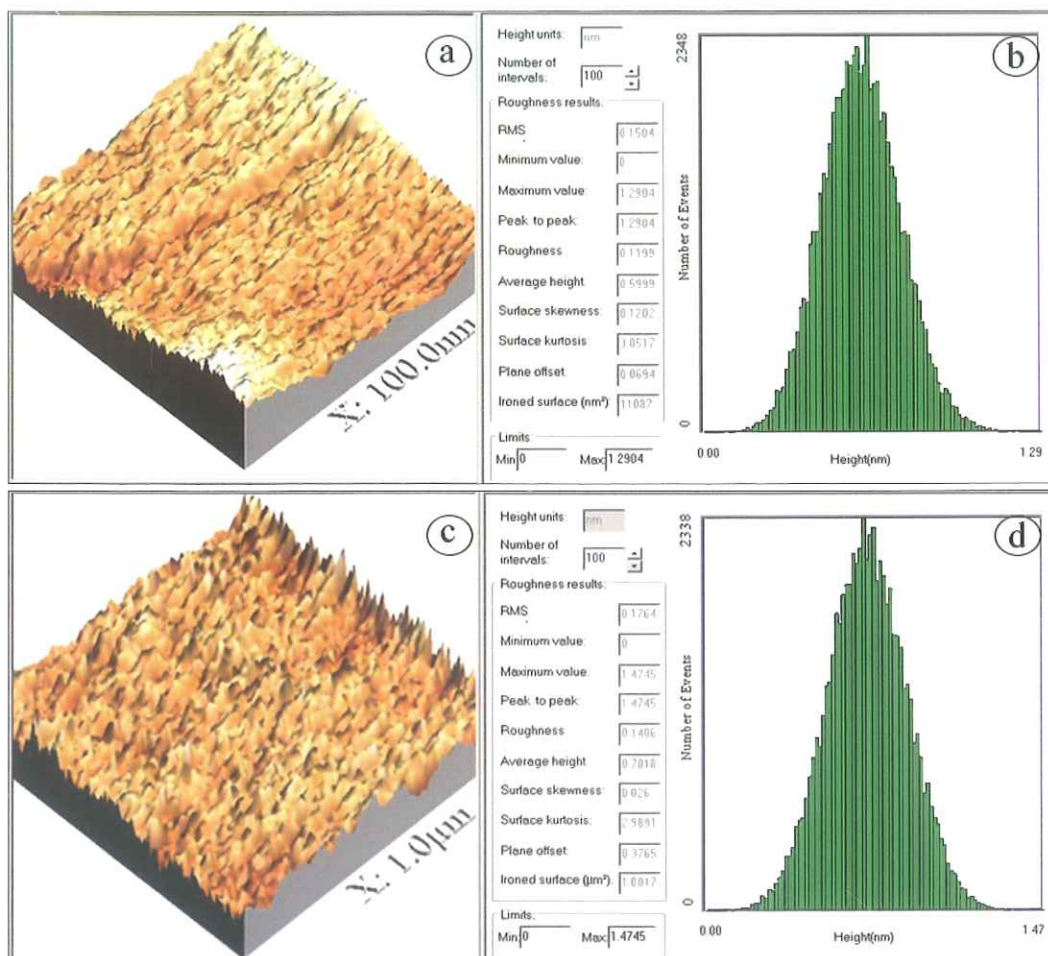
Figure 4. 39   3D Micro Topographies, Corresponding Histograms and Roughness Analyses of Biotite.

The tapping mode AFM 3D micro topographies (Figure 4.40a and 4.40c) and the corresponding histograms (Figure 4.40b and 4.40d) of the Aero 704-treated biotite revealed the roughness average as 0.3114nm, the maximum peak value as 3.5104nm and the average height value as 1.5631nm for 100nm x 100nm scanning size and 0.1446nm, 1.6333nm and 0.8655nm for 1μm x 1μm scanning size range, respectively (Figure 4.40). The tapping mode AFM image analysis of biotite and Aero 704-treated biotite based on their height profiles in 1μm were shown in Figure 4.41 for the scanned area. The biotite, shown in green, displayed almost similar height profiles to that of Aero 704-treated biotite for the scanned area.
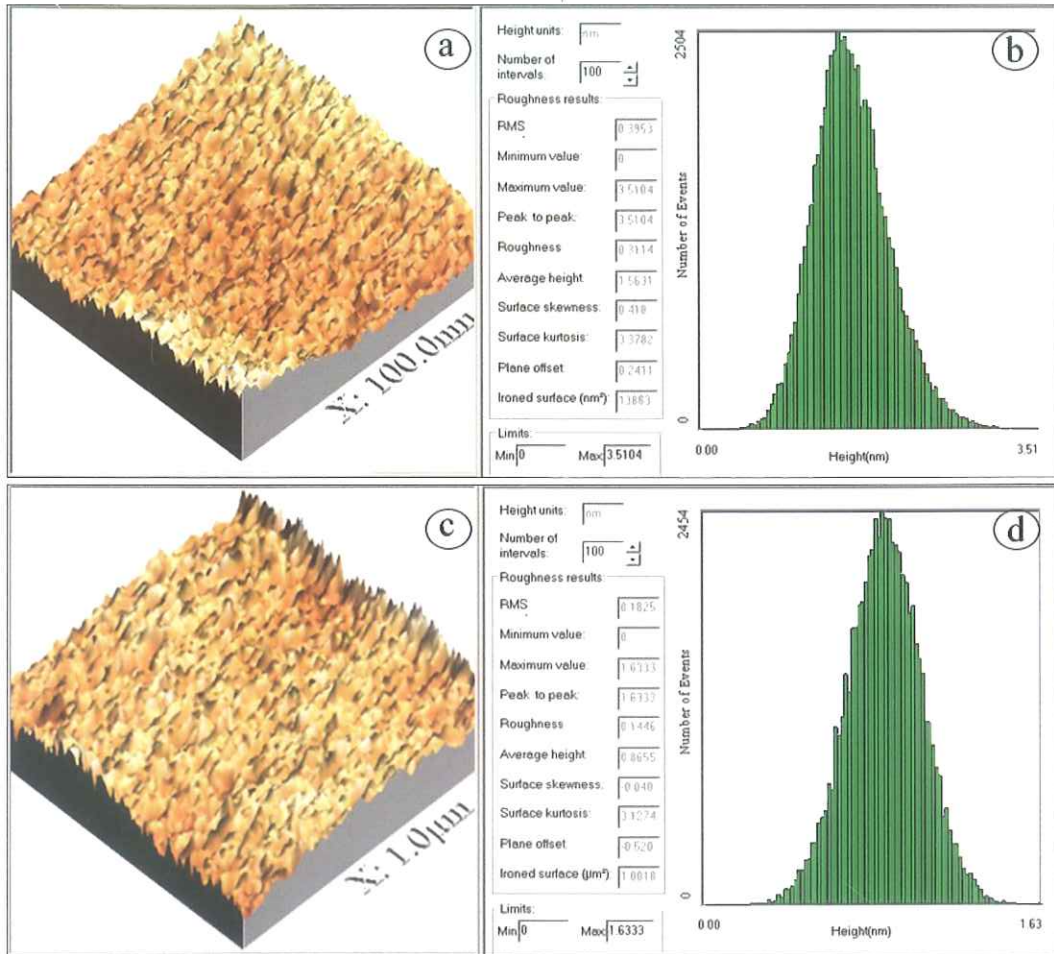
Figure 4. 40   3D Micro Topographies, Corresponding Histograms and Roughness Analyses of Aero 704-Treated Biotite.
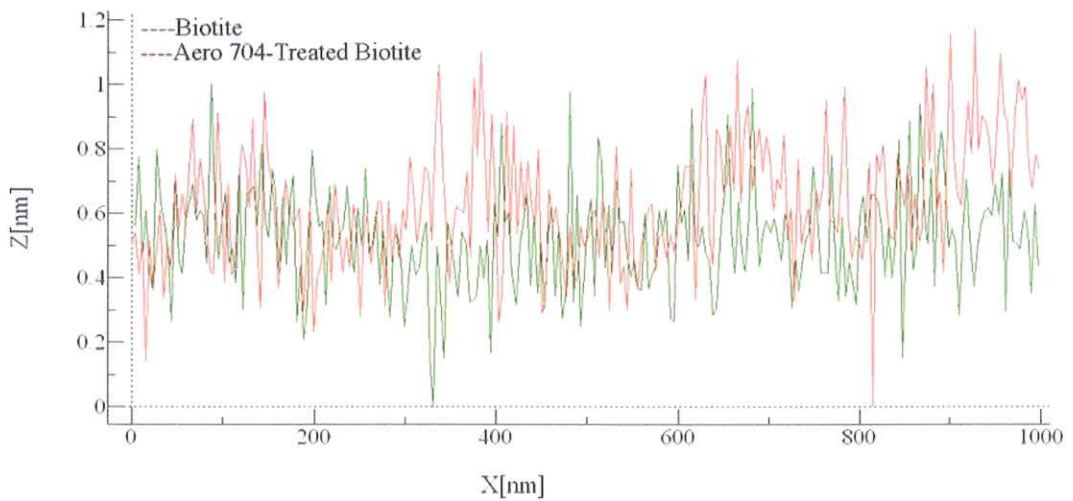
Figure 4. 41   Height Profiles of Biotite and Aero 704-Treated Biotite in 1μm Size.

The tapping mode AFM 3D micro topographies and the corresponding histograms of Aero 3000C-treated and Aero 825-treated biotite in 100nm x 100nm (Figure 4.42a-b for Aero 3000C-treated and Figure 4.44a-b for Aero 825-treated biotite) and 1μm x 1μm (Figure 4.42c-d for Aero 3000C-treated and Figure 4.44c-d for Aero 825-treated biotite) scanning size ranges were given in Figure 4.42 and Figure 4.44 respectively. For Aero 3000C-treated biotite, the histograms revealed that the roughness averages, the maximum peak values and the average height values as 0.1689nm, 1.9164nm and 1.0080nm for 100nm x 100nm scanning size and 0.3377nm, 3.3535nm and 1.5846nm for 1μm x 1μm scanning size ranges, respectively. In the case of Aero 825-treated biotite, the roughness averages, the maximum peak values and the average height values were obtained as 0.3054nm, 2.7129nm and 1.4045nm for 100nm x 100nm scanning size range and 0.4377nm, 6.6962nm, 2.2872nm for 1μm x 1μm scanning size range respectively

The tapping mode AFM image analysis of biotite and Aero 3000C-treated biotite based on their height profiles in 1μm was shown in Figure 4.43 for the scanned area. Similarly, the tapping mode AFM image analysis of biotite and Aero 825-treated biotite was shown in Figure 4.45. The height profiles of Aero 3000C-treated biotite reached to 2.5nm and Aero 825-treated biotite reached to 2.0nm while the biotite, shown in green in the figures, displayed height profiles less than 1.0nm for the scanned area.
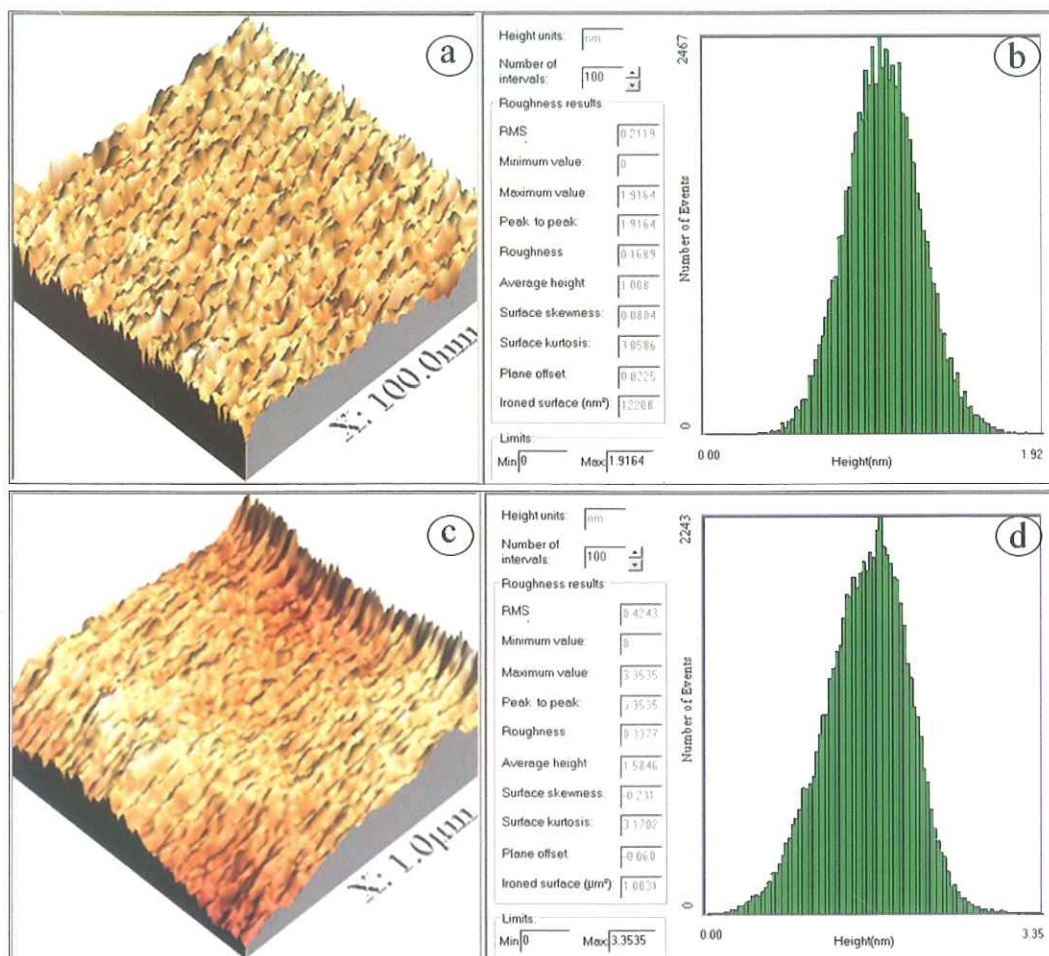
Figure 4. 42   3D Micro Topographies, Corresponding Histograms and Roughness Analyses of Aero 3000C-Treated Biotite.
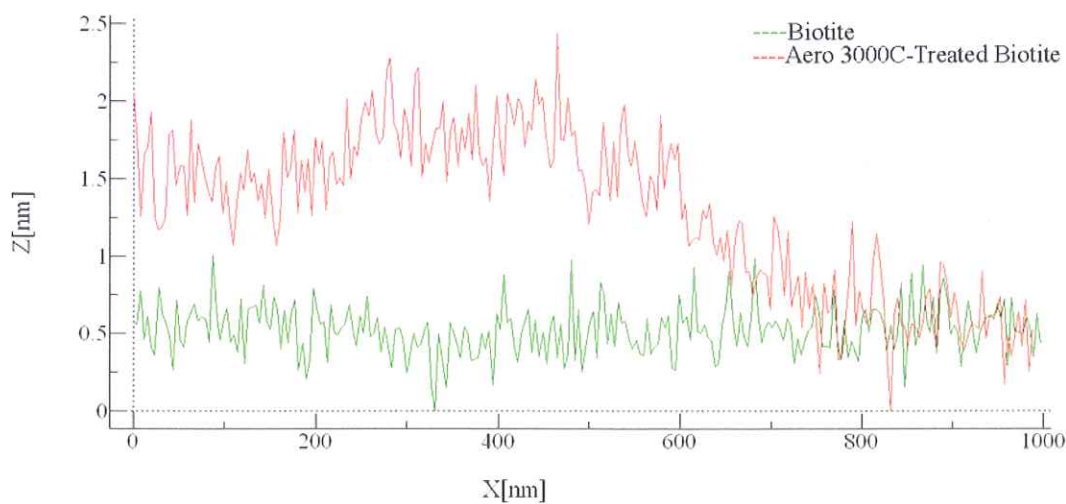
Figure 4. 43   Height Profiles of Biotite and Aero 3000C-Treated Biotite in 1μm Size.
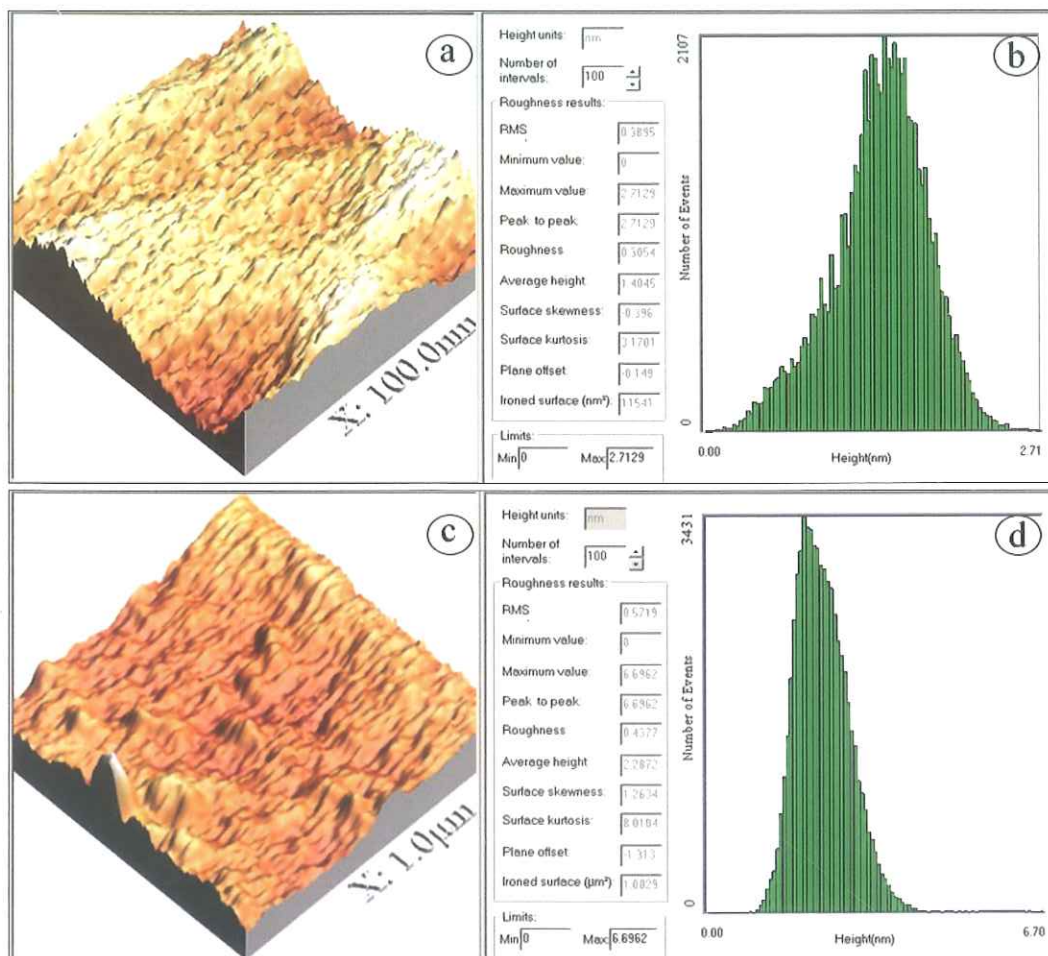
Figure 4. 44   3D Micro Topographies, Corresponding Histograms and Roughness Analyses of Aero 825-Treated Biotite.
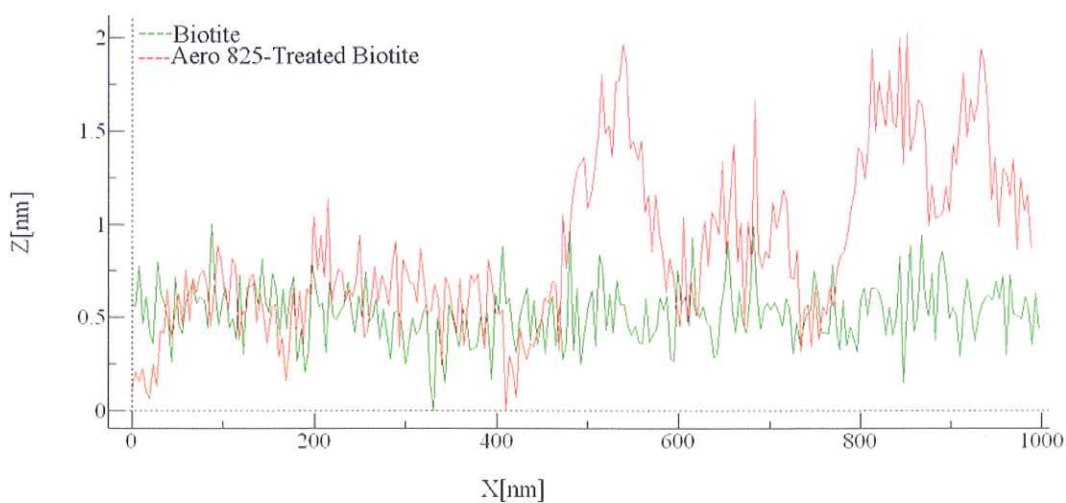
Figure 4. 45   Height Profiles of Biotite and Aero 825-Treated Biotite in 1μm Size.

4.2.4 FTIR Spectroscopy Studies on Biotite

In the similar way as albite, the FTIR analysis of the biotite, collector-treated biotite and acetone-washed biotite samples were examined and the resulting spectra were given in Figure 4.46, Figure 4.51 and Figure 4.56 for Aero 704, Aero 3000C and Aero 825 respectively.

In order to obtain more detailed FTIR spectra, the full scale FTIR spectra (4000-400 cm^{-1}) of collector, non-treated, collector-treated and acetone-washed biotite samples were analyzed in four major zones depending on the collector's FTIR peaks. Figures 4.47-4.50 show the FTIR ranges of biotite sample in the presence of Aero 704 as 3500-2750 cm^{-1}, 2750-1750 cm^{-1}, 1750-1250 cm^{-1} and 1250-400 cm^{-1} major wavelength's zones respectively.

The FTIR spectrum of Aero 704-treated biotite showed additional bands at 2961 cm^{-1}, 2926 cm^{-1} and 2854 cm^{-1} assigned as CH_2 stretching vibrations (Figure 4.47). The FTIR spectrum of the Aero 704-treated biotite upon washing with acetone was not altered keeping the bands which represent C-H vibrations.
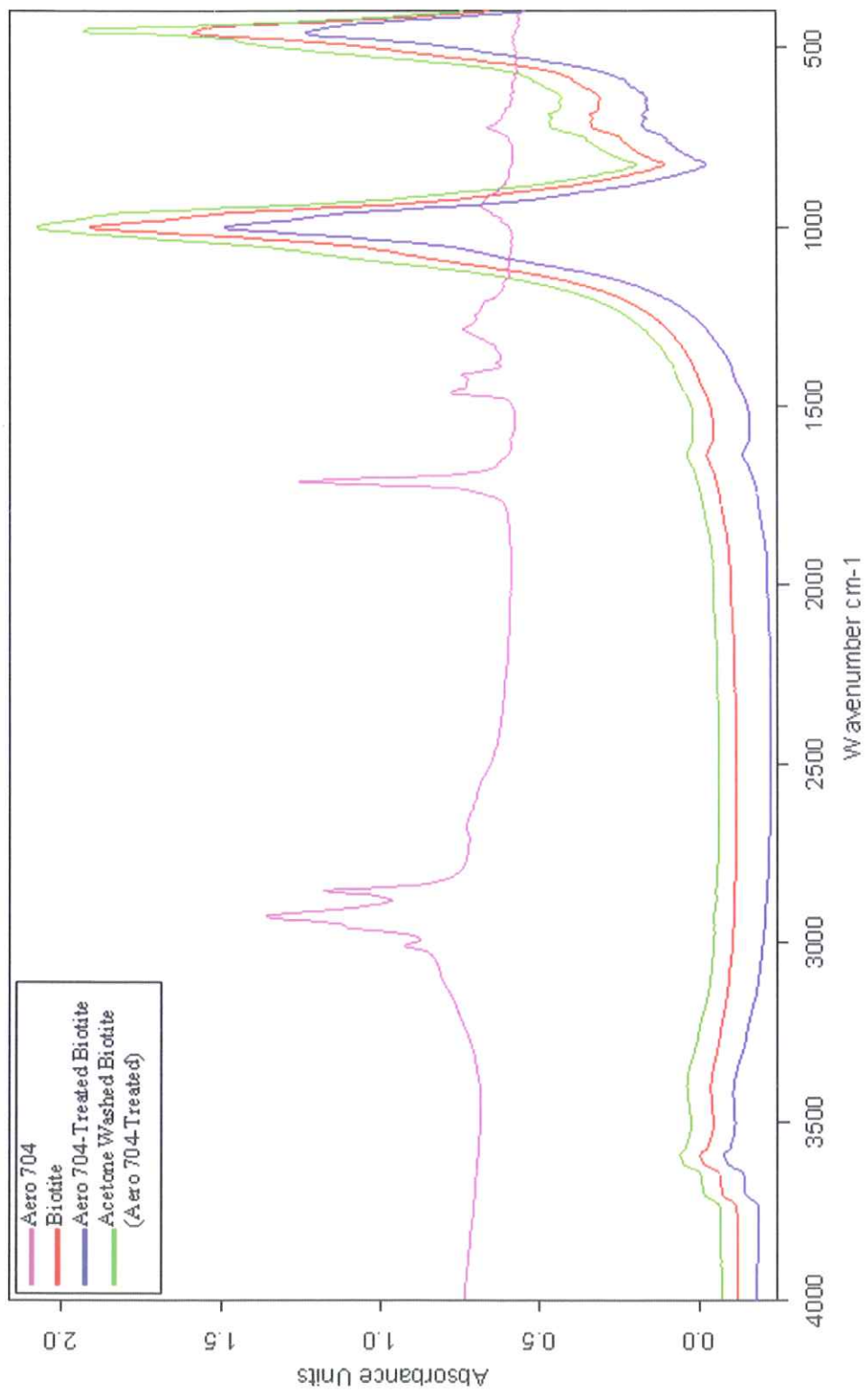
Figure 4. 46   FTIR Spectrum of Biotite in the Presence of Aero 704 in 4000–400 cm⁻¹ Wavelength Range.
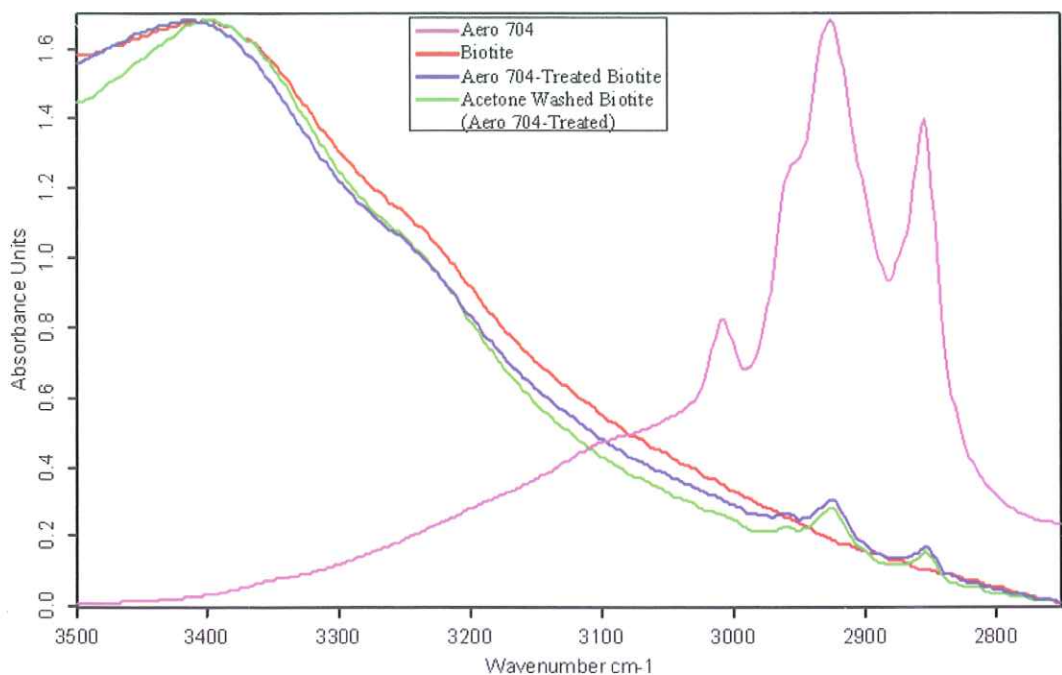
Figure 4. 47   FTIR Spectrum of Biotite in the Presence of Aero 704 in 3500–2750 cm^{-1} Wavelength Range.
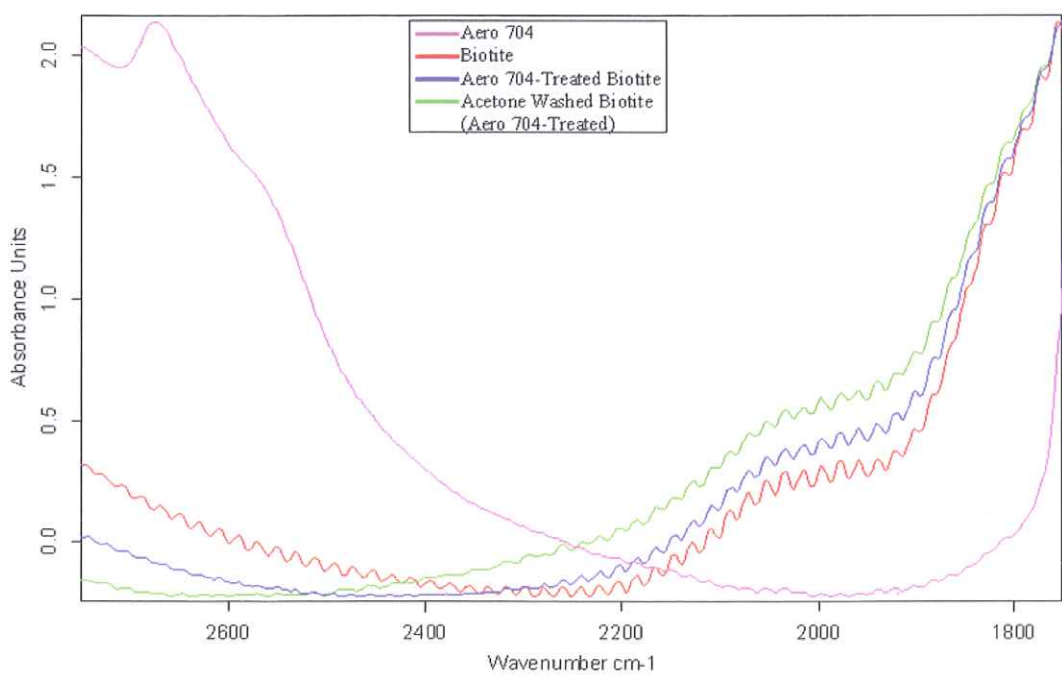
Figure 4. 48   FTIR Spectrum of Biotite in the Presence of Aero 704 in 2750–1750 cm^{-1} Wavelength Range.
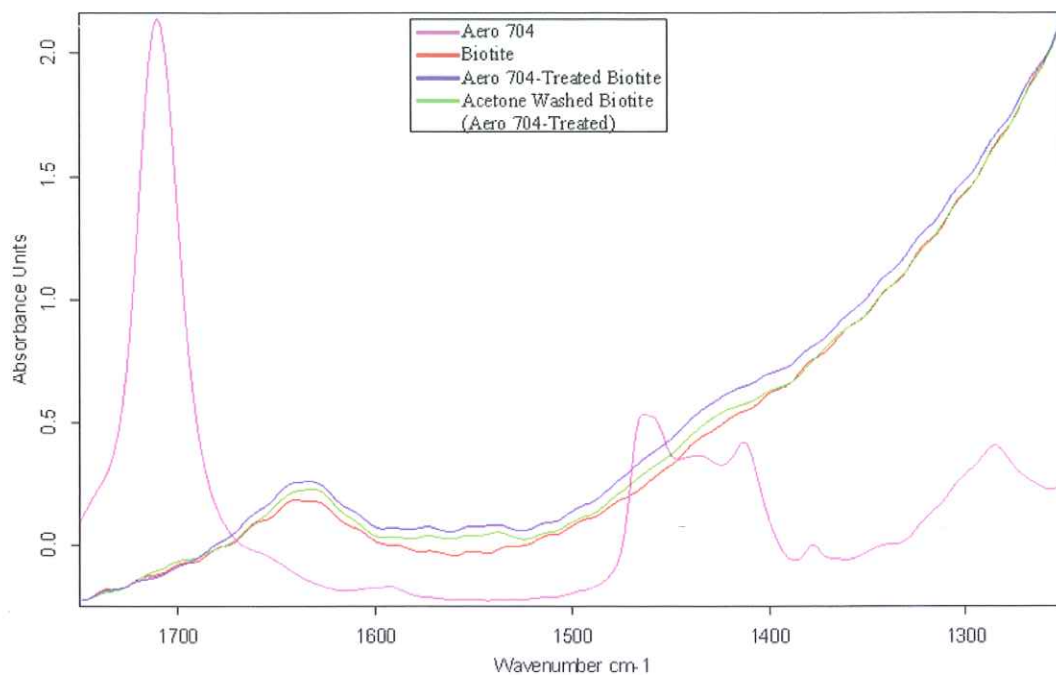
Figure 4. 49   FTIR Spectrum of Biotite in the Presence of Aero 704 in 1750–1250 cm^{-1} Wavelength Range.
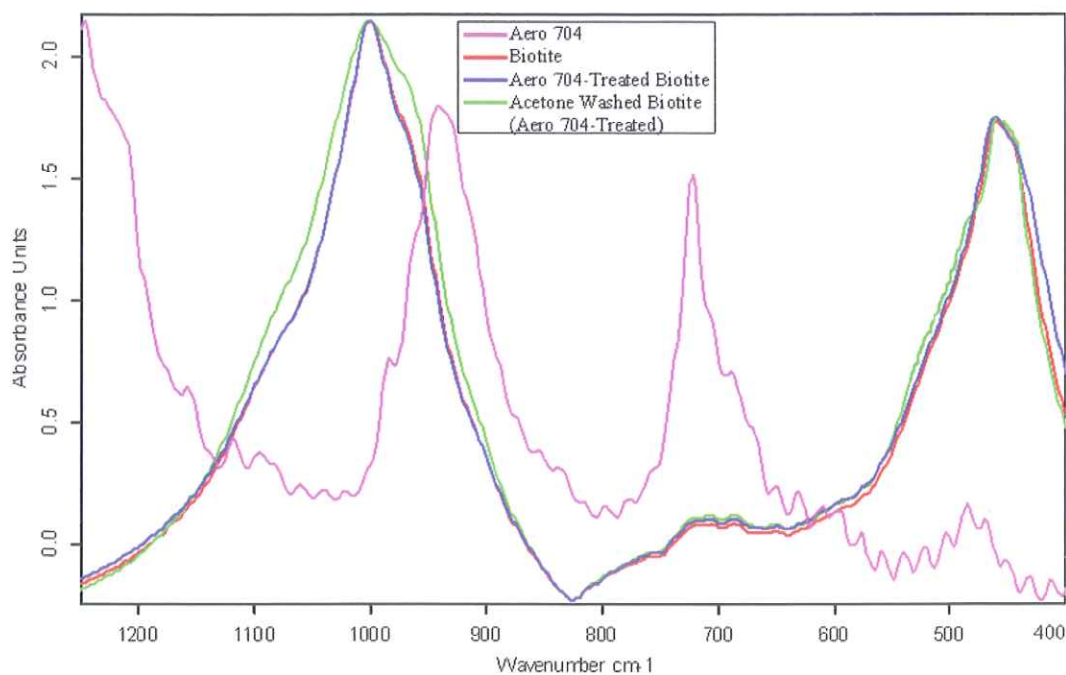
Figure 4. 50   FTIR Spectrum of Biotite in the Presence of Aero 704 in 1250–400 cm^{-1} Wavelength Range.

The spectra obtained with Aero 3000C, biotite, Aero 3000C-treated biotite and acetone-washed biotite were given in Figures 4.51 to 4.55. The major zones for the biotite in the presence of Aero 3000C were shown as 3250-2750 cm^{-1}, 2750-1750 cm^{-1}, 1750-1250 cm^{-1} and 1250-400 cm^{-1} wavelengths in Figures 4.52-4.55 respectively.

Aero 3000C-treated biotite showed additional bands at 2957 cm^{-1}, 2922 cm^{-1} and 2853 cm^{-1} with low intensities assigned as C-H stretching vibrations of Aero 3000C (Figure 4.52). The FTIR spectrum of the Aero 3000C-treated biotite upon washing with acetone was not altered; the bands were still exist.
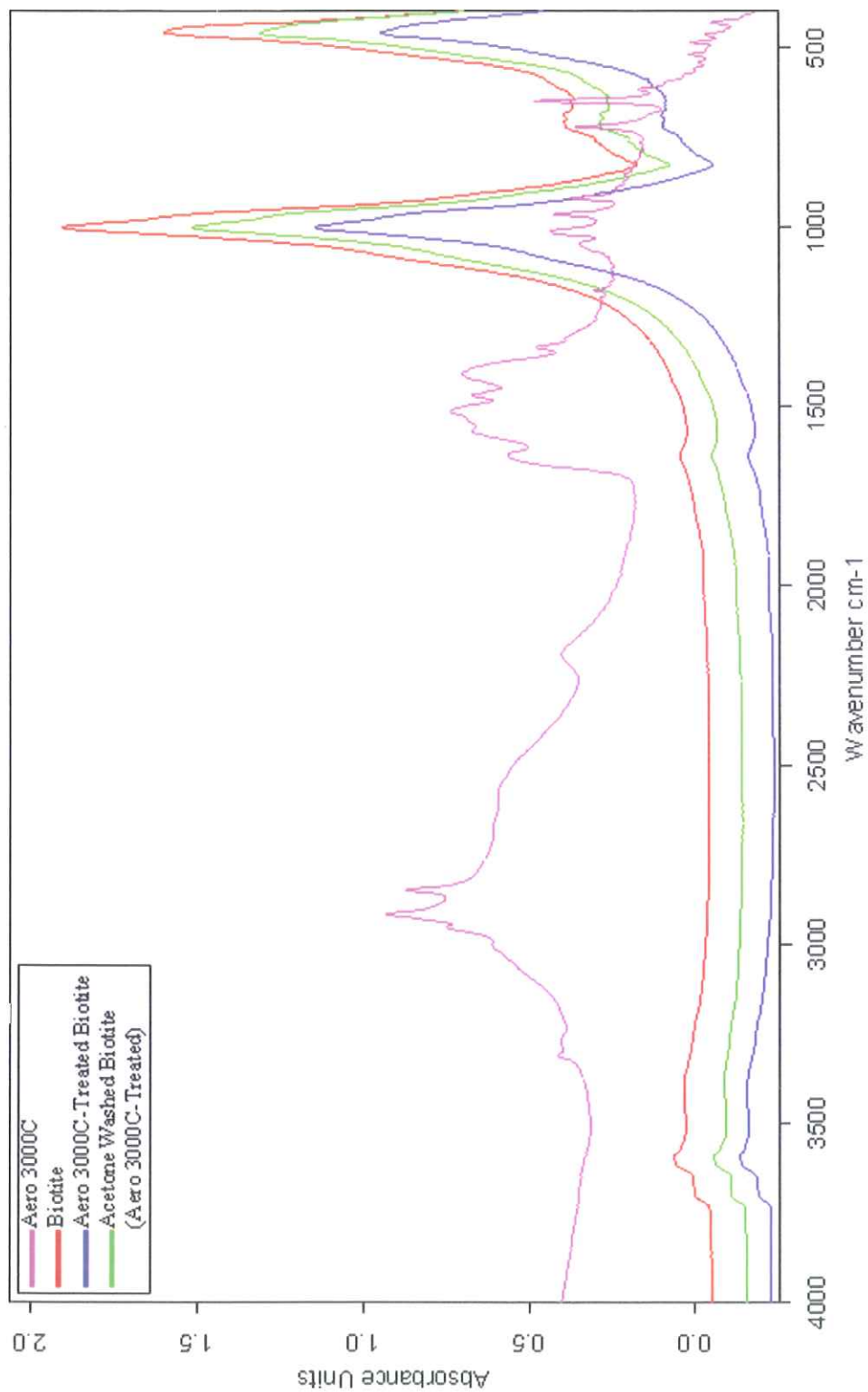
Figure 4. 51   FTIR Spectrum of Biotite in the Presence of Aero 3000C in 4000–400 cm^{-1} Wavelength Range.
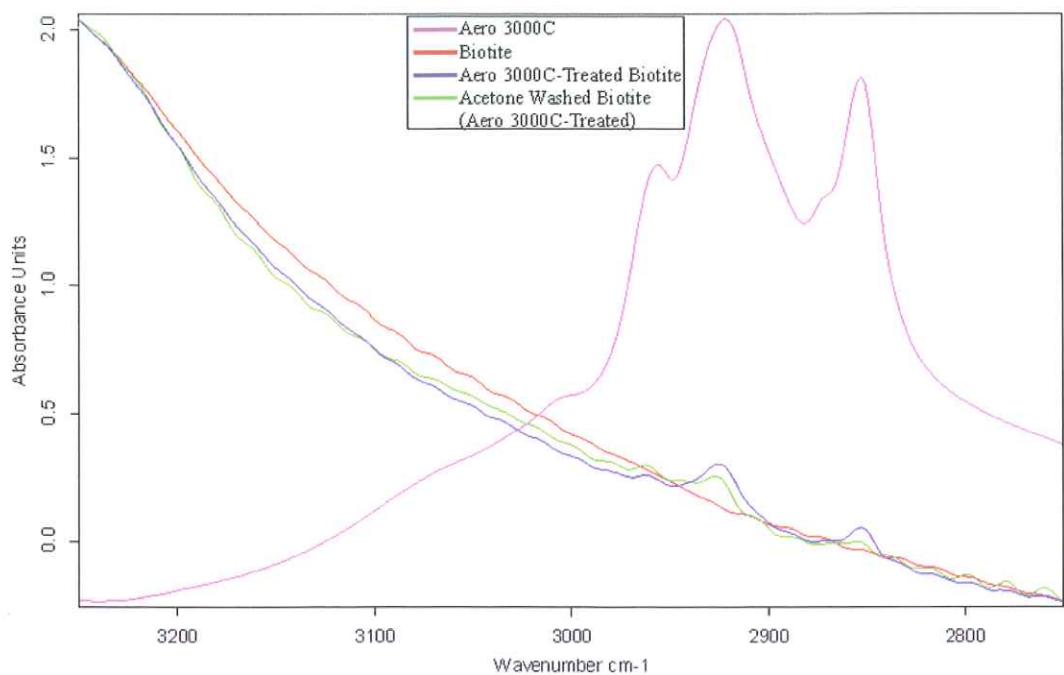
Figure 4. 52   FTIR Spectrum of Biotite in the Presence of Aero 3000C in 3250–2750 cm^{-1} Wavelength Range.
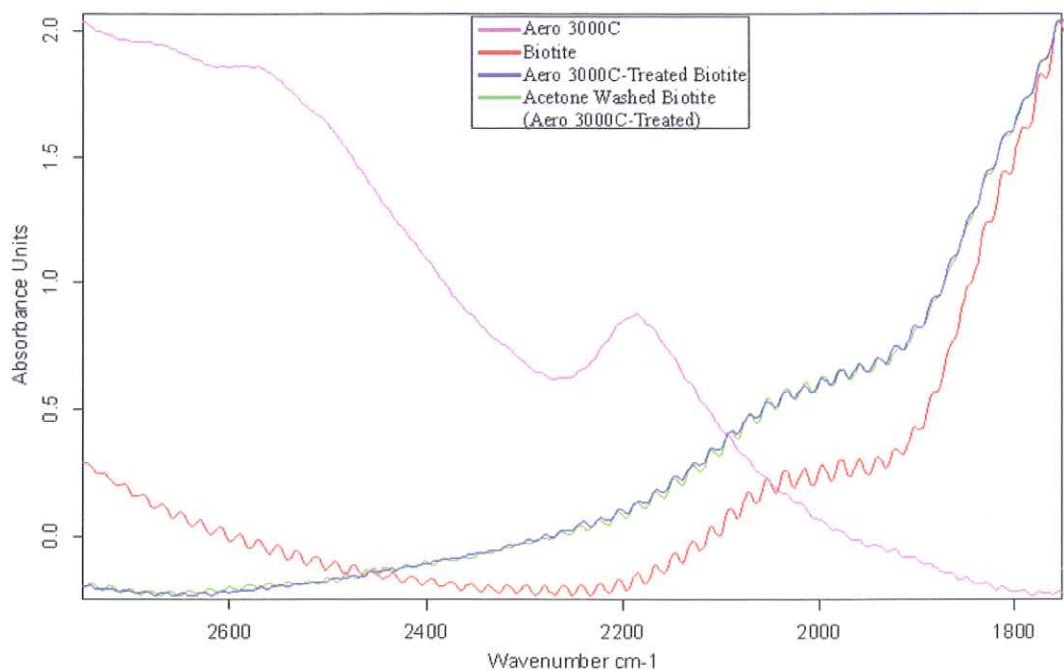
Figure 4. 53   FTIR Spectrum of Biotite in the Presence of Aero 3000C in 2750–1750 cm^{-1} Wavelength Range.
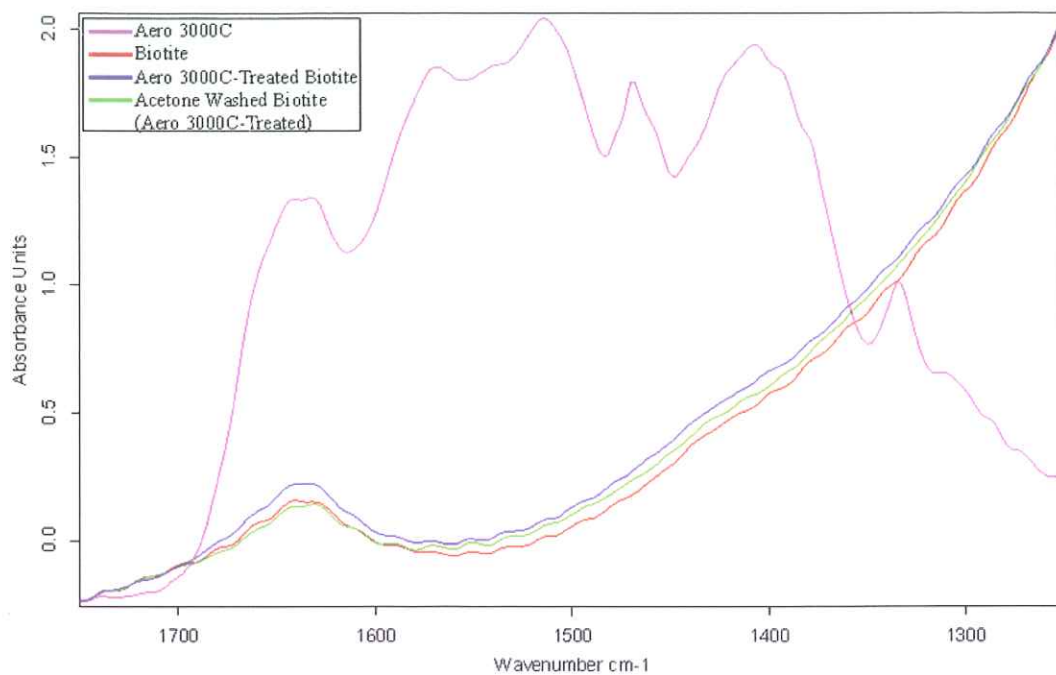
Figure 4. 54   FTIR Spectrum of Biotite in the Presence of Aero 3000C in 1750–1250 cm^{-1} Wavelength Range.
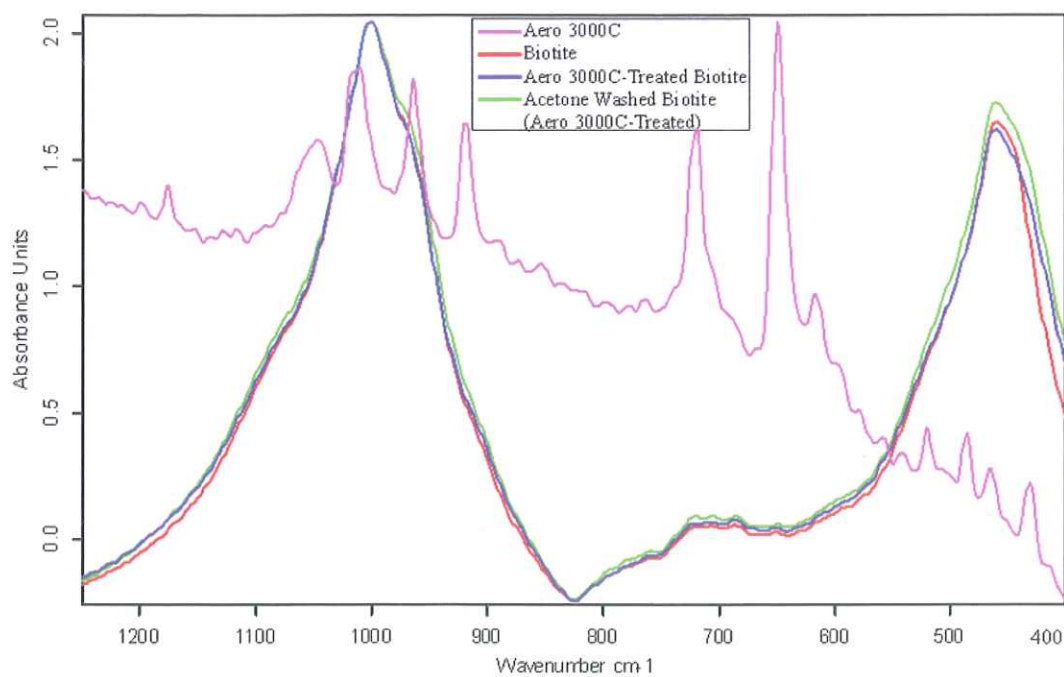
Figure 4. 55   FTIR Spectrum of Biotite in the Presence of Aero 3000C in 1250–400 cm^{-1} Wavelength Range.

The spectra obtained for Aero 825 are given in Figures 4.56-4.60. In order to provide more detailed spectra, the major zones for the biotite in the presence of Aero 825 were displayed in Figures 4.57-4.60 as 3750-2750 cm^{-1}, 2750-1500 cm^{-1}, 1500-1000 cm^{-1} and 1000-400 cm^{-1} wavelengths depending on the Aero 825's FTIR peaks.

In Figure 4.57, Aero 825-treated biotite had additional bands at 2951 cm^{-1}, 2924 cm^{-1} and 2854 cm^{-1} with very low intensities assigned as CH_2 stretching vibrations of Aero 825. However, upon washing with acetone, the bands at 2951 cm^{-1}, 2924 cm^{-1} and 2854 cm^{-1} disappeared.
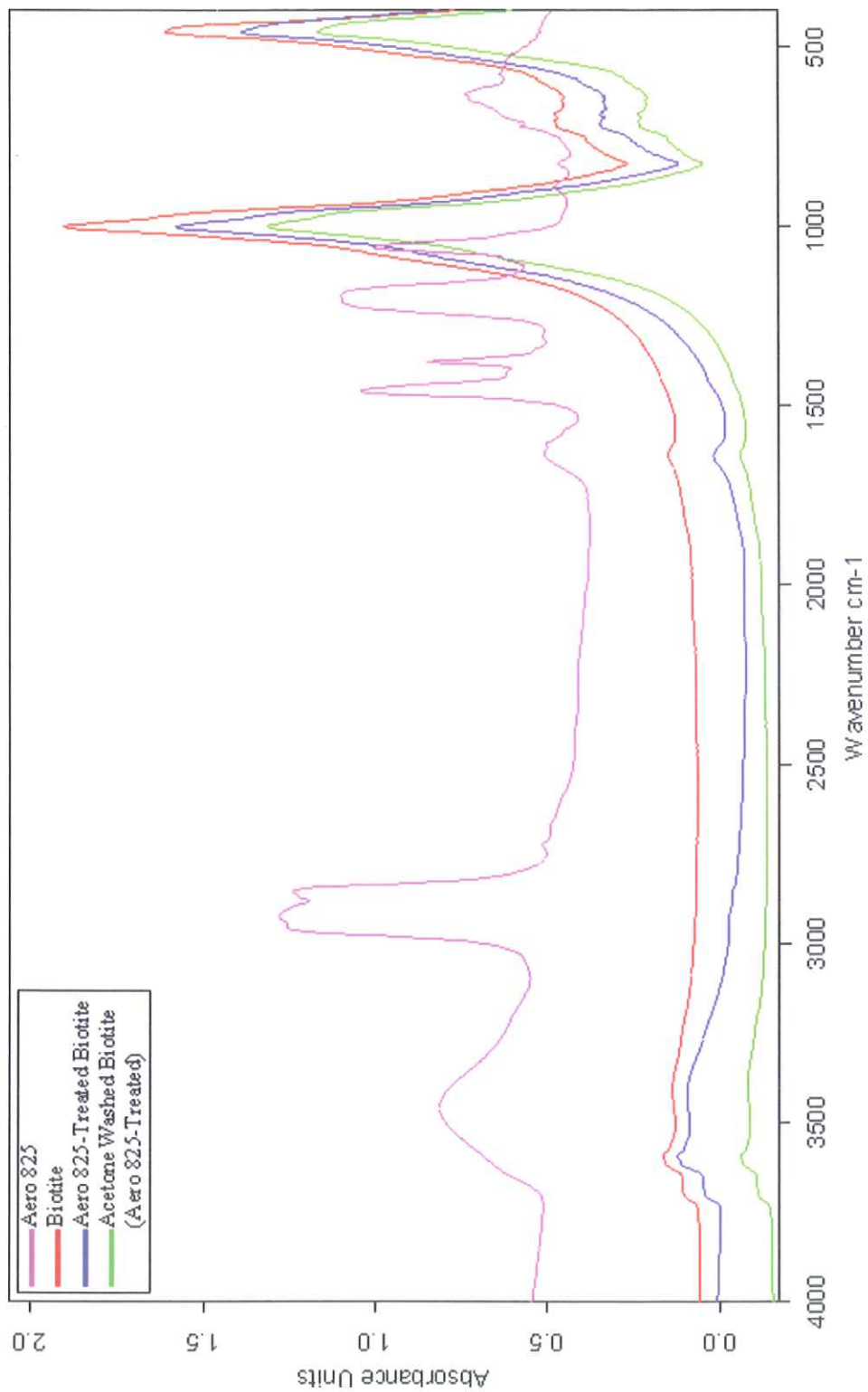
Figure 4. 56   FTIR Spectrum of Biotite in the Presence of Aero 825 in 4000–400 cm^{-1} Wavelength Range.
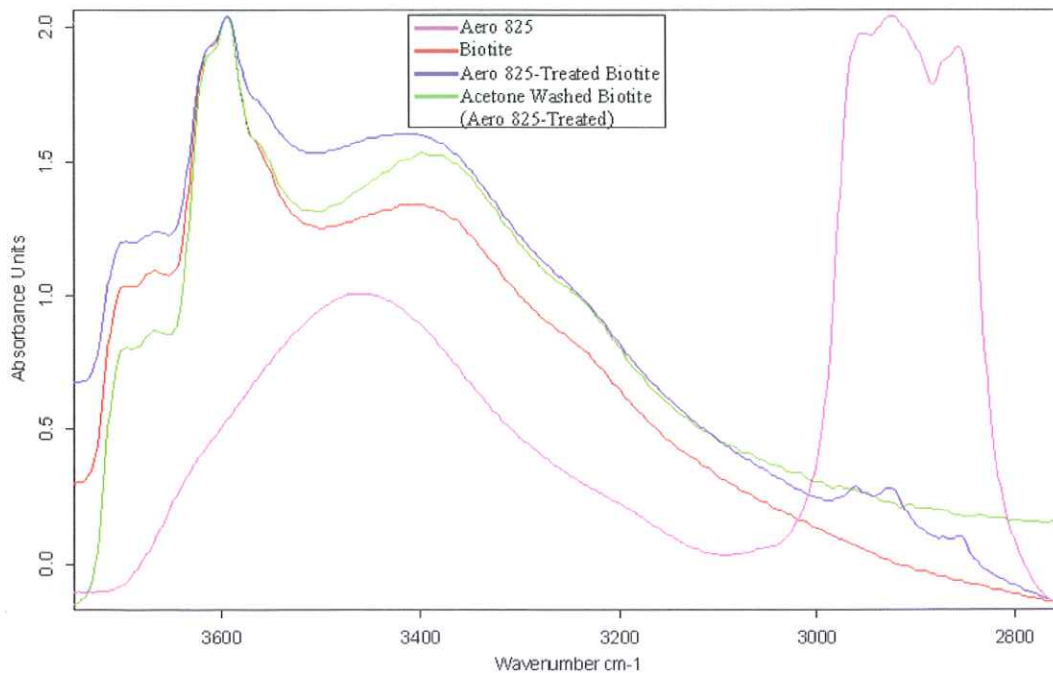
Figure 4. 57   FTIR Spectrum of Biotite in the Presence of Aero 825 in 3750–2750 cm^{-1} Wavelength Range.
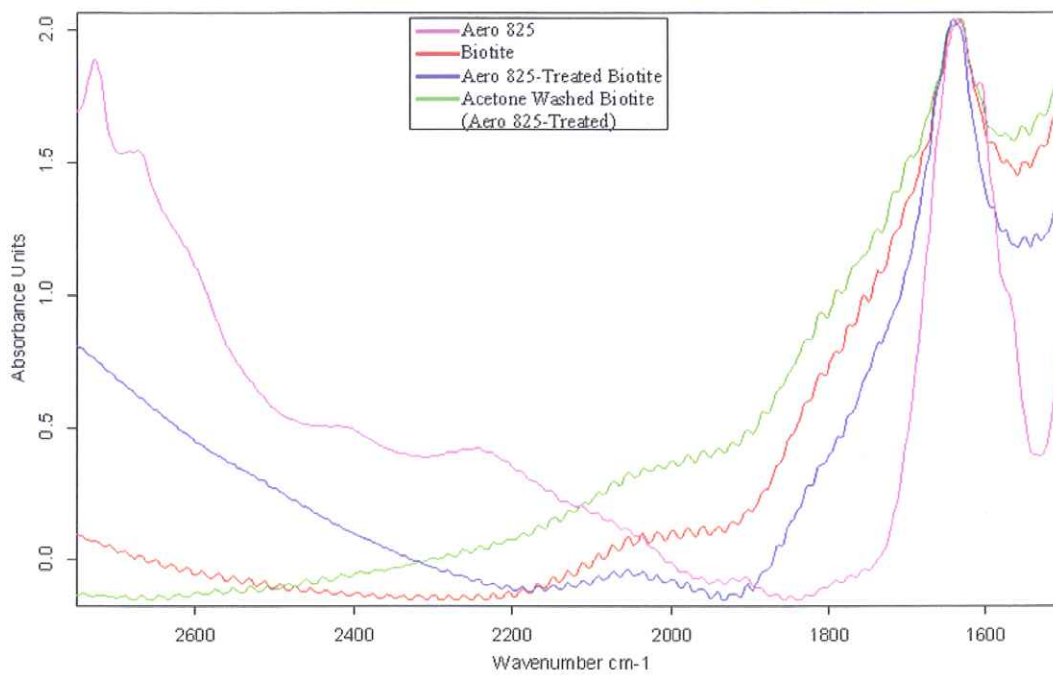
Figure 4. 58   FTIR Spectrum of Biotite in the Presence of Aero 825 in 2750–1500 cm^{-1} Wavelength Range.
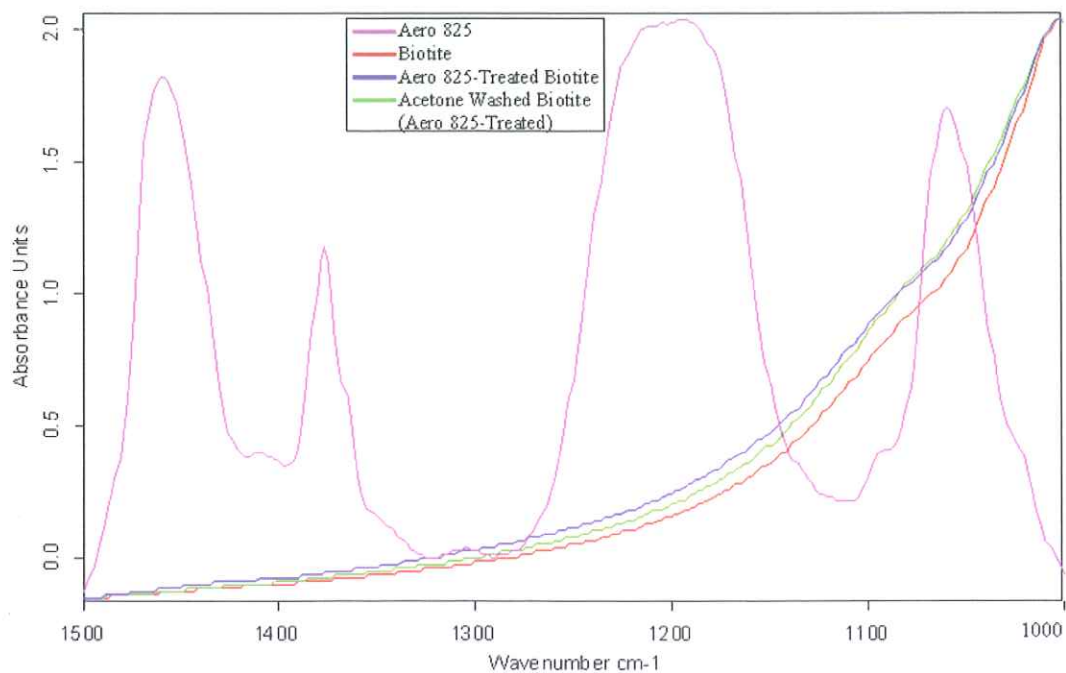
Figure 4. 59   FTIR Spectrum of Biotite in the Presence of Aero 825 in 1500–1000 cm^{-1} Wavelength Range.

Figure 4. 60   FTIR Spectrum of Biotite in the Presence of Aero 825 in 1000–400 cm^{-1} Wavelength Range.

4.3   Muscovite Sample

4.3.1   Electrokinetic Potential Measurements on Muscovite

When the similar procedure was applied in order to obtain the zeta potential values of muscovite, the i.e.p. was found to be about pH 3.0 in distilled water and in 1.0×10^{-3} M indifferent electrolyte, KCl. The results are given in Figure 4.61 as function of pH. Above the i.e.p. the zeta potential values became more negative towards the more basic region and below the i.e.p. the zeta potential values became more positive towards the more acidic region. The electrokinetic potential values of the muscovite found to be consistent with reported data by Nosrati et.al, 2012 [65].
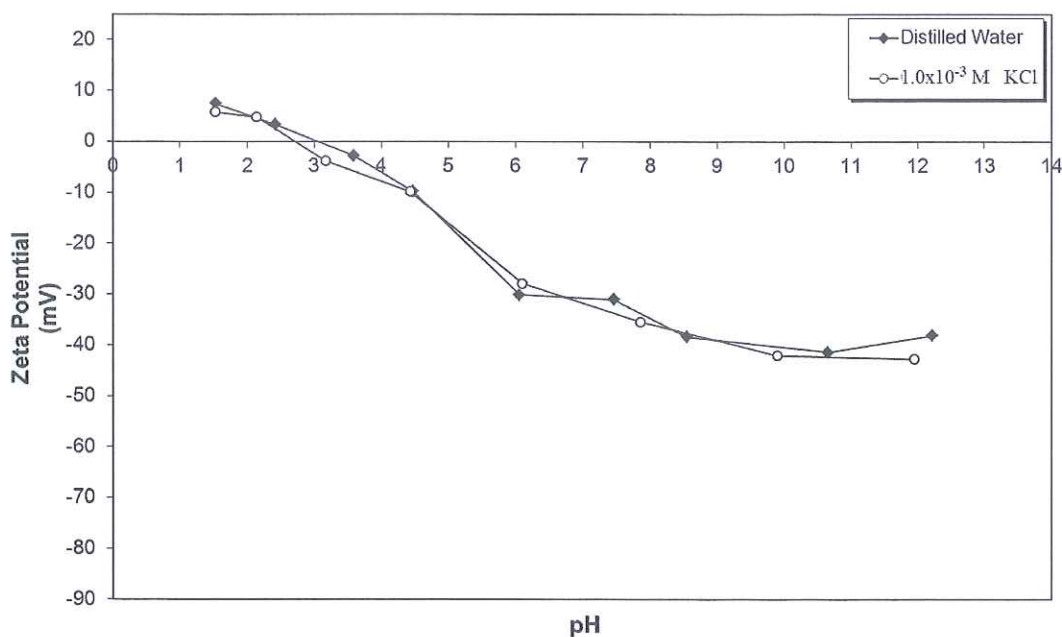
Figure 4. 61   Zeta Potential of Muscovite as a Function of pH.

Figure 4.62 shows the effect of 1.0×10^{-4} M, 5.0×10^{-4} M and 1.0×10^{-3} M of Aero 704 on the electrokinetic potential of muscovite. The zeta potential values of muscovite decreased with increasing Aero 704 concentration and pH. The i.e.p. was shifted towards the more acidic region (from pH 3.0 to about pH 1.5) with all Aero 704 concentrations and hence the positive charge of the muscovite decreased.

The zeta potential values of muscovite in the presence of 5.0×10^{-5} M, 1.0×10^{-4} M and 5.0×10^{-4} M of Aero 3000C as a function of pH were shown in Figure 4.63. The zeta potential values increased proportionally to Aero 3000C concentration and pH. The i.e.p. was shifted from about pH 3.0 to highly alkali conditions, about pH 10.8 and the surface of the sample was positively charged up to given pH.

Figure 4.64 displays the zeta potential values of muscovite in the presence of 1.0×10^{-4} M, 5.0×10^{-4} M and 1.0×10^{-3} M of Aero 825 as a function of pH. The zeta potential values of muscovite decreased with increasing Aero 825 concentration.
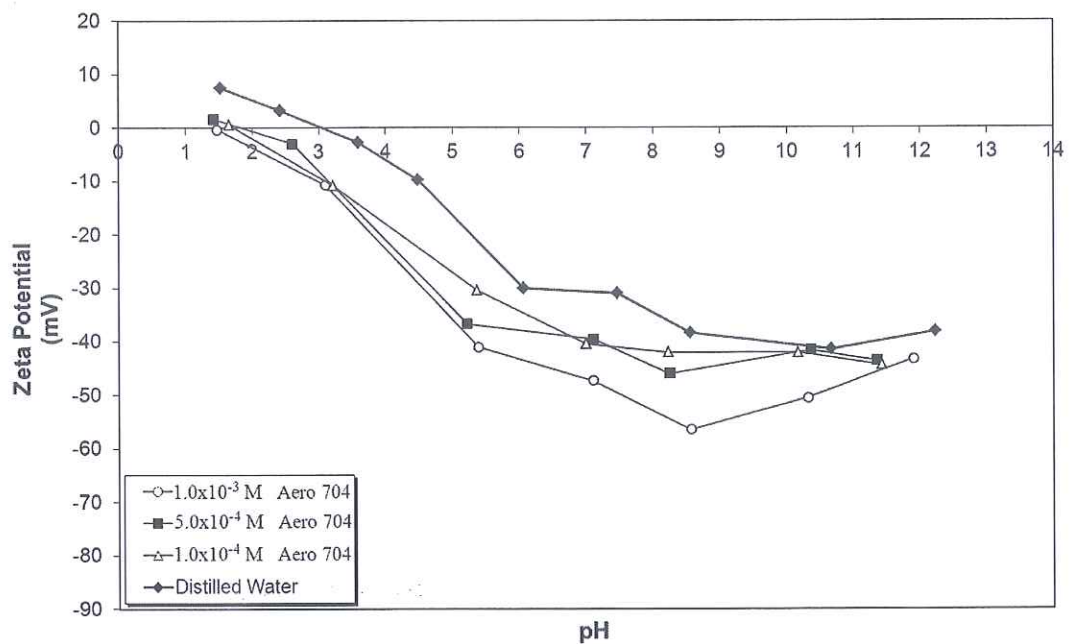
Figure 4. 62   Zeta Potential of Muscovite as a Function of pH and Aero 704 Concentration.
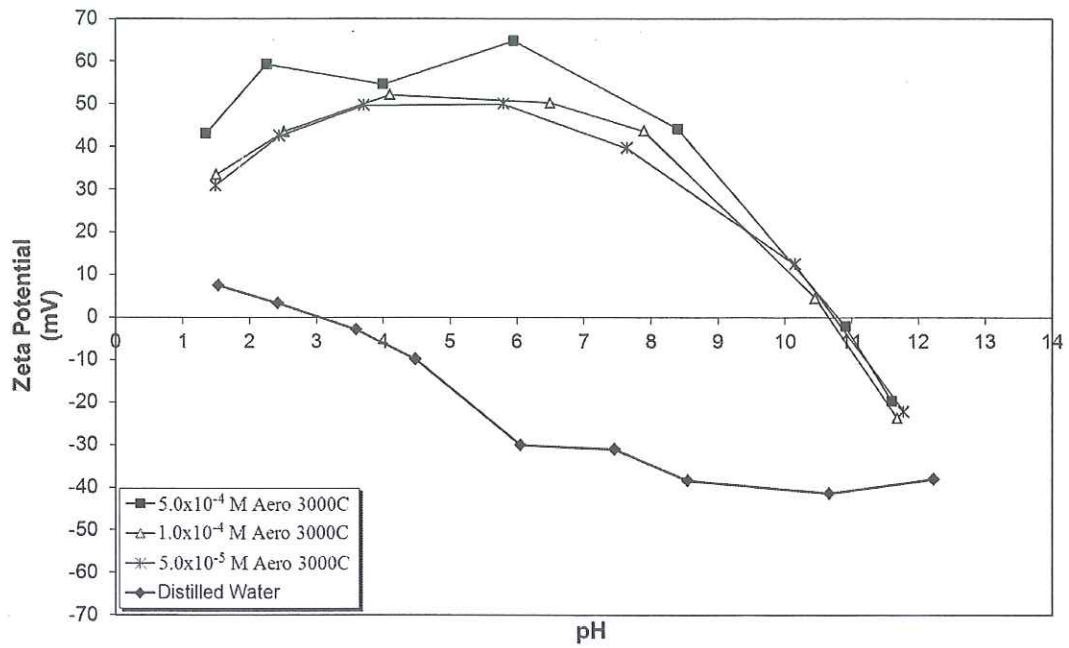
Figure 4. 63   Zeta Potential of Muscovite as a Function of pH and Aero 3000C Concentration.
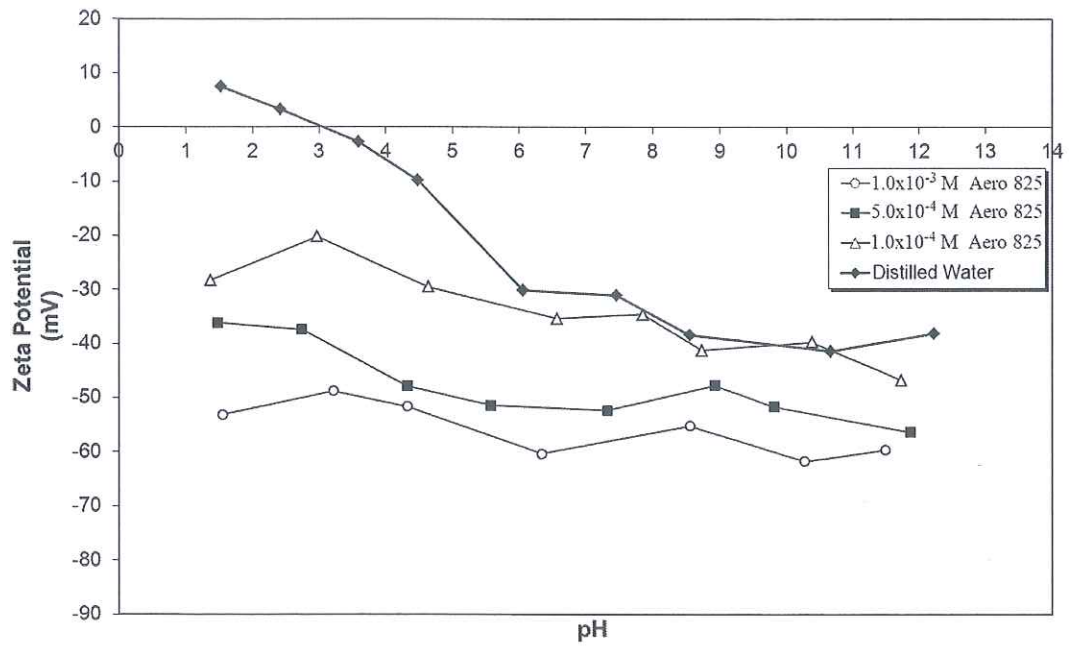
Figure 4. 64   Zeta Potential of Muscovite as a Function of pH and Aero 825 Concentration.

114

Additional electrokinetic potential measurements were carried out on acetone-washed muscovite samples which were conditioned with 3.5×10^{-4} M of Aero 704 about pH 9.5, 5.0×10^{-5} M of Aero 3000C about pH 3.0 and 2.0×10^{-4} M of Aero 825 about pH 5.0. The samples were first conditioned with each collector and then washed with acetone several times prior to electrokinetic potential measurements.

The effects of acetone washing on the electrokinetic potential values of collector-treated muscovite samples were shown in Figure 4.65 as a function of pH. The zeta potential values were found to be very similar to each other for all pH ranges.
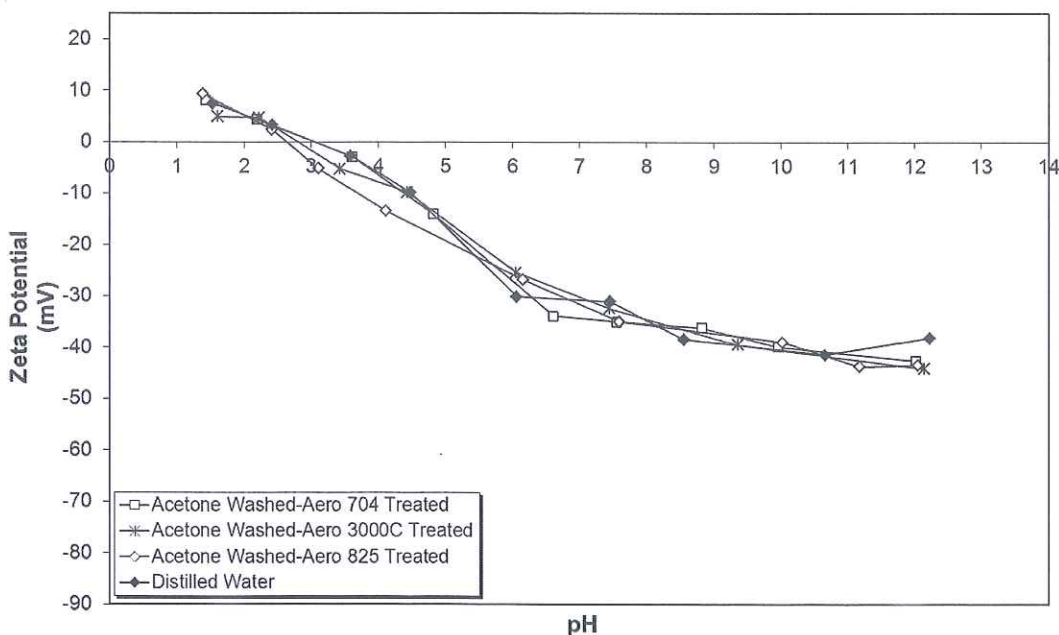
Figure 4. 65   Zeta Potentials of Aero 704, Aero 3000C and Aero 825 Treated Muscovite Samples After Acetone Washing.

4.3.2   Flotation Studies on Muscovite

The flotation recoveries of muscovite as a function of pH and Aero 704 concentration were shown in Figure 4.66. As the flotation recovery of muscovite was null below pH 7.0, the micro-flotation experiments were performed from this pH on with all Aero 704 concentrations. It is seen that the flotation recovery of the

muscovite increased proportionally to Aero 704 concentration. The maximum flotation recoveries were obtained as 25.0% with 2×10^{-4} M, 44.0% with 2.75×10^{-4} M, 75.0% with 5×10^{-4} M and 92.5% with 5×10^{-4} M of Aero 704 in the pH range of 9.0-10.5.

The flotation recoveries of the muscovite were maximum between the pH 3.5 and 10.5 with the values of 36.0% with 2.0×10^{-5}M, 86.5% with 5.0×10^{-5} M, 90.5% with 7.5×10^{-5} M and 93.0% with 1.0×10^{-4} M of Aero 3000C respectively (Figure 4.67). The flotation recoveries decreased sharply above pH 10.5 and below pH 3.5 in all Aero 3000C concentrations except for the lowest concentration, 2.0×10^{-5} M. In the latter case, the flotation recoveries gradually increased up to 36.0% about pH 8.0 and then decreased gradually above the given pH.

In the case of Aero 825, the flotation recoveries of muscovite were shown in Figure 4.68 as function of pH and concentration. The maximum recoveries were obtained as 16.5% with 5.0×10^{-4} M and as 20.0% with 1.0×10^{-3} M of Aero 825 between the pH range of 3.5 and 6.0. As shown in the figure, the flotation recoveries were almost null for the 1.5×10^{-4} M and 2.0×10^{-4} M.
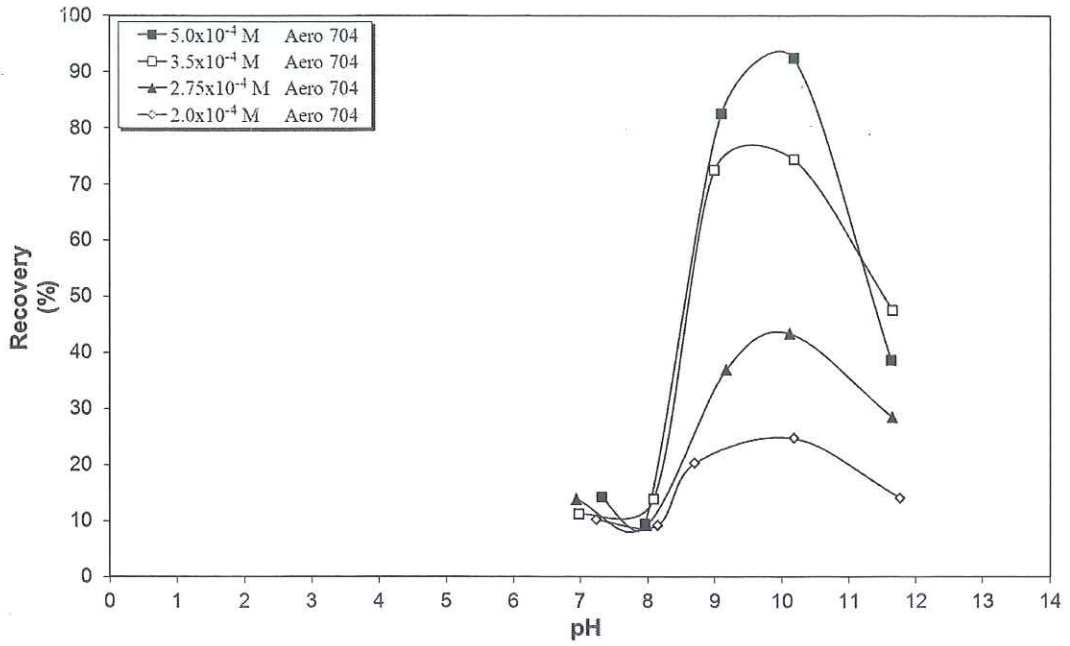
Figure 4. 66   Flotation Recovery of Muscovite as a Function of pH and Aero 704
                Concentration.
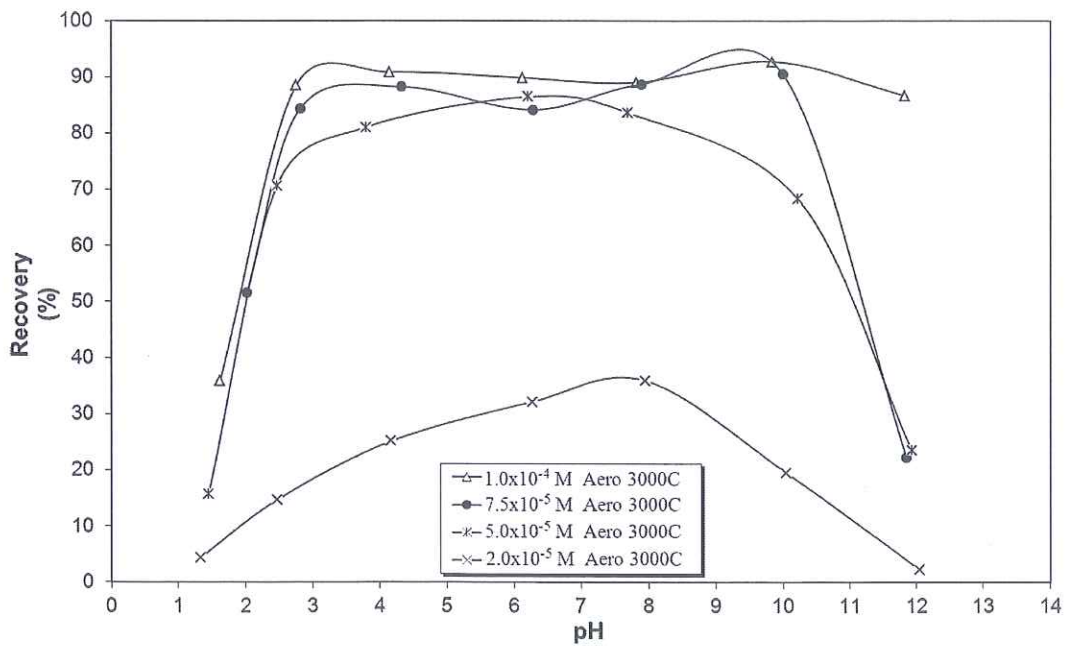
Figure 4. 67   Flotation Recovery of Muscovite as a Function of pH and Aero 3000C
                Concentration.

117
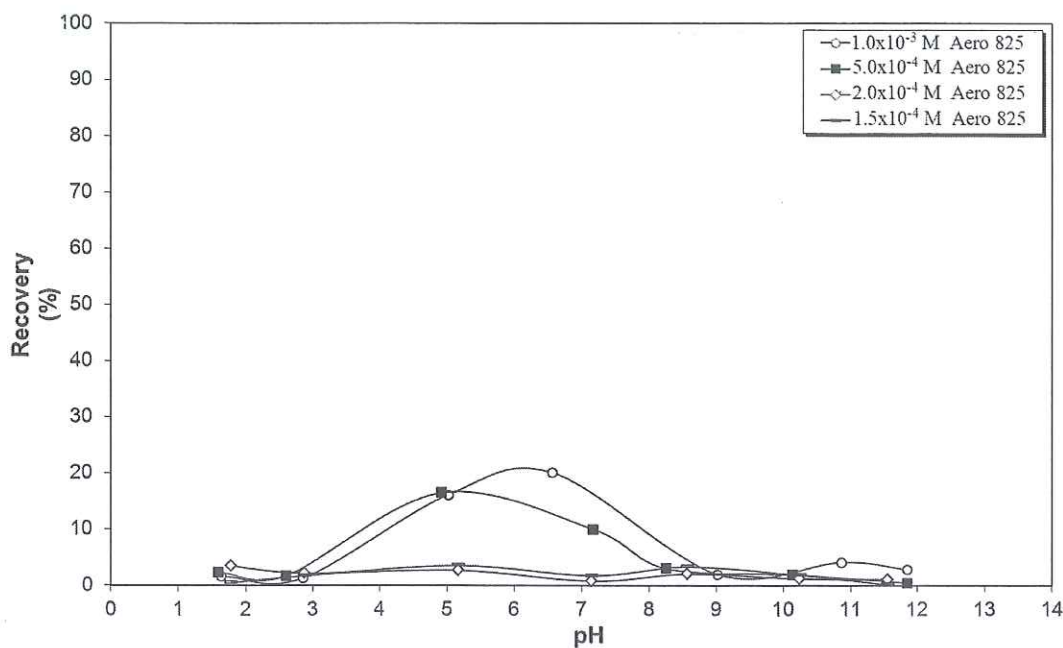
Figure 4. 68   Flotation Recovery of Muscovite as a Function of pH and Aero 825
Concentration.

4.3.3   AFM Studies on Muscovite

The tapping mode AFM 3D micro topographies of muscovite in 100nm (Figure 4.69a) and 1μm (Figure 4.69c) sizes and their corresponding histograms and roughness analyses (Figure 4.69b and Figure 4.69d) were given in Figure 4.69. The resulting histogram provides information about the surface roughness, the maximum peak value and the average height values of muscovite for 100nm x 100nm and 1μm x 1μm scanning size ranges. The corresponding histograms revealed the roughness average as 0.1431nm, the maximum peak value as 1.5289nm and the average height value as 0.6877nm for 100nm x 100nm scanning size range and 0.1452nm, 1.7224nm and 0.7433nm for 1μm x 1μm scanning size range respectively.
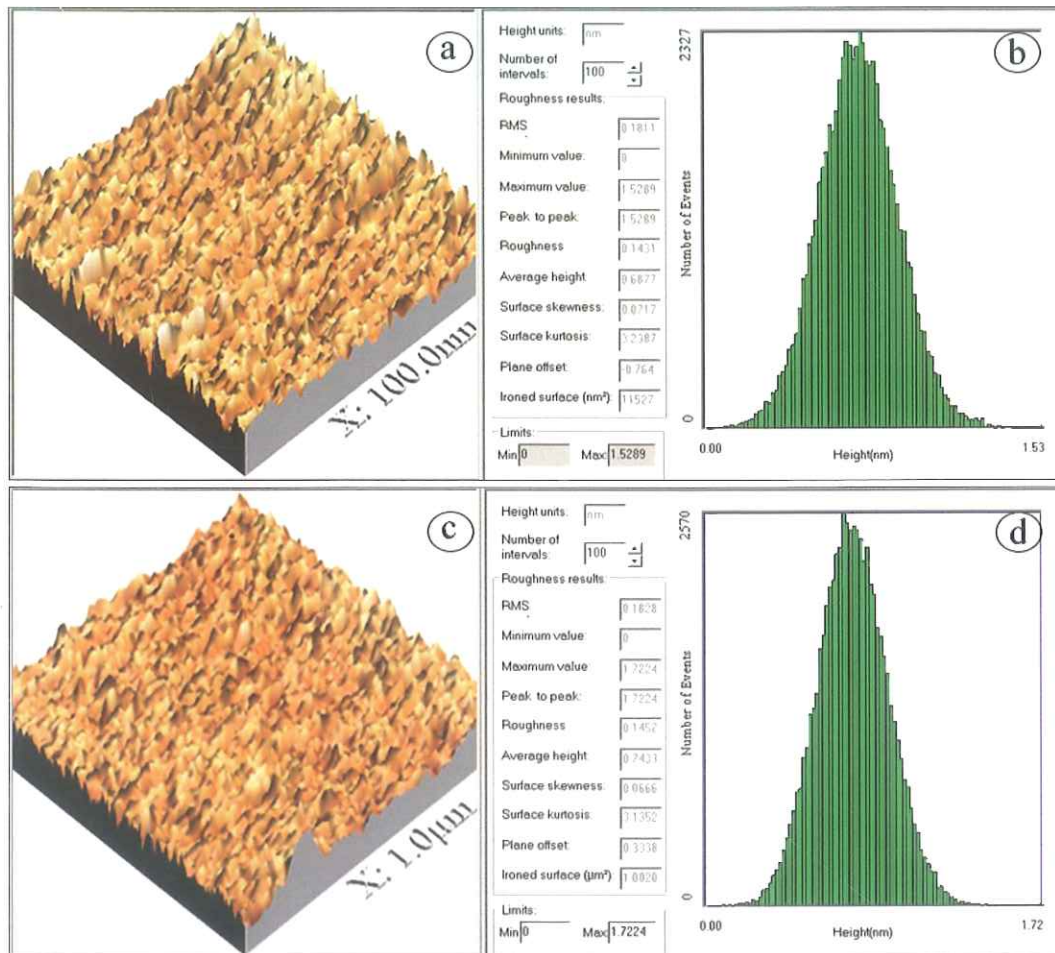
Figure 4. 69   3D Micro Topographies, Corresponding Histograms and Roughness
                Analyses of Muscovite.

The tapping mode AFM 3D micro topographies (Figure 4.70a and 4.70c) and the corresponding histograms (Figure 4.70b and 4.70d) of the Aero 704-treated muscovite revealed the roughness average as 0.2317nm, the maximum peak value as 2.2838nm and the average height value as 0.9840nm for 100nm x 100nm scanning size and 1.9939nm and 0.8730nm for 1μm x 1μm scanning size range, respectively (Figure 4.70). The tapping mode AFM image analysis of muscovite and Aero 704-treated muscovite based on their height profiles in 1μm were shown in Figure 4.71 for the scanned area. The muscovite, shown in green, displayed almost similar height profiles to that of Aero 704-treated muscovite for the scanned area.
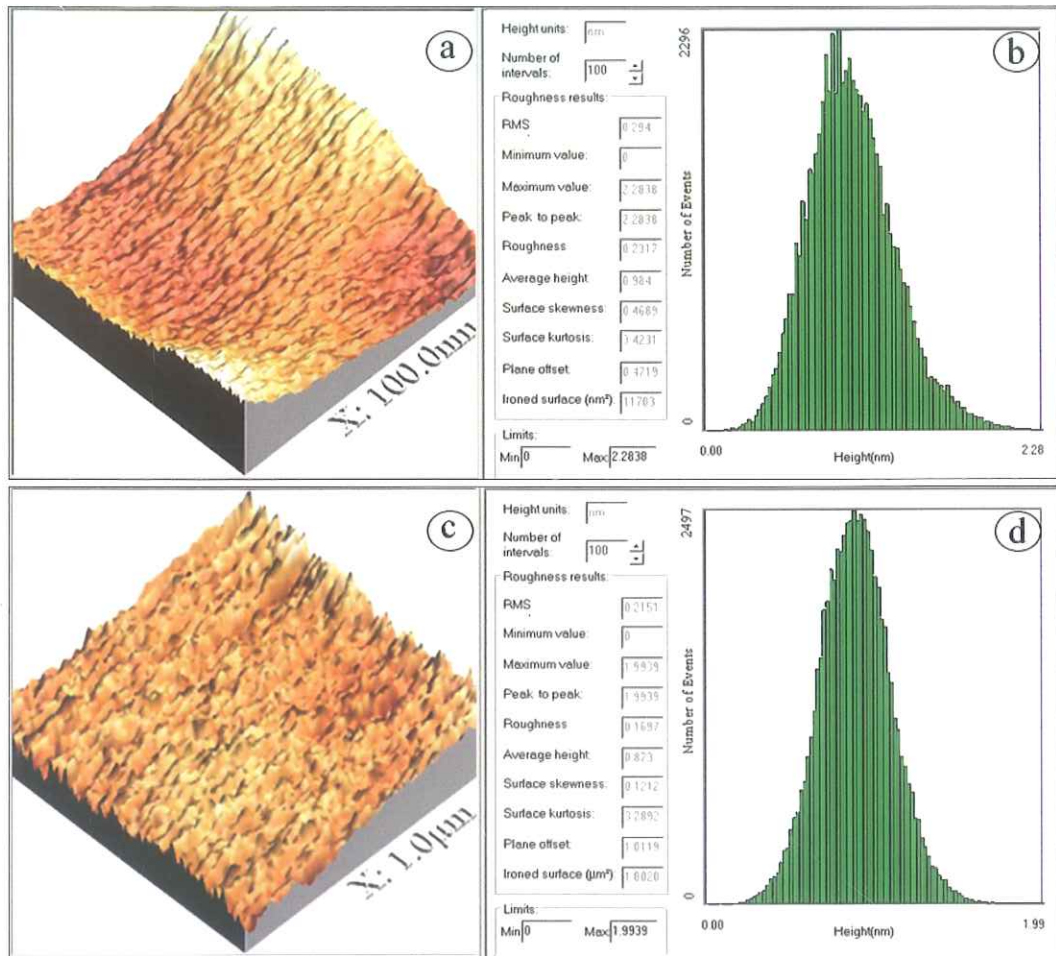
Figure 4. 70   3D Micro Topographies, Corresponding Histograms and Roughness
Analyses of Aero 704-Treated Muscovite.
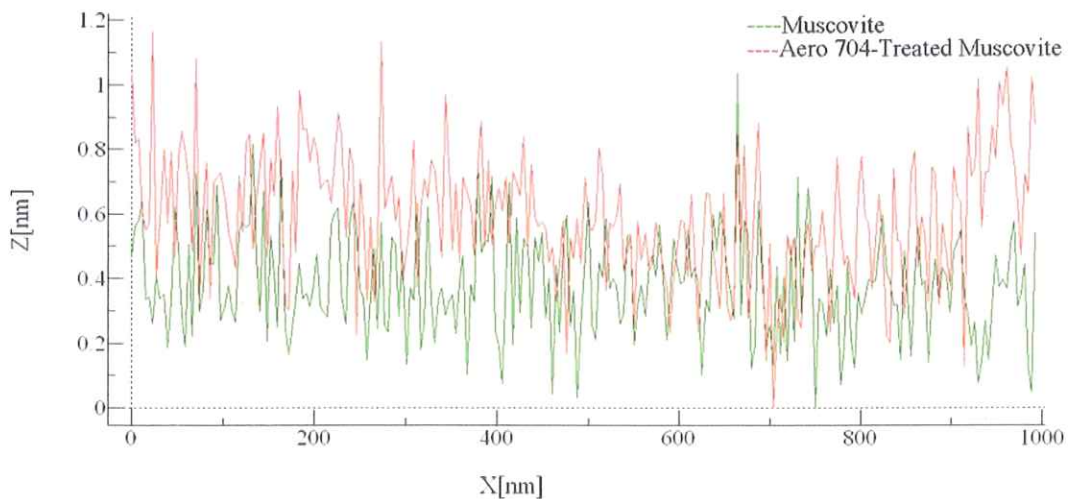
Figure 4. 71   Height Profiles of Muscovite and Aero 704-Treated Muscovite in 1μm
Size.

The tapping mode AFM 3D micro topographies and the corresponding histograms of Aero 3000C-treated and Aero 825-treated muscovite in 100nm x 100nm (Figure 4.72a-b for Aero 3000C-treated and Figure 4.74a-b for Aero 825-treated muscovite) and 1μm x 1μm (Figure 4.72c-d for Aero 3000C-treated and Figure 4.74c-d for Aero 825-treated muscovite) scanning size ranges were given in Figure 4.72 and Figure 4.74 respectively. For Aero 3000C-treated muscovite, the histograms revealed that the roughness averages, the maximum peak values and the average height values as 0.1463nm, 2.0060nm and 1.0953nm for 100nm x 100nm scanning size and 0.2209nm, 6.3128nm and 2.8661nm for 1μm x 1μm scanning size range, respectively. In the case of Aero 825-treated muscovite, the roughness averages, the maximum peak values and the average height values were obtained as 0.1478nm, 1.9988nm and 1.0383nm for 100nm x 100nm scanning size range and 0.1543nm, 2.0357nm, 0.7508nm for 1μm x 1μm scanning size range respectively.

The tapping mode AFM image analysis of muscovite and Aero 3000C-treated muscovite based on their height profiles in 1μm was shown in Figure 4.73 for the scanned area. Similarly, the tapping mode AFM image analysis of muscovite and Aero 825-treated muscovite was shown in Figure 4.75. The height profiles of Aero 3000C-treated muscovite reached to 4.0nm while the Aero 825-treated muscovite and muscovite (shown in green in the figures), displayed almost similar height profiles less than 1.0nm for the scanned area.

121
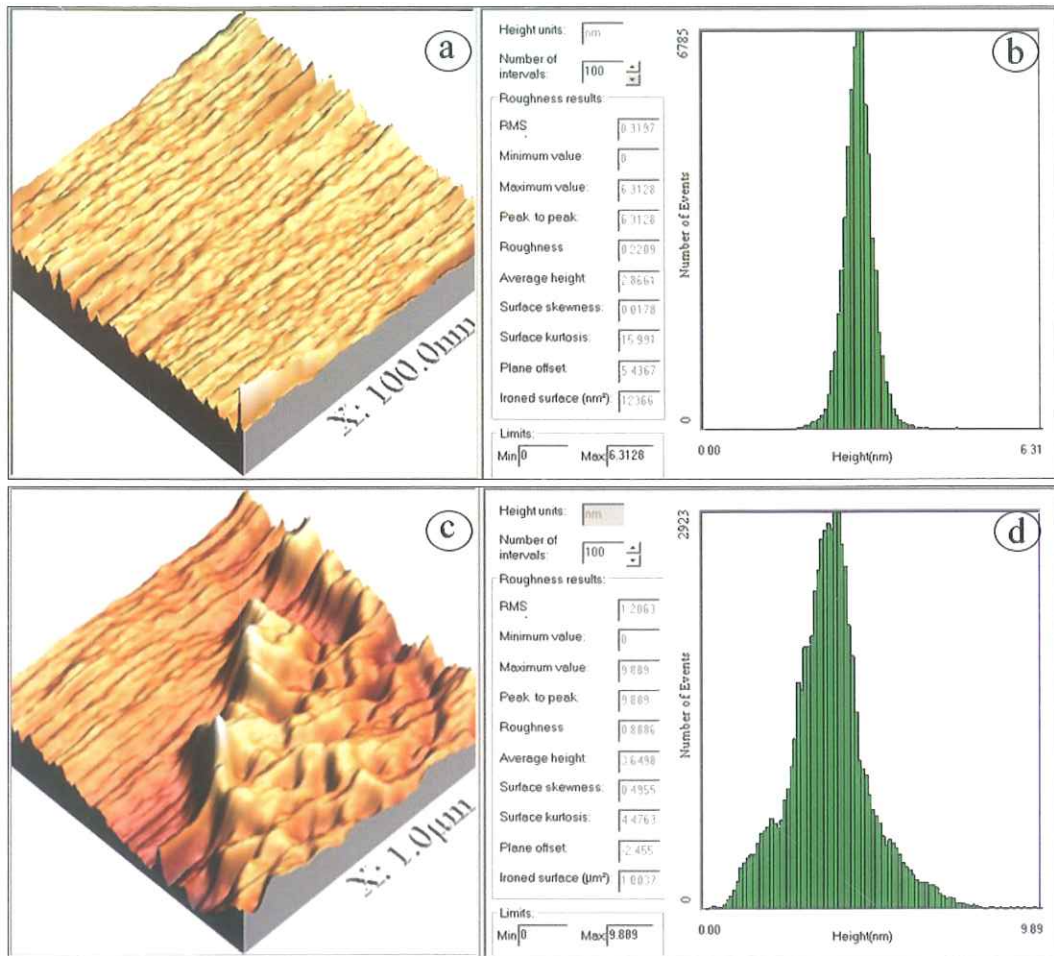
Figure 4. 72   3D Micro Topographies, Corresponding Histograms and Roughness Analyses of Aero 3000C-Treated Muscovite.
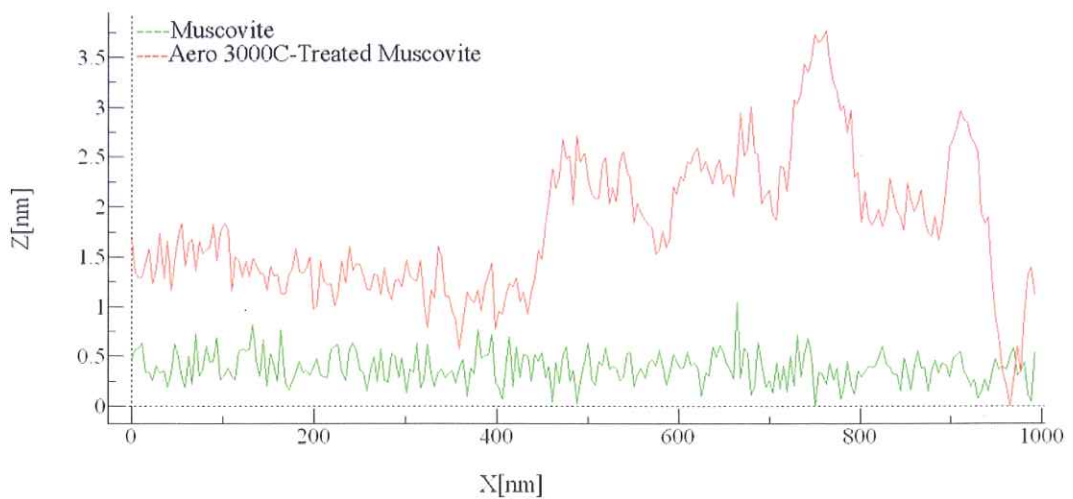
Figure 4. 73   Height Profiles of Muscovite and Aero 3000C-Treated Muscovite in 1μm Size.
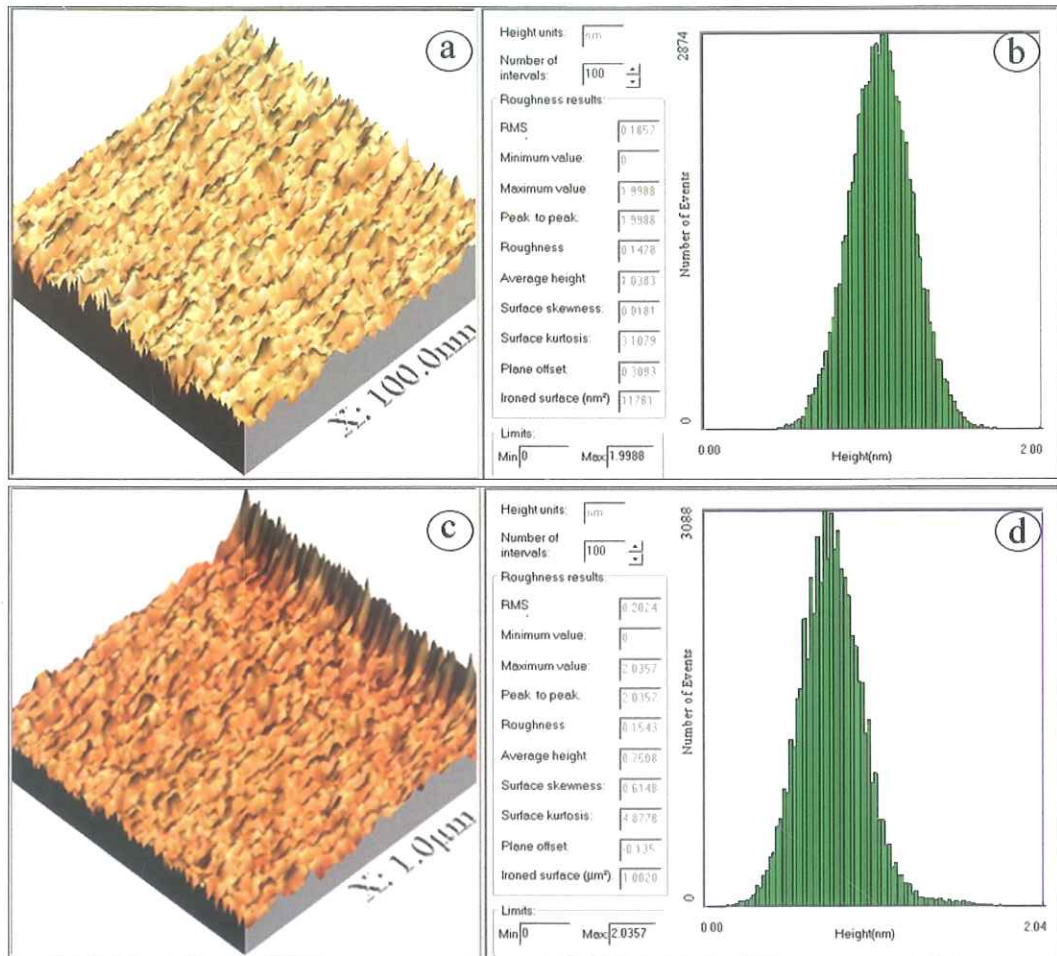
Figure 4. 74   3D Micro Topographies, Corresponding Histograms and Roughness
Analyses of Aero 825-Treated Muscovite.
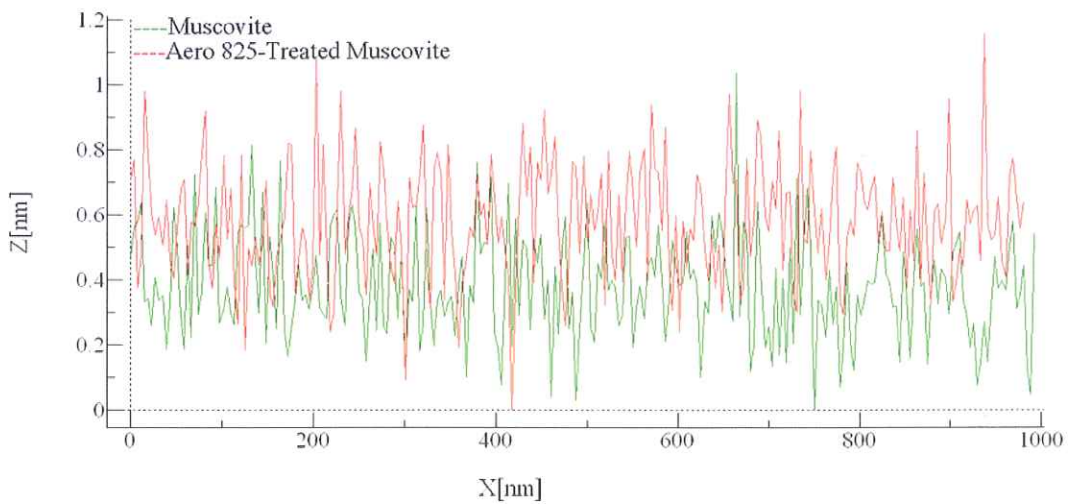
Figure 4. 75   Height Profiles of Muscovite and Aero 825-Treated Muscovite in 1 μm
Size.

4.3.4 FTIR Spectroscopy Studies on Muscovite

In the similar way as albite and biotite, the FTIR analysis of the muscovite, collector-treated muscovite and acetone-washed muscovite samples were examined and the resulting spectra were given in Figure 4.76, Figure 4.81 and Figure 4.86 for Aero 704, Aero 3000C and Aero 825 respectively.

In order to obtain more detailed FTIR spectra, the full scale FTIR spectra (4000-400 cm^{-1}) of collector, non-treated, collector-treated and acetone-washed muscovite samples were analyzed in four major zones depending on the collector's FTIR peaks. Figures 4.77-4.80 show the FTIR ranges of muscovite in the presence of Aero 704 as 3500-2750 cm^{-1}, 2750-1750 cm^{-1}, 1750-1250 cm^{-1} and 1250-400 cm^{-1} major wavelength's zones respectively.

The FTIR spectrum of Aero 704-treated muscovite showed additional bands at 2961 cm^{-1}, 2926 cm^{-1} and 2854 cm^{-1} assigned as CH_2 stretching vibrations (Figure 4.77). The FTIR spectrum of the Aero 704-treated muscovite upon washing with acetone was not altered keeping the bands which represent C-H vibrations.
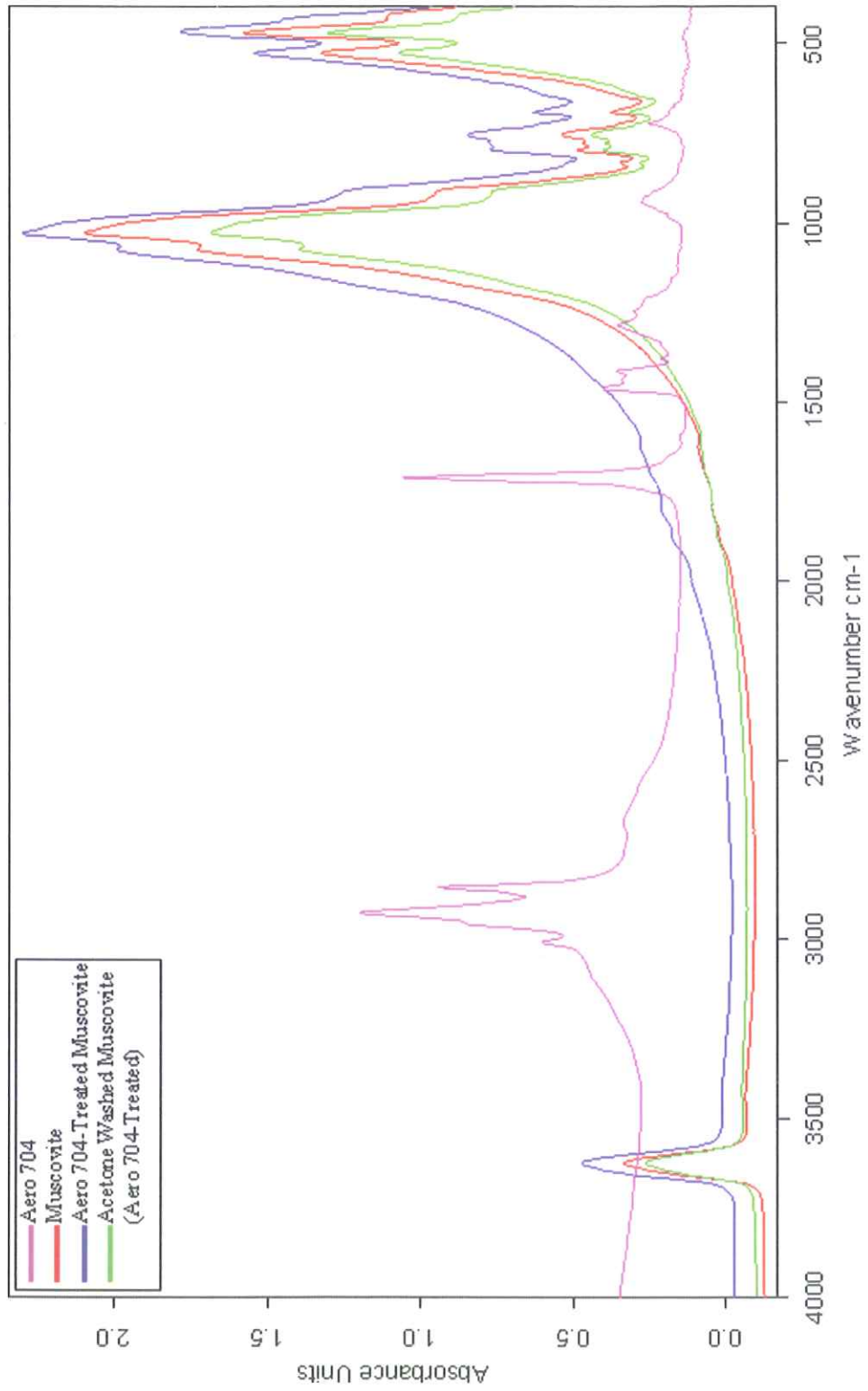
Figure 4. 76   FTIR Spectrum of Muscovite in the Presence of Aero 704 in 4000–400 cm⁻¹ Wavelength Range.

125
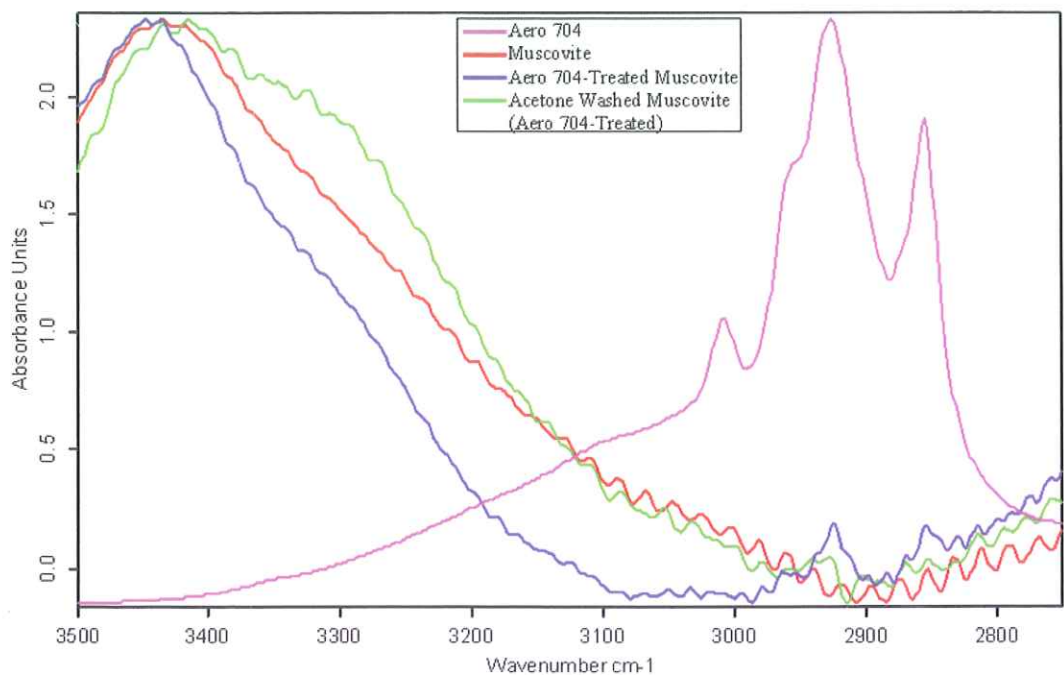
Figure 4. 77   FTIR Spectrum of Muscovite in the Presence of Aero 704 in 3500–2750 cm^{-1} Wavelength Range.
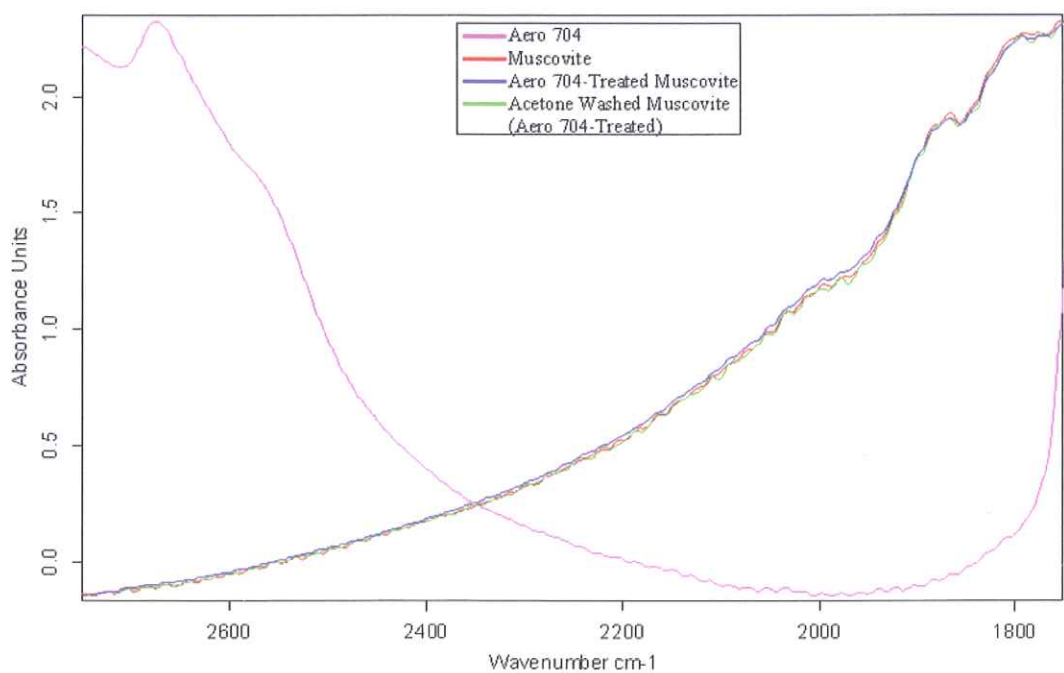
Figure 4. 78   FTIR Spectrum of Muscovite in the Presence of Aero 704 in 2750–1750 cm^{-1} Wavelength Range.

126

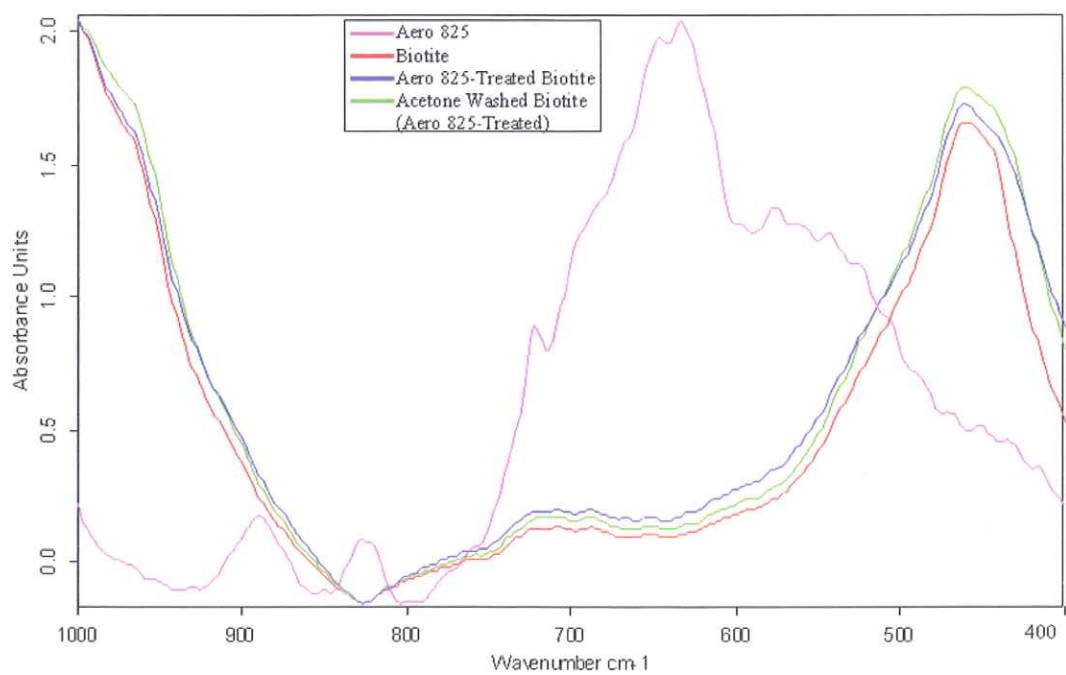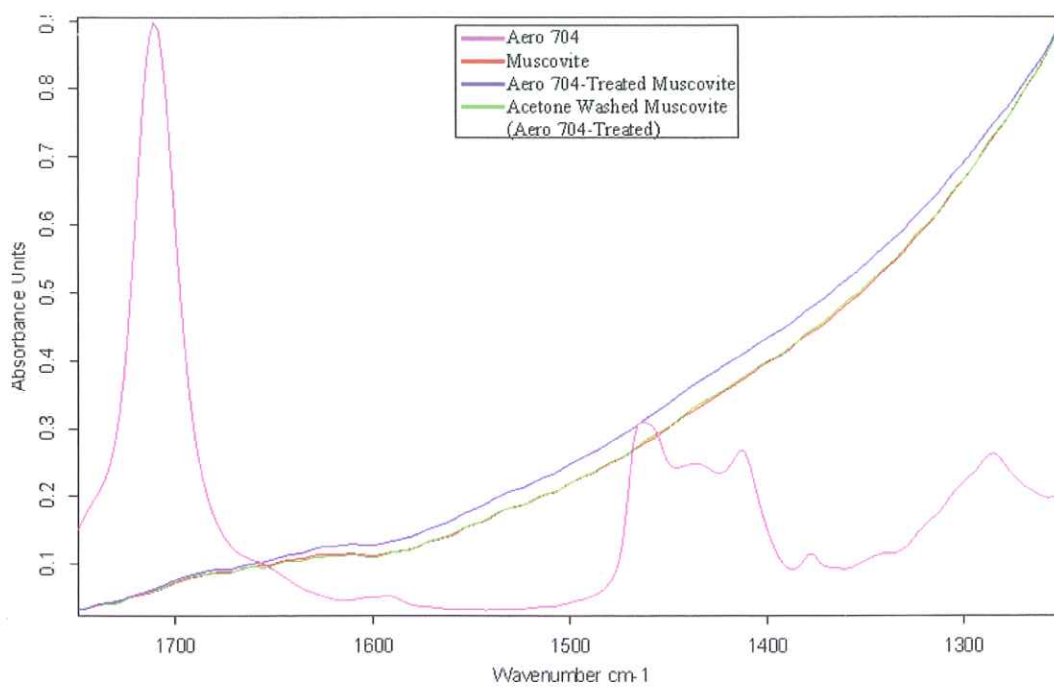Figure 4. 79   FTIR Spectrum of Muscovite in the Presence of Aero 704 in 1750–1250 cm^{-1} Wavelength Range.
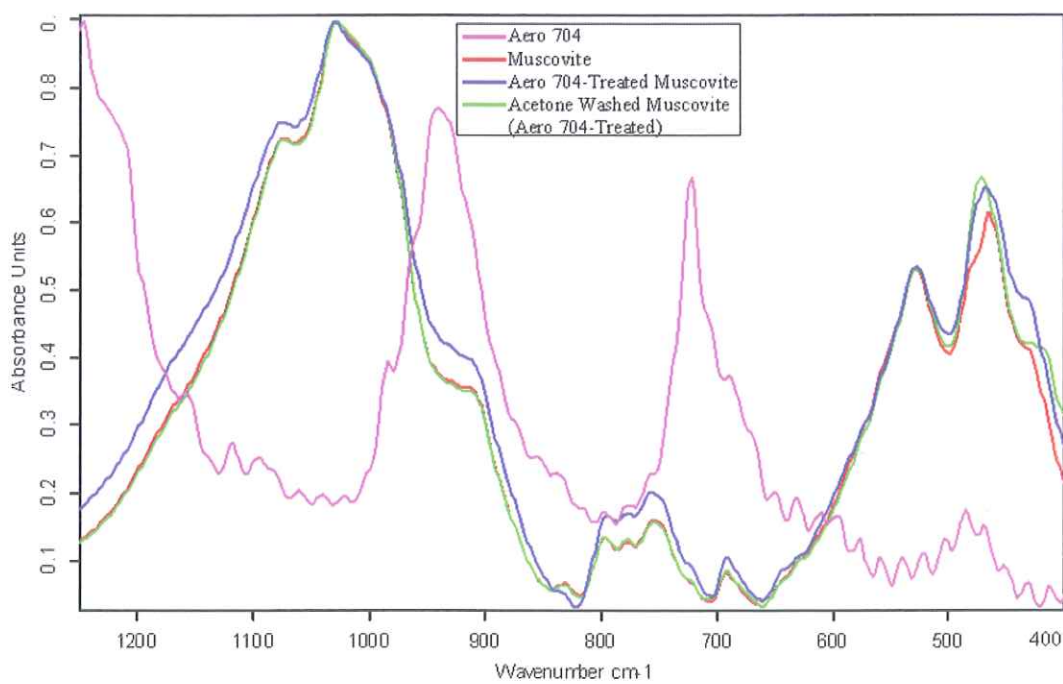
Figure 4. 80   FTIR Spectrum of Muscovite in the Presence of Aero 704 in 1250–400 cm^{-1} Wavelength Range.

The spectra obtained with Aero 3000C, muscovite, Aero 3000C-treated muscovite and acetone-washed muscovite were given in Figures 4.81 to 4.85. The major zones for the muscovite in the presence of Aero 3000C were shown as 3250-2750 cm^{-1}, 2750-1750 cm^{-1}, 1750-1250 cm^{-1} and 1250-400 cm^{-1} wavelengths in Figures 4.82-4.85 respectively.

Aero 3000C-treated muscovite showed additional bands at 2957 cm^{-1}, 2922 cm^{-1} and 2853 cm^{-1} with low intensities assigned as C-H stretching vibrations of Aero 3000C (Figure 4.82). The FTIR spectrum of the Aero 3000C-treated muscovite upon washing with acetone was not altered; the bands were still exist.
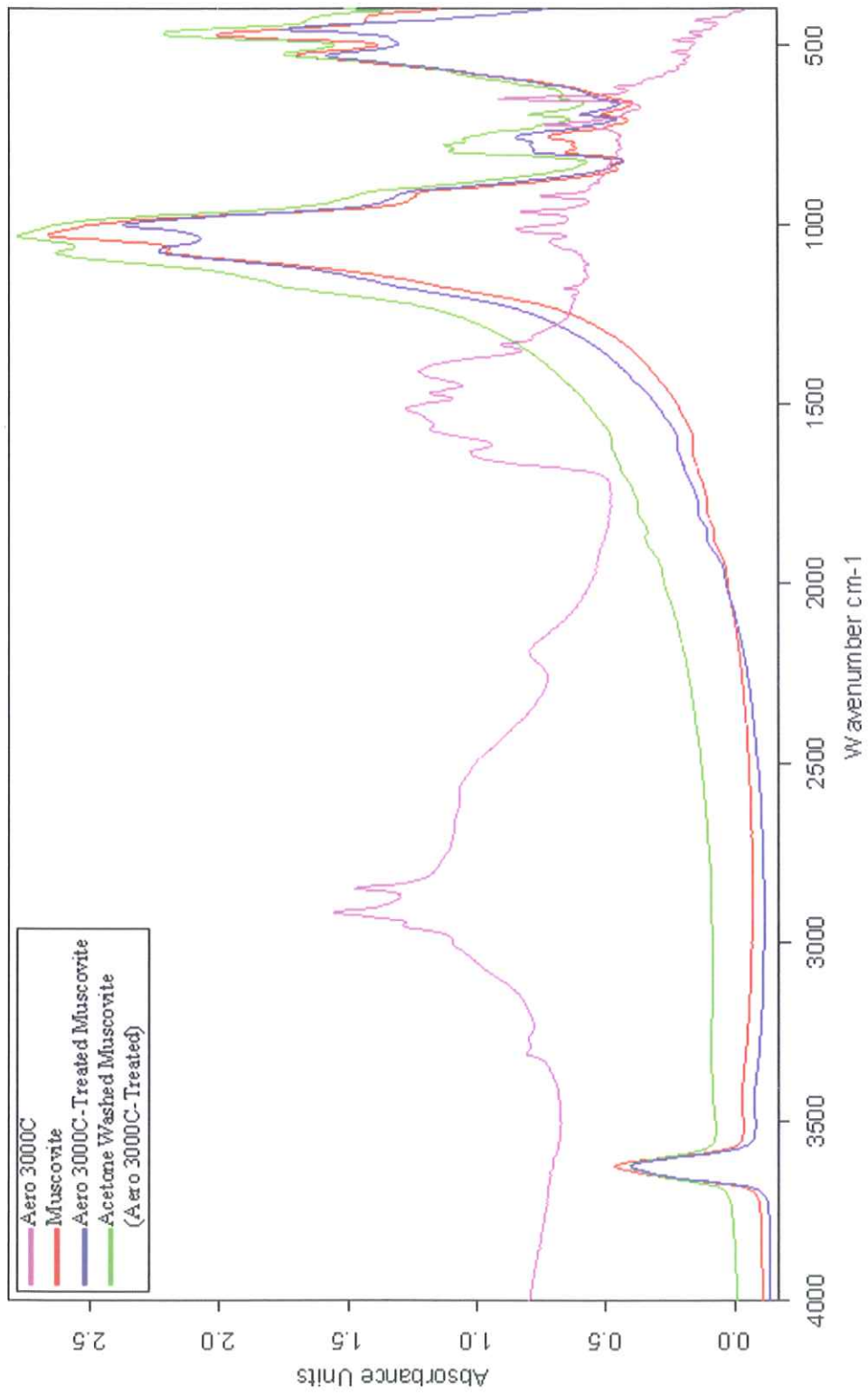
Figure 4. 81   FTIR Spectrum of Muscovite in the Presence of Aero 3000C in 4000–400 cm^{-1} Wavelength Range.
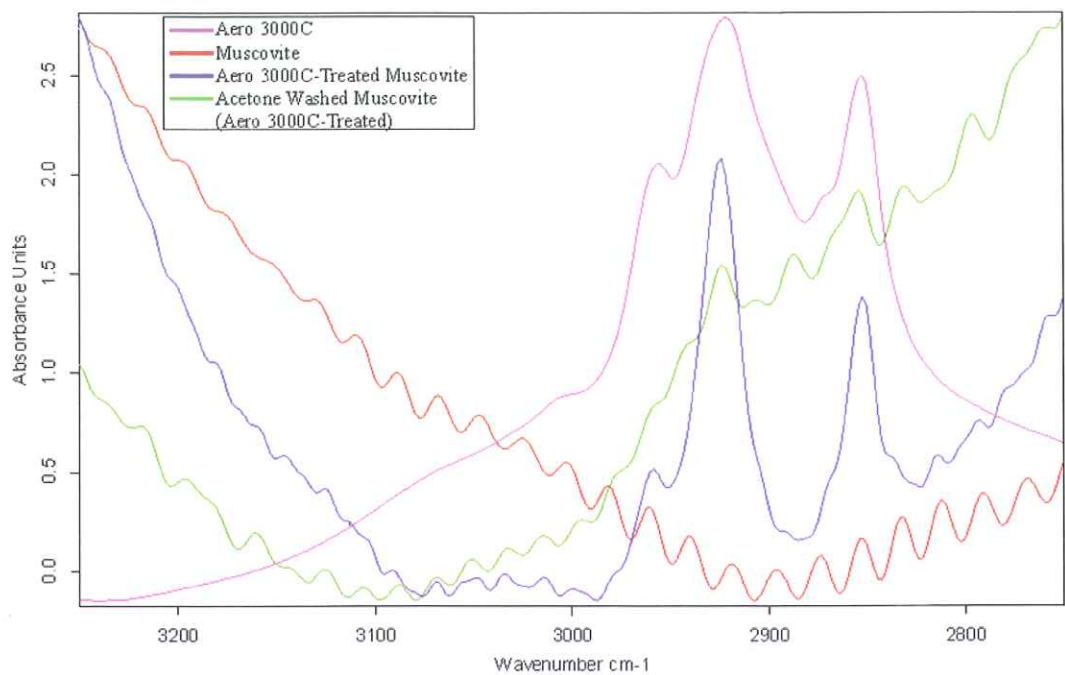
Figure 4. 82   FTIR Spectrum of Muscovite in the Presence of Aero 3000C in 3250–2750 cm^{-1} Wavelength Range.
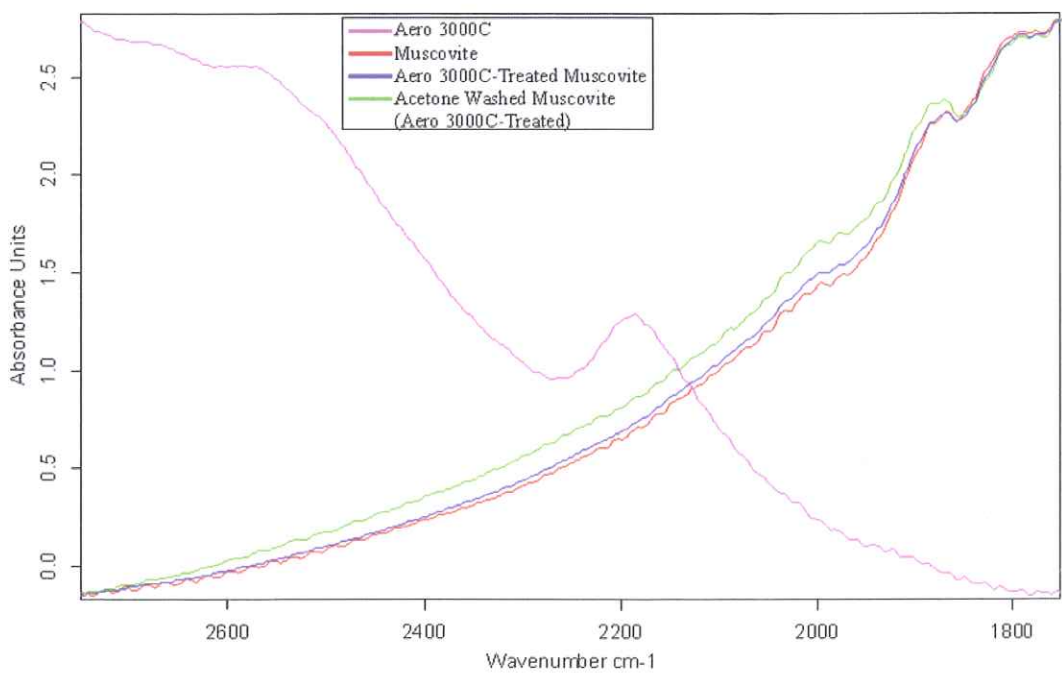
Figure 4. 83   FTIR Spectrum of Muscovite in the Presence of Aero 3000C in 2750–1750 cm^{-1} Wavelength Range.
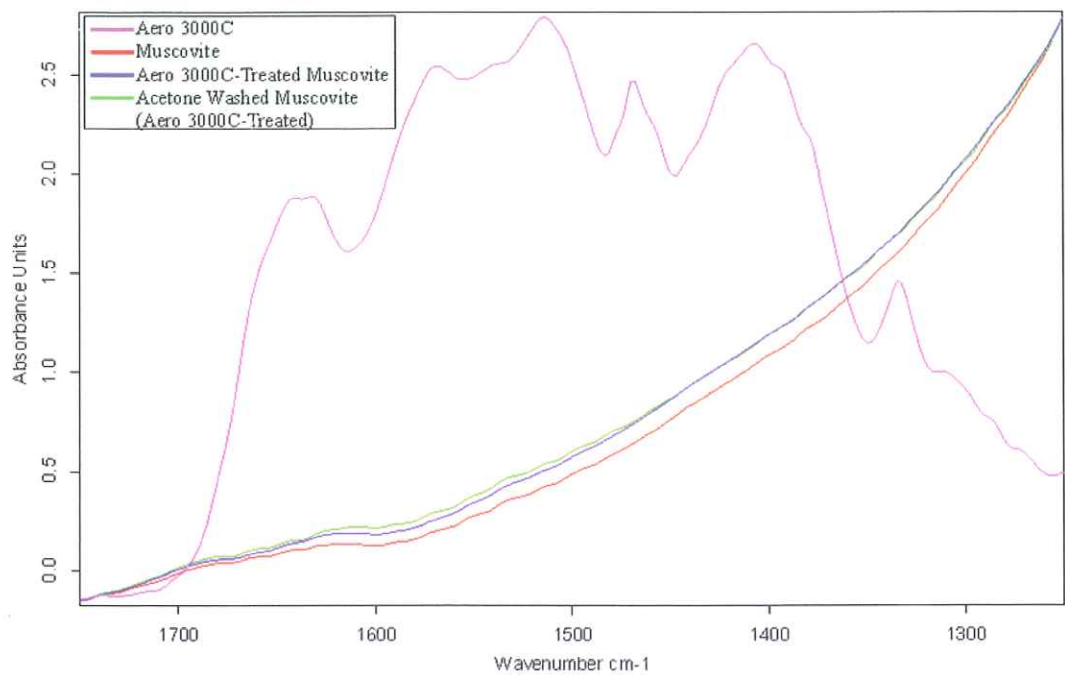
Figure 4. 84   FTIR Spectrum of Muscovite in the Presence of Aero 3000C in 1750–1250 cm^{-1} Wavelength Range.
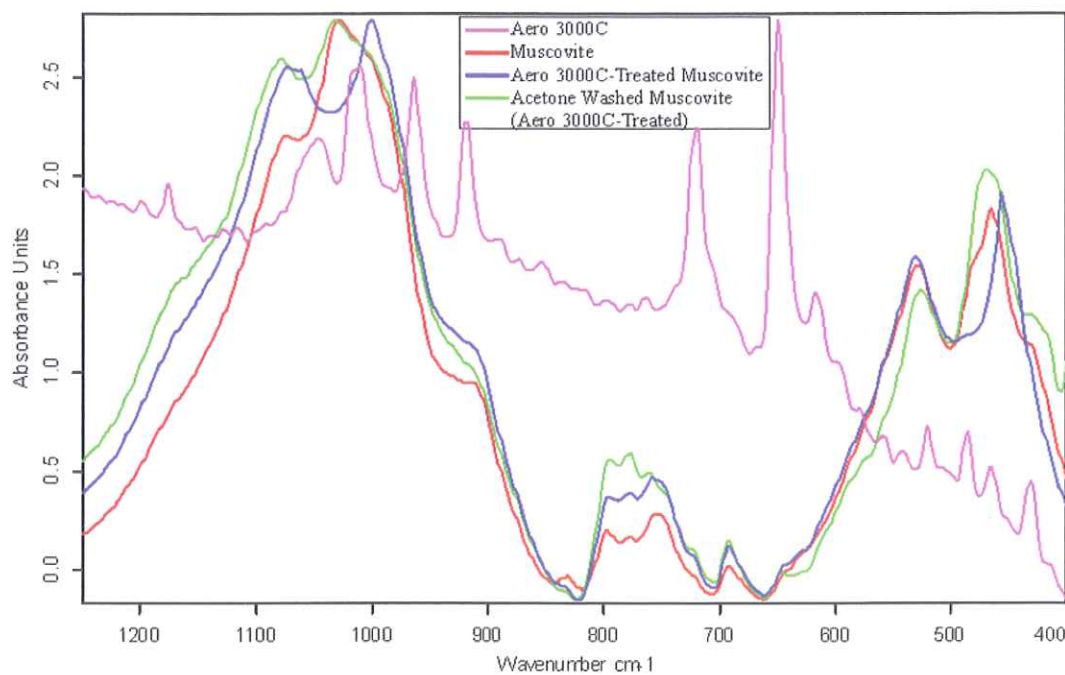
Figure 4. 85   FTIR Spectrum of Muscovite in the Presence of Aero 3000C in 1250–400 cm^{-1} Wavelength Range.

131

The spectra obtained for Aero 825 are given in Figures 4.86-4.90. In order to provide more detailed spectra, the major zones for the muscovite in the presence of Aero 825 were shown in Figures 4.87-4.90 as 3750-2750 cm^{-1}, 2750-1500 cm^{-1}, 1500-1000 cm^{-1} and 1000-400 cm^{-1} wavelengths depending on the Aero 825's FTIR peaks.

In Figure 4.87, the Aero 825-treated muscovite did not display any additional band belonging to Aero 825. The FTIR spectrum of the Aero 825-treated muscovite showed similarities compared to those of muscovite and Aero 825-treated muscovite samples in the given wavelength range upon washing with acetone several times.

Figure 4. 86   FTIR Spectrum of Muscovite in the Presence of Aero 825 in 4000–400 cm^{-1} Wavelength Range.

133

Figure 4. 87   FTIR Spectrum of Muscovite in the Presence of Aero 825 in 3750–2750 cm^{-1} Wavelength Range.
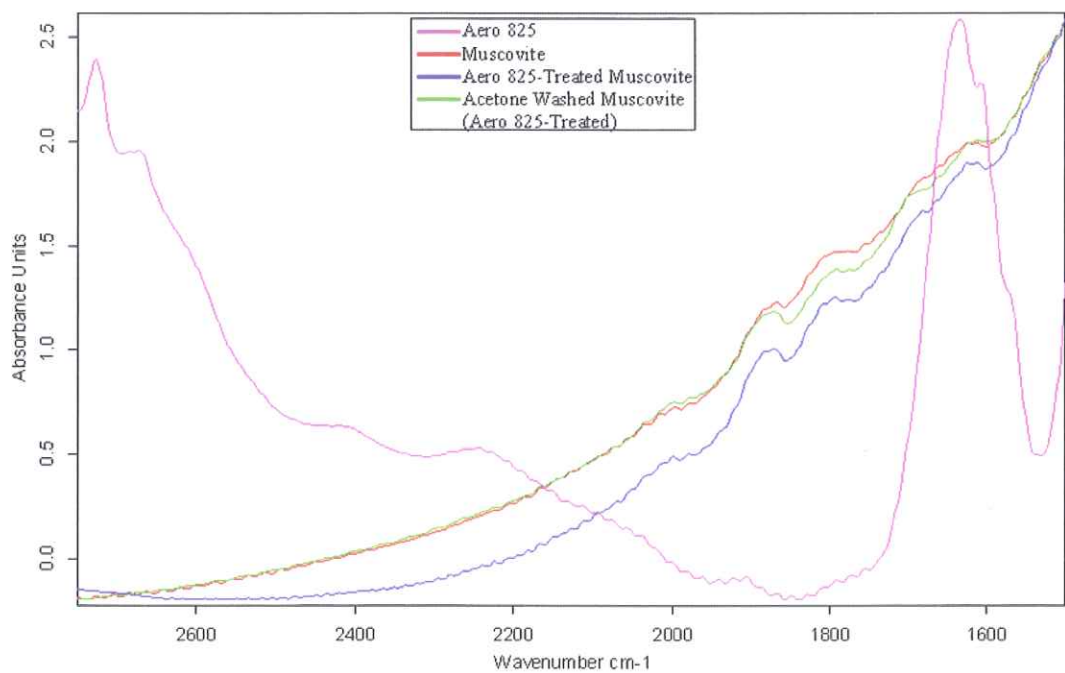
Figure 4. 88   FTIR Spectrum of Muscovite in the Presence of Aero 825 in 2750–1500 cm^{-1} Wavelength Range.

134

Figure 4. 89   FTIR Spectrum of Muscovite in the Presence of Aero 825 in 1500–1000 cm^{-1} Wavelength Range.

Figure 4. 90   FTIR Spectrum of Muscovite in the Presence of Aero 825 in 1000–400 cm^{-1} Wavelength Range.

4.4   Orthoclase Sample

4.4.1   Electrokinetic Potential Measurements on Orthoclase

When the similar procedure was applied in order to obtain the zeta potential values of orthoclase, the i.e.p. was found to be below pH 1.5 in distilled water and in 1.0×10^{-3} M of KCl. The results are given in Figure 4.91 as function of pH. It is seen that above the i.e.p. the zeta potential values became more negative towards the more basic region.
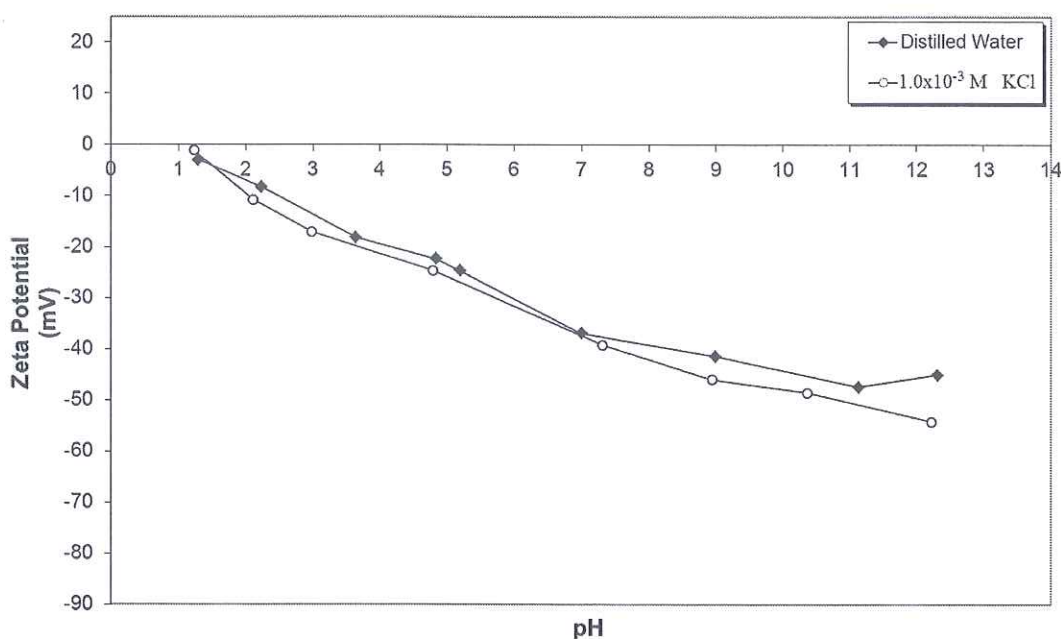
Figure 4. 91   Zeta Potential of Orthoclase as a Function of pH.

Figure 4.92 shows the effect of 1.0×10^{-4} M, 5.0×10^{-4} M and 1.0×10^{-3} M of Aero 704 on the electrokinetic potential of orthoclase. The zeta potential values of orthoclase decreased with increasing Aero 704 concentration and pH.

The zeta potential values of orthoclase in the presence of 5.0×10^{-5} M, 1.0×10^{-4} M and 5.0×10^{-4} M of Aero 3000C as a function of pH were shown in Figure 4.93. The zeta

potential values increased proportionally to Aero 3000C concentration and pH. The i.e.p. was shifted from about pH 1.5 to highly alkali conditions, about pH 10.8 and the surface of the sample was positively charged up to given pH.

Figure 4.94 displays the zeta potential values of orthoclase in the presence of 1.0×10^{-4} M, 5.0×10^{-4} M and 1.0×10^{-3} M of Aero 825 as a function of pH. The zeta potential values of orthoclase decreased with increasing Aero 825 concentration.

The results of the electrokinetic potential measurements in the presence of varying Aero 3000C (as amine) and Aero 825 (as sulfonate) concentrations are confirmed by the results of the electrokinetic potential measurements obtained by Vidyadhar et al., 2007 [45].
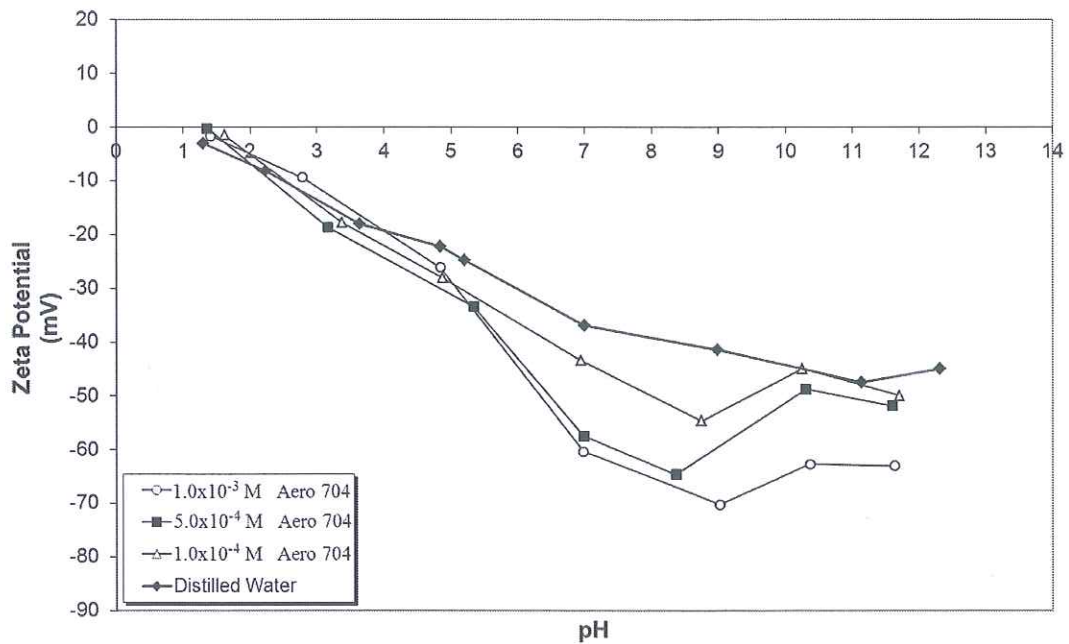
Figure 4. 92   Zeta Potential of Orthoclase as a Function of pH and Aero 704 Concentration.
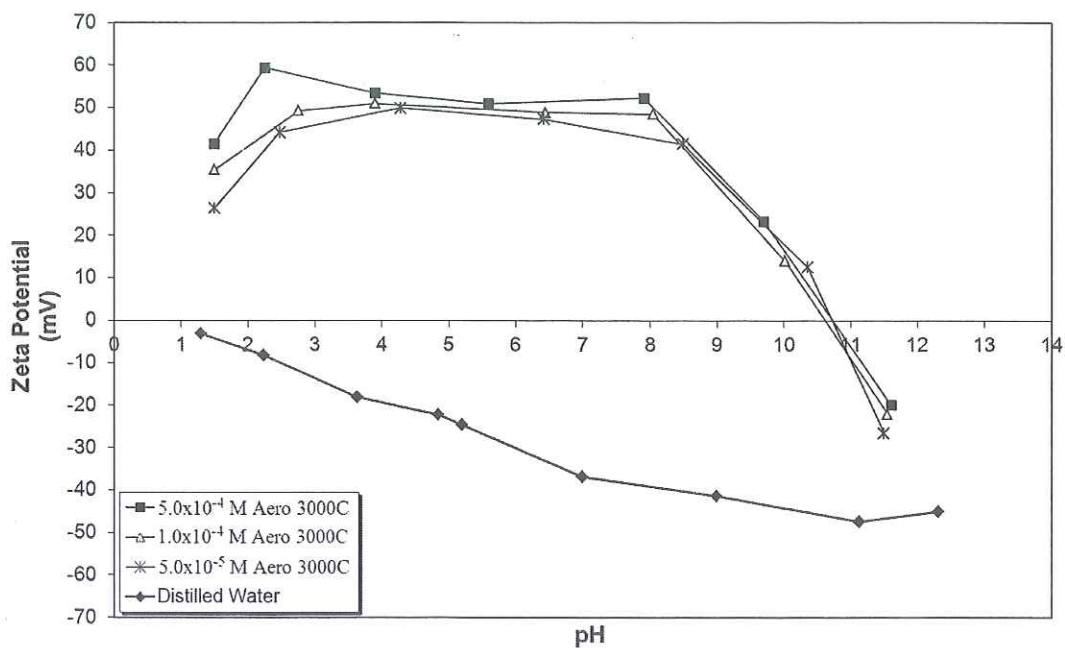
Figure 4. 93   Zeta Potential of Orthoclase as a Function of pH and Aero 3000C Concentration.
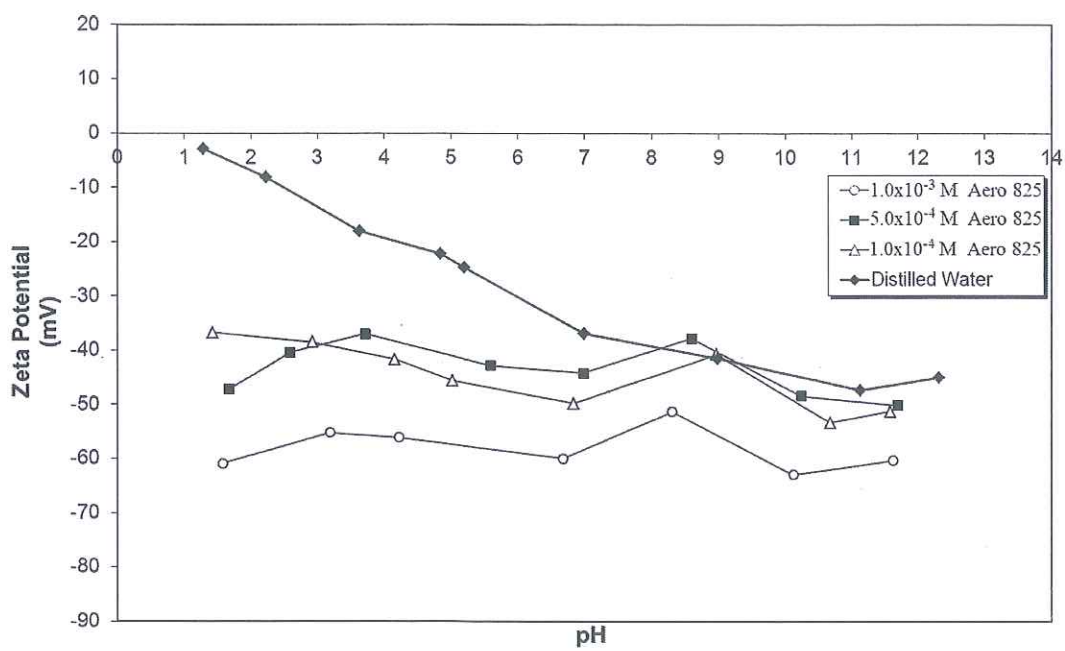
Figure 4. 94   Zeta Potential of Orthoclase as a Function of pH and Aero 825 Concentration.

Additional electrokinetic potential measurements in order to investigate the effect of acetone washing on the zeta potential values of the collector-treated orthoclase samples were carried out as a function on pH. The samples were first conditioned with each collector in optimum flotation conditions and then washed with acetone several times prior to electrokinetic potential measurements. The optimum conditions were 3.5×10^{-4} M of Aero 704 about pH 9.5, 5.0×10^{-5} M of Aero 3000C about pH 3.0, 2.0×10^{-4} M of Aero 825 about pH 5.0. The results showed that the zeta potential values were found to be very similar to each other for all pH ranges (Figure 4.95).

Figure 4. 95   Zeta Potentials of Aero 704, Aero 3000C and Aero 825 Treated Orthoclase Samples After Acetone Washing.

4.4.2   Flotation Studies on Orthoclase

The flotation recoveries of orthoclase as a function of pH and Aero 704 concentration were shown in Figure 4.96. As the flotation recovery of orthoclase was null below pH 7.0, the micro-flotation experiments were performed from this pH on with all Aero 704 concentrations. It is seen that the flotation recovery of the orthoclase increased proportionally to Aero 704 concentration. The maximum

flotation recoveries were obtained as 27.0% with 2.0×10^{-4} M, 75.0% with 2.75×10^{-4} M, 78.0% with 3.5×10^{-4} M and 74.0% in 5.0×10^{-4} M of Aero 704 in the pH range of 9.0-10.5.

The flotation recoveries of the orthoclase were maximum between the pH 3.5 and 10.5 with the values of 40.0% with 2.0×10^{-5} M, 86.5% with 5.0×10^{-5} M, 89.0% with 7.5×10^{-5} M and 90.0% with 1.0×10^{-4} M of Aero 3000C respectively (Figure 4.97). The flotation recoveries decreased sharply above and below pH where the maximum recoveries were obtained for all Aero 3000C concentrations.

In the case of Aero 825, the flotation recoveries of orthoclase were shown in Figure 4.98 as function of pH and concentration. As illustrated in the figure, the flotation recoveries were almost null in all Aero 825 concentrations, 1.5×10^{-4} M, 2.0×10^{-4} M, 5.0×10^{-4} M and 1.0×10^{-3} M and pH. The maximum flotation recovery obtained was about 10.0% even in the presence of highest Aero 825 concentration experimented, 1.0×10^{-3} M.
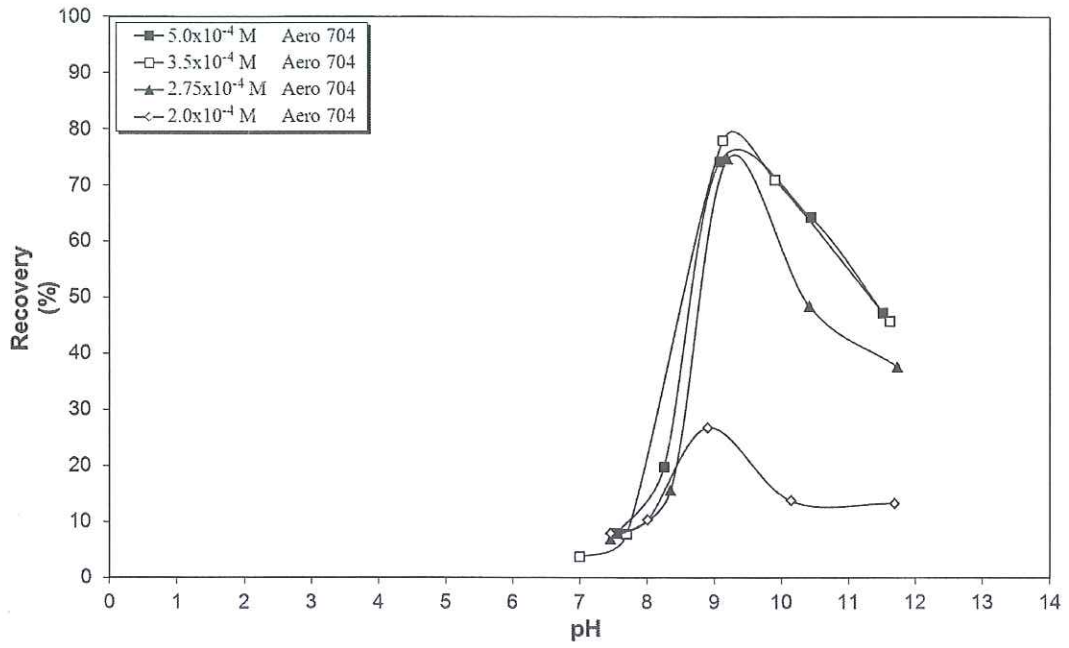
Figure 4. 96   Flotation Recovery of Orthoclase as a Function of pH and Aero 704
Concentration.
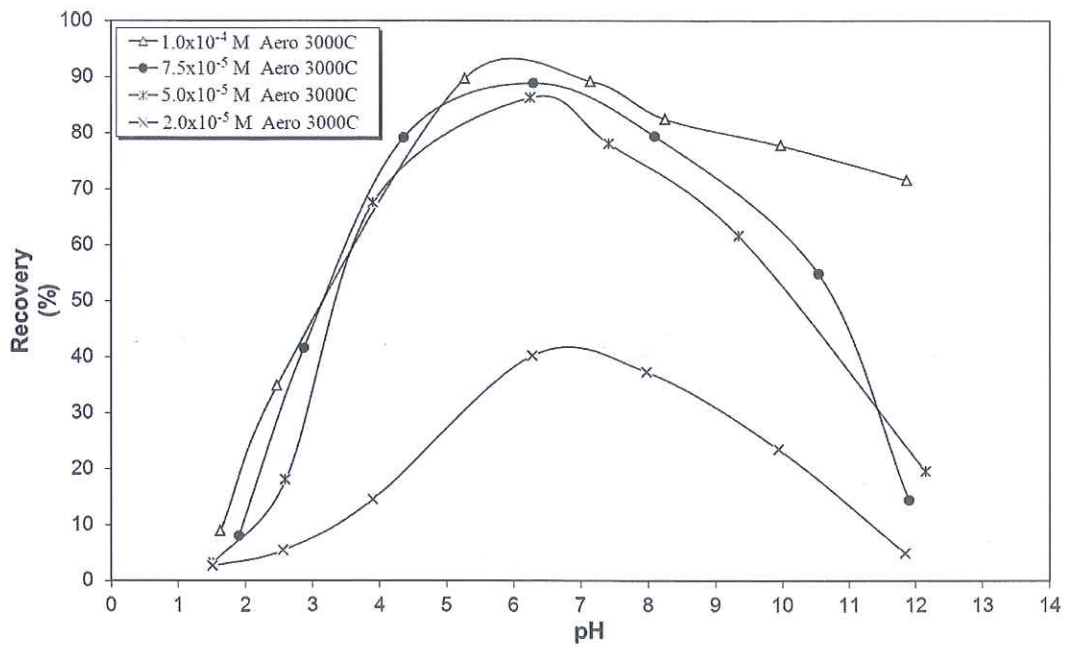
Figure 4. 97   Flotation Recovery of Orthoclase as a Function of pH and Aero
3000C Concentration.

141
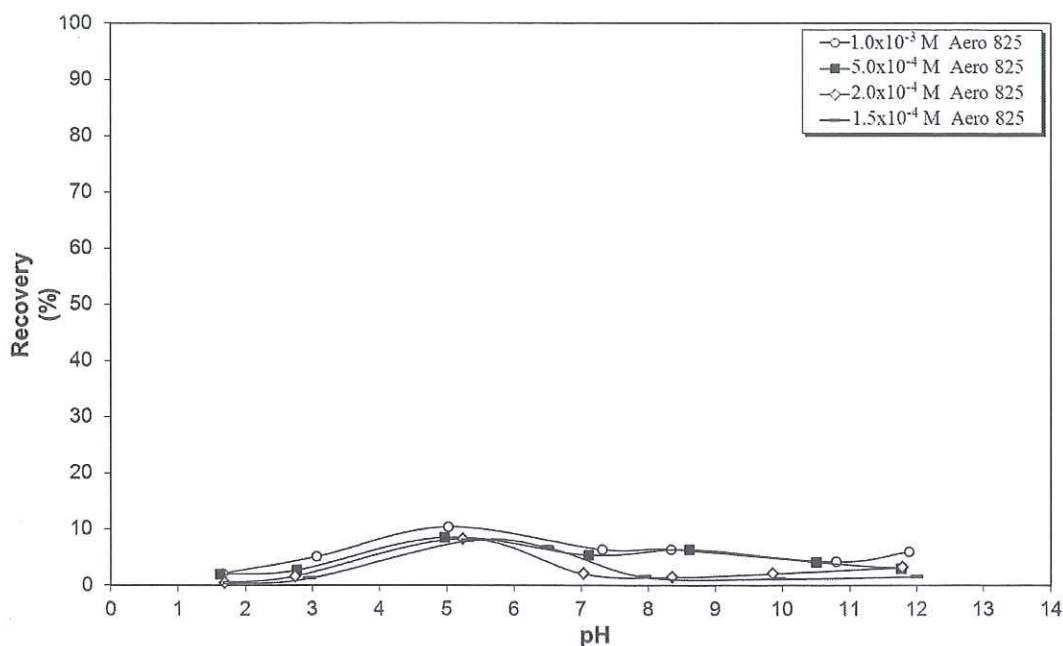
Figure 4. 98   Flotation Recovery of Orthoclase as a Function of pH and Aero 825
Concentration.

4.4.3 AFM Studies on Orthoclase

The tapping mode AFM 3D micro topographies of orthoclase in 100nm (Figure 4.99a) and 1μm (Figure 4.99c) sizes and their corresponding histograms and roughness analyses (Figure 4.99b and Figure 4.99d) were given in Figure 4.99. The resulting histogram provides information about the surface roughness, the maximum peak value and the average height values of orthoclase for 100nm x 100nm and 1μm x 1μm scanning size ranges. The corresponding histograms revealed the roughness average as 0.2001nm, the maximum peak value as 1.8966nm and the average height value as 0.8434nm for 100nm x 100nm scanning size range and 0.8953nm, 7.1194nm and 3.2007nm for 1μm x 1μm scanning size range respectively.

142
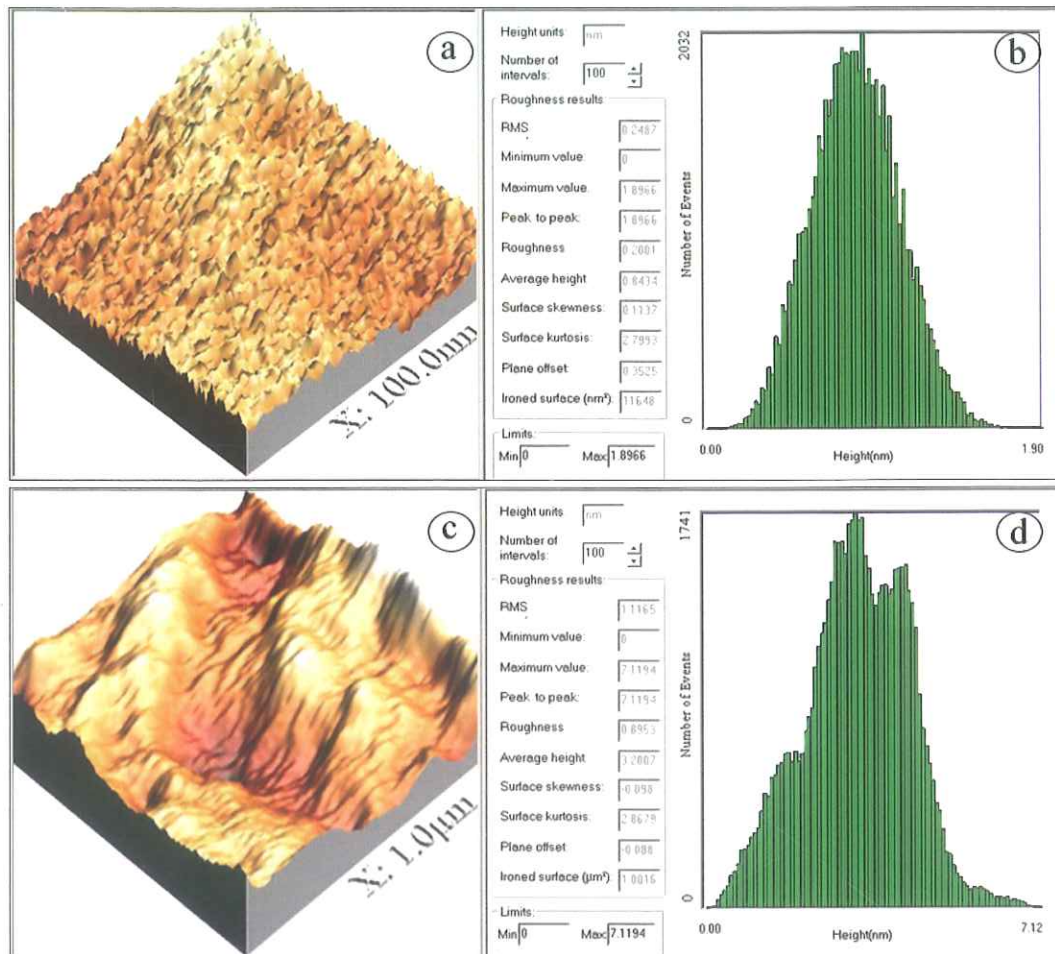
Figure 4. 99   3D Micro Topographies, Corresponding Histograms and Roughness
Analyses of Orthoclase.

The tapping mode AFM 3D micro topographies (Figure 4.100a and 4.100c) and the
corresponding histograms (Figure 4.100b and 4.100d) of the Aero 704-treated
orthoclase revealed the roughness average as 0.4264nm, the maximum peak value as
3.5243nm and the average height value as 1.2551nm for 100nm x 100nm scanning
size and 1.1422nm, 11.6450nm and 3.7867nm for 1μm x 1μm scanning size range,
respectively (Figure 4.100). The tapping mode AFM image analysis of orthoclase
and Aero 704-treated orthoclase based on their height profiles in 1μm were shown in
Figure 4.101 for the scanned area. The orthoclase, shown in green, displayed height
profiles less than 3.0nm while the height profiles of Aero 704-treated orthoclase
reached up to 5.0nm.

143
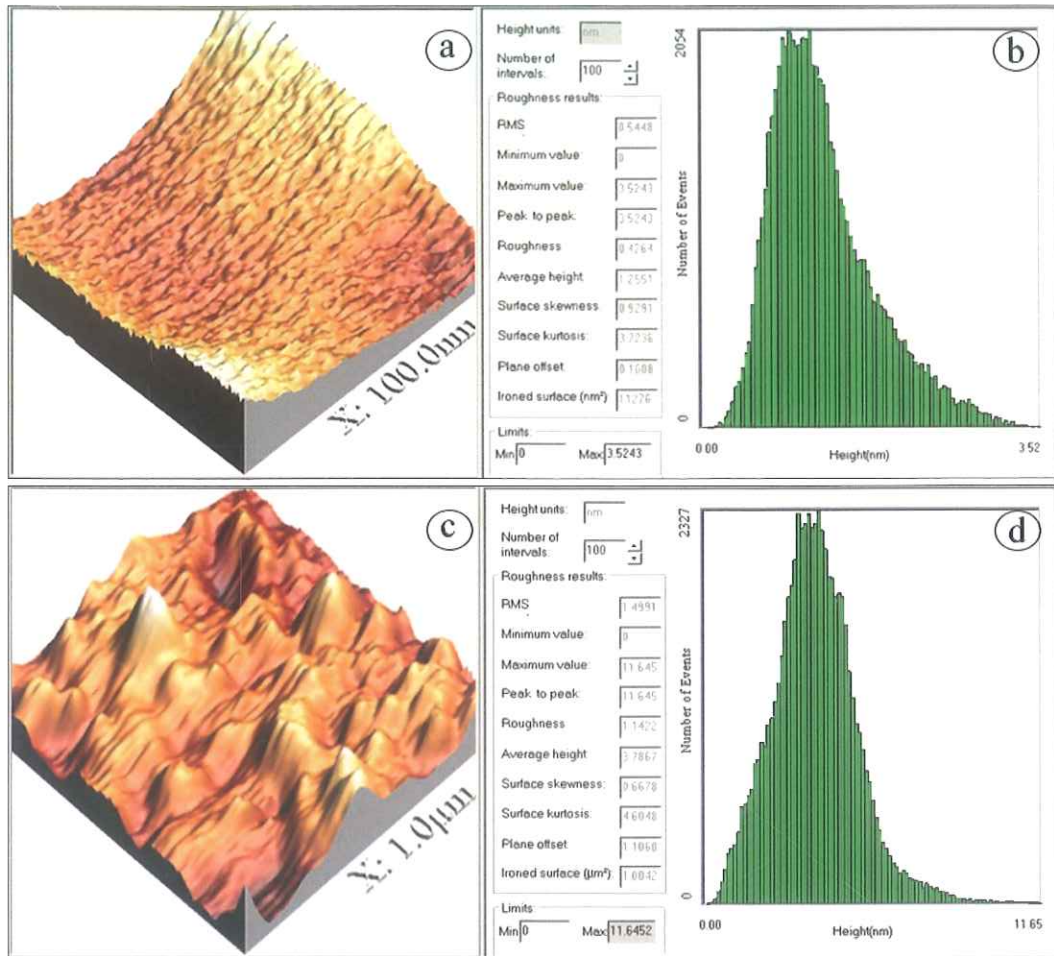
Figure 4. 100 3D Micro Topographies, Corresponding Histograms and Roughness Analyses of Aero 704-Treated Orthoclase.
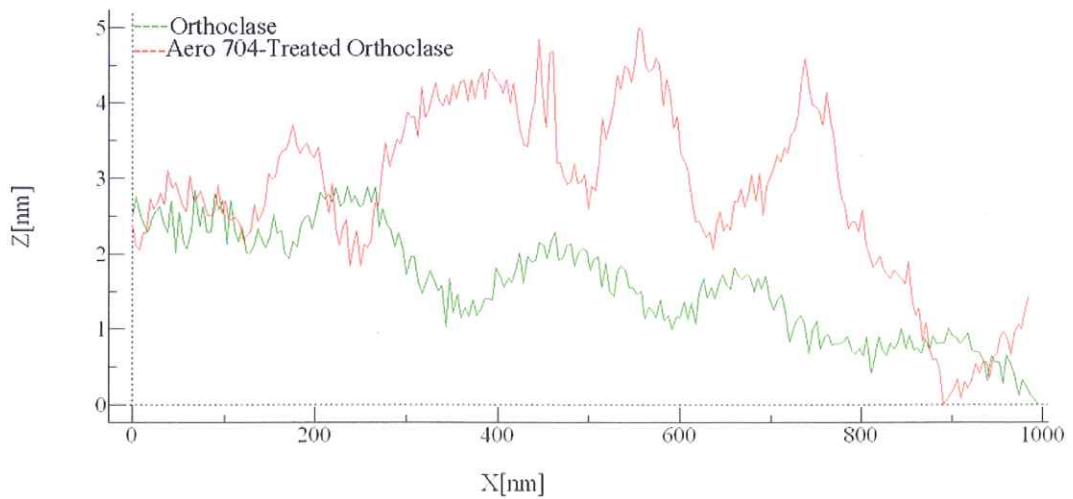
Figure 4. 101 Height Profiles of Orthoclase and Aero 704-Treated Orthoclase in 1μm Size.

The tapping mode AFM 3D micro topographies and the corresponding histograms of Aero 3000C-treated and Aero 825-treated orthoclase in 100nm x 100nm (Figure 4.102a-b for Aero 3000C-treated and Figure 4.104a-b for Aero 825-treated orthoclase) and 1μm x 1μm (Figure 4.102c-d for Aero 3000C-treated and Figure 4.104c-d for Aero 825-treated orthoclase) scanning size ranges were given in Figure 4.102 and Figure 4.104 respectively. For Aero 3000C-treated orthoclase, the histograms revealed that the roughness averages, the maximum peak values and the average height values as 0.5131nm, 4.3604nm and 1.6793nm for 100nm x 100nm scanning size and 1.4677nm, 11.0950nm and 4.3441nm for 1μm x 1μm scanning size range, respectively. In the case of Aero 825-treated orthoclase, the roughness averages, the maximum peak values and the average height values were obtained as 0.2687nm, 3.1966nm and 1.0676nm for 100nm x 100nm scanning size range and 2.1019nm, 20.5560nm, 10.2350nm for 1μm x 1μm scanning size range respectively

The tapping mode AFM image analysis of orthoclase and Aero 3000C-treated orthoclase based on their height profiles in 1μm was shown in Figure 4.103 for the scanned area. Similarly, the tapping mode AFM image analysis of orthoclase and Aero 825-treated orthoclase was shown in Figure 4.105. The height profiles of Aero 3000C-treated orthoclase reached to 6.0nm while the orthoclase, shown in green, displayed height profiles less than 3.0nm. In the case of Aero 825, the Aero 825-treated orthoclase and orthoclase (shown in green in the figures), displayed similarities with very low height profile difference, less than 1.5nm, compared to each other for the scanned area.
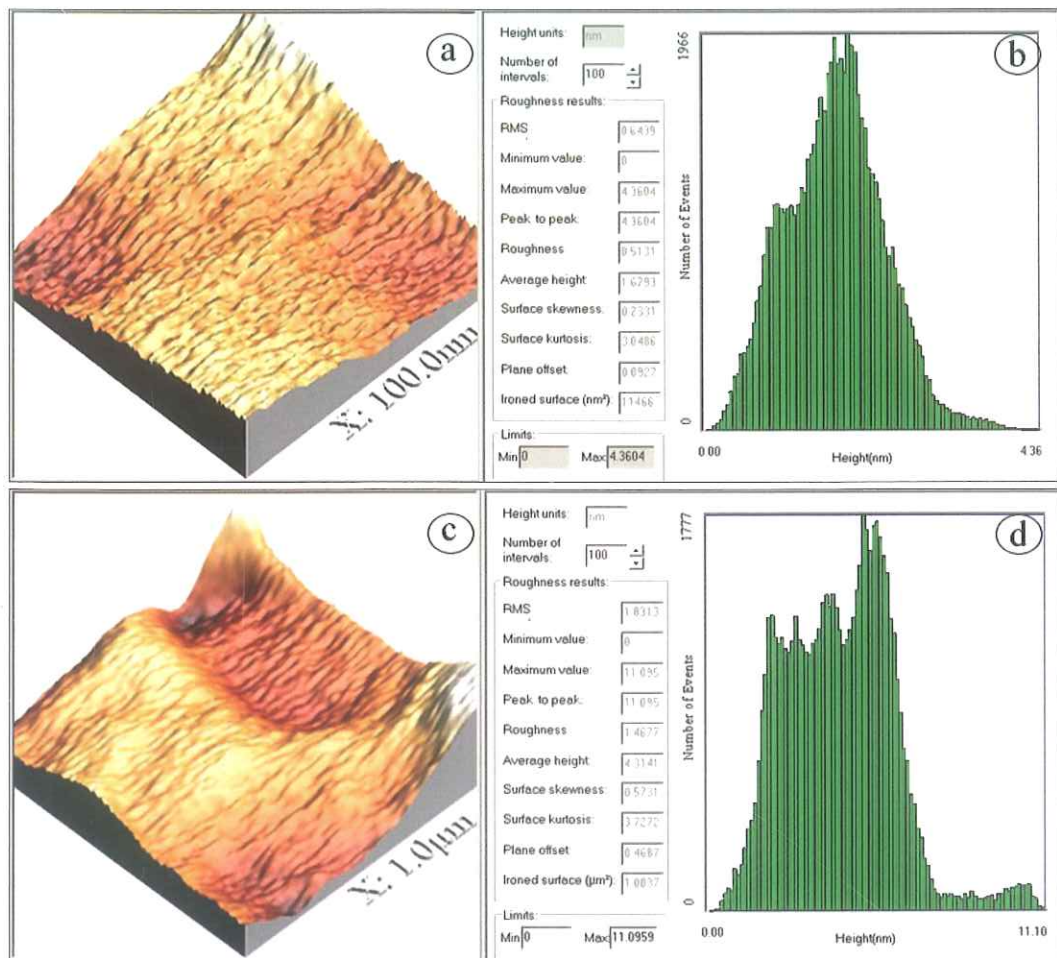
Figure 4. 102 3D Micro Topographies, Corresponding Histograms and Roughness Analyses of Aero 3000C-Treated Orthoclase.
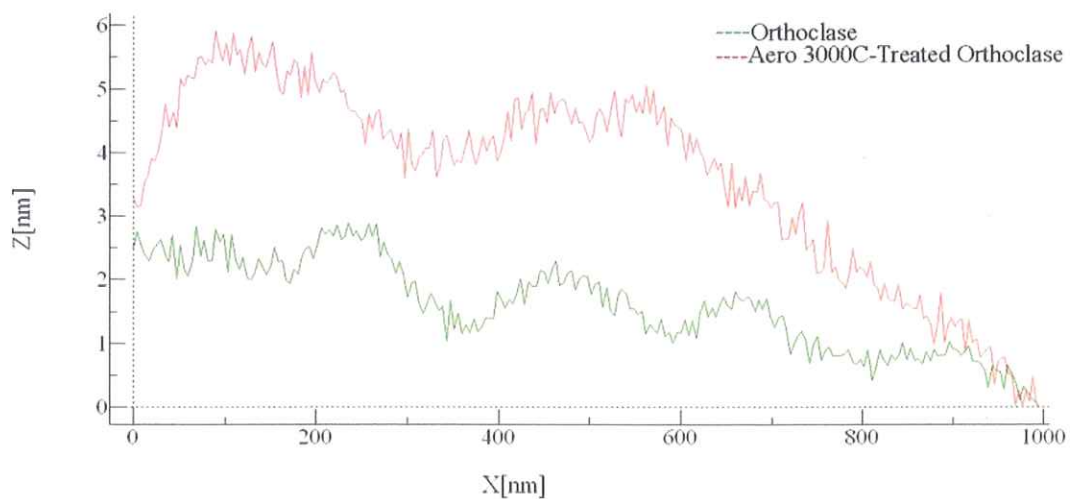
Figure 4. 103 Height Profiles of Orthoclase and Aero 3000C-Treated Orthoclase in 1μm Size.

Figure 4. 104 3D Micro Topographies, Corresponding Histograms and Roughness Analyses of Aero 825-Treated Orthoclase.
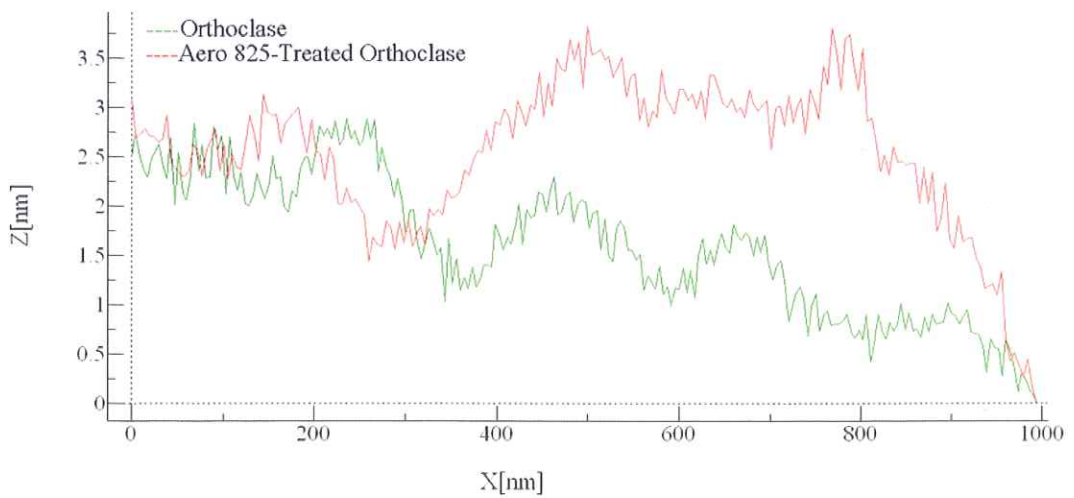
Figure 4. 105 Height Profiles of Orthoclase and Aero 825-Treated Orthoclase in 1μm Size.

147

4.4.4   FTIR Spectroscopy Studies on Orthoclase

In the similar way as previous mineral samples, the FTIR analysis of the orthoclase, collector-treated orthoclase and acetone-washed orthoclase samples were examined and the resulting spectra were given in Figure 4.106, Figure 4.111 and Figure 4.116 for Aero 704, Aero 3000C and Aero 825 respectively.

In order to obtain more detailed FTIR spectra, the full scale FTIR spectra (4000-400 cm^{-1}) of collector, non-treated, collector-treated and acetone-washed orthoclase samples were analyzed in four major zones depending on the collector's FTIR peaks. Figures 4.107-4.110 show the FTIR ranges of orthoclase in the presence of Aero 704 as 3500-2750 cm^{-1}, 2750-1750 cm^{-1}, 1750-1250 cm^{-1} and 1250-400 cm^{-1} major wavelength's zones respectively.

The FTIR spectrum of Aero 704-treated orthoclase showed additional weak bands at 2961 cm^{-1}, 2926 cm^{-1} and 2854 cm^{-1} assigned as CH_2 stretching vibrations (Figure 4.107). The FTIR spectrum of the Aero 704-treated orthoclase was altered upon washing several times with acetone and the bands at 2961 cm^{-1}, 2926 cm^{-1} and 2854 cm^{-1} disappeared.
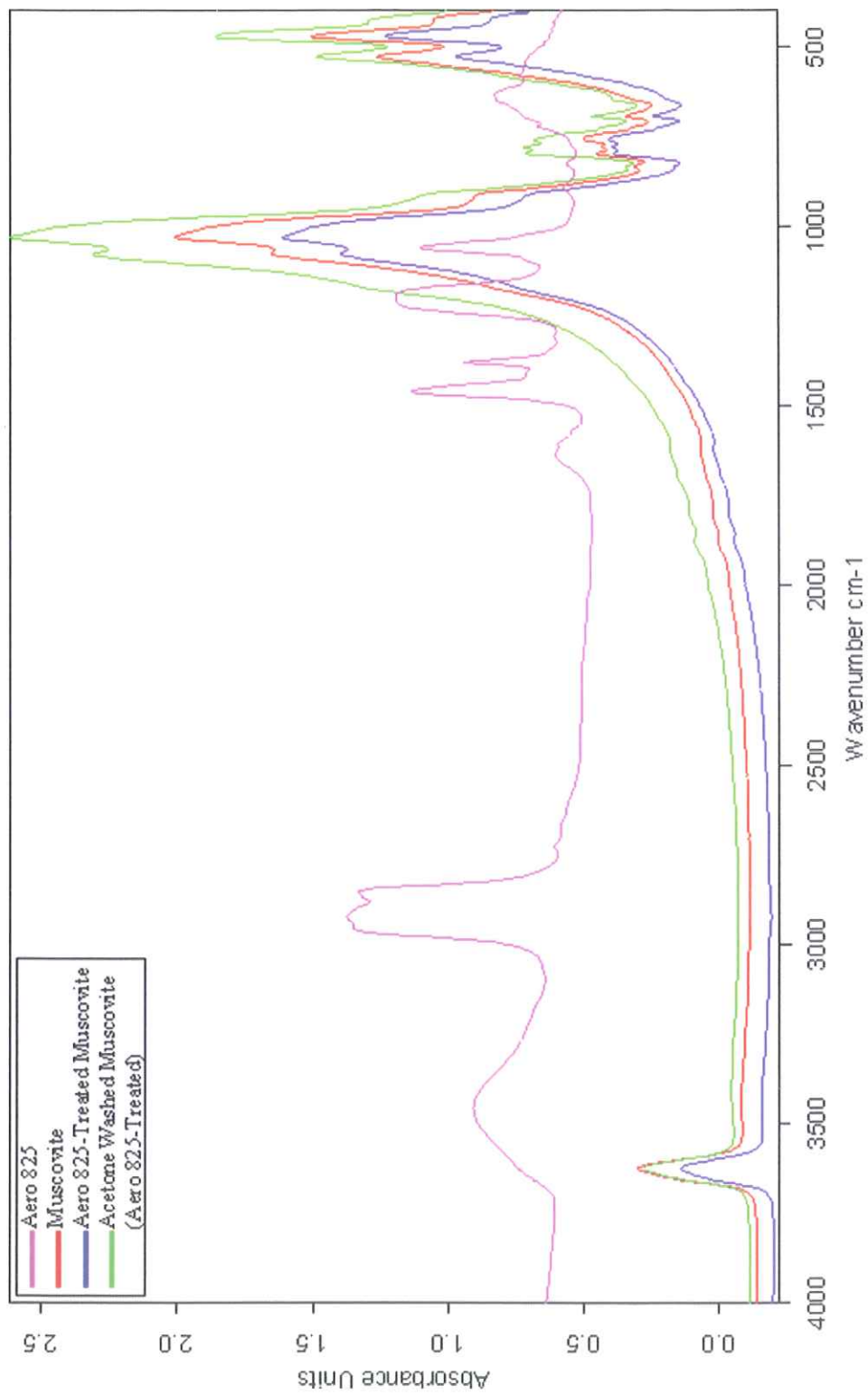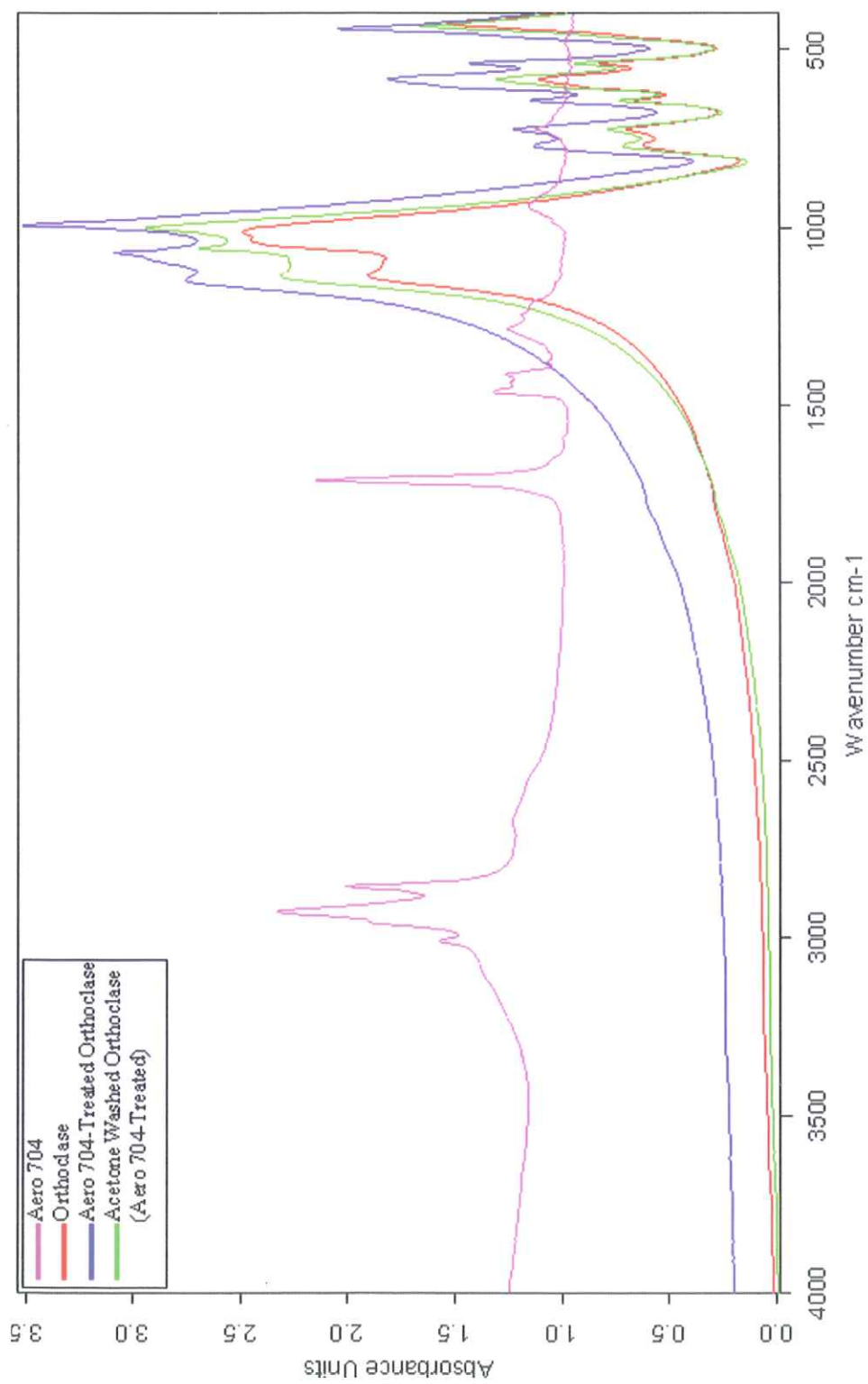
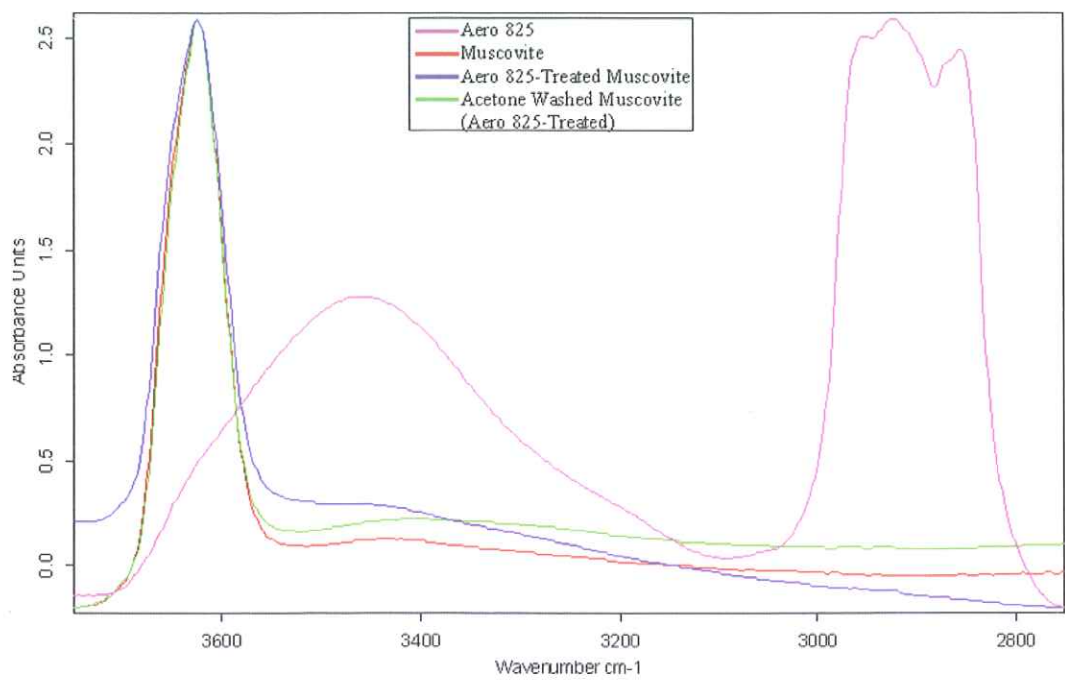Figure 4. 106 FTIR Spectrum of Orthoclase in the Presence of Aero 704 in 4000–400 cm^{-1} Wavelength Range.
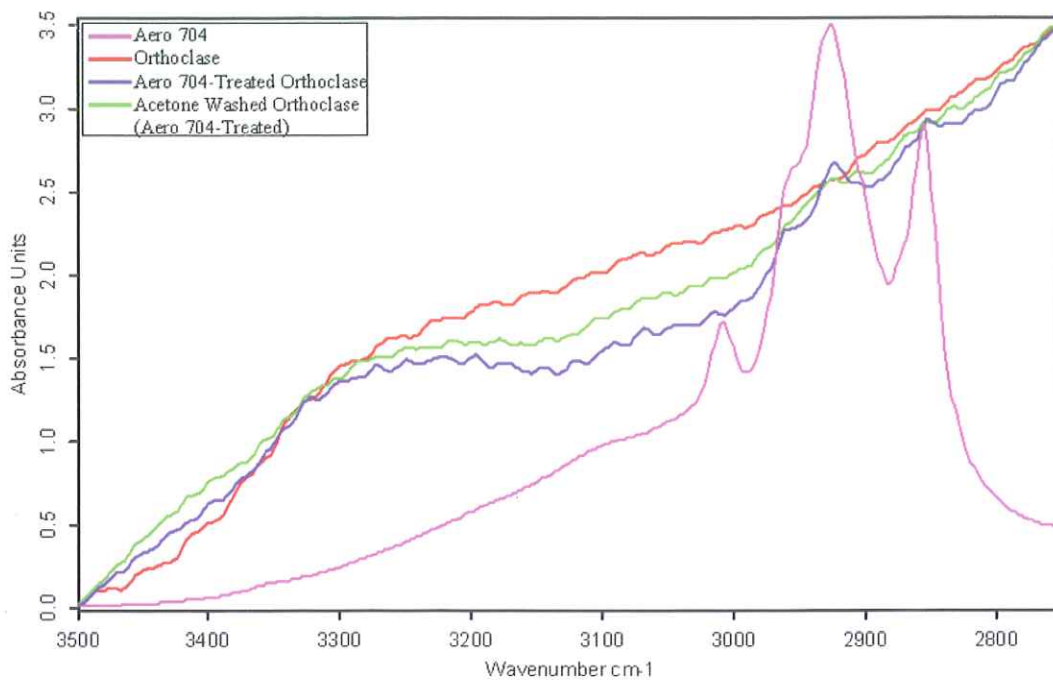
Figure 4. 107 FTIR Spectrum of Orthoclase in the Presence of Aero 704 in 3500–2750 cm^{-1} Wavelength Range.
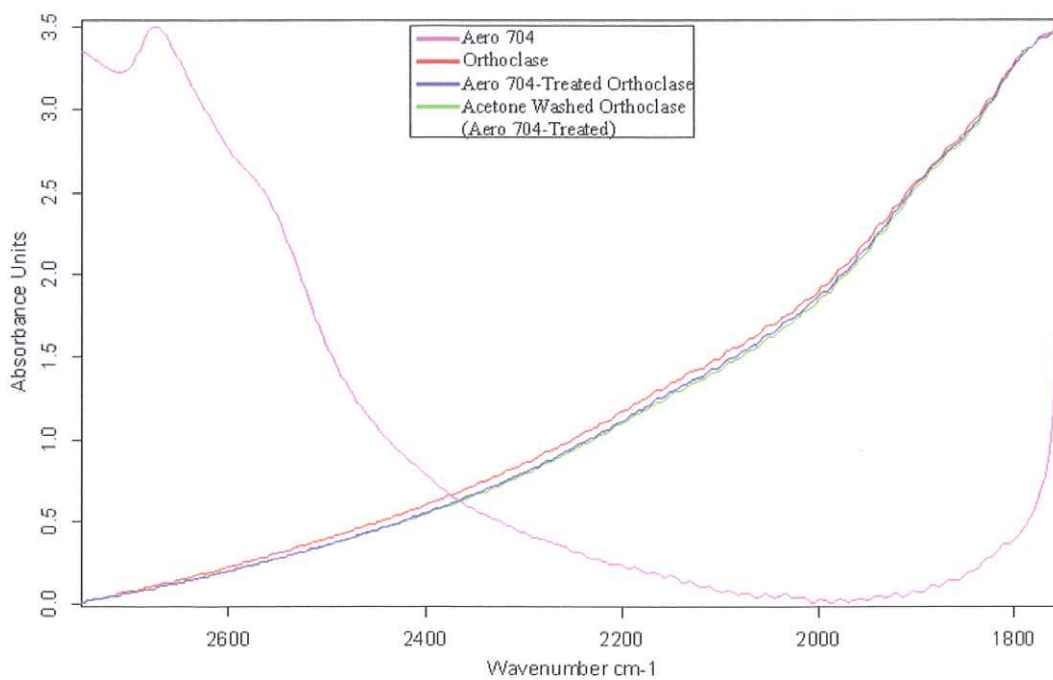

Figure 4. 108 FTIR Spectrum of Orthoclase in the Presence of Aero 704 in 2750–1750 cm^{-1} Wavelength Range.
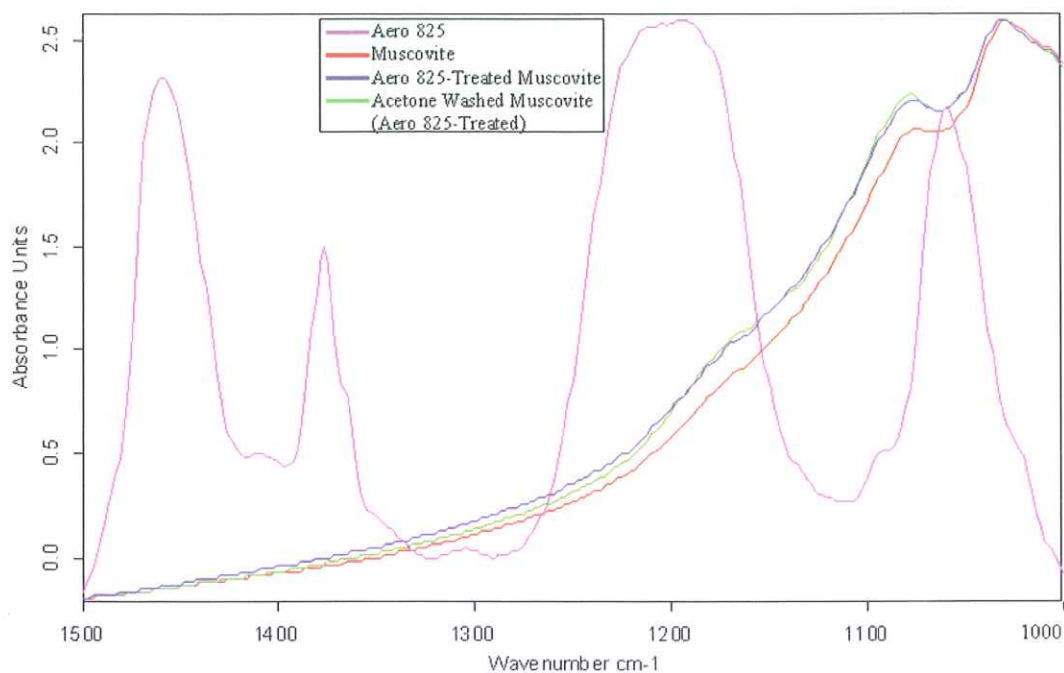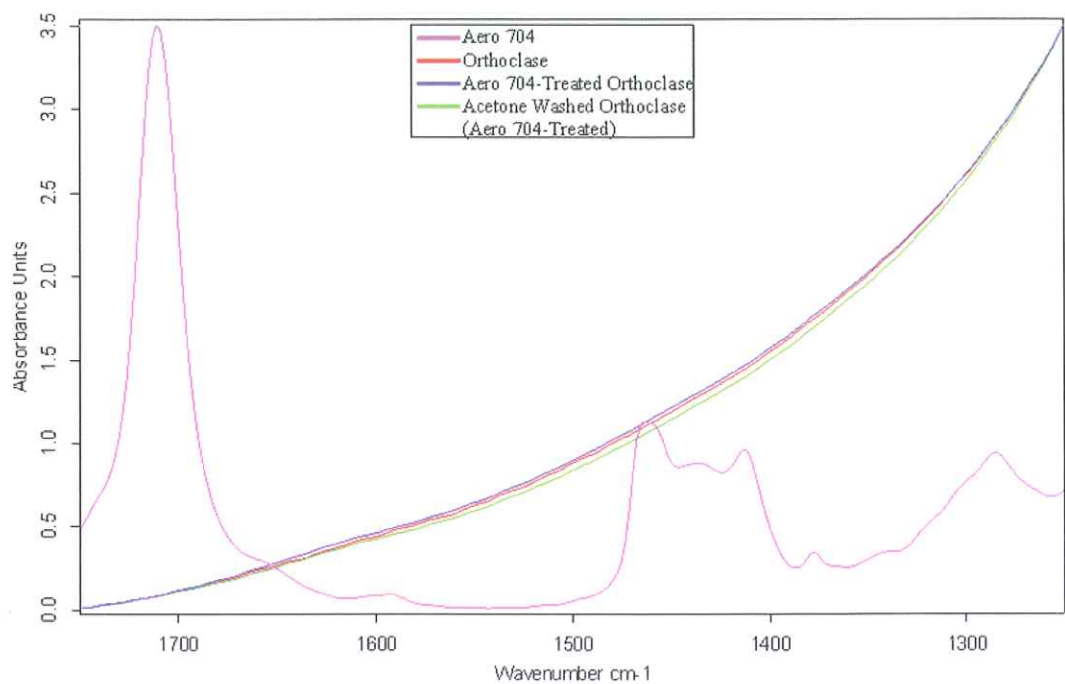
Figure 4. 109 FTIR Spectrum of Orthoclase in the Presence of Aero 704 in 1750–1250 cm^{-1} Wavelength Range.
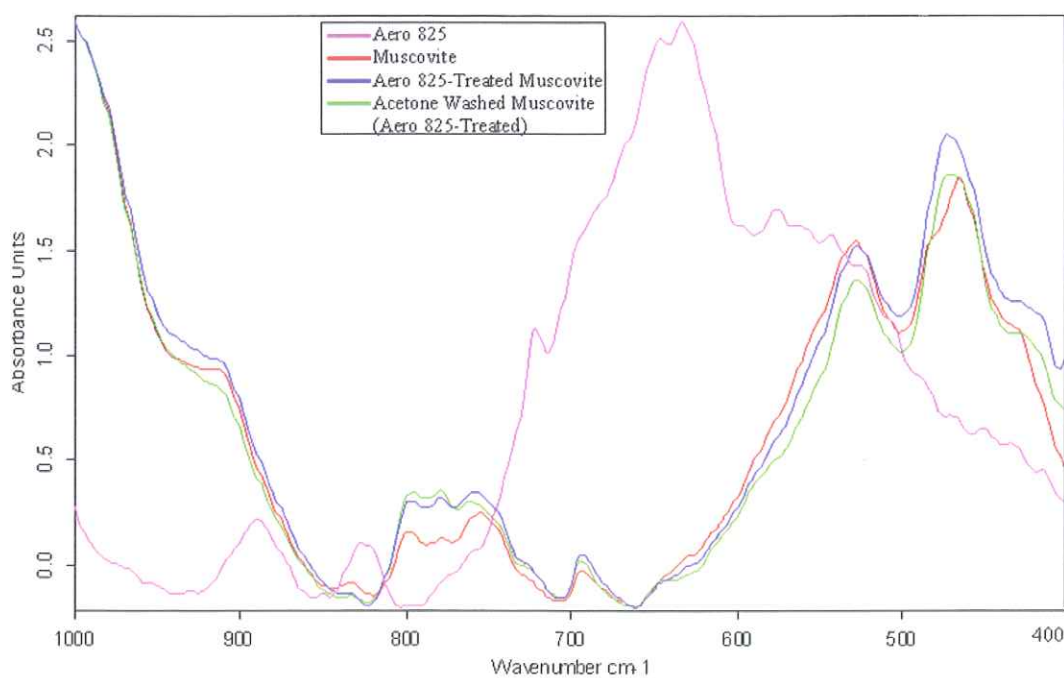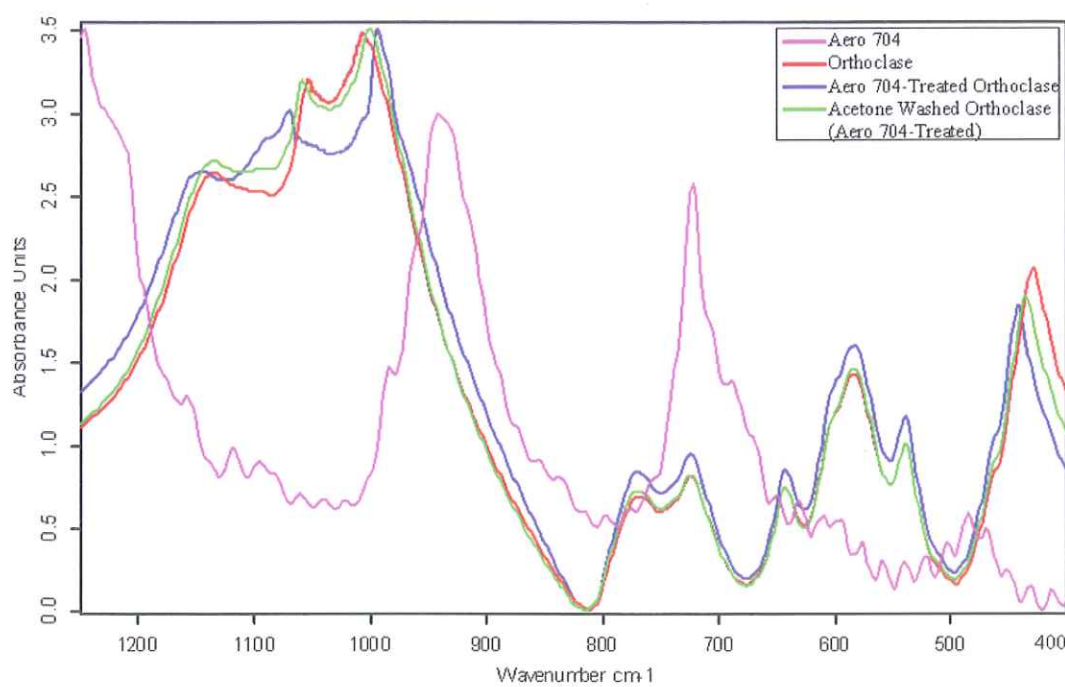

Figure 4. 110 FTIR Spectrum of Orthoclase in the Presence of Aero 704 in 1250–400 cm^{-1} Wavelength Range.

The spectra obtained with Aero 3000C, orthoclase, Aero 3000C-treated orthoclase and acetone-washed orthoclase were given in Figures 4.111 to 4.115. The major zones for the orthoclase in the presence of Aero 3000C were shown as 3250-2750 cm^{-1}, 2750-1750 cm^{-1}, 1750-1250 cm^{-1} and 1250-400 cm^{-1} wavelengths in Figures 4.112-4.115 respectively.

Aero 3000C-treated orthoclase showed additional bands at 2957 cm^{-1}, 2922 cm^{-1} and 2853 cm^{-1} with low intensities assigned as C-H stretching vibrations of Aero 3000C (Figure 4.112). However, the FTIR spectrum of the Aero 3000C-treated orthoclase upon washing with acetone was altered; the additional bands disappeared.
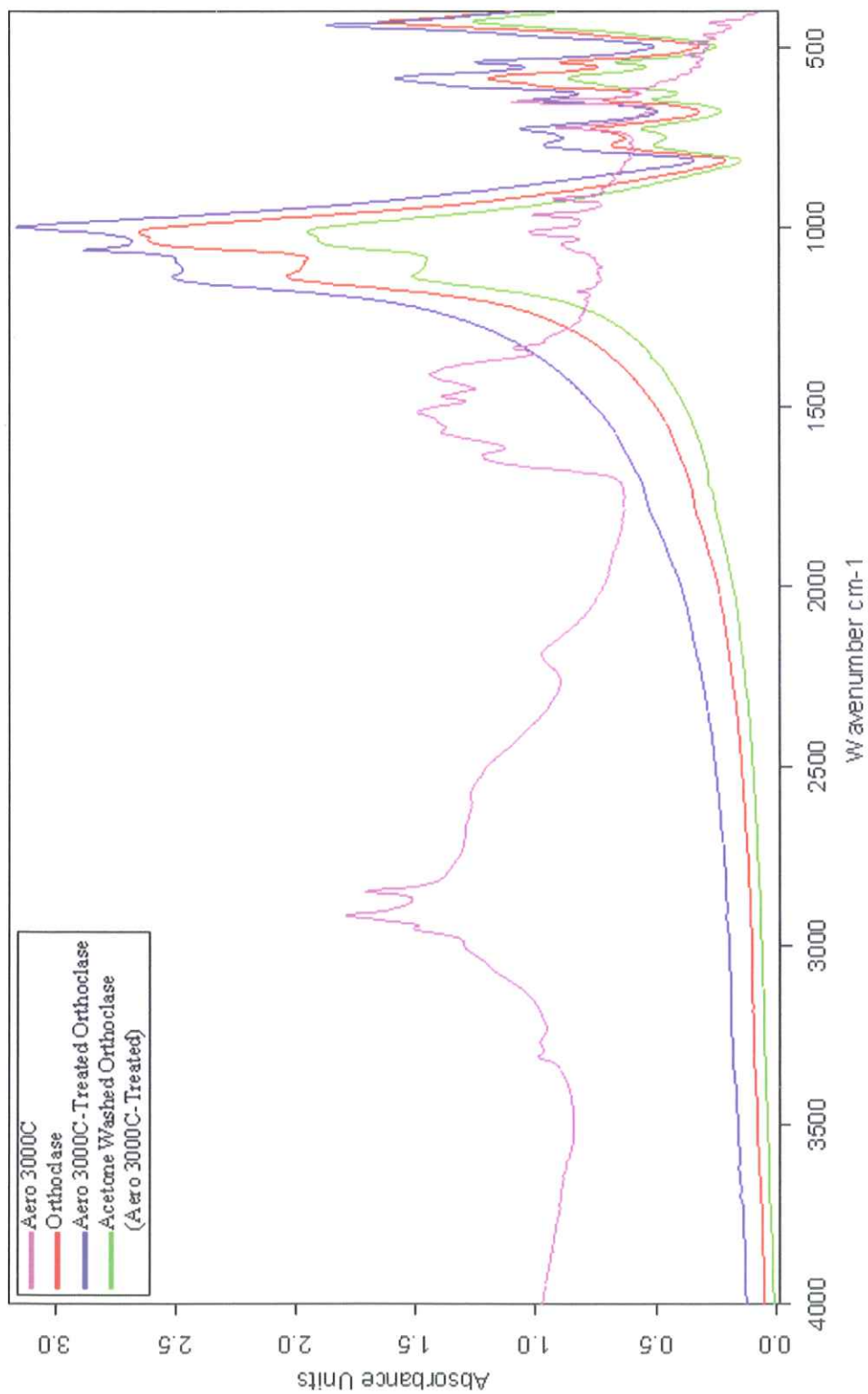
Figure 4. 111 FTIR Spectrum of Orthoclase in the Presence of Aero 3000C in 4000–400 cm^{-1} Wavelength Range.

Figure 4. 112 FTIR Spectrum of Orthoclase in the Presence of Aero 3000C in 3250–2750 cm⁻¹ Wavelength Range.

Figure 4. 113 FTIR Spectrum of Orthoclase in the Presence of Aero 3000C in 2750–1750 cm⁻¹ Wavelength Range.

Figure 4. 114 FTIR Spectrum of Orthoclase in the Presence of Aero 3000C in 1750–1250 cm^{-1} Wavelength Range.

Figure 4. 115 FTIR Spectrum of Orthoclase in the Presence of Aero 3000C in 1250–400 cm^{-1} Wavelength Range.

The spectra obtained for Aero 825 are given in Figures 4.116-4.120. In order to provide more detailed spectra, the major zones for the orthoclase in the presence of Aero 825 were displayed in Figures 4.117-4.120 as 3750-2750 cm^{-1}, 2750-1500 cm^{-1}, 1500-1000 cm^{-1} and 1000-400 cm^{-1} wavelengths depending on the Aero 825's FTIR peaks.

In Figure 4.117, Aero 825-treated orthoclase had additional bands at 2951 cm^{-1}, 2924 cm^{-1} and 2854 cm^{-1} with very low intensities assigned as CH$_2$ vibrations of Aero 825. However, upon washing with acetone, the bands at 2951 cm^{-1}, 2924 cm^{-1} and 2854 cm^{-1} disappeared.
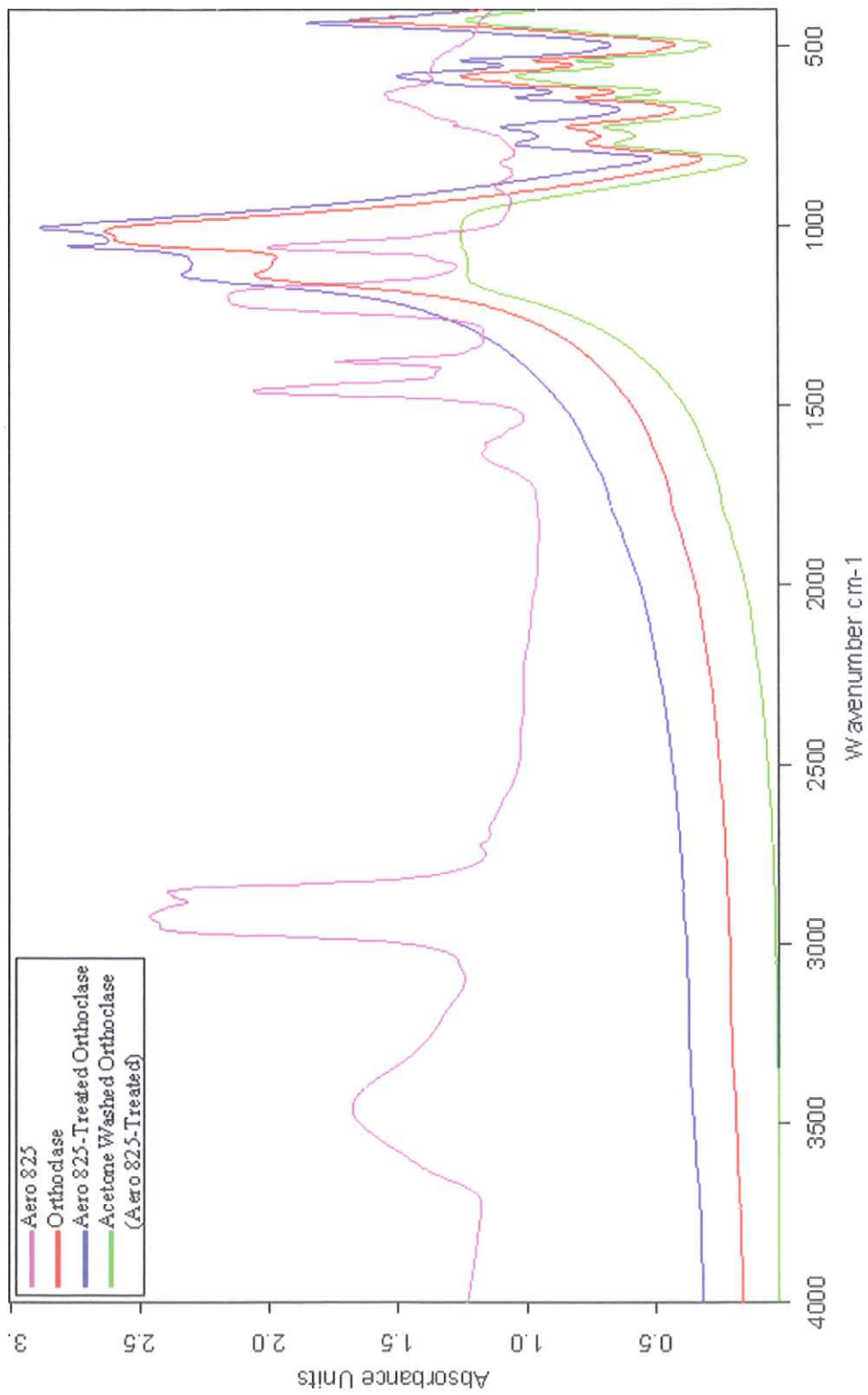
Figure 4. 116 FTIR Spectrum of Orthoclase in the Presence of Aero 825 in 4000–400 cm^{-1} Wavelength Range.

157
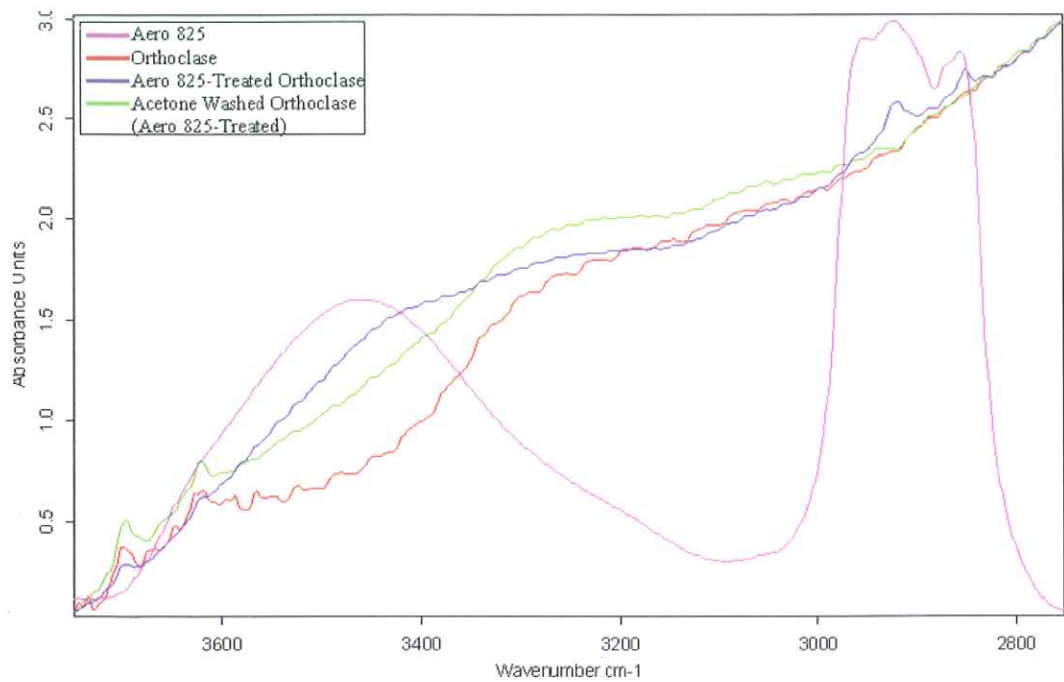
Figure 4. 117 FTIR Spectrum of Orthoclase in the Presence of Aero 825 in 3750–2750 cm^{-1} Wavelength Range.

Figure 4. 118 FTIR Spectrum of Orthoclase in the Presence of Aero 825 in 2750–1500 cm^{-1} Wavelength Range.

Figure 4. 119 FTIR Spectrum of Orthoclase in the Presence of Aero 825 in 1500–1000 cm^{-1} Wavelength Range.

Figure 4. 120 FTIR Spectrum of Orthoclase in the Presence of Aero 825 in 1000–400 cm^{-1} Wavelength Range.

159

4.5   Quartz Sample

4.5.1   Electrokinetic Potential Measurements on Quartz

When the similar procedure was applied in order to obtain the zeta potential values of quartz, the i.e.p. was found about pH 1.5 in distilled water and in 1.0×10^{-3} M of KCl. The results are given in Figure 4.121 as function of pH. It is seen that above the i.e.p. the zeta potential values became more negative towards the more basic region. The results of the experiments are confirming the electrokinetic potential measurements on quartz in distilled water obtained by Vidyadhar et al., 2007 [45].
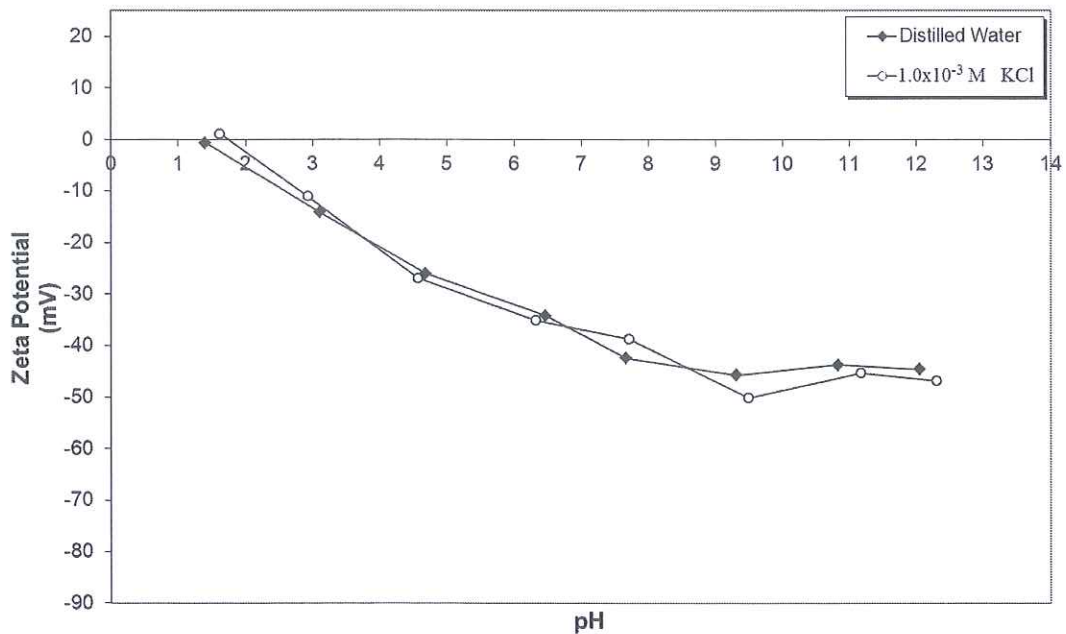
Figure 4.121   Zeta Potential of Quartz as a Function of pH.

Figure 4.122 shows the effect of 1.0×10^{-4} M, 5.0×10^{-4} M and 1.0×10^{-3} M of Aero 704 on the electrokinetic potential of quartz. The zeta potential values of quartz decreased proportionally to Aero 704 concentration and pH. The results of the electrokinetic potential measurements in the presence of varying Aero 704 (as oleate) concentrations are confirmed by the electrokinetic potential measurements obtained by Vidyadhar et al., 2002 [10].

160

The zeta potential values of quartz in the presence of 5.0×10^{-5} M, 1.0×10^{-4} M and 5.0×10^{-4} M of Aero 3000C as a function of pH were shown in Figure 4.123. The zeta potential values increased proportionally to both Aero 3000C concentration and pH. The i.e.p. was shifted from about pH 1.5 to highly alkali conditions, about pH 10.8 and the surface of the sample was positively charged up to given pH.

Figure 4.124 displays the zeta potential values of quartz in the presence of 1.0×10^{-4} M, 5.0×10^{-4} M and 1.0×10^{-3} M of Aero 825 as a function of pH. The zeta potential values of quartz decreased with increasing Aero 825 concentration.

The results of the electrokinetic potential measurements in the presence of varying Aero 3000C (as amine) and Aero 825 (as sulfonate) concentrations are confirming the electrokinetic potential measurements on quartz obtained by Vidyadhar et al., 2007 [45].
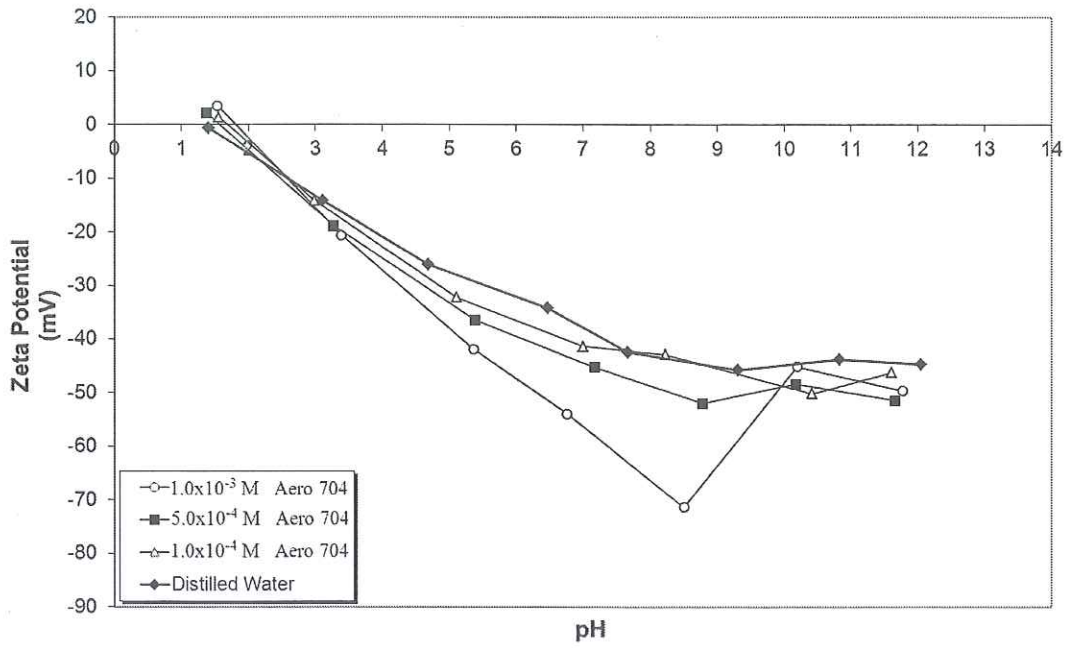
Figure 4.122 Zeta Potential of Quartz as a Function of pH and Aero 704 Concentration.
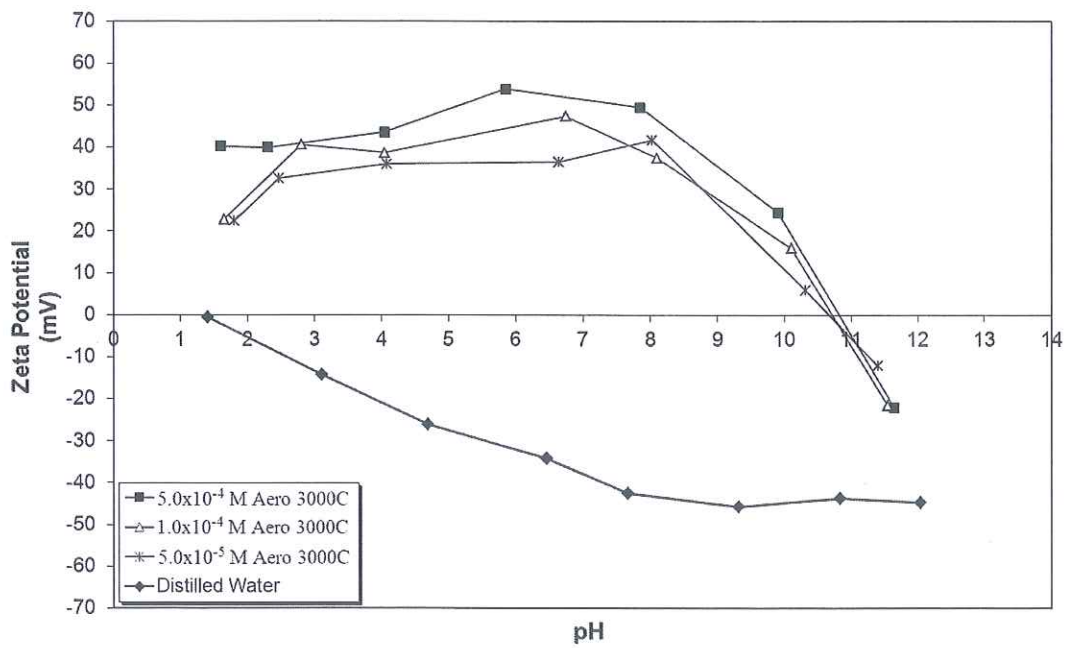
Figure 4.123 Zeta Potential of Quartz as a Function of pH and Aero 3000C Concentration.

162

Figure 4.124 Zeta Potential of Quartz as a Function of pH and Aero 825
Concentration.

Additional electrokinetic potential measurements were carried out on acetone-washed quartz samples which were conditioned with 3.5×10^{-4} M of Aero 704 about pH 9.5, 5.0×10^{-5} M of Aero 3000C about pH 3.0 and 2.0×10^{-4} M of Aero 825 about pH 5.0. The samples were first conditioned with each collector and then washed with acetone several times prior to electrokinetic potential measurements.

The effect of acetone washing on the electrokinetic potential values of collector-treated quartz samples were shown in Figure 4.125 as a function of pH. The zeta potential values were found to be very similar to each other for all pH ranges.
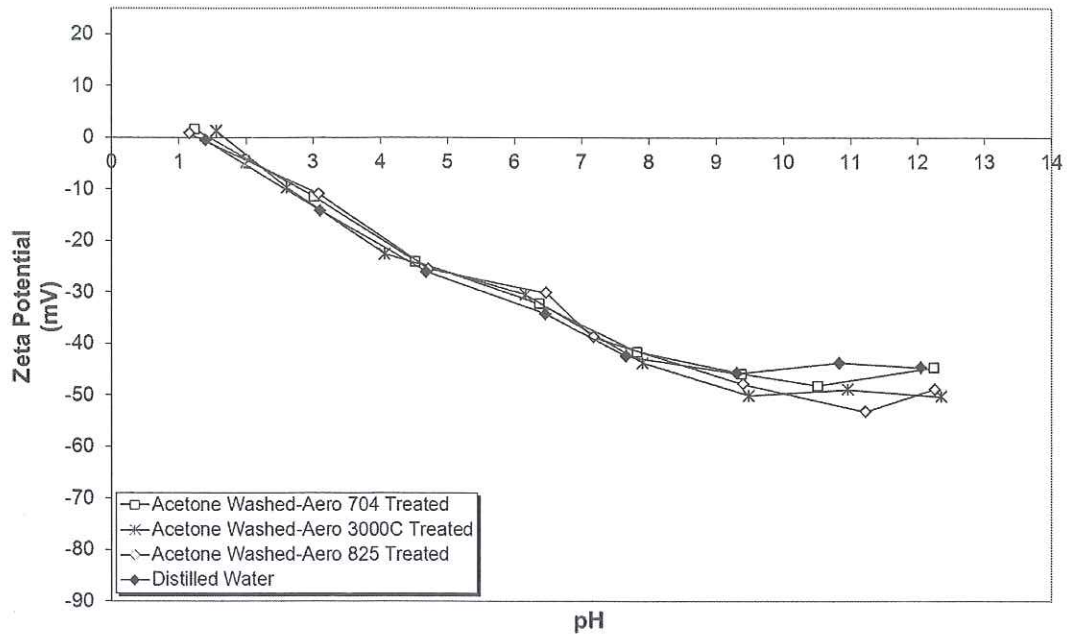
Figure 4.125   Zeta Potentials of Aero 704, Aero 3000C and Aero 825 Treated Quartz Samples After Acetone Washing.

4.5.2   Flotation Studies on Quartz

The flotation recoveries of quartz as a function of pH and Aero 704 concentration were shown in Figure 4.126. As the Aero 704's collecting power lost below pH 7.0, experienced in the previous studies, the micro-flotation studies were performed above the given pH. It is apparent that the flotation recovery of quartz is irrespective of both pH and Aero 704 concentration. The effective pH range and concentration on the flotation recovery of quartz cannot be determined.

The flotation recoveries of the quartz were maximum between the pH 3.50 and 10.50 with the values of 80.5% with 2.0×10^{-5}M, 90.0% with 5.0×10^{-5} M, 91.5% with 7.5×10^{-5} M and 94.0% with 1.0×10^{-4} M of Aero 3000C respectively (Figure 4.127). The flotation recoveries decreased sharply above pH 10.5 and below pH 3.5 in all Aero 3000C concentrations.

In the case of Aero 825, the flotation recoveries of quartz were shown in Figure 4.128 as function of pH and concentration. As illustrated in the figure, the flotation recoveries were almost null in all Aero 825 concentrations, 1.5×10^{-4} M, 2.0×10^{-4} M, 5.0×10^{-4} M and 1.0×10^{-3} M and pH. It is clear that the flotation recovery of quartz was found irrespective of both pH and Aero 825 concentration. The maximum flotation recovery obtained was less than 5.0% even in the presence of the highest Aero 825 concentration, 1.0×10^{-3} M. The effective pH range and concentration on the flotation recovery of quartz cannot be determined.
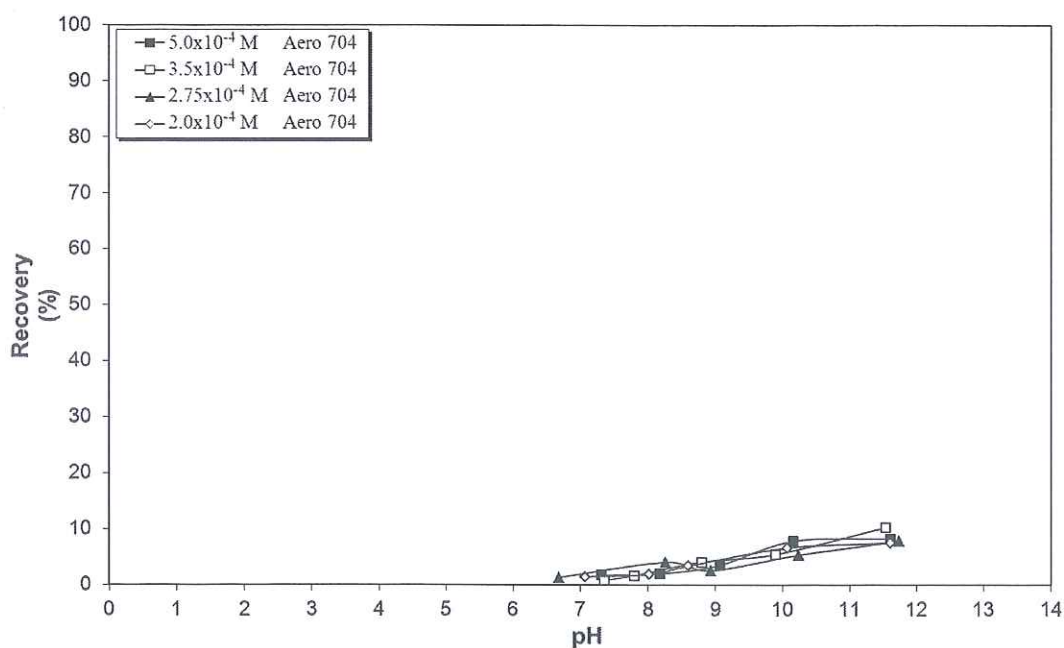
Figure 4.126 Flotation Recovery of Quartz as a Function of pH and Aero 704 Concentration.
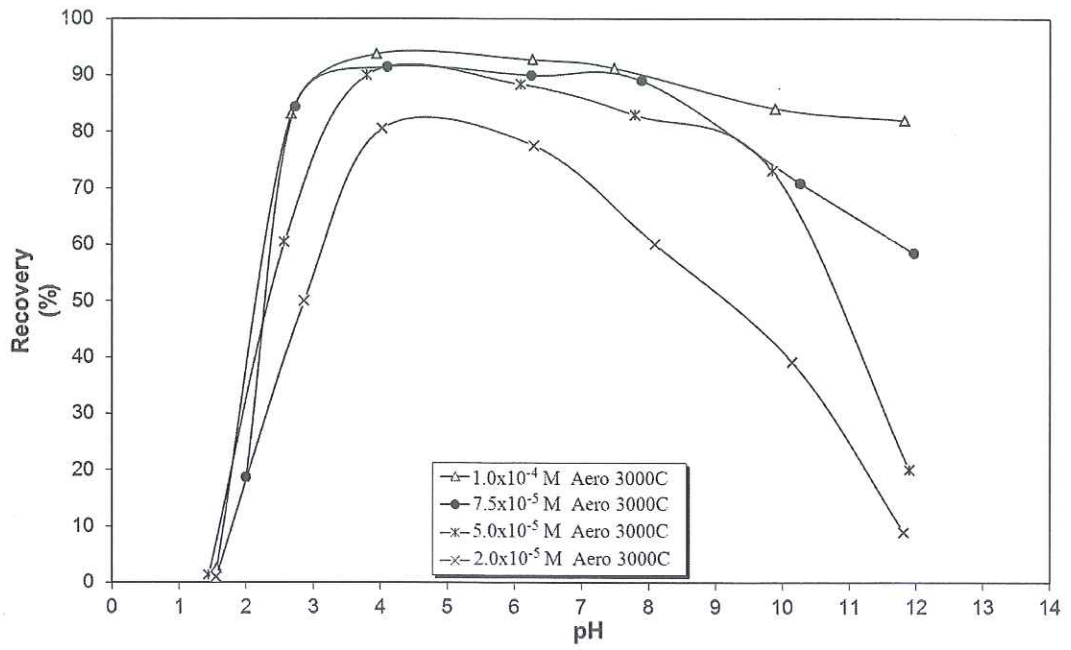
Figure 4.127   Flotation Recovery of Quartz as a Function of pH and Aero 3000C
Concentration.

Figure 4.128   Flotation Recovery of Quartz as a Function of pH and Aero 825
Concentration.

166

4.5.3   AFM Studies on Quartz

The tapping mode AFM 3D micro topographies of quartz in 100nm (Figure 4.129a) and 1μm (Figure 4.129c) sizes and their corresponding histograms and roughness analyses (Figure 4.129b and Figure 4.129d) were given in Figure 4.129. The resulting histogram provides information about the surface roughness, the maximum peak value and the average height values of quartz for 100nm x 100nm and 1μm x 1μm scanning size ranges. The corresponding histograms revealed the roughness average as 0.1376nm, the maximum peak value as 1.3682nm and the average height value as 0.6441nm for 100nm x 100nm scanning size range and 0.1755nm, 2.2845nm and 0.8615nm for 1μm x 1μm scanning size range respectively.
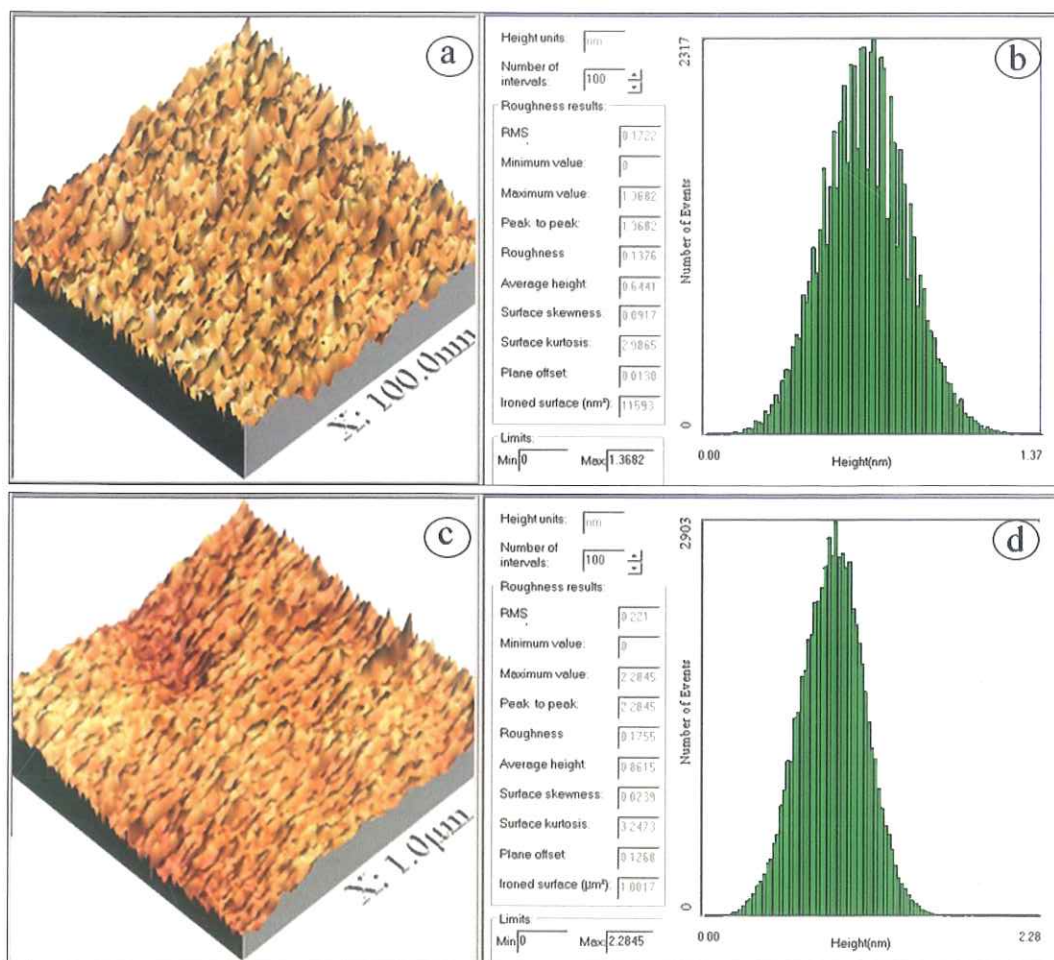
Figure 4.129   3D Micro Topographies, Corresponding Histograms and Roughness Analyses of Quartz.

The tapping mode AFM 3D micro topographies (Figure 4.130a and 4.130c) and the corresponding histograms (Figure 4.130b and 4.130d) of the Aero 704-treated quartz revealed the roughness average as 0.1434nm, the maximum peak value as 1.5090nm and the average height value as 0.7349nm for 100nm x 100nm scanning size and 0.2223nm, 3.4031nm and 1.1880nm for 1µm x 1µm scanning size range, respectively (Figure 4.130).

The tapping mode AFM image analysis of quartz and Aero 704-treated quartz based on their height profiles in 1µm were shown in Figure 4.131 for the scanned area. The quartz and the Aero 704-treated quartz showed similarities with a low height difference compared to each other.
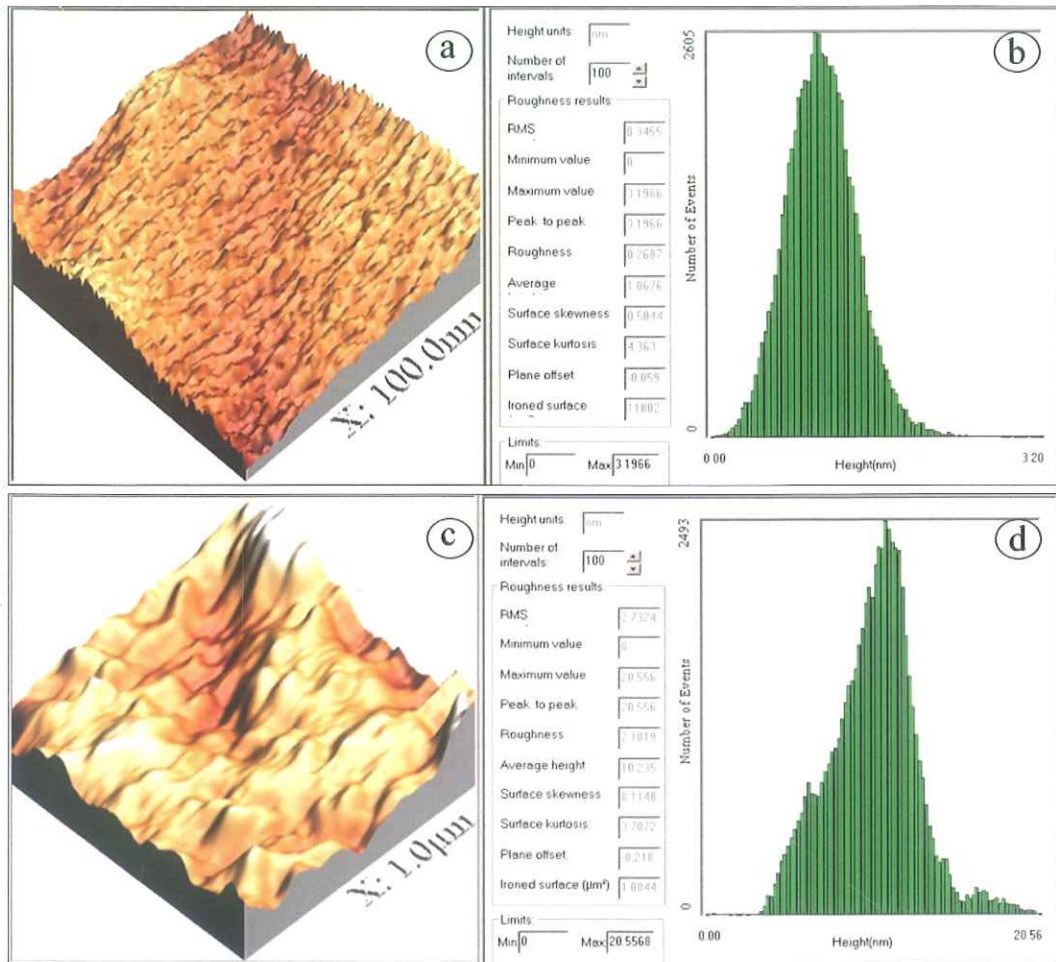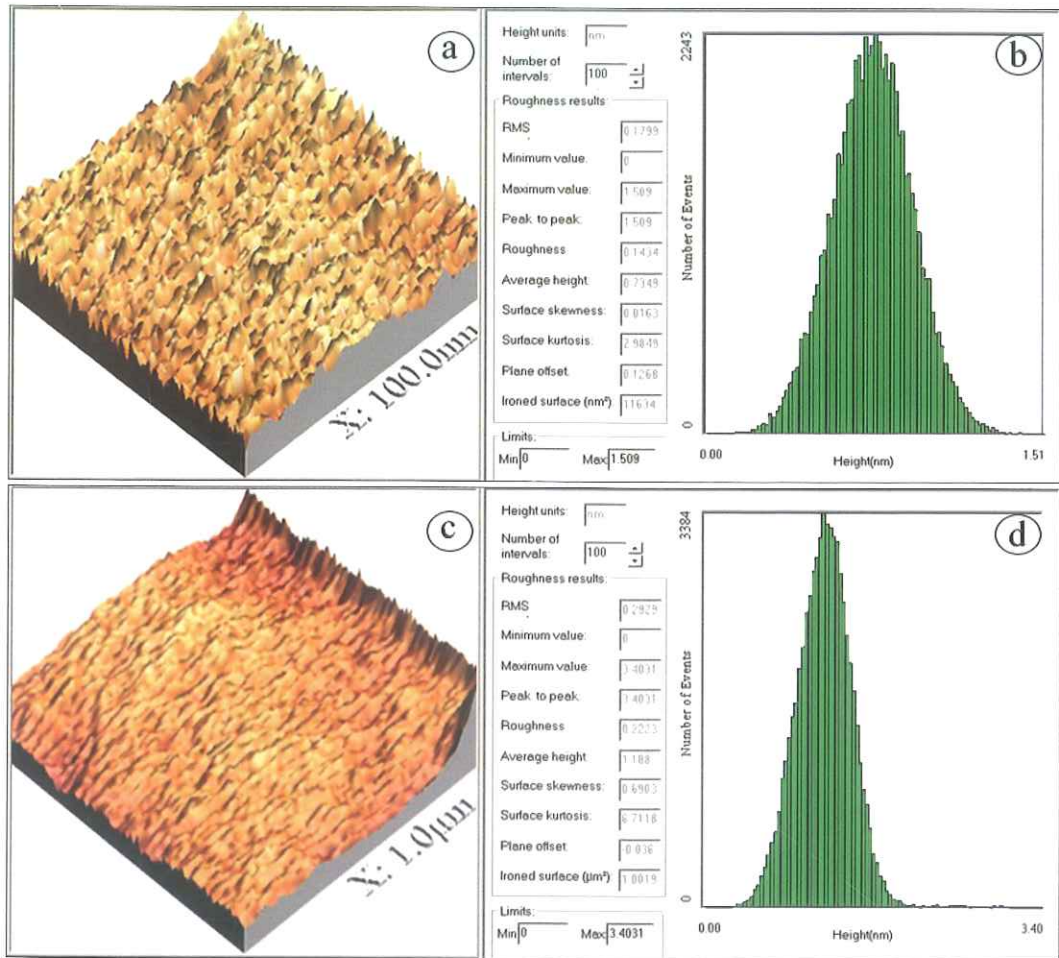
Figure 4.130 3D Micro Topographies, Corresponding Histograms and Roughness Analyses of Aero 704-Treated Quartz.
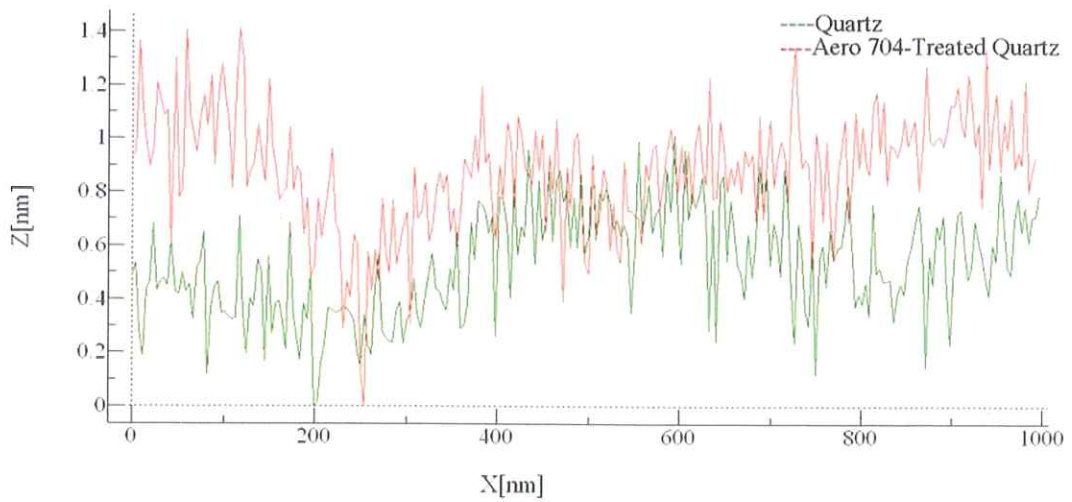
Figure 4.131 Height Profiles of Quartz and Aero 704-Treated Quartz in 1μm Size.

169

The tapping mode AFM 3D micro topographies and the corresponding histograms of Aero 3000C-treated and Aero 825-treated quartz in 100nm x 100nm (Figure 4.132a-b for Aero 3000C-treated and Figure 4.134a-b for Aero 825-treated quartz) and 1μm x 1μm (Figure 4.132c-d for Aero 3000C-treated and Figure 4.134c-d for Aero 825-treated quartz) scanning size ranges were given in Figure 4.132 and Figure 4.134 respectively. For Aero 3000C-treated quartz, the histograms revealed that the roughness averages, the maximum peak values and the average height values as 0.2675nm, 2.2152nm and 0.9537nm for 100nm x 100nm scanning size and 1.2534nm, 9.7774nm and 3.7770nm for 1μm x 1μm scanning size range, respectively. In the case of Aero 825-treated quartz, the roughness averages, the maximum peak values and the average height values were obtained as 0.2172nm, 2.1719nm and 0.9827nm for 100nm x 100nm scanning size range and 1.2443nm, 10.7070nm and 5.1508nm for 1μm x 1μm scanning size range respectively.

The tapping mode AFM image analysis of quartz and Aero 3000C-treated quartz based on their height profiles in 1μm was shown in Figure 4.133 for the scanned area. Similarly, the tapping mode AFM image analysis of quartz and Aero 825-treated quartz was shown in Figure 4.135. The height profiles of Aero 3000C-treated quartz reached to 4.60nm and the Aero 825-treated quartz reached to 5.0nm while the quartz (shown in green in the figures) displayed height profiles less than 1.0nm for the scanned area.

Figure 4.132   3D Micro Topographies, Corresponding Histograms and Roughness Analyses of Aero 3000C-Treated Quartz.

Figure 4.133   Height Profiles of Quartz and Aero 3000C-Treated Quartz in 1μm Size.

171

Figure 4.134   3D Micro Topographies, Corresponding Histograms and Roughness Analyses of Aero 825-Treated Quartz.
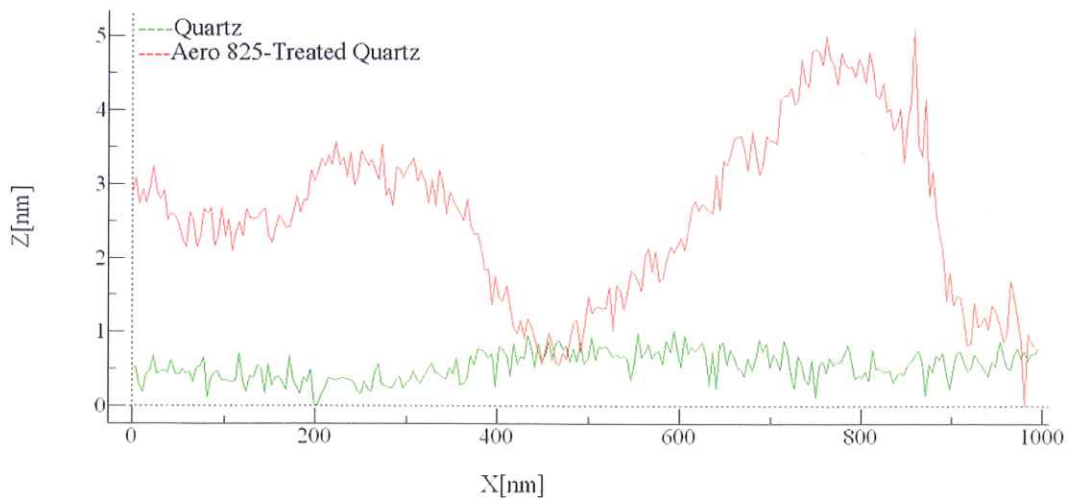
Figure 4.135   Height Profiles of Quartz and Aero 825-Treated Quartz in 1µm Size.

172

4.5.4 FTIR Spectroscopy Studies on Quartz

In the similar way as previous mineral samples, the FTIR analysis of the quartz, collector-treated quartz and acetone-washed quartz samples were examined and the resulting spectra were given in Figure 4.136, Figure 4.141 and Figure 4.146 for Aero 704, Aero 3000C and Aero 825 respectively.

In order to obtain more detailed FTIR spectra, the full scale FTIR spectra (4000-400 cm^{-1}) of collector, non-treated, collector-treated and acetone-washed quartz samples were analyzed in four major zones depending on the collector's FTIR peaks. Figures 4.137-4.140 show the FTIR ranges of quartz in the presence of Aero 704 as 3500-2750 cm^{-1}, 2750-1750 cm^{-1}, 1750-1250 cm^{-1} and 1250-400 cm^{-1} major wavelength's zones respectively.

The FTIR spectrum of Aero 704-treated quartz showed additional weak bands at 2961 cm^{-1}, 2926 cm^{-1} and 2854 cm^{-1} assigned as CH_2 stretching vibrations which come from Aero 704 (Figure 4.137). The FTIR spectrum of the Aero 704-treated quartz was altered upon washing several times with acetone and the bands at 2961 cm^{-1}, 2926 cm^{-1} and 2854 cm^{-1} disappeared.
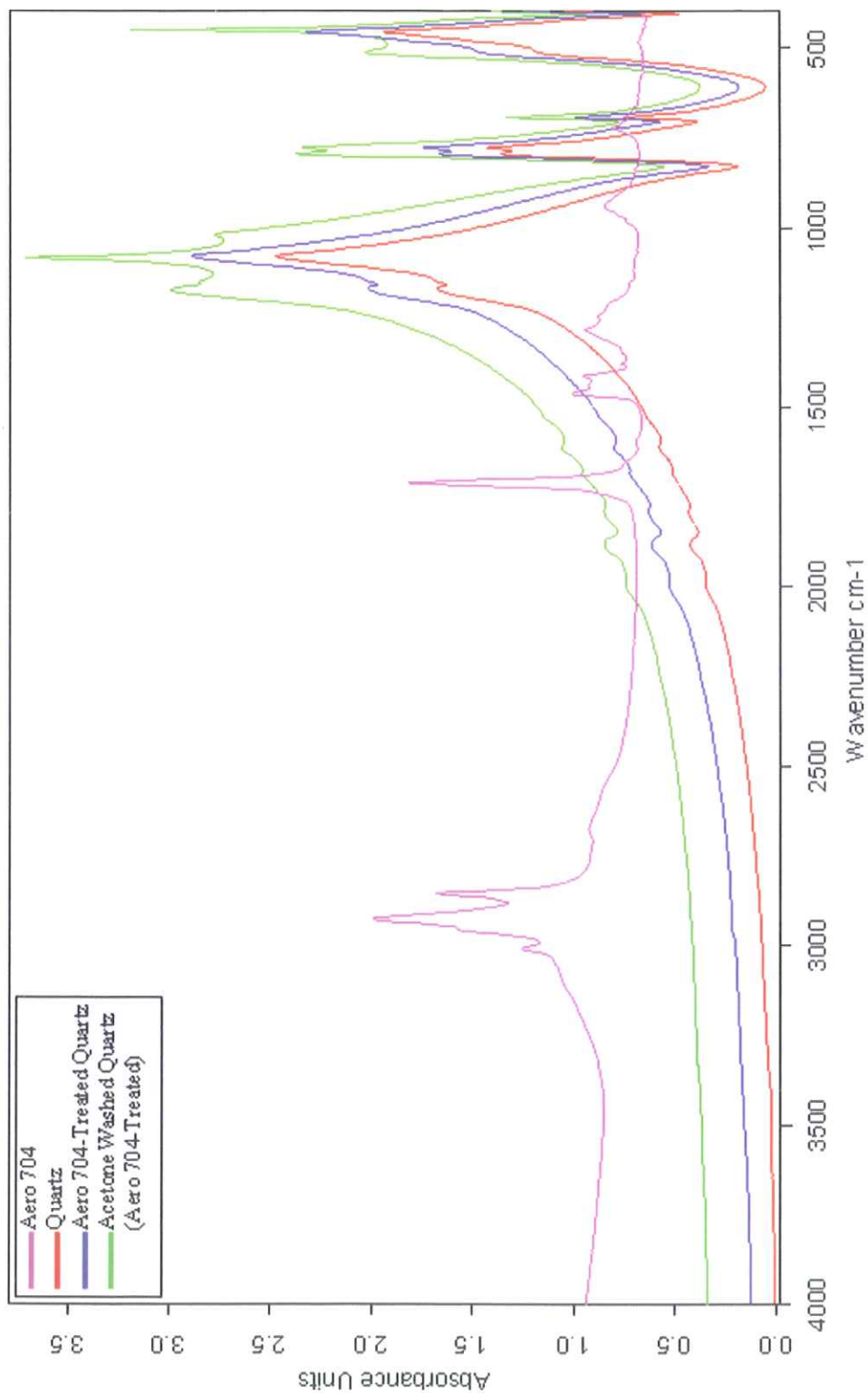
Figure 4.136   FTIR Spectrum of Quartz in the Presence of Aero 704 in 4000–400 cm^{-1} Wavelength Range.

174

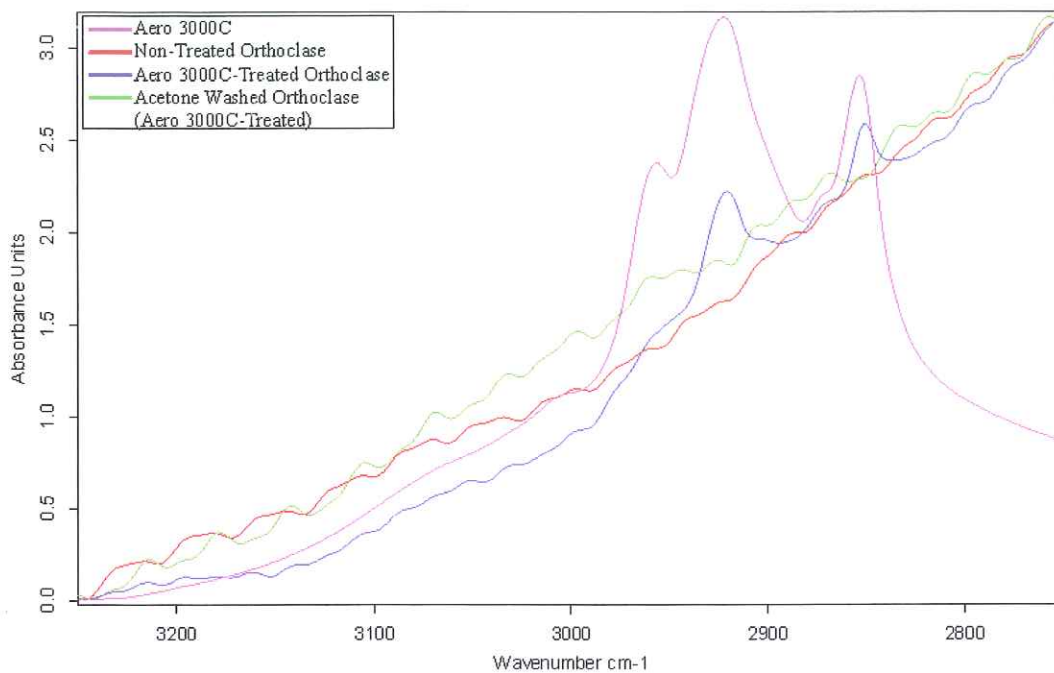Figure 4.137 FTIR Spectrum of Quartz in the Presence of Aero 704 in 3500–2750 cm^{-1} Wavelength Range.
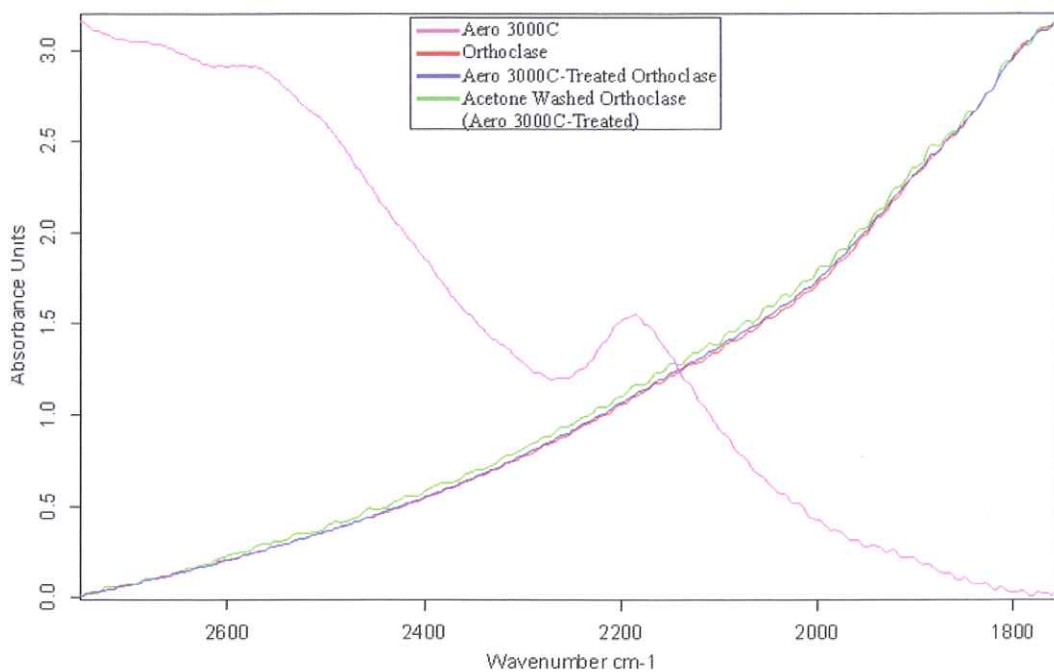

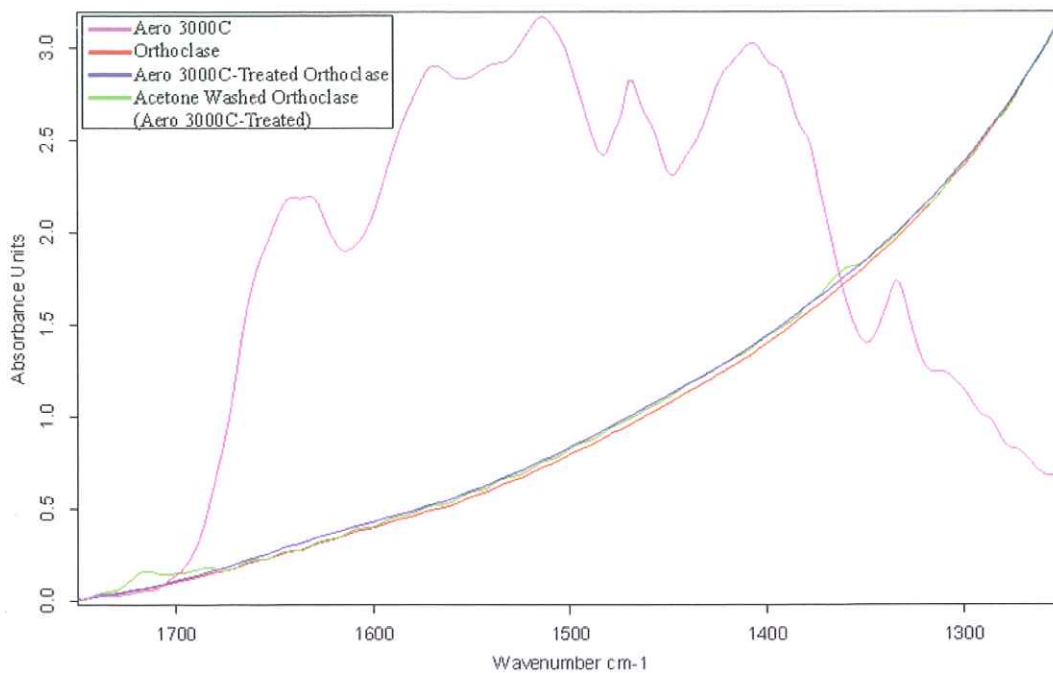Figure 4.138 FTIR Spectrum of Quartz in the Presence of Aero 704 in 2750–1750 cm^{-1} Wavelength Range.

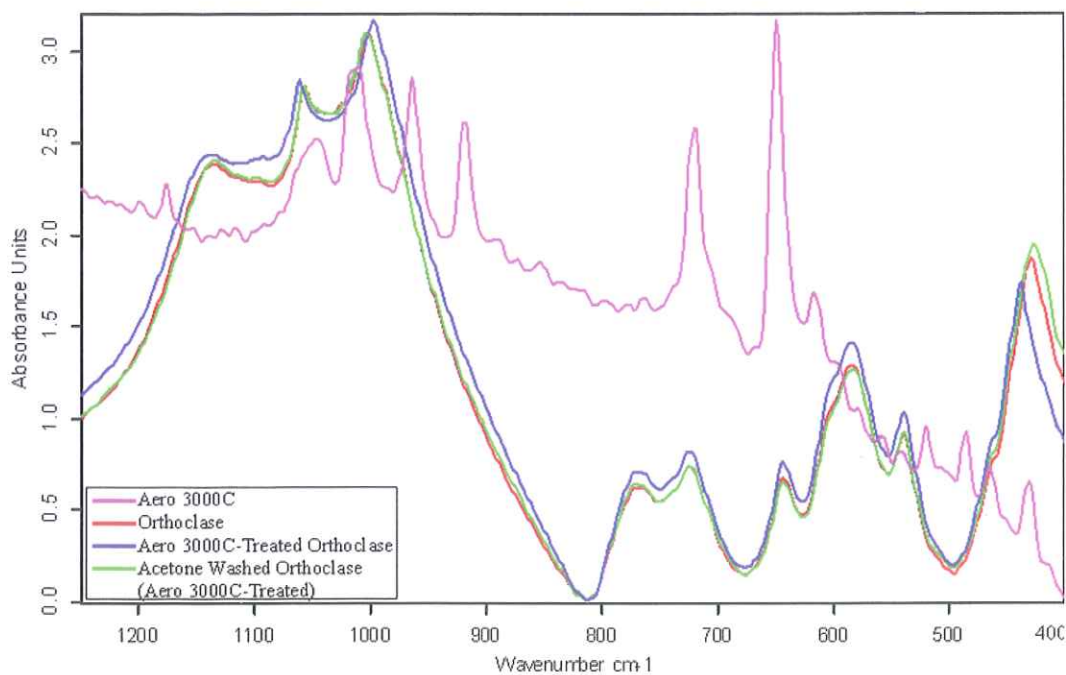Figure 4.139 FTIR Spectrum of Quartz in the Presence of Aero 704 in 1750–1250 cm^{-1} Wavelength Range.

Figure 4.140 FTIR Spectrum of Quartz in the Presence of Aero 704 in 1250–400 cm^{-1} Wavelength Range.

176

The spectra obtained with Aero 3000C, quartz, Aero 3000C-treated quartz and acetone-washed quartz were given in Figures 4.141 to 4.145. The major zones for the quartz in the presence of Aero 3000C were shown as 3250-2750 cm^{-1}, 2750-1750 cm^{-1}, 1750-1250 cm^{-1} and 1250-400 cm^{-1} wavelengths in Figures 4.142-4.145 respectively.

Aero 3000C-treated quartz showed additional bands at 2957 cm^{-1}, 2922 cm^{-1} and 2853 cm^{-1} with low intensities assigned as C-H stretching vibrations of Aero 3000C (Figure 4.142). However, the FTIR spectrum of the Aero 3000C-treated quartz upon washing with acetone was altered; the additional bands disappeared.

Figure 4.141 FTIR Spectrum of Quartz in the Presence of Aero 3000C in 4000–400 cm^{-1} wavelength range.

178

Figure 4.142   FTIR Spectrum of Quartz in the Presence of Aero 3000C in 3250–2750 cm^{-1} Wavelength Range.
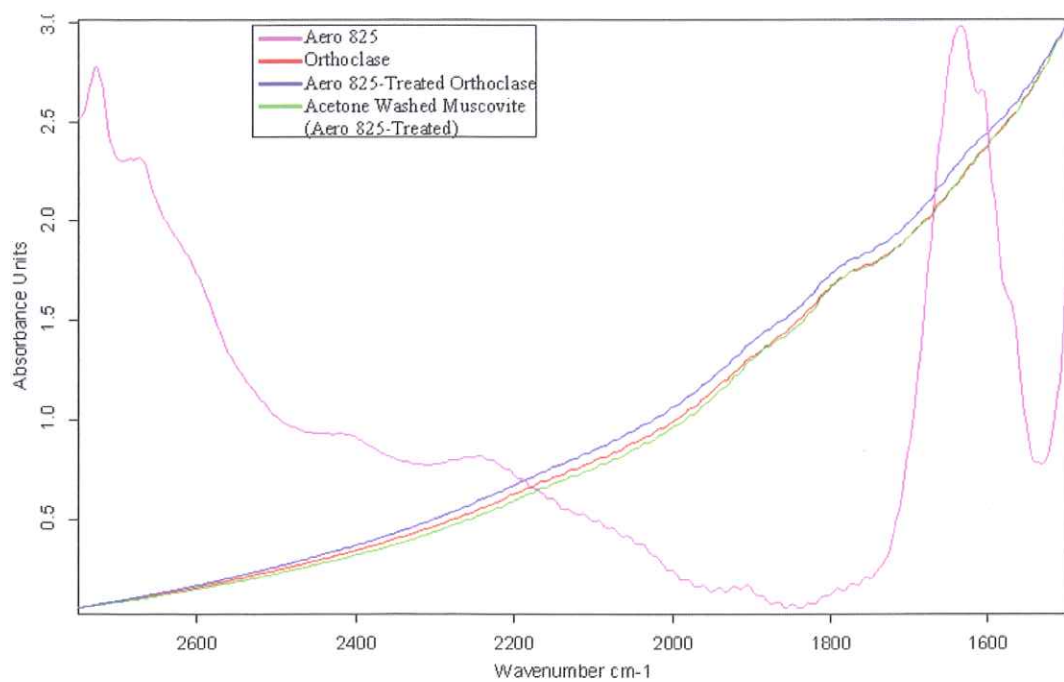

Figure 4.143   FTIR Spectrum of Quartz in the Presence of Aero 3000C in 2750–1750 cm^{-1} Wavelength Range.

179

Figure 4.144   FTIR Spectrum of Quartz in the Presence of Aero 3000C in 1750–1250 cm^{-1} Wavelength Range.

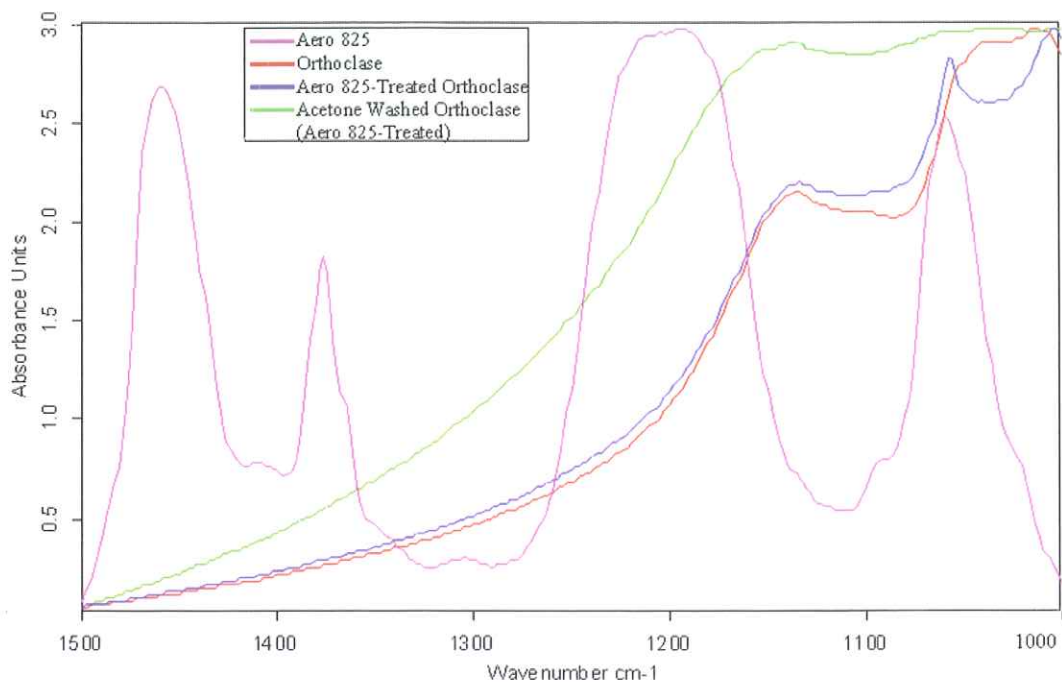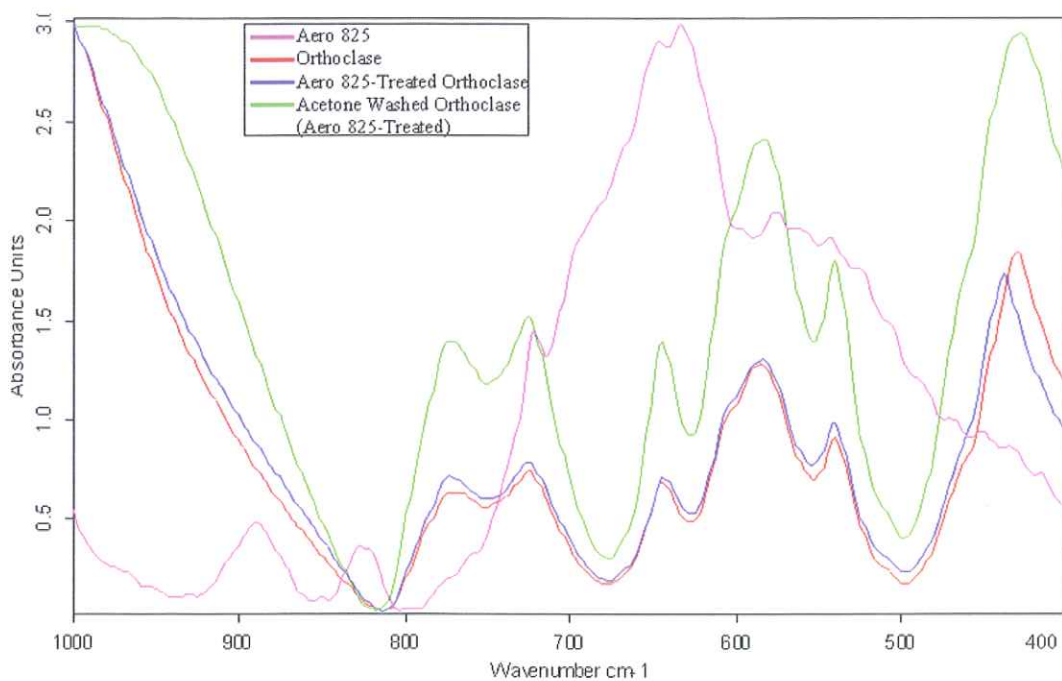Figure 4.145   FTIR Spectrum of Quartz in the Presence of Aero 3000C in 1250–400 cm^{-1} Wavelength Range.

180

The spectra obtained for Aero 825 are given in Figures 4.146-4.150. In order to provide more detailed spectra, the major zones for the quartz in the presence of Aero 825 were displayed in Figures 4.147-4.150 as 3750-2750 cm^{-1}, 2750-1500 cm^{-1}, 1500-1000 cm^{-1} and 1000-400 cm^{-1} wavelengths depending on the Aero 825's FTIR peaks.

If the characteristic peak positions of quartz and Aero 825-treated quartz were taken into account, the Aero 825-treated quartz did not display any additional band belonging to Aero 825. The FTIR spectrum of Aero 825-treated quartz showed similarities upon washing with acetone compared to the characteristic bands of quartz.
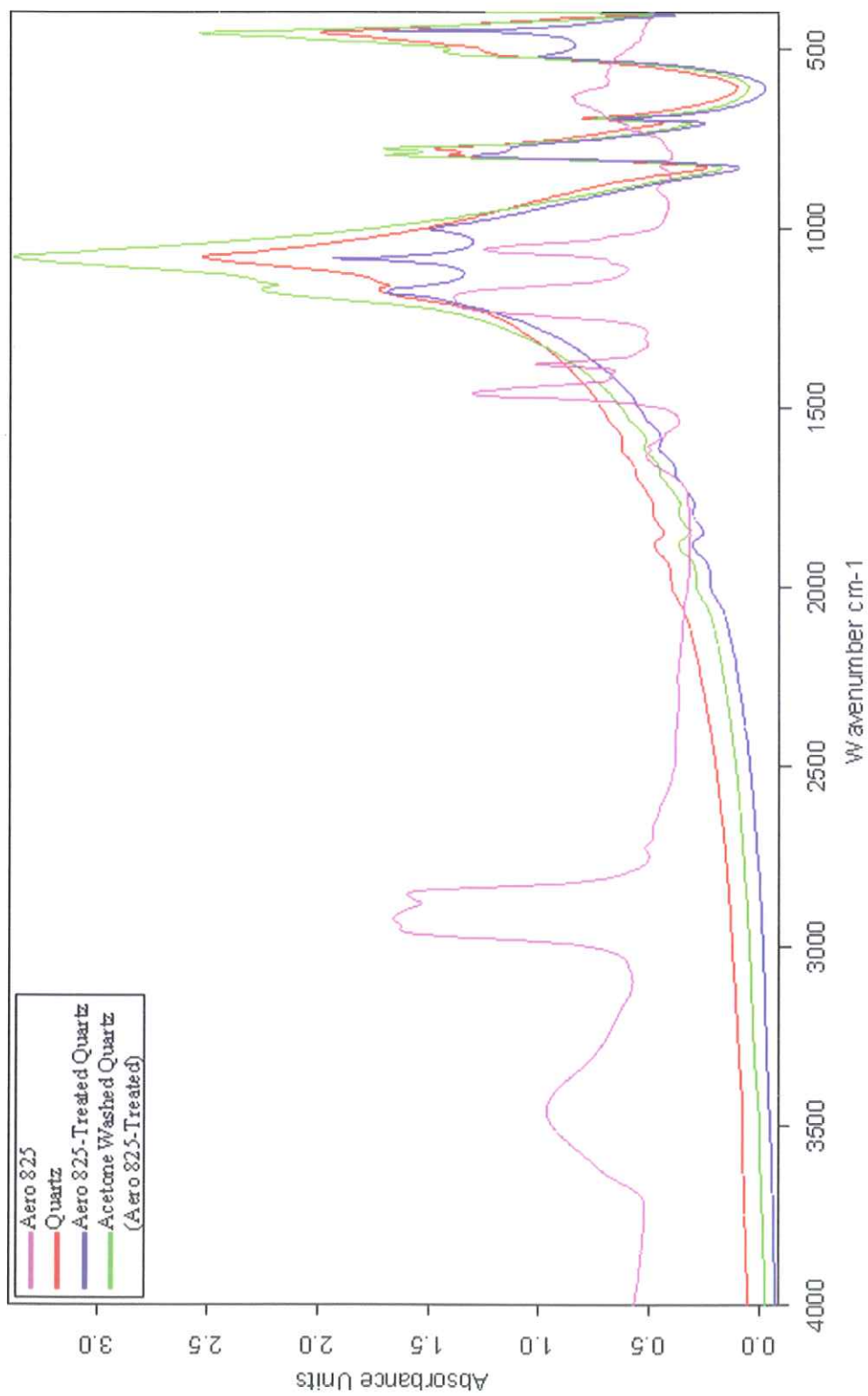
Figure 4.146 FTIR Spectrum of Quartz in the Presence of Aero 825 in 4000–400 cm^{-1} Wavelength Range.

Figure 4.147   FTIR Spectrum of Quartz in the Presence of Aero 825 in 3750–2750 cm^{-1} Wavelength Range.

Figure 4.148   FTIR Spectrum of Quartz in the Presence of Aero 825 in 2750–1500 cm^{-1} Wavelength Range.

Figure 4.149 FTIR Spectrum of Quartz in the Presence of Aero 825 in 1500–1000 cm^{-1} Wavelength Range.

Figure 4.150 FTIR Spectrum of Quartz in the Presence of Aero 825 in 1000–400 cm^{-1} Wavelength Range.

184

4.6 Rutile Sample

4.6.1 Electrokinetic Potential Measurements on Rutile

When the similar procedure was applied in order to obtain the zeta potential values of rutile, the i.e.p. was found about pH 3.3 in distilled water and in 1.0×10^{-3} M indifferent electrolyte, KCl. The results are given in Figure 4.151 as function of pH. Above the i.e.p. the zeta potential values became more negative towards the more basic region and below the i.e.p. the zeta potential values became more positive towards the more acidic region. The electrokinetic potential measurement's results are confirmed by the electrokinetic potential measurements on rutile in distilled water obtained by Pugh, 1973 [66].
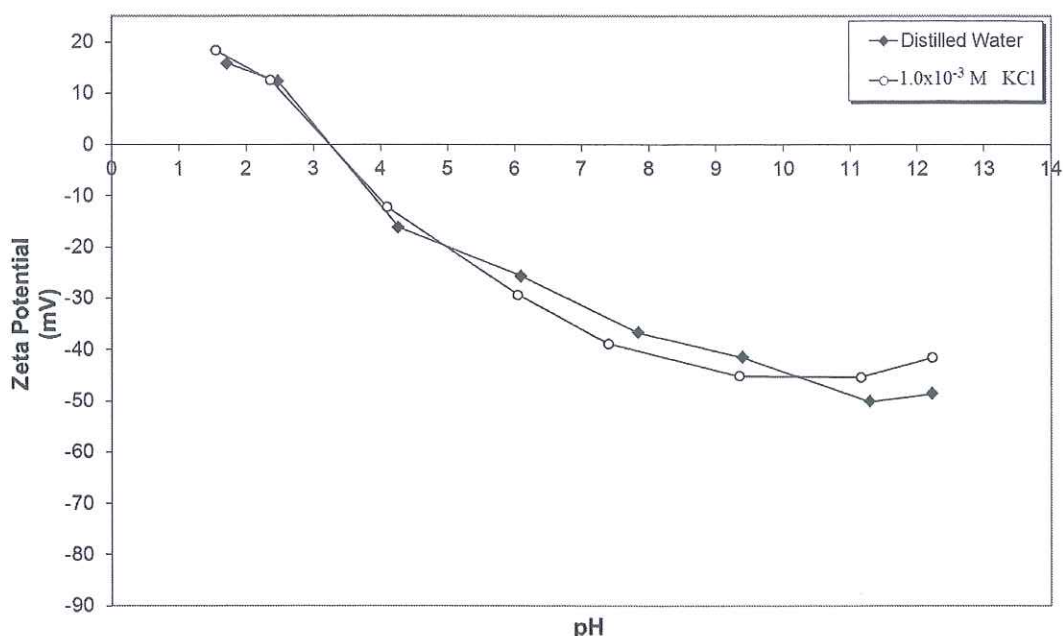
Figure 4.151   Zeta Potential of Rutile as a Function of pH.

Figure 4.152 shows the effect of 1.0×10^{-4} M, 5.0×10^{-4} M and 1.0×10^{-3} M of Aero 704 on the electrokinetic potential of rutile. The zeta potential values of rutile decreased with increasing Aero 704 concentration and pH. The i.e.p. was shifted towards the

more acidic region (from pH 3.3 to about pH 1.8) with all Aero 704 concentrations and hence the positive charge of the rutile decreased.

The zeta potential values of rutile in the presence of 5.0×10^{-5} M, 1.0×10^{-4} M and 5.0×10^{-4} M of Aero 3000C as a function of pH were shown in Figure 4.153. The zeta potential values increased proportionally to Aero 3000C concentration and pH. The i.e.p. was shifted from about pH 3.3 to highly alkali conditions, about pH 10.8 and the surface of the sample was positively charged up to given pH.

Figure 4.154 displays the zeta potential values of rutile in the presence of 1.0×10^{-4} M, 5.0×10^{-4} M and 1.0×10^{-3} M of Aero 825 as a function of pH. The zeta potential values decreased with increasing Aero 825 concentration and pH. It is seen from the figure that there were sharp increase in the zeta potential values about pH 3.3, where the i.e.p. of the rutile was found in distilled water, for all Aero 825 concentrations.
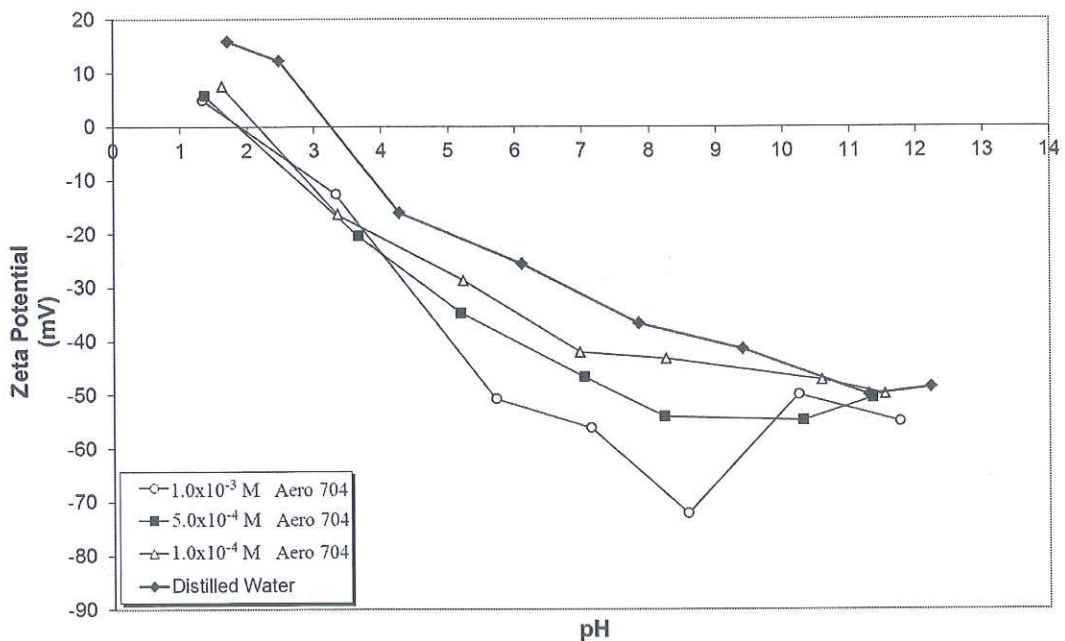
Figure 4.152   Zeta Potential of Rutile as a Function of pH and Aero 704 Concentration.

186
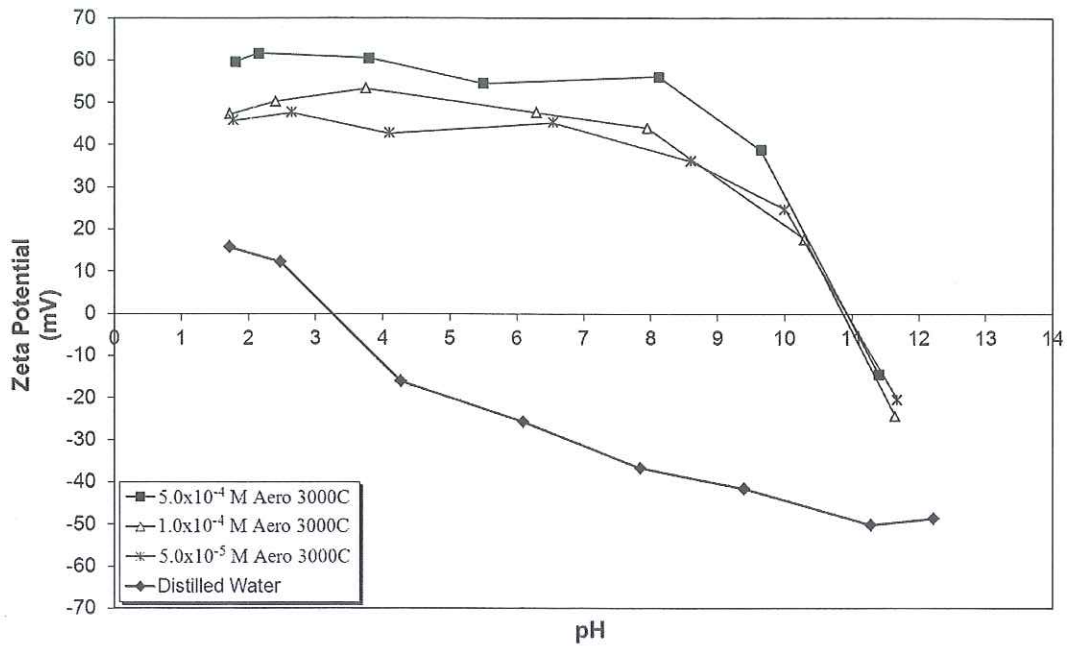
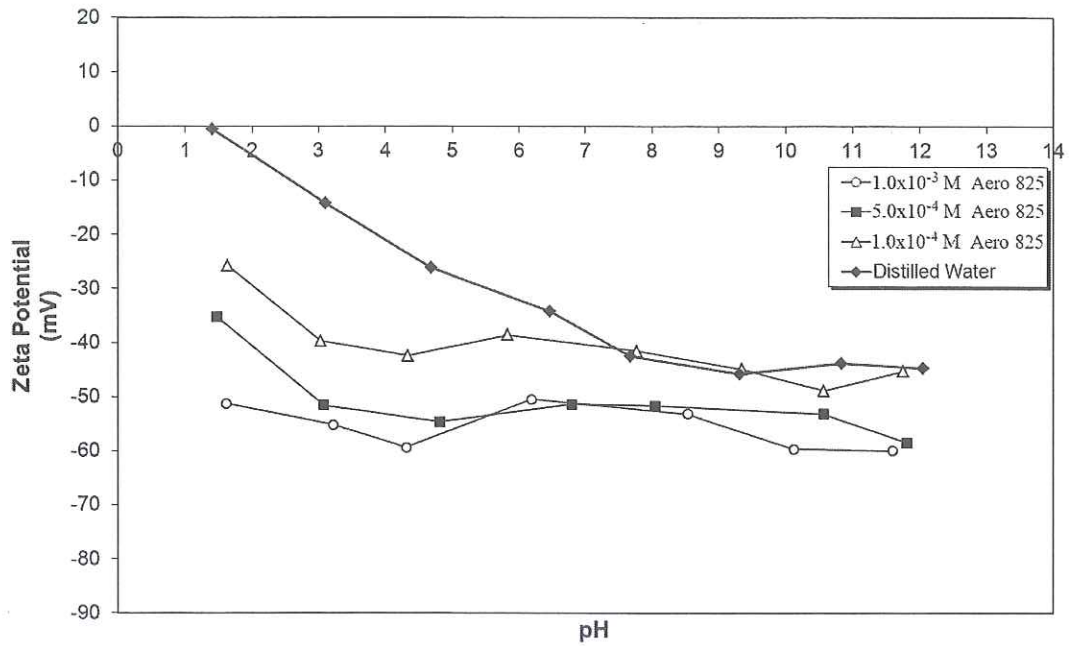Figure 4.153 Zeta Potential of Rutile as a Function of pH and Aero 3000C Concentration.
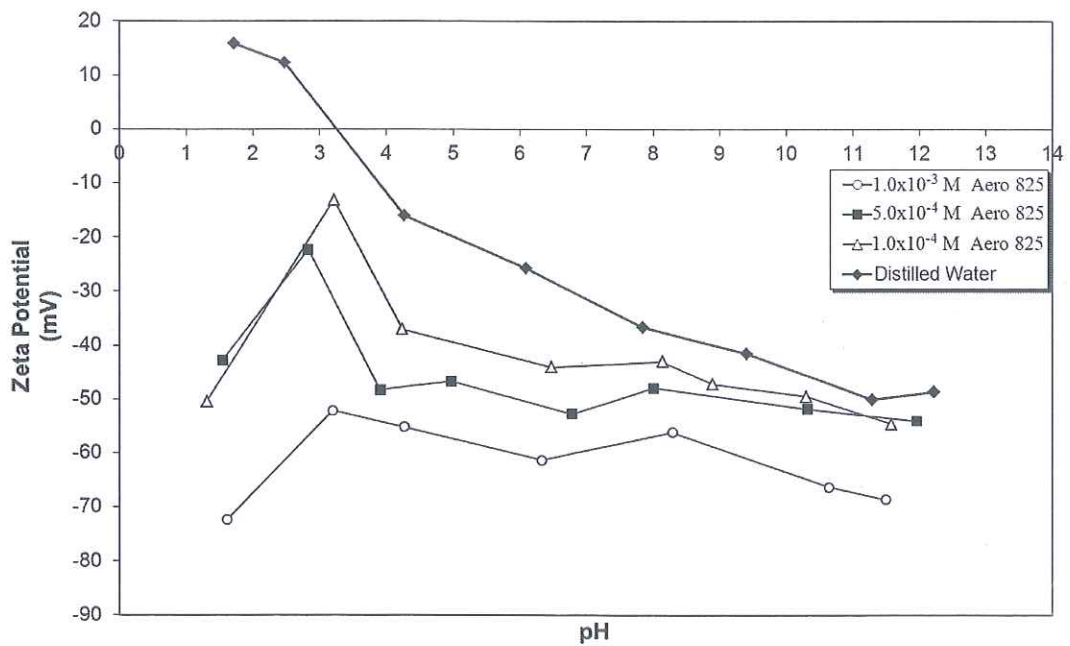
Figure 4.154 Zeta Potential of Rutile as a Function of pH and Aero 825 Concentration.

The additional electrokinetic potential measurements in order to investigate the effect of acetone washing on the zeta potential values of the collector-treated rutile samples were carried out as a function on pH. The samples were first conditioned with each collector in optimum flotation conditions and then washed with acetone several times prior to electrokinetic potential measurements. The optimum conditions were 3.5×10^{-4}M of Aero 704 about pH 9.5, 5.0×10^{-5}M of Aero 3000C about pH 3.0, 2.0×10^{-4}M of Aero 825 about pH 5.0. The results showed that the zeta potential values were found to be very similar to each other for all pH ranges (Figure 4.155).
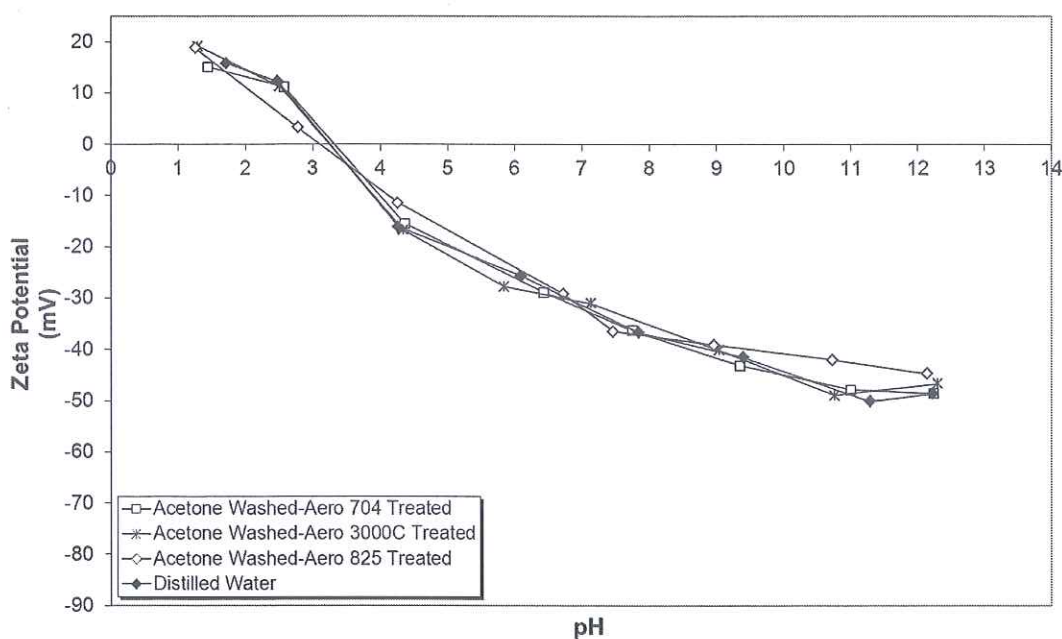
Figure 4.155   Zeta Potentials of Aero 704, Aero 3000C and Aero 825 Treated Rutile Samples After Acetone Washing.

4.6.2   Flotation Studies on Rutile

The flotation recoveries of rutile as a function of pH and Aero 704 concentration were shown in Figure 4.156. As the flotation recovery of rutile was null below pH 7.0, the micro-flotation experiments were performed from this pH on with all Aero 704 concentrations. It is seen that the flotation recovery of rutile in the presence of varying Aero 704 concentration was very pH dependent and increased proportionally

188

to Aero 704 concentration below the highest concentration experimented, 5.0×10^{-4} M. The maximum flotation recoveries were obtained as 46.0% with 2.0×10^{-4} M, 67.5% with 2.75×10^{-4} M, 85.0% with 3.5×10^{-4} M and 75.5% with 5.0×10^{-4} M of Aero 704. The flotation recoveries decreased sharply below and above the pH where the maximum recoveries obtained for all Aero 704 concentrations.

The flotation recoveries of the rutile were maximum between the pH 3.5 and 10.5 with the values of 67.5% with 2.0×10^{-5} M, 90.0% with 5.0×10^{-5} M, 92.0% with 7.5×10^{-5} M and 97.0% with 1.0×10^{-4} M of Aero 3000C respectively (Figure 4.157). The flotation recoveries decreased sharply above and below pH where the maximum recoveries were obtained for all Aero 3000C concentrations.

In the case of Aero 825, the flotation recoveries of rutile were shown in Figure 4.158 as function of pH and concentration. The flotation recovery increased with increasing Aero 825 concentration. From the figure, the effective pH range on the flotation recovery of rutile was found between the pH range of 3.5 and 6.0. The maximum recoveries were obtained as 31.0% with 1.5×10^{-4} M, 69.0% with 2.0×10^{-4} M, 76.0% with 5.0×10^{-4} M and 80.0% with 1.0×10^{-3} M of Aero 825 respectively. The flotation recoveries of rutile in all Aero 825 concentrations decreased sharply below and above the given pH range.
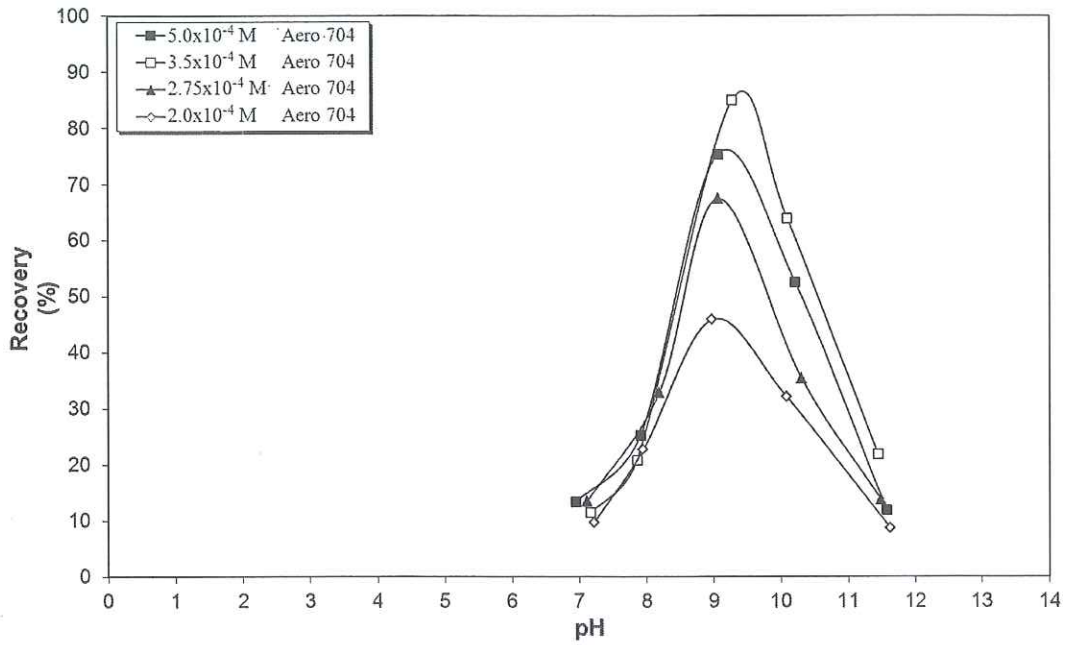
Figure 4.156 Flotation Recovery of Rutile as a Function of pH and Aero 704 Concentration.
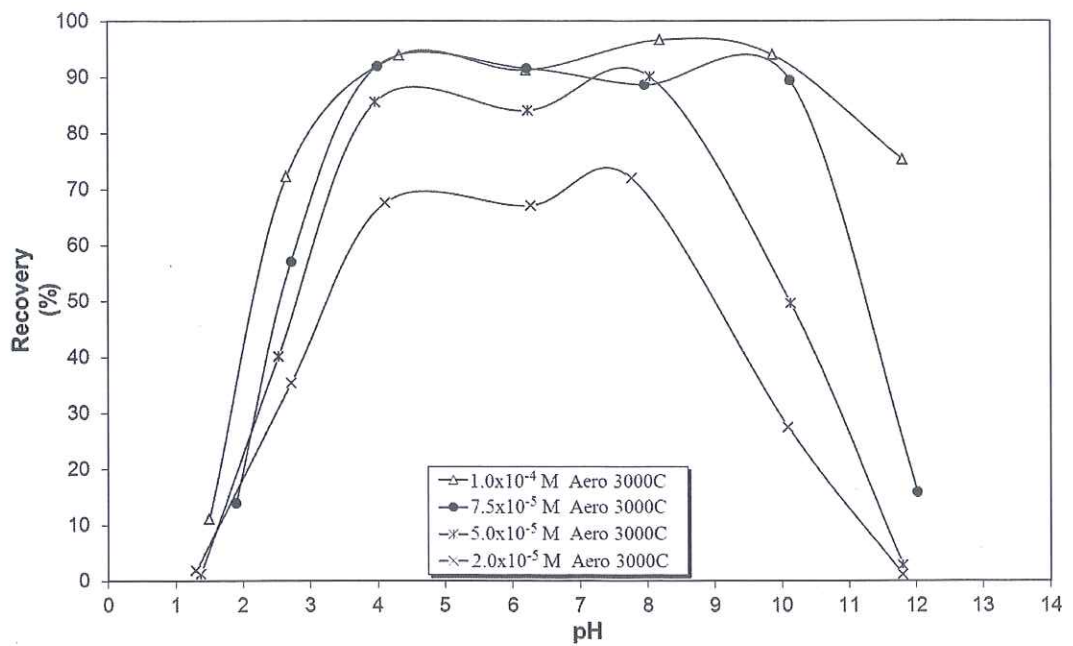
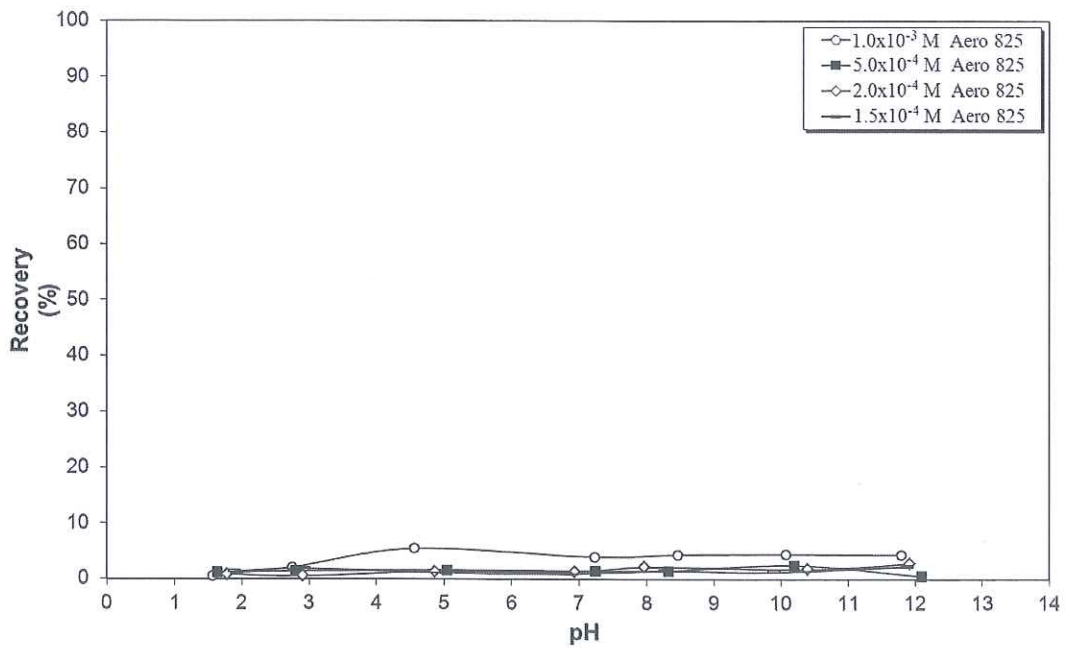Figure 4.157 Flotation Recovery of Rutile as a Function of pH and Aero 3000C Concentration.
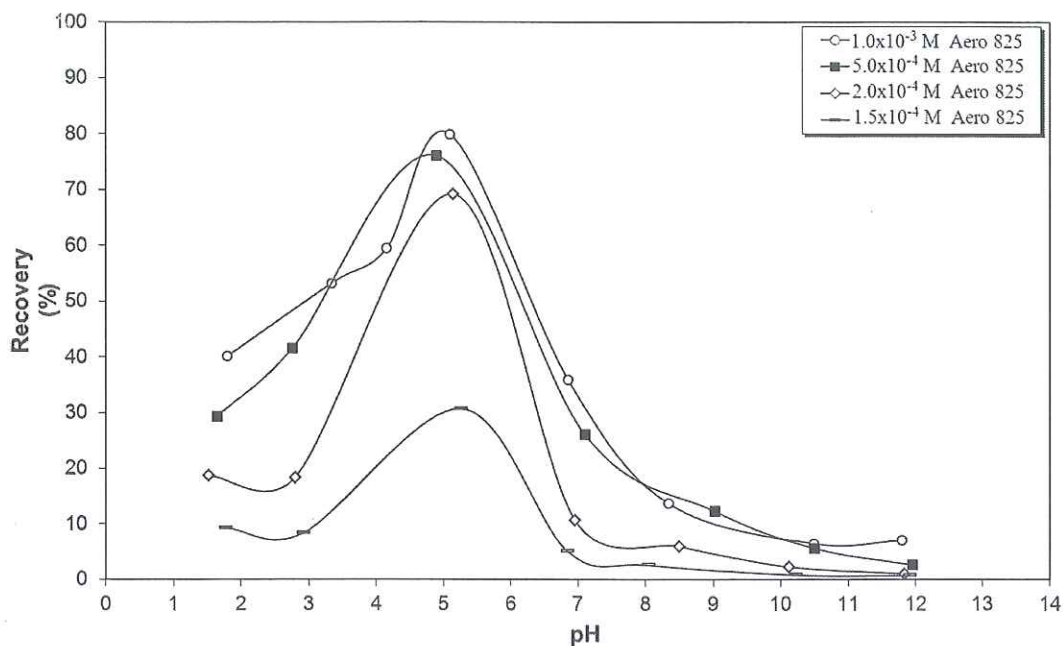
Figure 4.158   Flotation Recovery of Rutile as a Function of pH and Aero 825 Concentration.

4.6.3   AFM Studies on Rutile

The tapping mode AFM 3D micro topographies of rutile in 100nm (Figure 4.159a) and 1μm (Figure 4.159c) sizes and their corresponding histograms and roughness analyses (Figure 4.159b and Figure 4.159d) were given in Figure 4.159. The resulting histogram provides information about the surface roughness, the maximum peak value and the average height values of rutile for 100nm x 100nm and 1μm x 1μm scanning size ranges. The corresponding histograms revealed the roughness average as 0.1922nm, the maximum peak value as 1.7995nm and the average height value as 0.8350nm for 100nm x 100nm scanning size range and 0.6772nm, 5.8584nm and 2.4952nm for 1μm x 1μm scanning size range respectively.
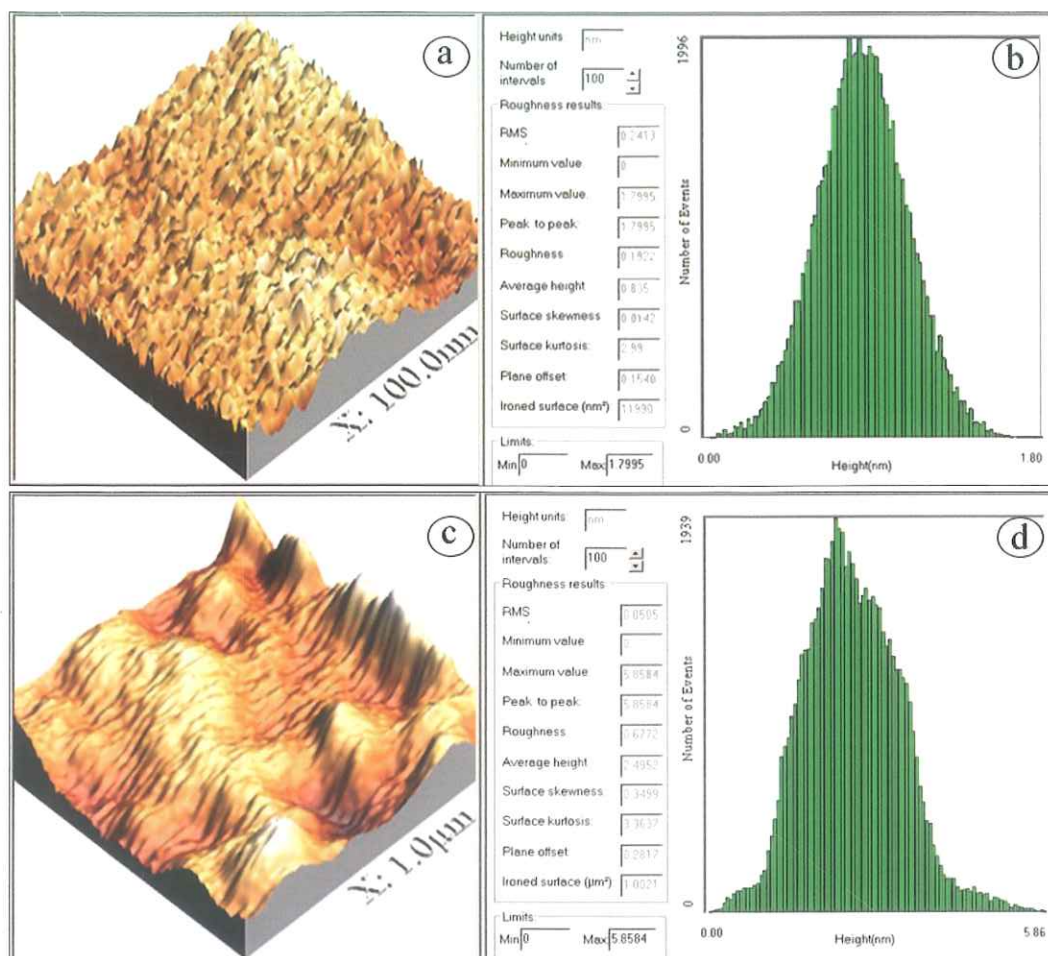
Figure 4.159   3D Micro Topographies, Corresponding Histograms and Roughness Analyses of Rutile.

The tapping mode AFM 3D micro topographies (Figure 4.160a and 4.160c) and the corresponding histograms (Figure 4.160b and 4.160d) of the Aero 704-treated rutile revealed the roughness average as 0.2806nm, the maximum peak value as 2.5235nm and the average height value as 1.2403nm for 100nm x 100nm scanning size and 0.7480nm, 6.1523nm and 2.9825nm for 1μm x 1μm scanning size range, respectively (Figure 4.160). The tapping mode AFM image analysis of rutile and Aero 704-treated rutile based on their height profiles in 1μm were shown in Figure 4.161 for the scanned area. The rutile and the Aero 704-treated rutile showed similarities with a low height difference compared to each other.
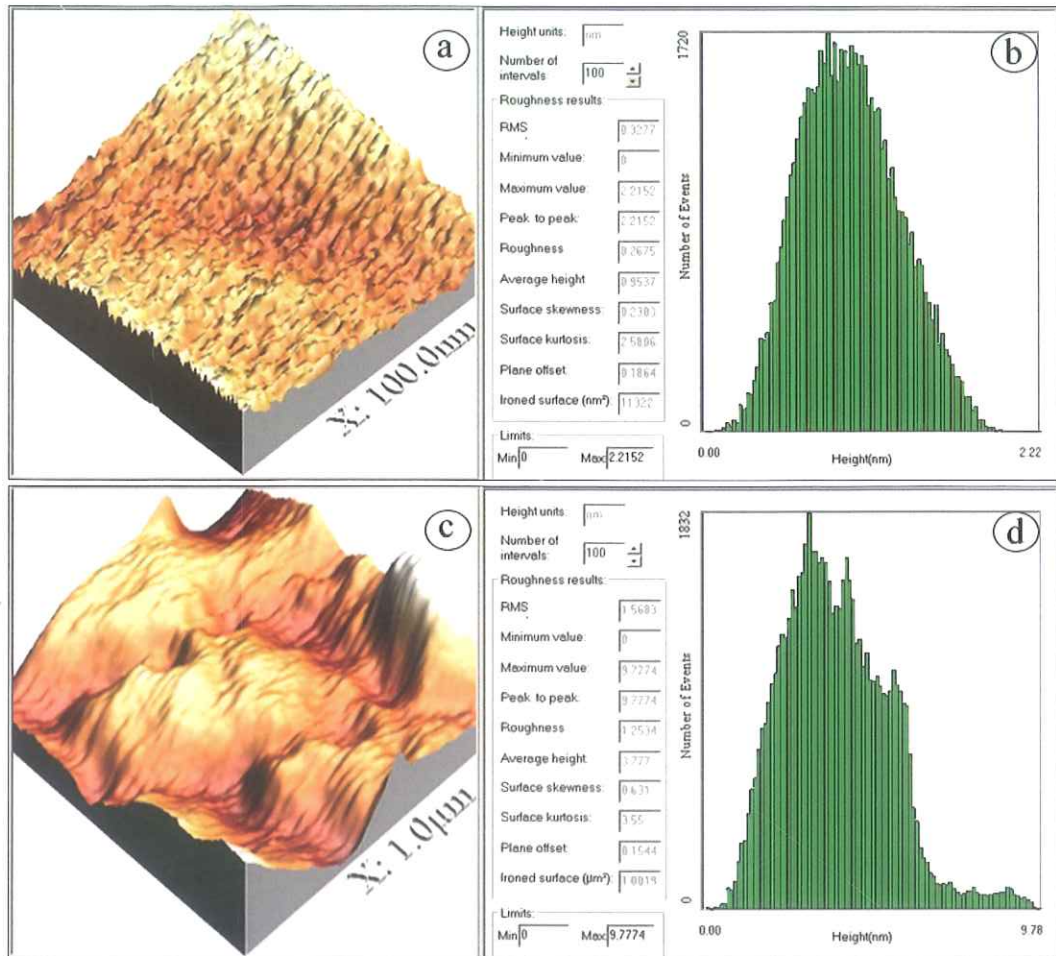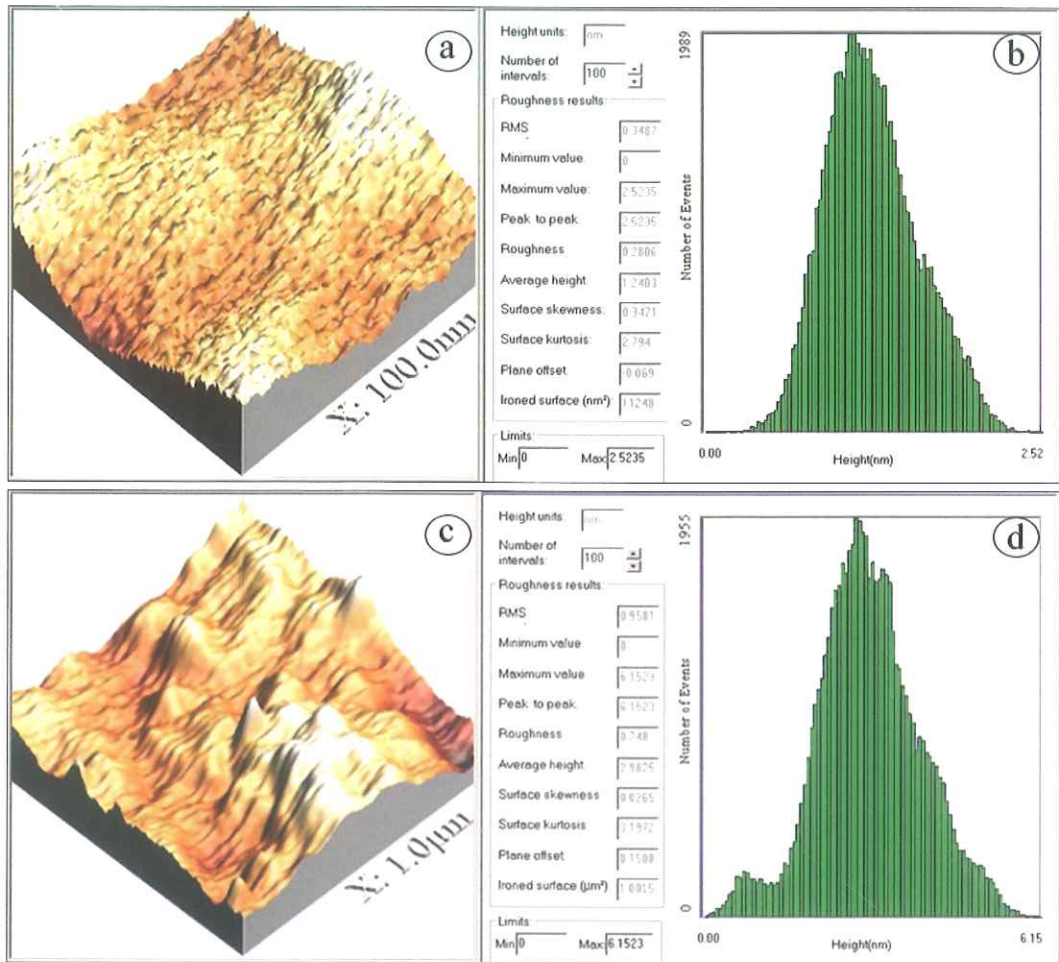
Figure 4.160   3D Micro Topographies, Corresponding Histograms and Roughness Analyses of Aero 704-Treated Rutile.
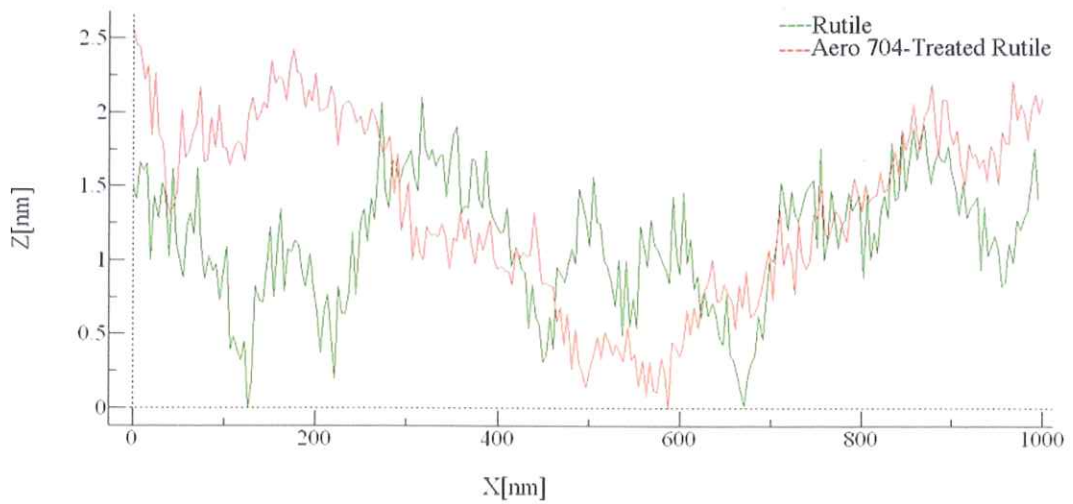
Figure 4.161   Height Profiles of Rutile and Aero 704-Treated Rutile in 1μm Size.

The tapping mode AFM 3D micro topographies and the corresponding histograms of Aero 3000C-treated and Aero 825-treated rutile in 100nm x 100nm (Figure 4.162a-b for Aero 3000C-treated and Figure 4.164a-b for Aero 825-treated rutile) and 1μm x 1μm (Figure 4.162c-d for Aero 3000C-treated and Figure 4.164c-d for Aero 825-treated rutile) scanning size ranges were given in Figure 4.162 and Figure 4.164 respectively. For Aero 3000C-treated rutile, the histograms revealed that the roughness averages, the maximum peak values and the average height values as 0.2104nm, 2.0564nm and 0.8765nm for 100nm x 100nm scanning size and 0.7167nm, 9.9664nm and 3.0709nm for 1μm x 1μm scanning size range, respectively. In the case of Aero 825-treated rutile, the roughness averages, the maximum peak values and the average height values were obtained as 0.2343nm, 2.1051nm and 1.0657nm for 100nm x 100nm scanning size range and 1.8716nm, 18.632nm and 6.0682nm for 1μm x 1μm scanning size range respectively.

The tapping mode AFM image analysis of rutile and Aero 3000C-treated rutile based on their height profiles in 1μm was shown in Figure 4.163 for the scanned area. Similarly, the tapping mode AFM image analysis of rutile and Aero 825-treated rutile was shown in Figure 4.165. The height profiles of Aero 3000C-treated rutile reached to 4.0nm and the Aero 825-treated rutile reached to 8.5nm while the rutile (shown in green in the figures) displayed height profiles less than 2.0nm for the scanned area.
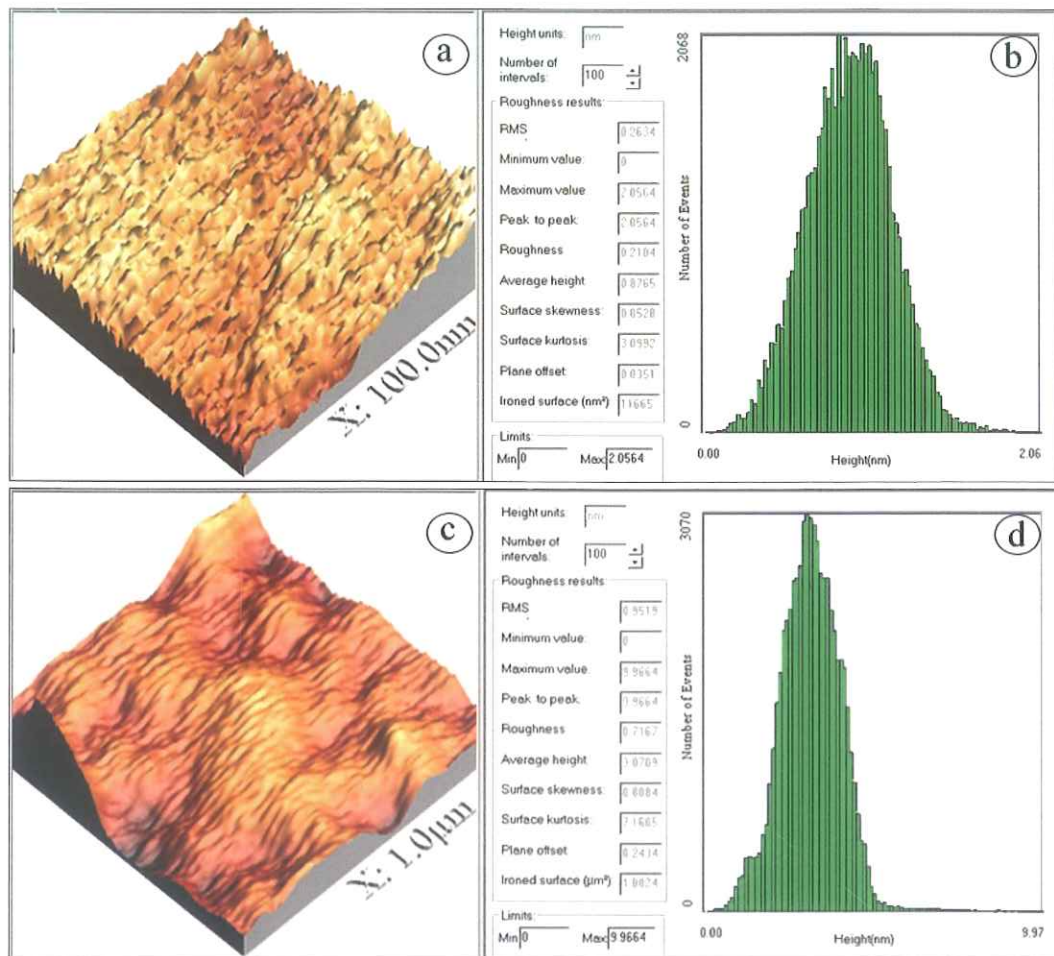
Figure 4.162   3D Micro Topographies, Corresponding Histograms and Roughness Analyses of Aero 3000C-Treated Rutile.
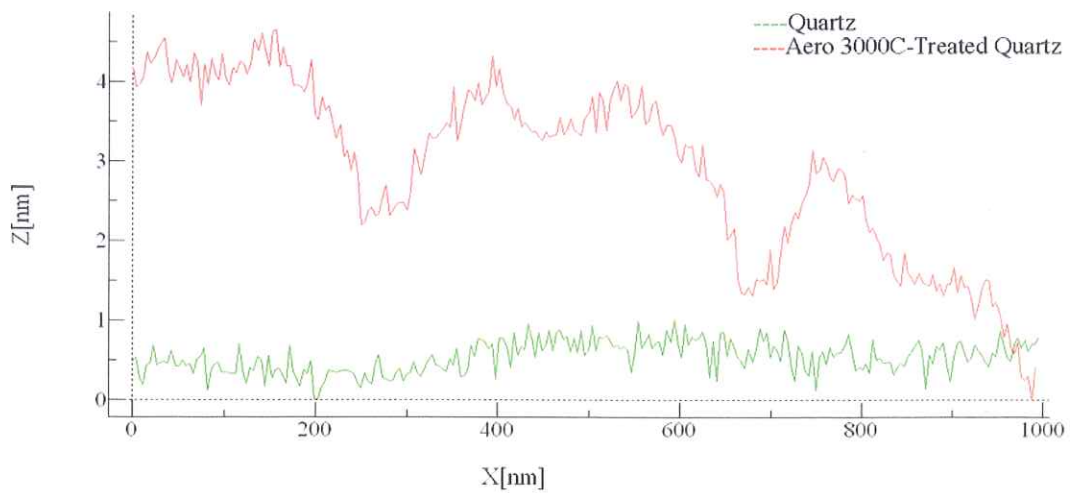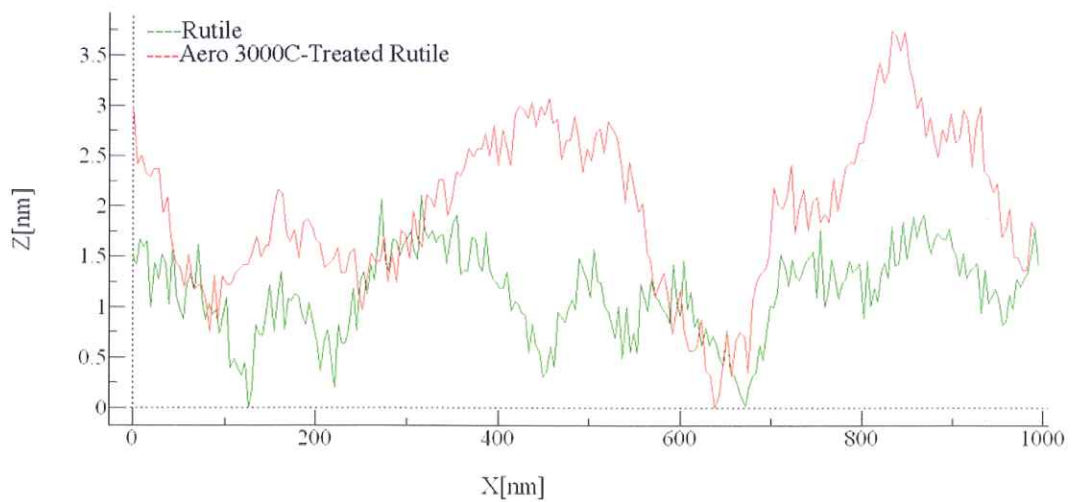

Figure 4.163   Height Profiles of Rutile and Aero 3000C-Treated Rutile in 1µm Size.
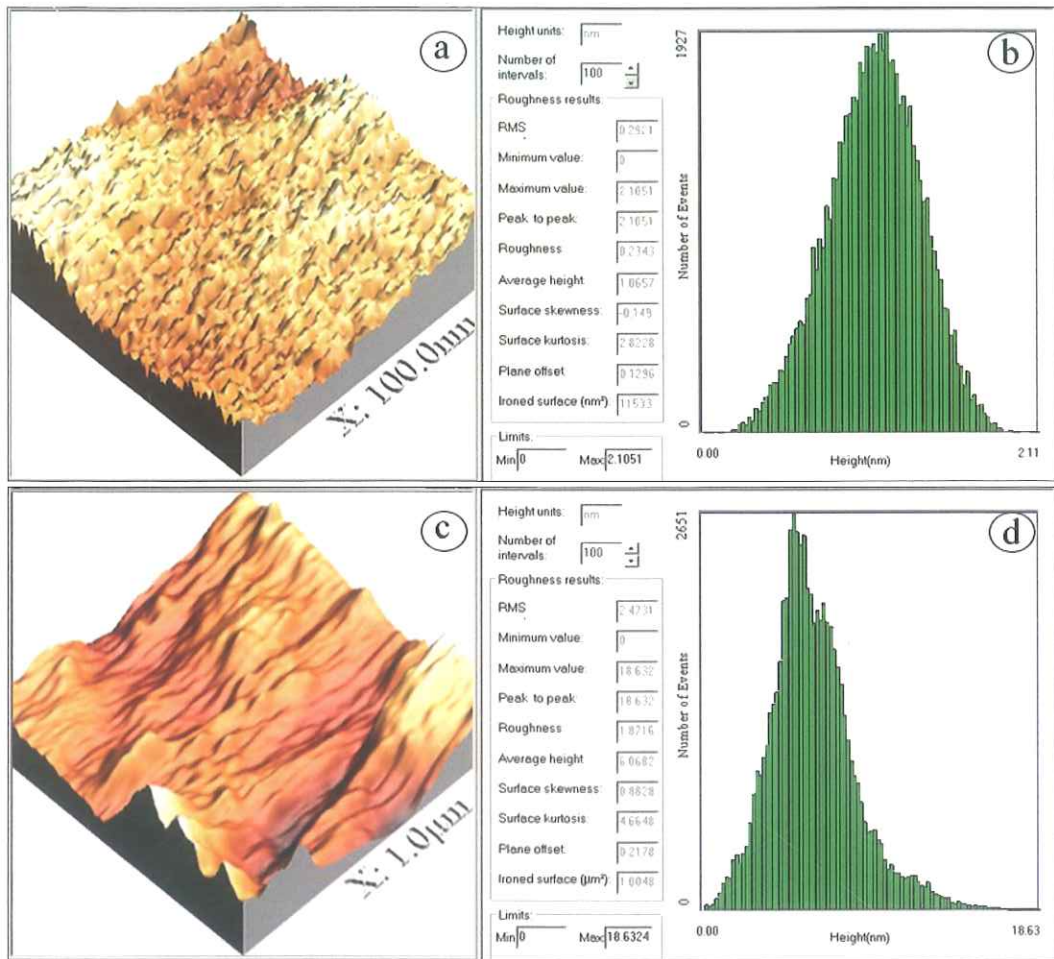
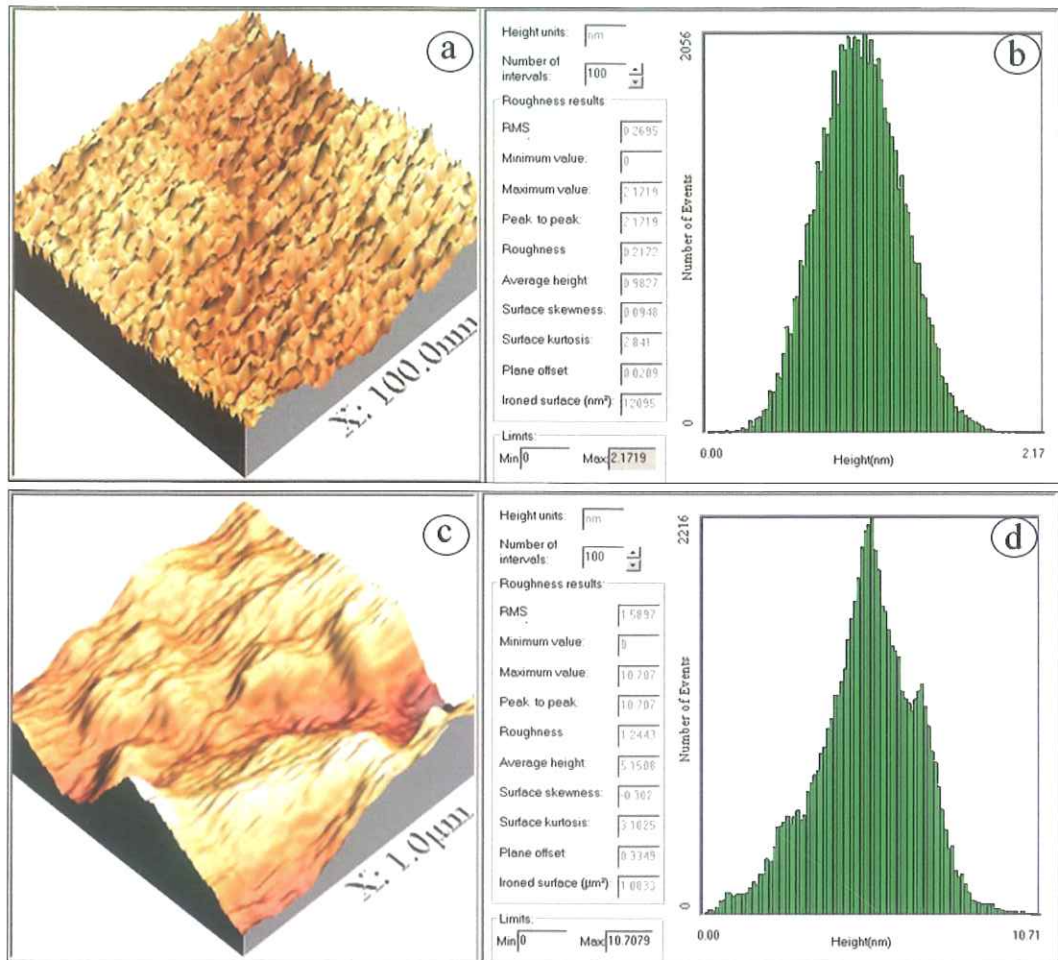Figure 4.164   3D Micro Topographies, Corresponding Histograms and Roughness Analyses of Aero 825-Treated Rutile.
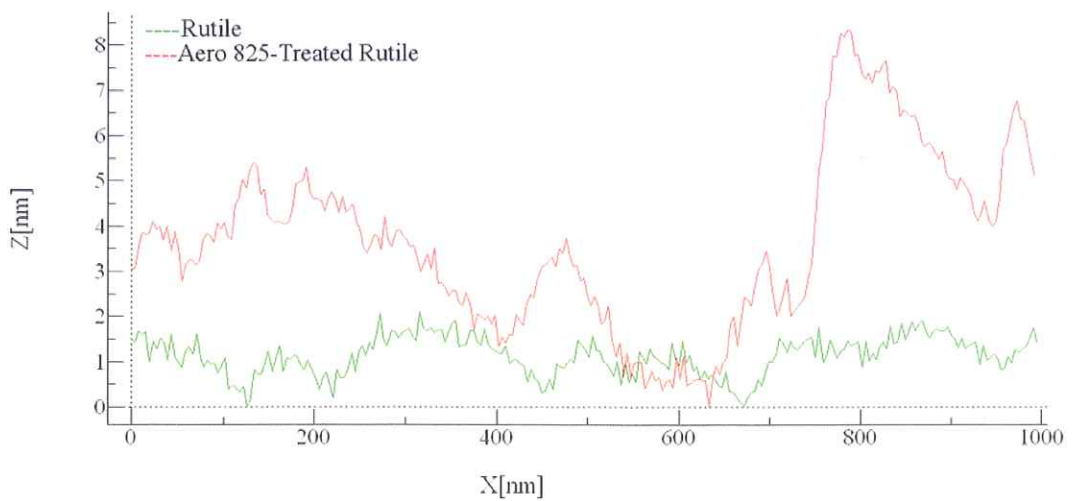
Figure 4.165   Height Profiles of Rutile and Aero 825-Treated Rutile in 1µm Size.

4.6.4 FTIR Spectroscopy Studies on Rutile

In the similar way as previous mineral samples, the FTIR analysis of the rutile, collector-treated rutile and acetone-washed rutile samples were examined and the resulting spectra were given in Figure 4.166, Figure 4.171 and Figure 4.176 for Aero 704, Aero 3000C and Aero 825 respectively.

In order to obtain more detailed FTIR spectra, the full scale FTIR spectra (4000-400 cm^{-1}) of collector, non-treated, collector-treated and acetone-washed rutile samples were analyzed in four major zones depending on the collector's FTIR peaks. Figures 4.167-4.180 show the FTIR ranges of rutile in the presence of Aero 704 as 3500-2750 cm^{-1}, 2750-1750 cm^{-1}, 1750-1250 cm^{-1} and 1250-400 cm^{-1} major wavelength's zones respectively.

The FTIR spectrum of Aero 704-treated rutile showed additional weak bands at 2961 cm^{-1}, 2926 cm^{-1} and 2854 cm^{-1} assigned as CH_2 stretching vibrations which come from Aero 704 (Figure 4.167). However, the FTIR spectrum of the Aero 704-treated rutile was altered upon washing several times with acetone and the bands at 2961 cm^{-1}, 2926 cm^{-1} and 2854 cm^{-1} disappeared.
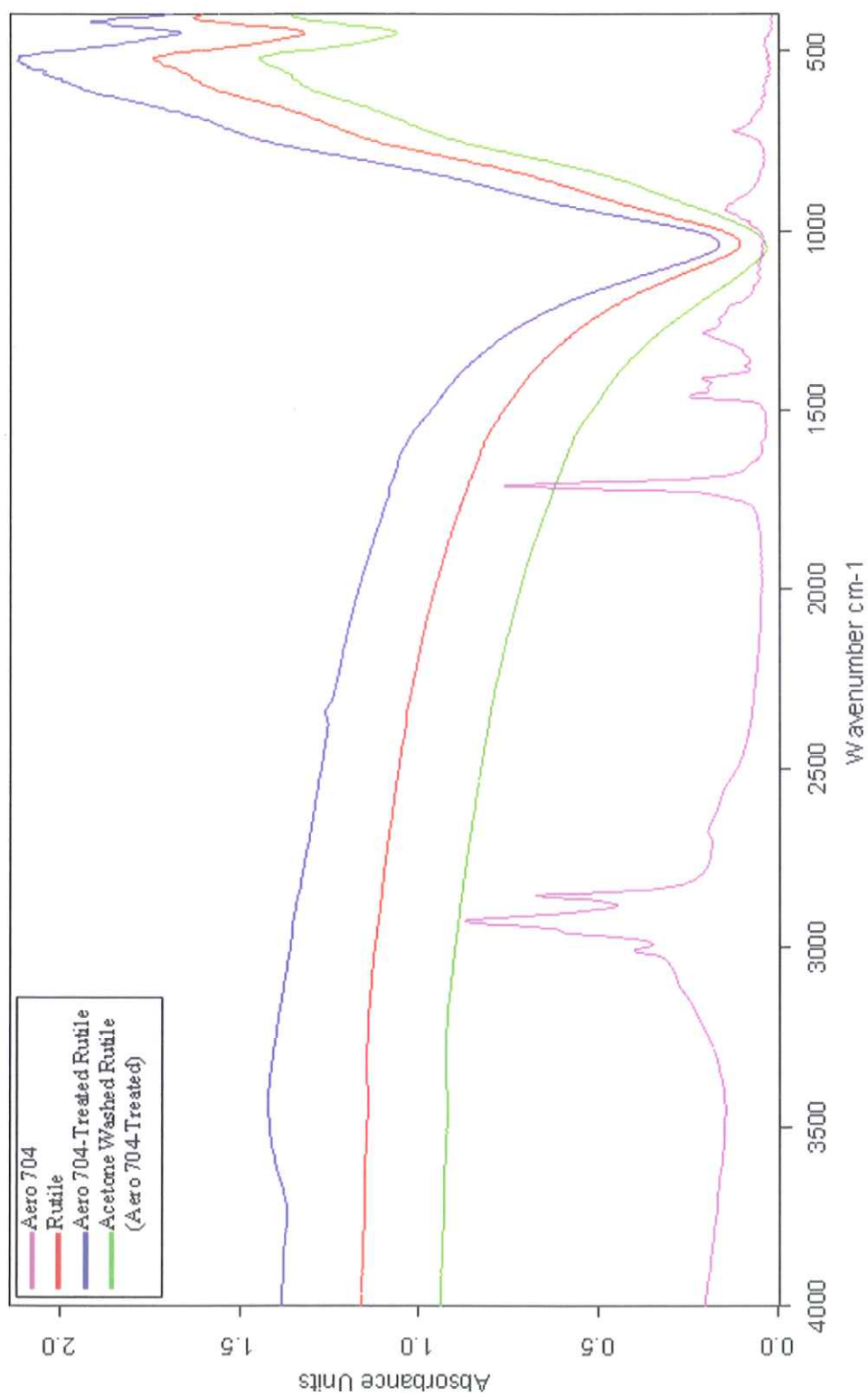
Figure 4.166   FTIR Spectrum of Rutile in the Presence of Aero 704 in 4000–400 cm^{-1} Wavelength Range.
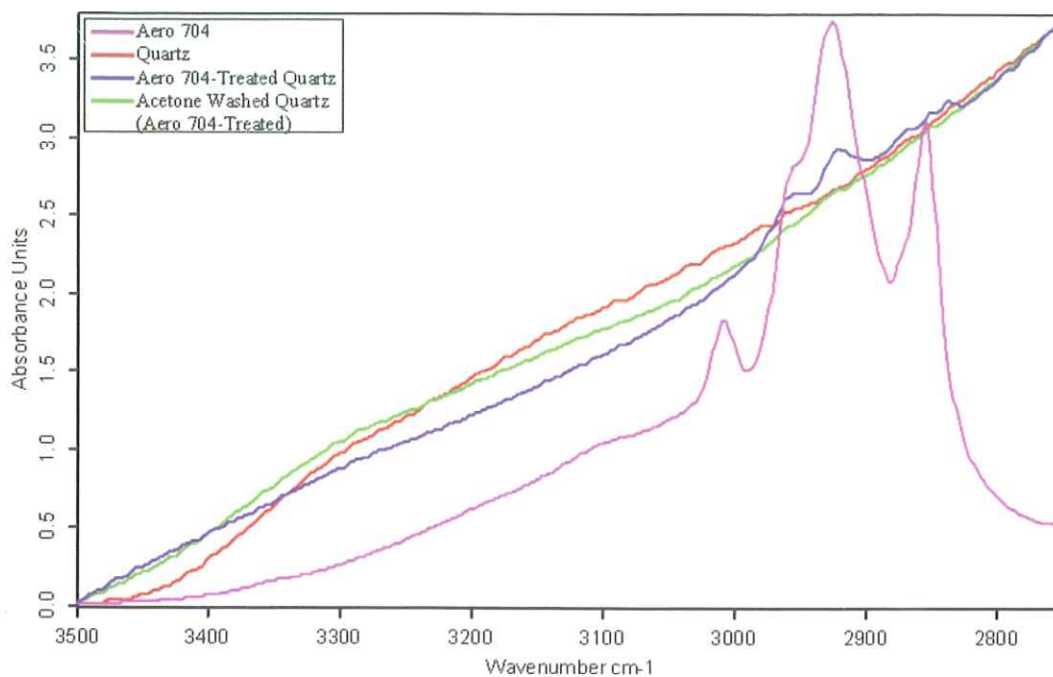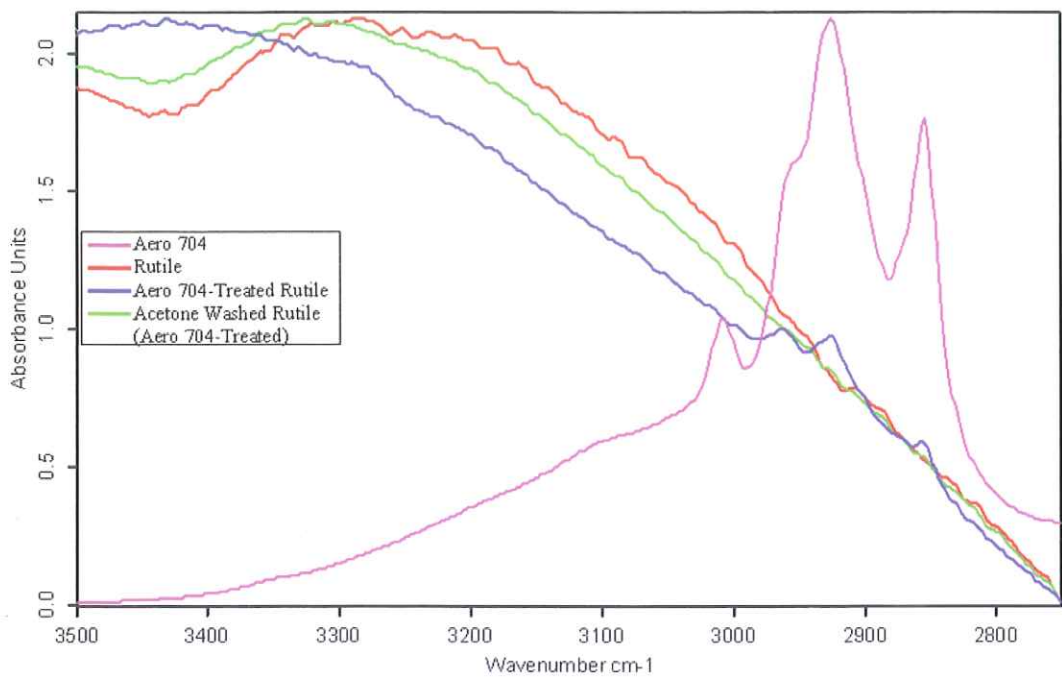
Figure 4.167   FTIR Spectrum of Rutile in the Presence of Aero 704 in 3500–2750 cm^{-1} Wavelength Range.
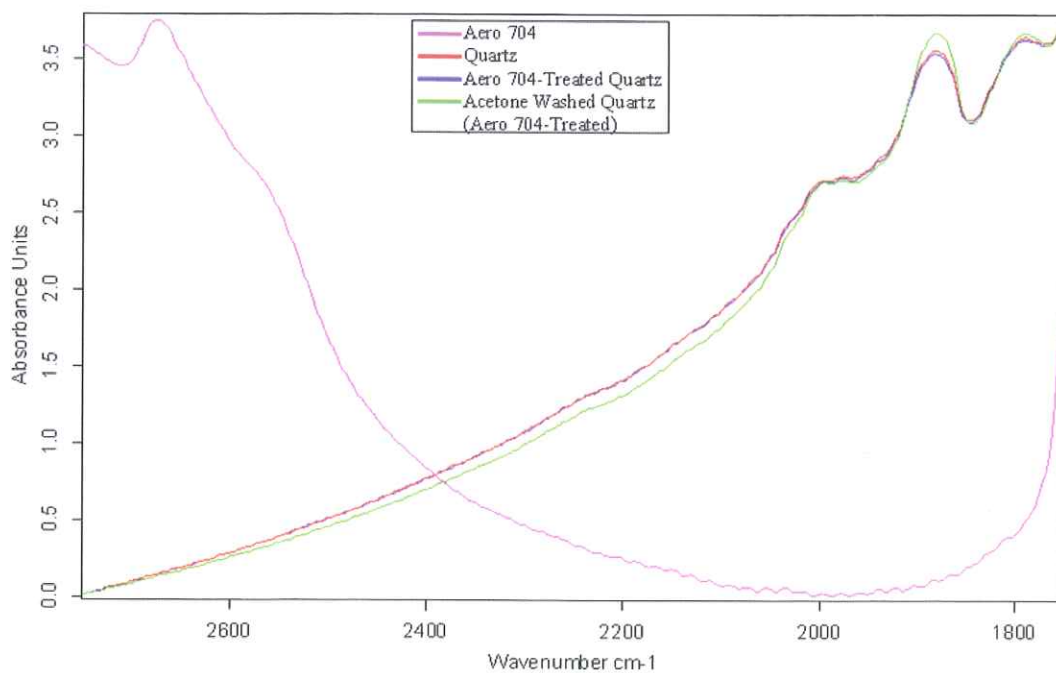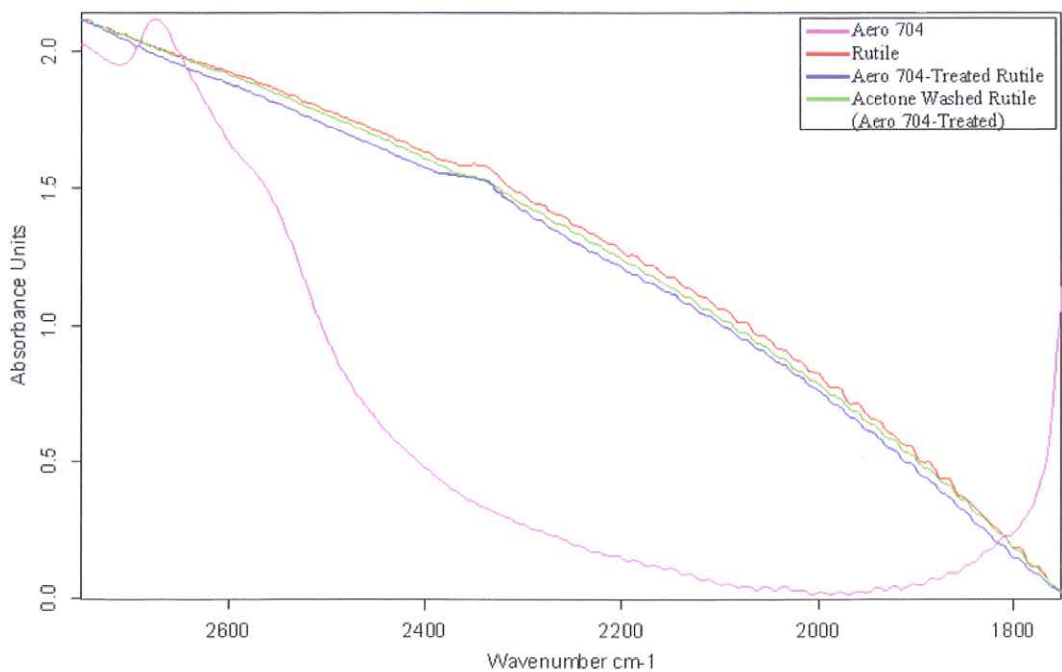

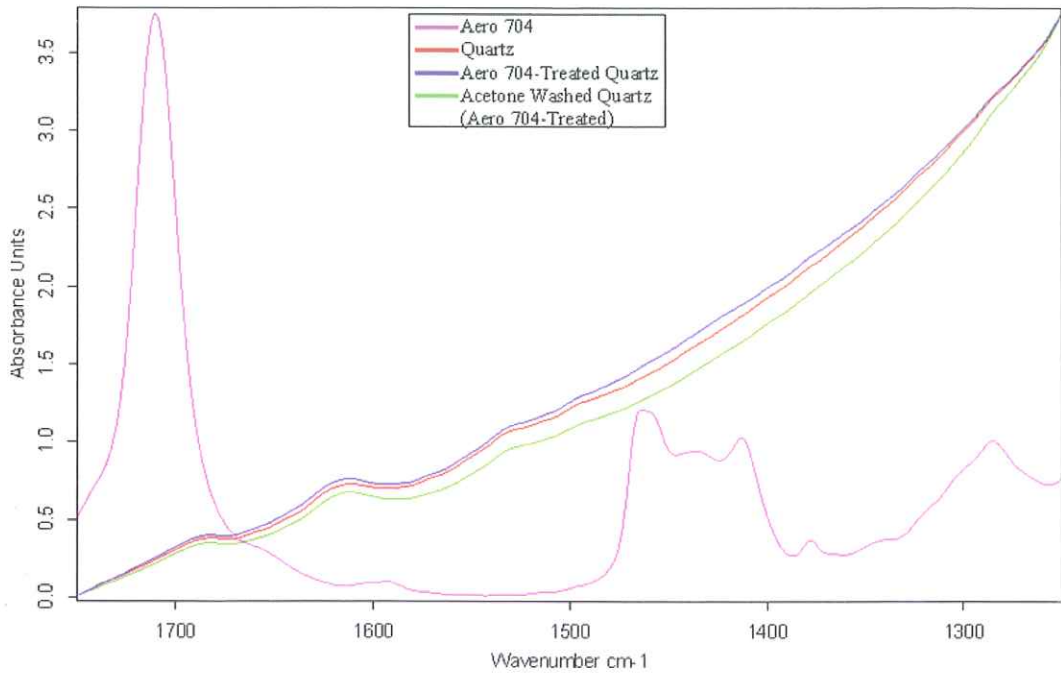Figure 4.168   FTIR Spectrum of Rutile in the Presence of Aero 704 in 2750–1750 cm^{-1} Wavelength Range.
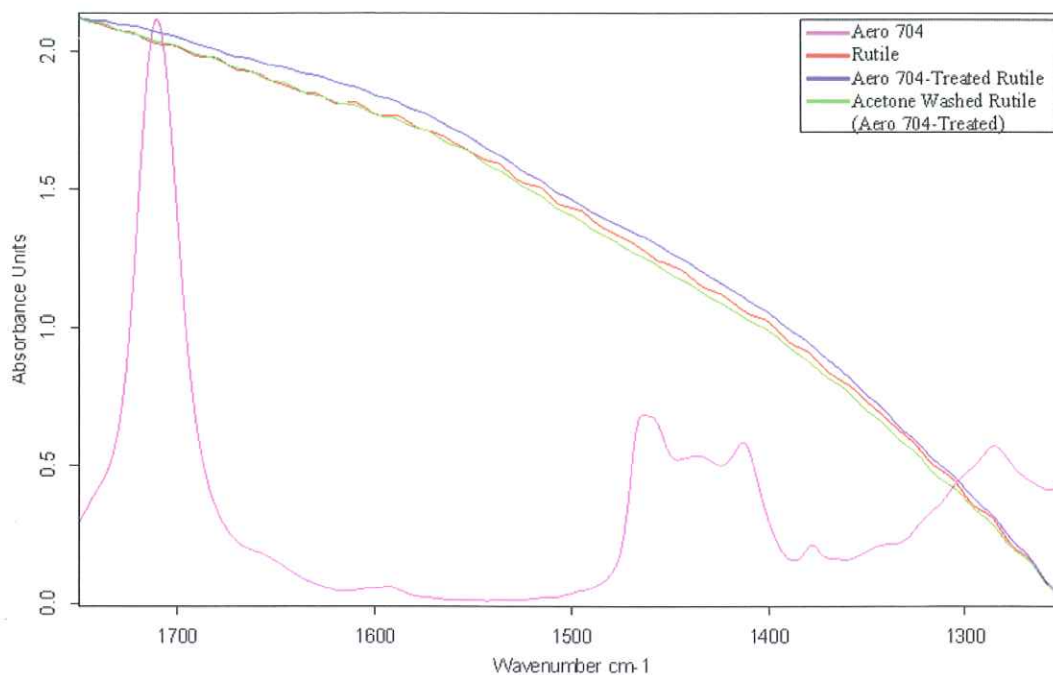
Figure 4.169   FTIR Spectrum of Rutile in the Presence of Aero 704 in 1750–1250 cm^{-1} Wavelength Range.
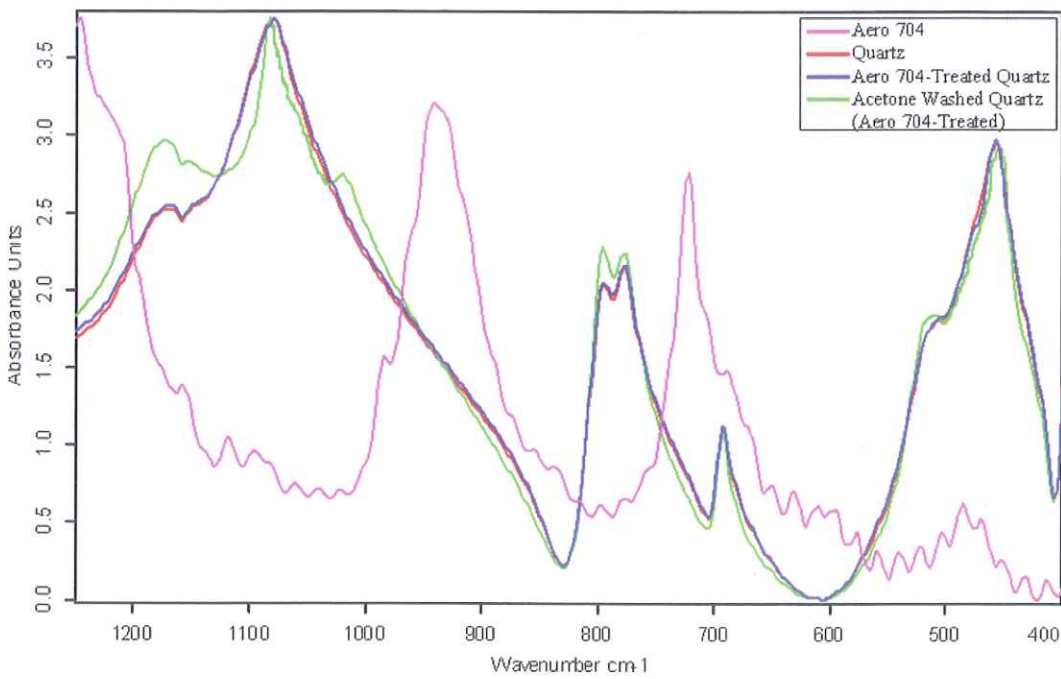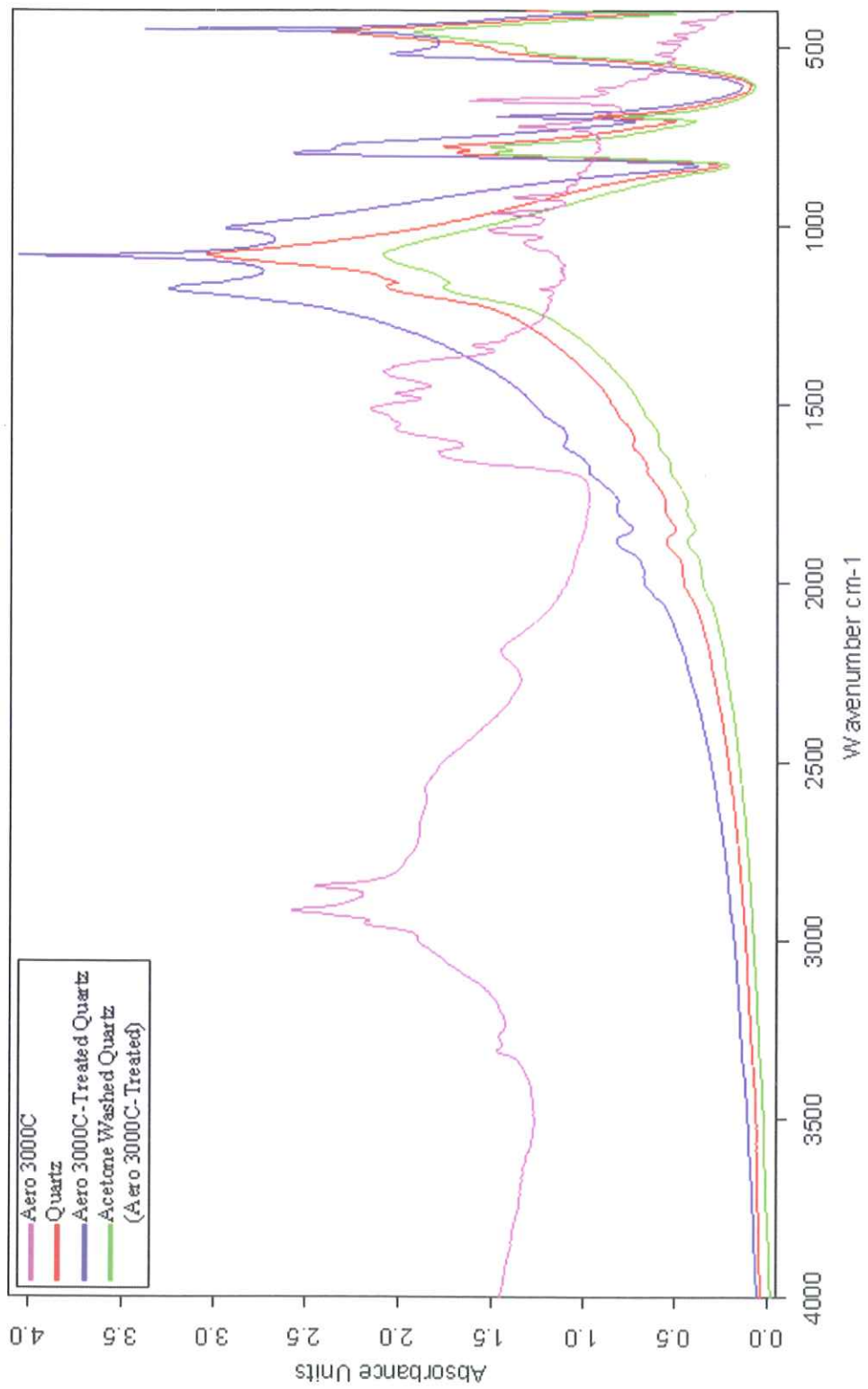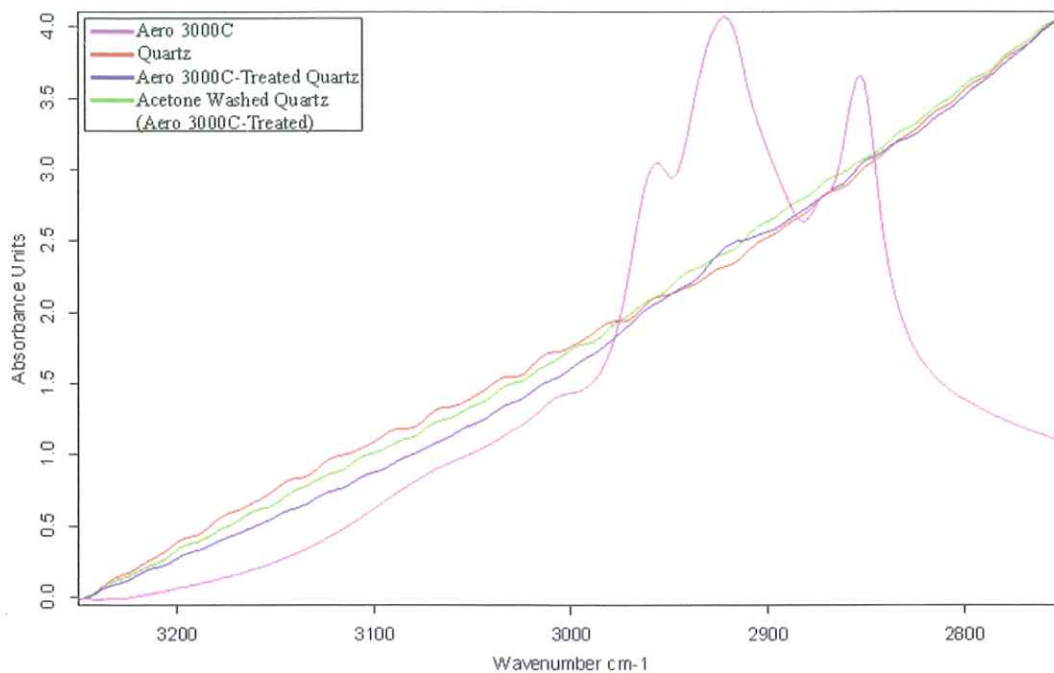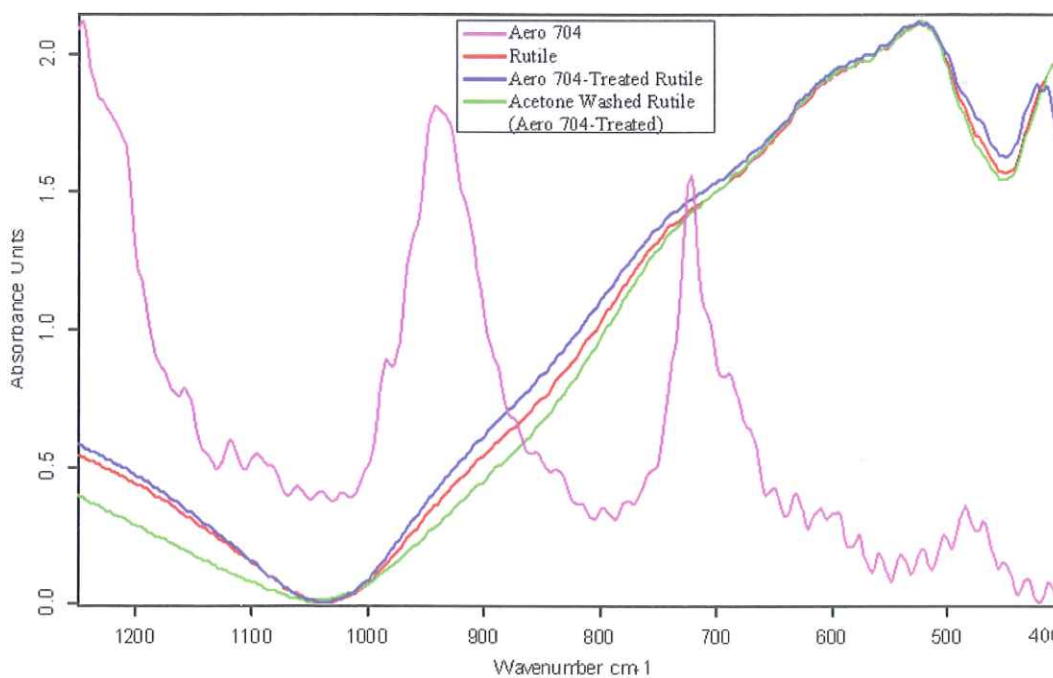

Figure 4.170   FTIR Spectrum of Rutile in the Presence of Aero 704 in 1250–400 cm^{-1} Wavelength Range.

The spectra obtained with Aero 3000C, rutile, Aero 3000C-treated rutile and acetone-washed rutile were given in Figures 4.171 to 4.175. The major zones for the rutile in the presence of Aero 3000C were shown as 3250-2750 cm^{-1}, 2750-1750 cm^{-1}, 1750-1250 cm^{-1} and 1250-400 cm^{-1} wavelengths in Figures 4.172-4.175 respectively.

Aero 3000C-treated rutile showed additional bands at 2957 cm^{-1}, 2922 cm^{-1} and 2853 cm^{-1} with low intensities assigned as C-H stretching vibrations of Aero 3000C (Figure 4.172). However, the FTIR spectrum of the Aero 3000C-treated rutile upon washing with acetone was altered; the additional bands disappeared.

As the rutile had only two bands at 523 cm^{-1} and 409 cm^{-1}, it was easy to determine additional bands below 2750 cm^{-1} wavelength region. In this respect, in Figures 4.173 to 4.175, Aero 3000C-treated and acetone-washed rutile samples did not display any additional band belonging to Aero 3000C in the given wavelength region.
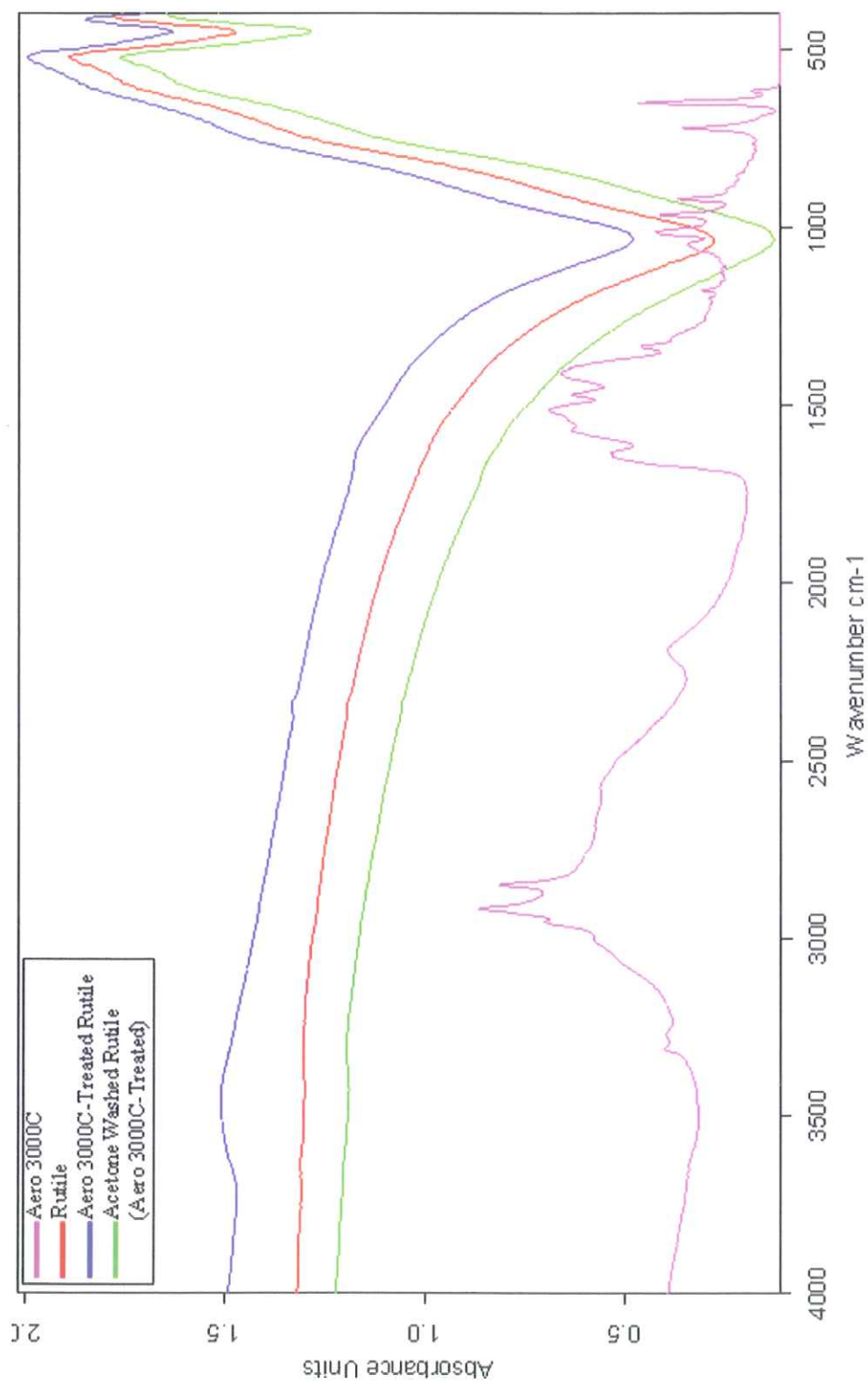
Figure 4.171   FTIR Spectrum of Rutile in the Presence of Aero 3000C in 4000–400 cm^{-1} Wavelength Range.
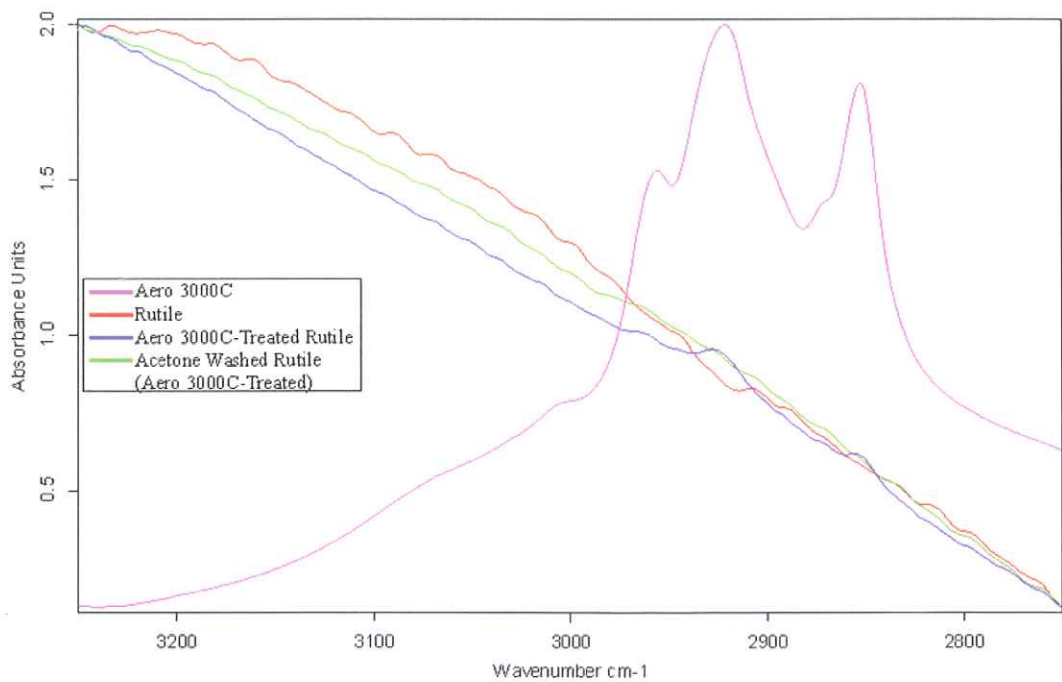
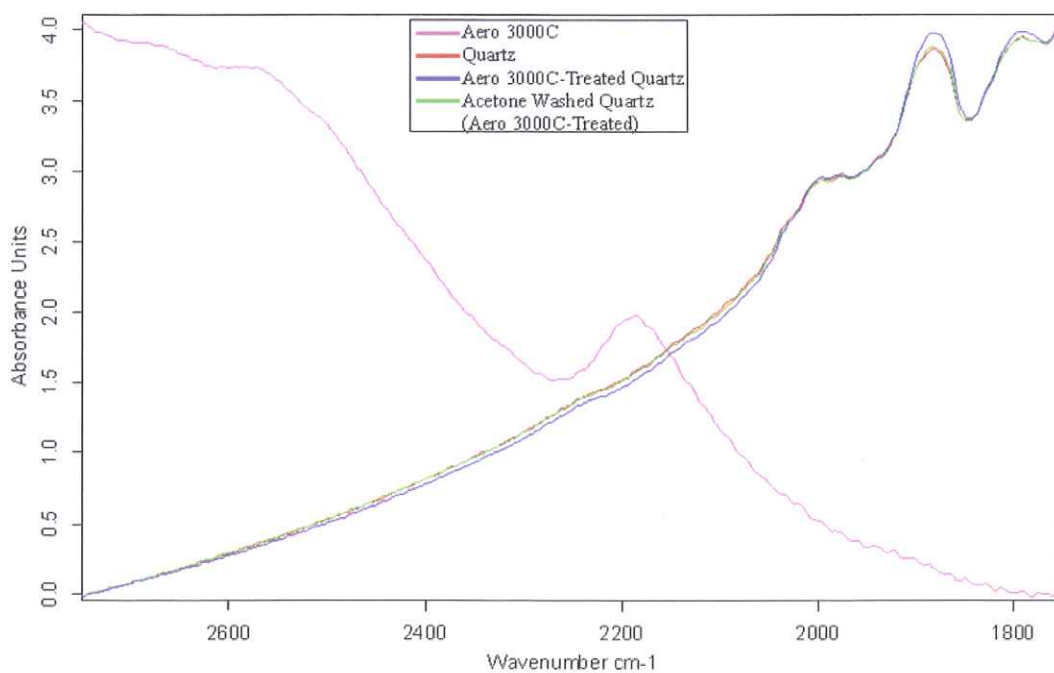Figure 4.172   FTIR Spectrum of Rutile in the Presence of Aero 3000C in 3250–2750 cm⁻¹ Wavelength Range.
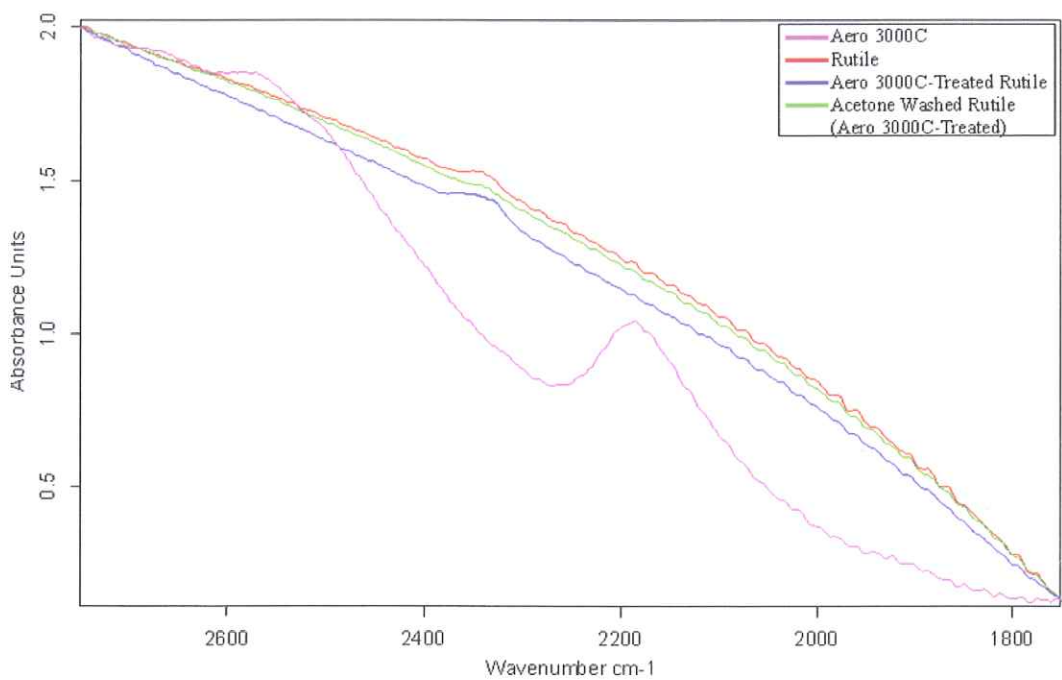
Figure 4.173   FTIR Spectrum of Rutile in the Presence of Aero 3000C in 2750–1750 cm⁻¹ Wavelength Range.
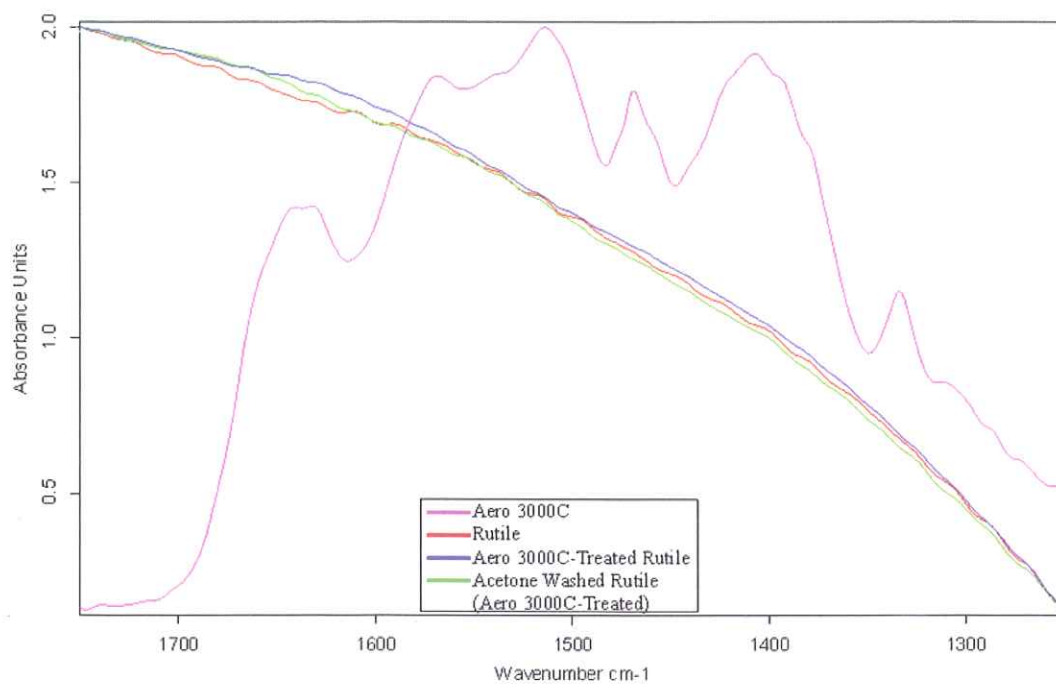
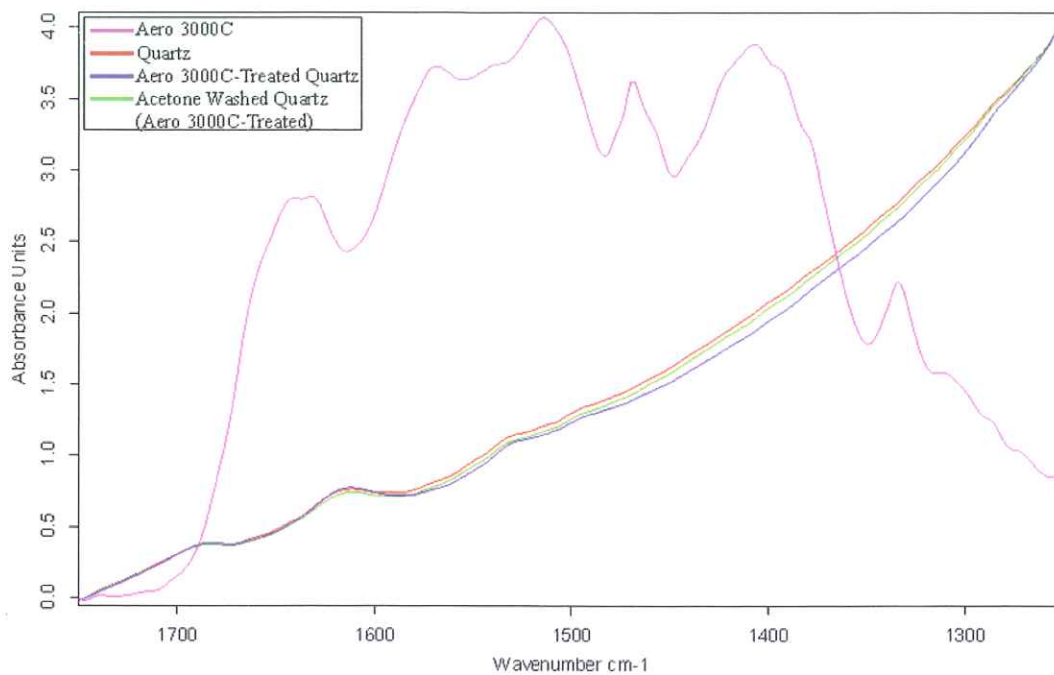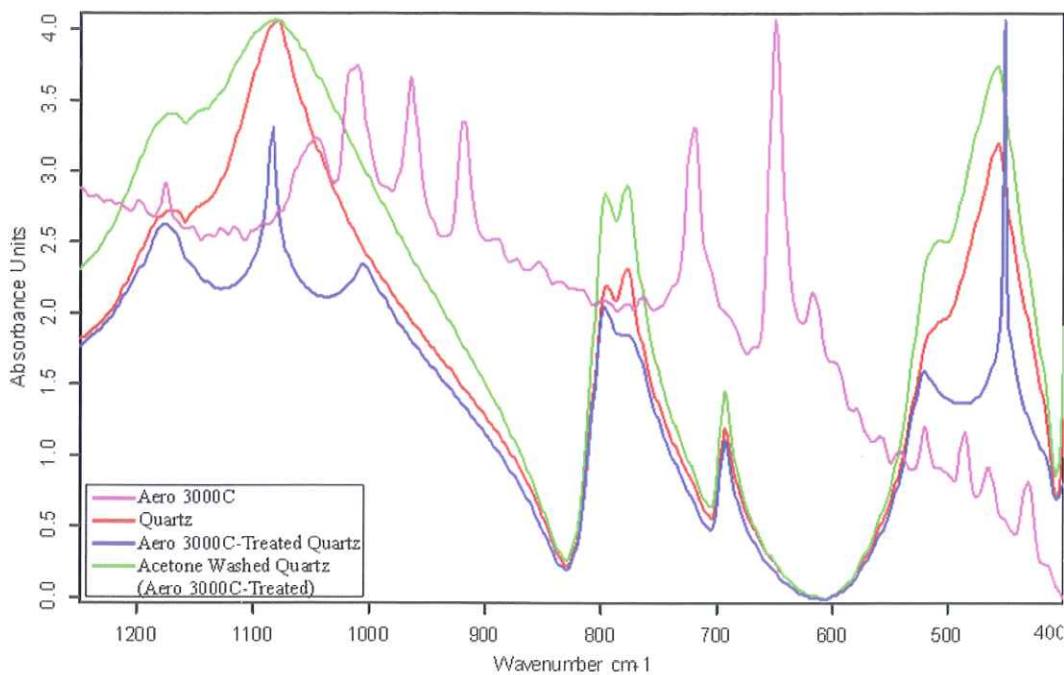Figure 4.174   FTIR Spectrum of Rutile in the Presence of Aero 3000C in 1750–1250 cm^{-1} Wavelength Range.
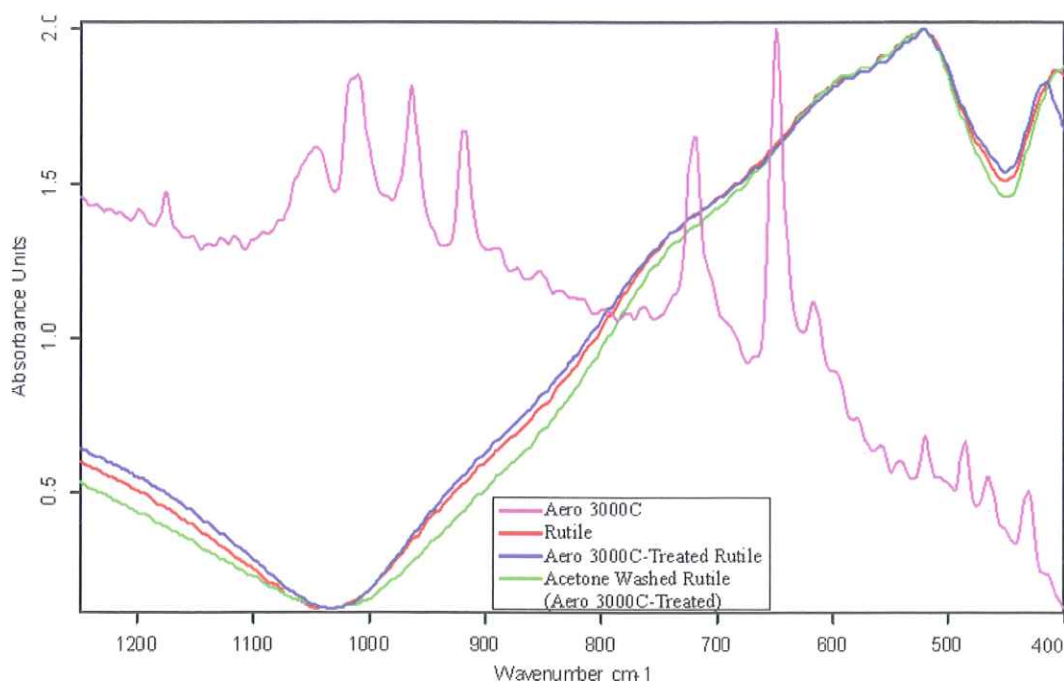
Figure 4.175   FTIR Spectrum of Rutile in the Presence of Aero 3000C in 1250–400 cm^{-1} Wavelength Range.

The spectra obtained for Aero 825 are given in Figures 4.176-4.180. In order to provide more detailed spectra, the major zones for the rutile in the presence of Aero 825 were displayed in Figures 4.177-4.180 as 3750-2750 cm^{-1}, 2750-1500 cm^{-1}, 1500-1000 cm^{-1} and 1000-400 cm^{-1} wavelengths depending on the Aero 825's FTIR peaks.

If the characteristic peak positions of rutile and the Aero 825-treated rutile were taken into account (Figure 4.177), the Aero 825-treated rutile displayed additional broad band at 3457 cm^{-1} which assigned to O-H vibration while rutile did not. In addition to this band, there were also additional bands at 2951 cm^{-1}, 2924 cm^{-1} and 2854 cm^{-1} with very low intensities assigned as CH_2 stretching vibrations of Aero 825. The FTIR spectrum of the Aero 825-treated rutile about pH 5.0 was altered upon washing several times with acetone, the broad band at 3457 cm^{-1} and other additional bands of Aero 825 disappeared.
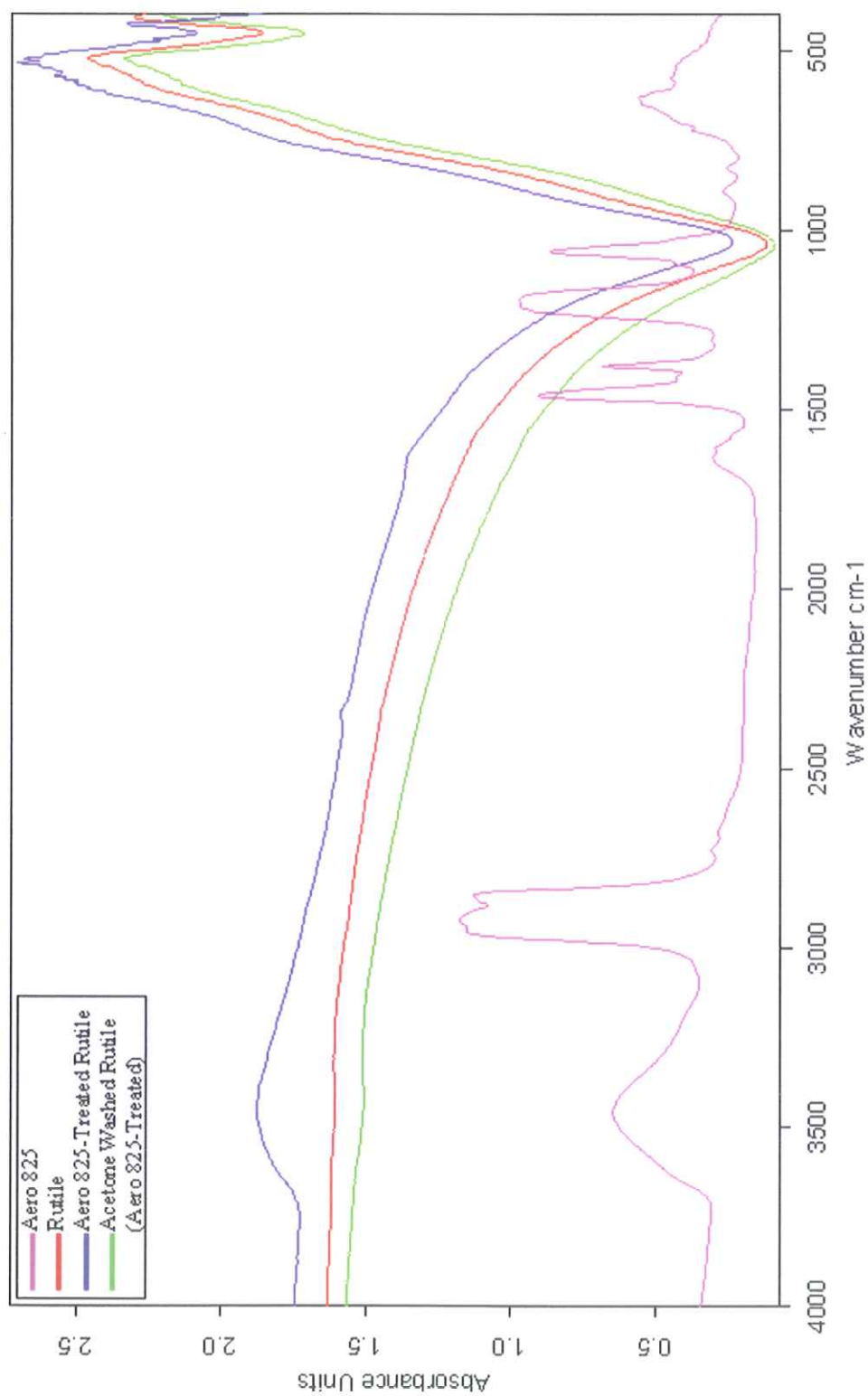
Figure 4.176   FTIR Spectrum of Rutile in the Presence of Aero 825 in 4000–400 cm^{-1} Wavelength Range.
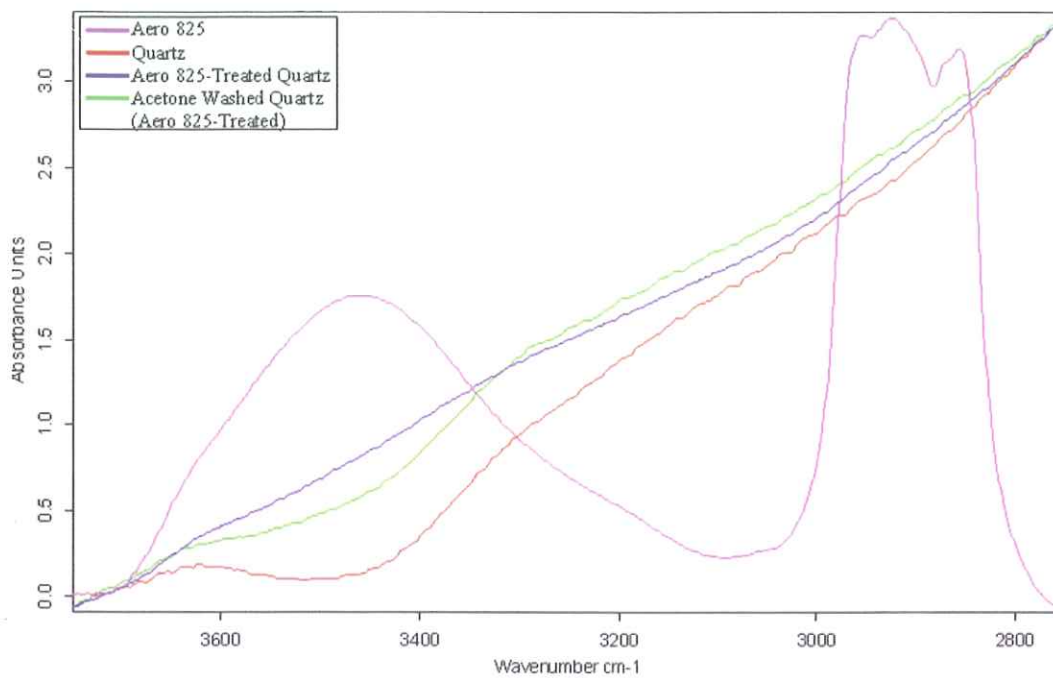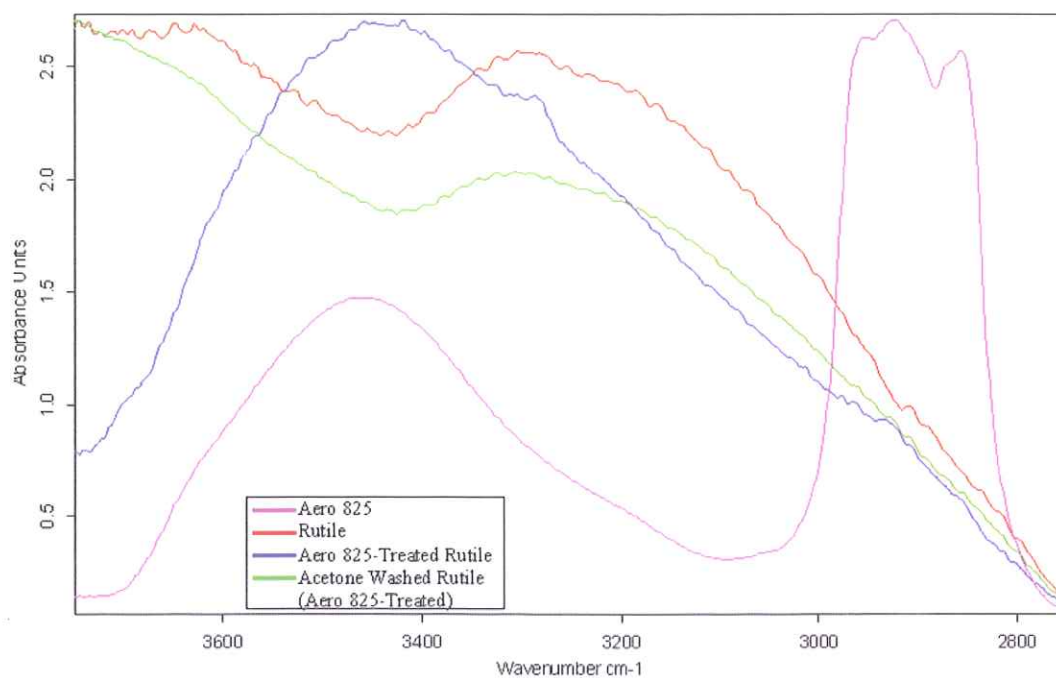
Figure 4.177   FTIR Spectrum of Rutile in the Presence of Aero 825 in 3750–2750 cm^{-1} Wavelength Range.
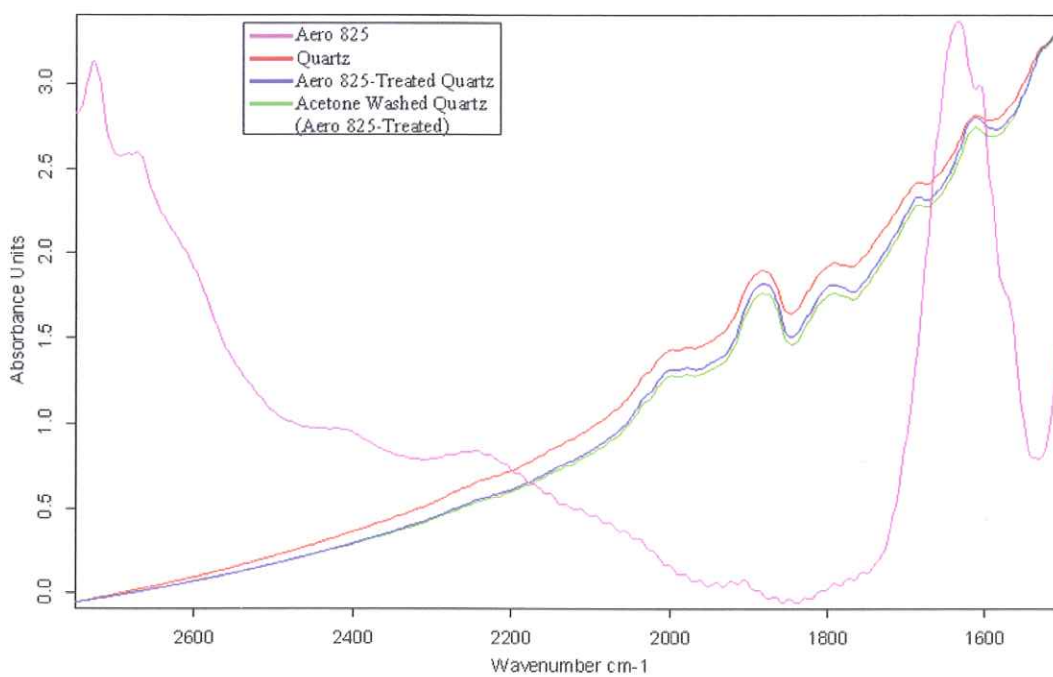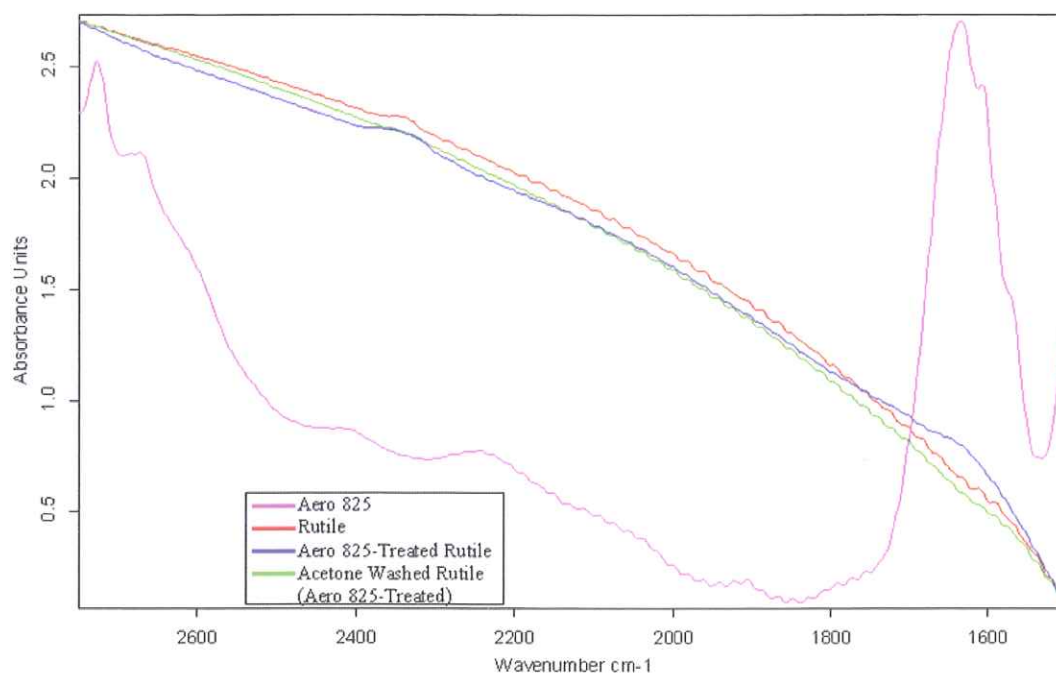

Figure 4.178   FTIR Spectrum of Rutile in the Presence of Aero 825 in 2750–1500 cm^{-1} Wavelength Range.
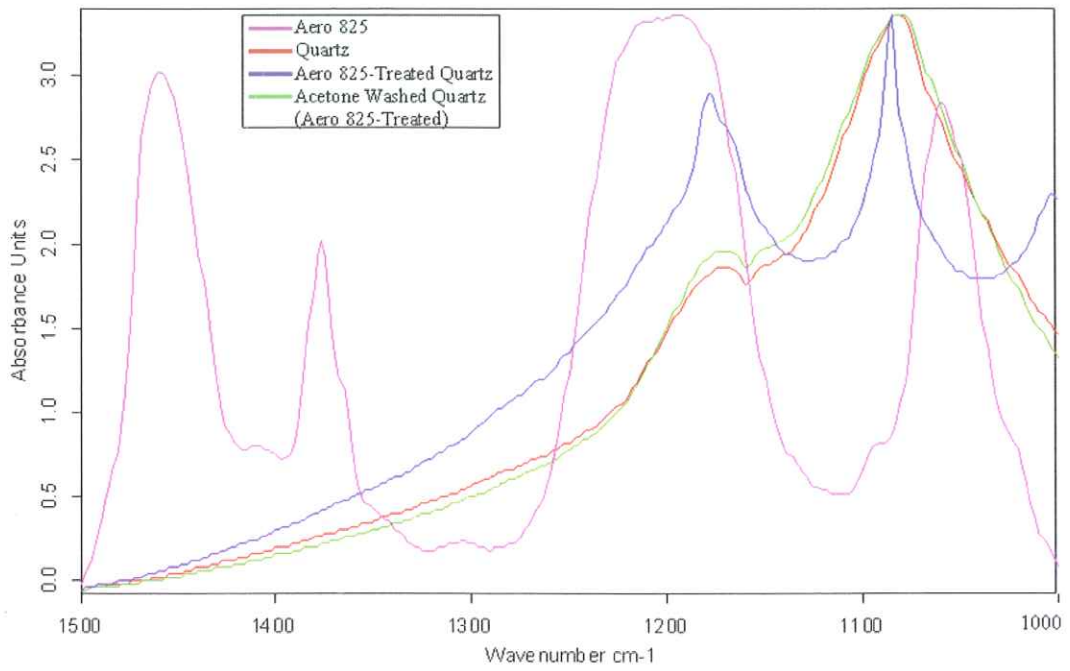
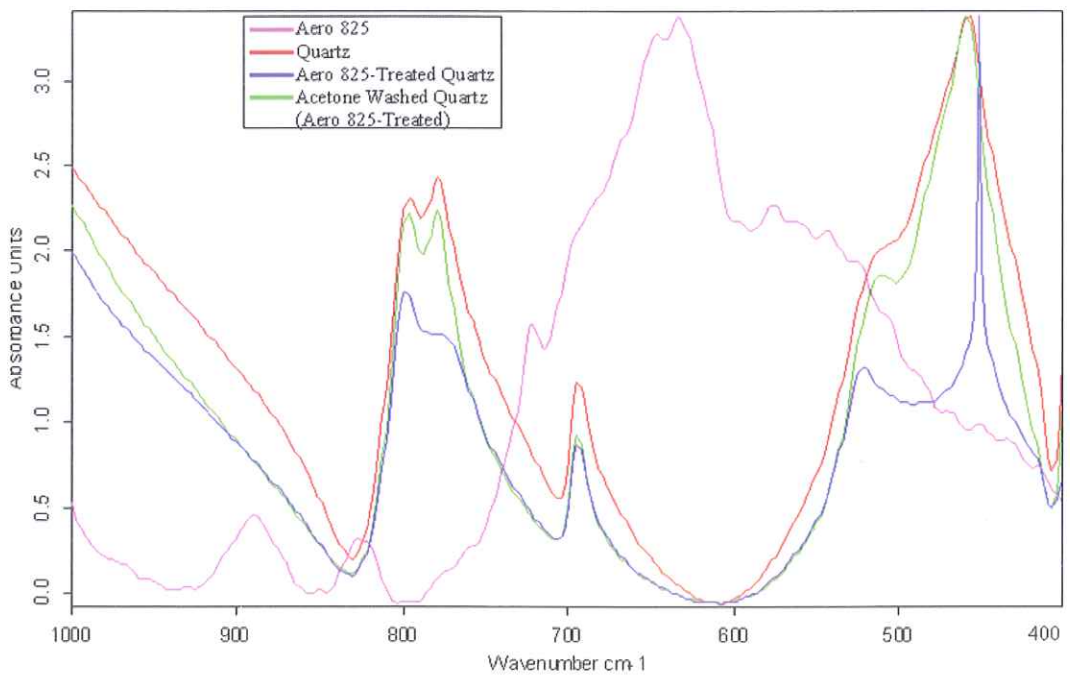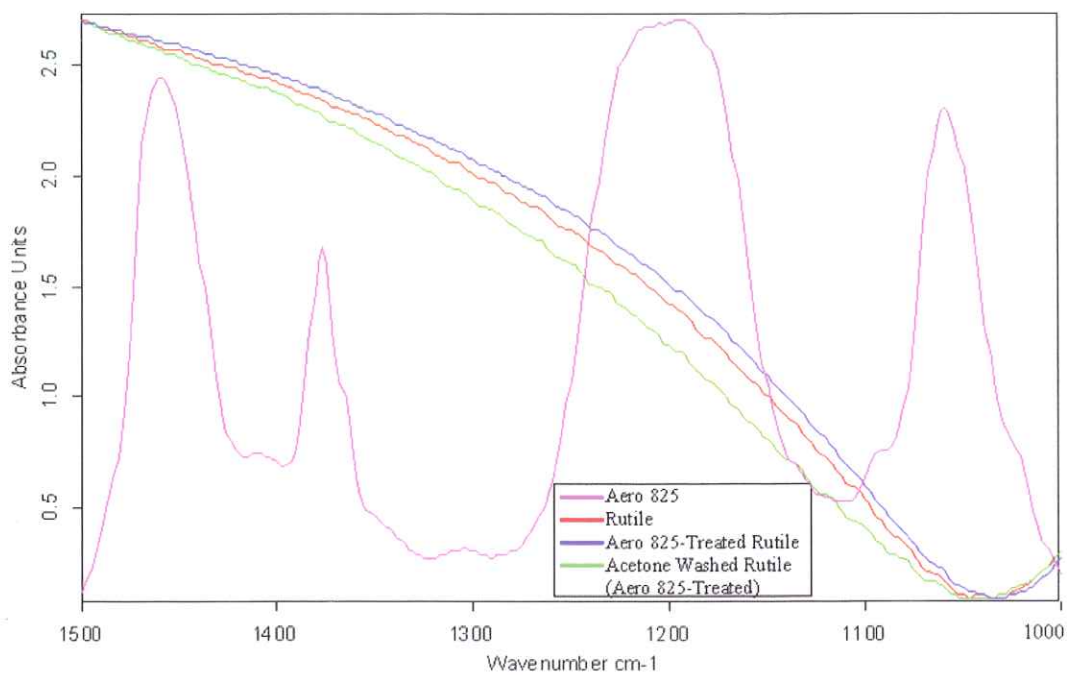Figure 4.179 FTIR Spectrum of Rutile in the Presence of Aero 825 in 1500–1000 cm^{-1} Wavelength Range.
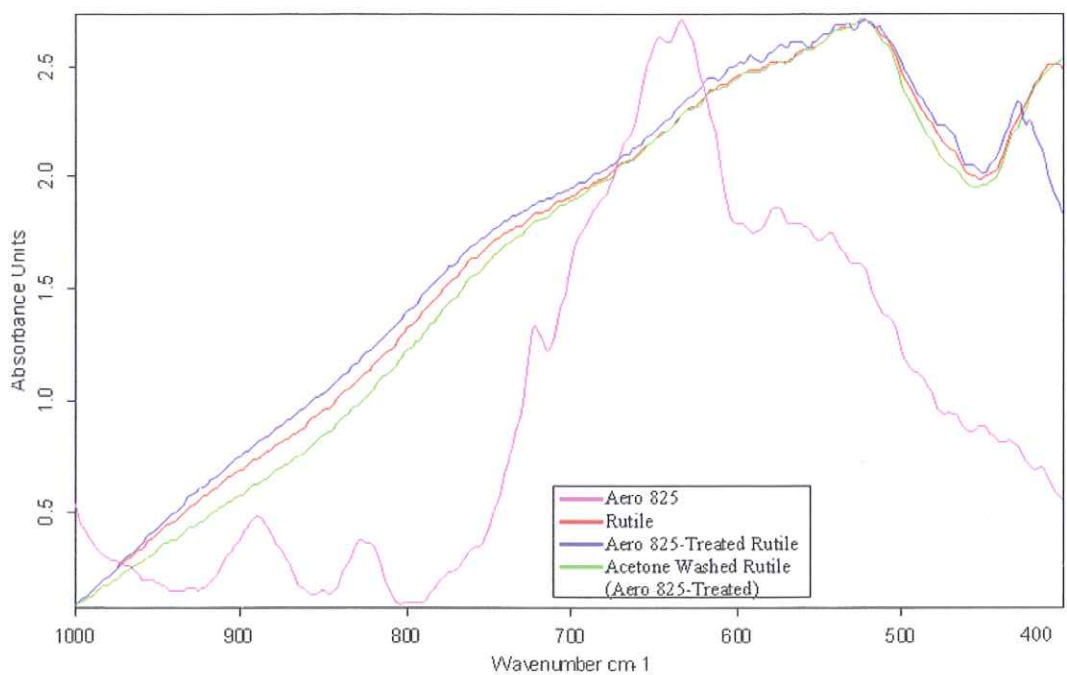
Figure 4.180 FTIR Spectrum of Rutile in the Presence of Aero 825 in 1000–400 cm^{-1} Wavelength Range.

CHAPTER 5

DISCUSSIONS

Discussion of the results was presented under four headings;

1. Electrokinetic potential values
2. Micro-flotation studies
3. AFM and FTIR analyses
4. Overall interpretation of the results

5.1 Electrokinetic Potential Values

The electrical charge on the surface of the minerals studied here can be generated by three mechanisms;

a) Selective adsorption of ions by physical adsorption (weak interaction) or even by chemisorption (strong interaction).

b) Isomorphous substitution in the lattice of minerals.

The isomorphous substitution is one of the main charge mechanisms in clay and mica minerals. In a polyhedra formation, the coordination number, in other words, the number of anions present around a given cation is related with radius ratio of cation to that of anion (Table 5.1).

Table 5. 1   The Correlation between the Coordination Number and the Radius Ratio [106].

Coordination Number of the Cation	Radius Ratio* r Cation / r Anion
1	0 - ∞
2	0 - ∞
3	0.155 – 0.225
4	0.225 – 0.414
6	0.414 – 0.732
8	0.732 – 1.0
12	1.0 – 1.0

* The radius ratio given in the table corresponds to the lowest value for the given coordination number. For example; the cation in any cation/anion combination having a radius ratio greater than 0.255 would be capable of being in close contact with four anion and would not be capable to coordinate with six anions until the radius ratio react to a value of 0.414.

It is also possible to say that the structure is determined mainly by the packing of the anions and the cations which associate with any anion group depend upon the relative size of the cation compared to the size of the opening available in the anion group. Thus, any given anion group would be compatible with a number of different cations if their sizes were similar (Table 5.2). For example, as it is seen in Table 5.2, aluminum, iron and magnesium can be present in octahedral (six-fold) coordination with oxygen (r Al^{3+} / r O^{2-}: 0.57/1.32: 0.4318, similar consideration can also be given for Fe^{2+}, Fe^{3+} and Mg^{2+}). On the other hand, aluminum or given cations can also be located in the tetrahedral coordination by substituting for silicon. Generally, it could be stated that "one ion may substitute for another if their ionic radii differ by less than fifteen per cent" [106]. Upon substitution, geometry is not changed, but resultant structure may be charged. For example, when Al^{3+} or Fe^{3+} is substituted Si^{4+}, the resultant structure will be negatively charged. If substitution occurs between Mg^{2+} and Al^{3+}, again the resultant structure becomes negatively charged.

Table 5. 2   Ionic Radii of Certain Elements [106].

Element	Valence	Ionic Radius (a.u.)
Li	+1	0.78
Na	+1	0.98
K	+1	1.33
Be	+2	0.34
Mg	+2	0.78
Ca	+2	1.06
Fe	+2	0.83
Fe	+3	0.67
Al	+3	0.57
Si	+4	0.39
O	-2	1.32
F	-2	1.33

c) Ionization of hydroxylated surface groups. Hydroxylated surface groups may have three types;

i.   Silanol group,~SiOH,

The group ionizes in the following ways:

- ~SiOH $\leftrightarrow$ ~SiO$^-$ + H$^+$ .... (I)

  or

- ~SiOH+ OH$^-$ $\leftrightarrow$ ~SiO$^-$ + H$_2$O [55] ....(II)

- ~SiOH+ H$^+$ $\leftrightarrow$ ~SiOH$_2^+$ ....(III)

Due to these ionizations, the surface of the minerals becomes positively or negatively charged dependent on pH of the medium.

ii.   On the surface, Al, aluminum may undergo hydrolysis and form ~AlOH.

211

~AlOH dissociates in two ways;

- ~AlOH $\leftrightarrow$ ~AlO$^-$ + H$^+$ ....(IV)
- ~AlOH + H$^+$ $\leftrightarrow$ ~AlOH$_2^+$ ....(V)

In acids, surface becomes positive, in basis surface becomes negative.

Similar consideration can also be done for titanium containing minerals such as rutile. In this case, Ti on the surface may undergo hydrolysis and form ~TiOH.

~TiOH dissociates in two ways;

- ~TiOH $\leftrightarrow$ ~TiO$^-$ + H$^+$ ....(VI)
- ~TiOH + H$^+$ $\leftrightarrow$ ~TiOH$_2^+$ ....(VII)

Whichever the mechanism(s) is/are the case, the mineral surfaces become charged. In aqueous solutions, oppositely charged species will migrate to the mineral/water interface until equilibrium conditions are established. As a result, a region of electrical inhomogeneity forms across the mineral/water interface. The excess (positive or negative) charge fixed at the mineral surface is balanced by a diffuse region of equal but opposite charge on the liquid side [67]. "The net charge on the surface is compensated by the counter ions which are located on the unit-layer surfaces. These counter ions have a tendency to diffuse away from the layer surface since their concentration will be smaller in the bulk solution. On the other hand, they are attracted electrostatically to the charged lattice. The result of these opposing trends is the creation of an atmospheric distribution of the compensating ions in a diffuse electrical double layer on the exterior layer surfaces" of the mineral particle [68] (Figure 5.1).
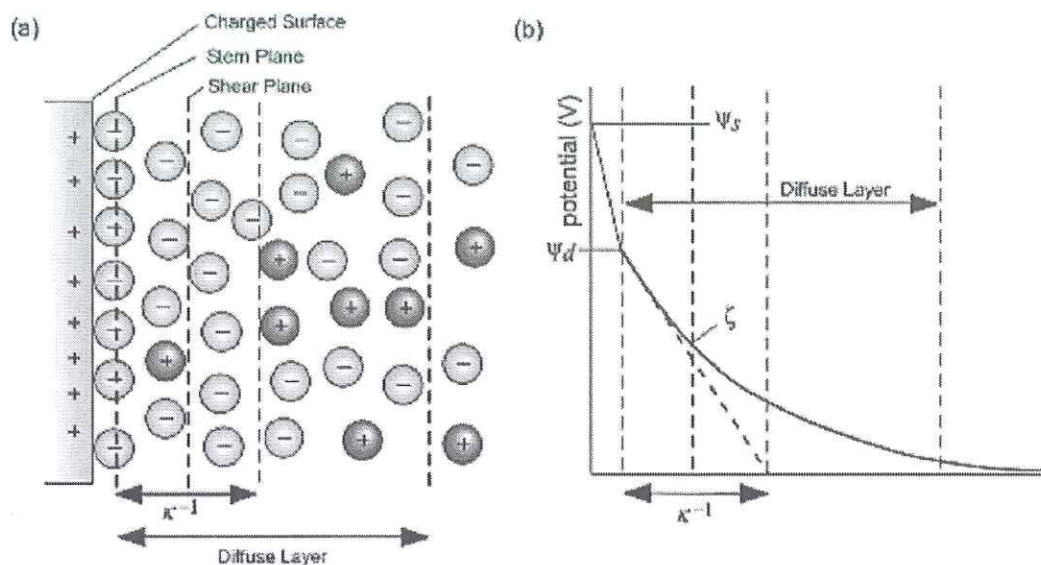
Figure 5. 1   (a) Schematic Representation of the Electric Double Layer (b) Schematic Representation of the Electric Potential Profile Showing the Debye Length [69].

The results of electrokinetic measurement of albite in distilled water and in 1.0×10^{-3} M of KCl are given as a function of pH in Figure 4.1. The isoelectric point (i.e.p.) was found very close to pH 1.5 in distilled water and in 1.0×10^{-3}M of KCl. The corresponding zeta potential values decrease with increasing pH and become more negative towards the more basic region. The reason for the negative charge on the surface might be due to the dissociation of silanol and aluminum hydroxide groups according to reaction I, II and IV. When similar considerations have been taken into account for biotite, orthoclase and quartz, the zeta potential values change in the same way as shown in Figure 4.31, Figure 4.91 and Figure 4.121. The zeta potential values of these minerals in distilled water are in agreement with the results found before [44, 45, 64]. So, it is possible to say that charging mechanisms of these minerals are the same as discussed for albite, in other words, dissociation of silanol and aluminum hydroxide groups (reactions I, II, III, IV and V).

In the case of muscovite, as given in Figure 4.61, the i.e.p. was found about pH 3.0 in distilled water and in 1.0×10^{-3} M of KCl. The zeta potential values become more negative, above the i.e.p., towards the more basic region and become positive below

213

the i.e.p. point. The positive surface charge might come from the dissociation of aluminum hydroxide group according to reaction V. Thus, the effect of silanol group dissociation might be less than the effect of aluminum hydroxide group dissociation below the i.e.p. of the muscovite. The similar results were also observed for rutile (Figure 4.151). The i.e.p. of rutile was found very close to pH 3.3. In this case, the surface charge of the rutile may come from hydrolysis of Ti, titanium on the surface to form (~TiOH) as given before (reactions VI and VII). The positive surface charge may come from the hydrolysis reaction VI whereas the negative charge may come the hydrolysis reaction VII. The electrokinetic potential values of the muscovite and rutile also found to be consistent with literature values for distilled water [65, 66].

Although there has been considerable amount of study on constraining theoretical models of surface protonation and reaction rates, the nature of the actual surface species, even for quartz and aluminosilicates, is subject to controversy (James and Parks, 1982; Davis and Kent, 1990) [70, 71]. The existence of hydroxyl groups on feldspar surfaces in aqueous solution include $>AlO^-$, $>AlOH$, $>AlOH_2^+$, $>SiO^-$, $>SiOH$ and $>SiOH_2^+$ groups (Casey et al., 1988; Brady and Walther, 1989; Blum and Lasaga, 1991; Hellman, 1995) [72-75], and $>Al-OH^+- Si<$ groups (Blum and Lasaga, 1991) [76, 77].

5.1.1 The effect of Aero 704 on the Electrokinetic Potential Values of the Minerals

As discussed before (Chapter 3.1), Aero 704 is a oleic acid related base collector so, it was converted into oleate form before electrokinetic potential measurements.

The oleate species distribution diagram (Figure 5.2) provides a useful tool for the examination of the change in the active chemical form of sodium oleate with changing pH. It is also used in understanding the role of various oleic acid species

and complexes in solution and their role in governing the surface energy of the liquid/gas interface [67].
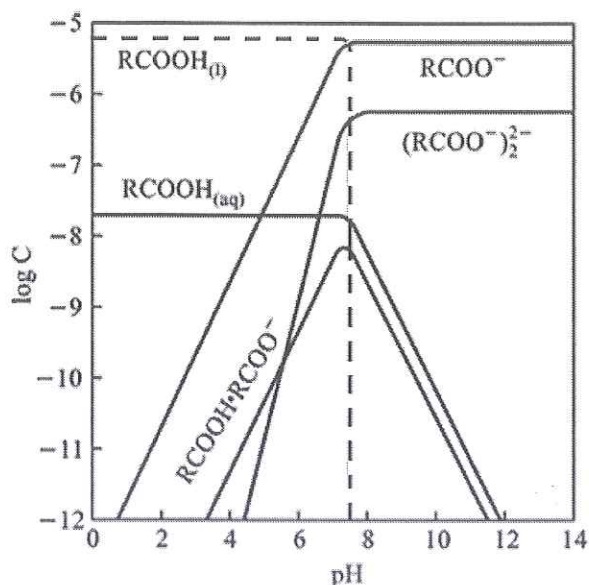
Figure 5. 2   Species Distribution Diagram of Oleate as a Function of pH [67].

The oleic acid undergoes "dissociation to form ion (RCOO⁻) at high pH values and neutral molecules (RCOOH) at low pH values. In the intermediate pH region, the ions and neutral molecules can associate to form ionomolecular (RCOOH • RCOO⁻) complexes. As the collector concentration is increased, micellization or precipitation of the collector will occur. In addition, collector species can undergo associative interactions to form other aggregates such as dimers $(RCOO_2^{2-})$" [67]. The concentrations of $(RCOO)^-$, $(RCOO)_2^{2-}$ and ionomolecular forms keep increasing up to about pH value of 8.0. The concentration of molecular and dimeric form remains constant from pH value of 8.0 on while the concentration of ionomolecular form levels off only after a pH value of 11.0 (Figure 5.2). In both cases, the concentration of the ionomolecular species is less than that of the ionic oleate and its dimer at any specific value of pH. Since the surface activities of these species will vary from those of each other, flotation of minerals with these collectors can also be expected to be dependent upon pH and such solution conditions [67].

Ionization in solution is complicated by the formation of oleate dimers, acid soap (ionomolecular complex). The solution equilibria of oleic acid are summarized as follows [67];
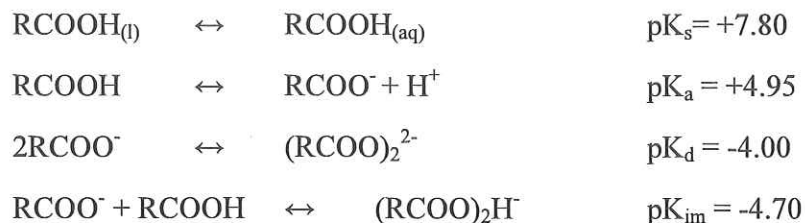
$$RCOOH_{(l)} \leftrightarrow RCOOH_{(aq)} \qquad pK_s = +7.80$$

$$RCOOH \leftrightarrow RCOO^- + H^+ \qquad pK_a = +4.95$$

$$2RCOO^- \leftrightarrow (RCOO)_2^{2-} \qquad pK_d = -4.00$$

$$RCOO^- + RCOOH \leftrightarrow (RCOO)_2H^- \qquad pK_{im} = -4.70$$

(K_a: acid dissociation constant, K_d: dimer formation constant, K_{im}: ionomolecular complex constant)

As it is seen from the diagram,

- The maximum activity of ionomolecular species ($RCOOH \bullet RCOO^-$) occurs at a pH value of 7.8 for a total oleate concentration of $5.0 \times 10^{-5} M$.
- "The activities of the ionic oleate ($RCOO^-$) and its dimer ($(RCOO)_2^{2-}$) increase as pH is increased up to a value of 7.8 and then remain constant at higher pH values.
- The neutral oleic acid ($RCOOH$) starts to precipitate from the aqueous solution at pH values below 7.8" [78].

Based on charge and molecular size considerations, one can expect the surface activities of different oleate species to be markedly different. The estimation of the surface activities of various species suggests that "the surface activity of the acid-soap is five orders of magnitude higher than that of the neutral molecule and about seven orders of magnitude higher than that of the oleate monomer" [67, 79]. Since the surface activities of the species are different from each other, flotation of minerals with these collectors can also be expected to be dependent upon pH and such solution conditions.

A large number of electrokinetic potential measurements have been performed in order to clarify the respective change in the sign and magnitude of the electrokinetic potential and the floatability of minerals in the presence of oleate at various pH values. The increasing Aero 704 concentration resulted in an increase in the negative electrokinetic potential of the albite, biotite, muscovite, orthoclase, quartz and rutile minerals.

In order to discuss the effect of oleate concentration on the electrokinetic potential values of the minerals as a function of pH, the pH region on the study is divided into three sub-groups; acidic region, neutral region and basic region. In highly acidic region (up to about pH 4.0), the predominant species is the neutral molecules (RCOOH) besides the ionic oleate (RCOO$^-$) and the ionomolecular oleate (RCOOH $\bullet$ RCOO$^-$) are also present. About neutral pH region (between pH 6.0 and 8.0), the predominant species seem to be the ionic oleate, the ionomolecular oleate and the dimer (RCOO$_2^{2-}$), the neutral form seem to be less. In the basic region (between pH 9.0 and pH 11.0), the predominant species are the ionic oleate and the dimer. The ionomolecular and the neutral forms of oleate are less in amount.

It is expected that the charged species of oleate effect the surface charge of the minerals. The results showed that their effect changes depending on the type of the minerals. When the i.e.p. of the albite, biotite, orthoclase and quartz in distilled water are taken into account, no considerable shifting on their i.e.p.' were observed.

On the other hand, in the presence of Aero 704, as the pH increases towards the basic region, their zeta potential values become more negative. This might be due to decreasing effect of AlOH$_2^+$ and/or SiOH$_2^+$ by electrostatic interaction of negatively charged oleate species.

In the case of muscovite, the i.e.p. was shifted from about pH 3.0 to about pH 1.5 in the presence of Aero 704 (Figure 4.62). In the presence of Aero 704 at this pH 3.0

217

the surface charge becomes negative due to the electrostatic and/or chemical interaction of the dominant negatively charged oleate species (RCOO⁻, RCOOH • RCOO⁻) on the surface.

In the case of rutile, the i.e.p. was shifted from about pH 3.3 to about pH 1.5 in the presence of Aero 704 (Figure 4.152). The similar consideration done for muscovite is also done for rutile mineral at pH 3.3, the surface becomes negatively charged because of the interaction of dominant oleate species on the positively charged surface coming from $TiOH_2^+$.

Above the i.e.p. of these minerals, their zeta potential values become more negative due to the decreasing positively charged surfaces by electrostatic and/or chemical interaction of negatively charged oleate species.

5.1.2 The effect of Aero 3000C on the Electrokinetic Potential values of the minerals

The behavior of the cationic collector Aero 3000C (RNH_2) in aqueous solution is similar to that of oleate (here Aero 704). The equilibria in the solution of RNH_2 can be given as follows;
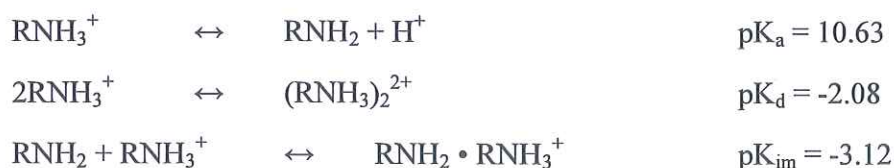
RNH_3^+	$\leftrightarrow$	$RNH_2 + H^+$	$pK_a = 10.63$
$2RNH_3^+$	$\leftrightarrow$	$(RNH_3)_2^{2+}$	$pK_d = -2.08$
$RNH_2 + RNH_3^+$	$\leftrightarrow$	$RNH_2 • RNH_3^+$	$pK_{im} = -3.12$

(K_a: acid dissociation constant, K_d: dimer formation constant, K_{im}: ionomolecular complex constant) (acidic form of RNH_2 is RNH_3^+) [67].

The species distribution of dodecyl amine at total concentration of 5.0×10^{-5} M is shown in Figure 5.3. In this case the neutral molecule (RNH_2) precipitates in the high

218

pH range and the ionic form (RNH_3^+) and the dimer form (($RNH_3)_2^{2+}$) dominate in the acidic pH range. Again, the ionomolecular (ion-molecule, $RNH_2 \cdot RNH_3^+$) complex exhibits a maximum at certain pH values (about pH 10.5 for 5.0×10^{-5} M).
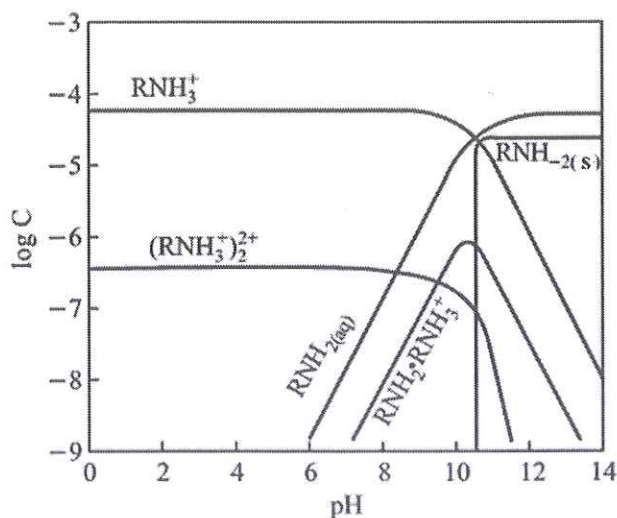
Fiigure 5. 3   Species Distribution Diagram of Dodecyl Amine as a Function of pH (total conc.=5.0×10^{-5}M) [67].

The electrokinetic potential values of the minerals, albite, biotite, muscovite, orthoclase, quartz and rutile (Figure 4.3, Figure 4.33, Figure 4.63, Figure 4.93, Figure 4.123 and Figure 4.153) increased appreciably with increasing concentration of Aero 3000C.

Albite, biotite, orthoclase and quartz in distilled water have no significant i.e.p. and they all have negative surface charge above pH 1.5. However, in the presence of Aero 3000C, the zeta potential values of those minerals became positive up to about pH 11.0 and above that became negative. The reason for the reversal of the surface charges up to about pH 11.0 may come from the interaction of positively charged species of amine (the ionic, RNH_3^+, the dimer, ($RNH_3)_2^{2+}$ and the ionomolecular complex, $RNH_2 \cdot RNH_3^+$, with the negatively charged mineral surfaces. Above about pH 11.0, the RNH_3^+, ($RNH_3)_2^{2+}$, $RNH_2 \cdot RNH_3^+$ concentrations decrease. Their charge reversal effect become insufficient and the zeta potential values of the

minerals again become negative (Figure 4.3, Figure 4.33, Figure 4.93 and Figure 4.123).

In the case of muscovite and rutile, their i.e.p. in distilled water were shifted from pH 3.0 for muscovite and pH 3.3 for rutile to about pH 11.0 in the presence of Aero 3000C. The effect of amine species on those mineral surfaces can be assumed to be the similar as explained before for the other minerals, albite, biotite, orthoclase and quartz.

5.1.3 The effect of Aero 825 on the Electrokinetic Potential Values of the Minerals

The behavior of the anionic collector Aero 825 (may be shown as R^- corresponding to sodium dodecyl sulfonate) in aqueous solution can be displayed by species distribution diagram given in Figure 5.4. The diagram provides an useful tool for the examination of the change in the active chemical form of sulfonate with pH.
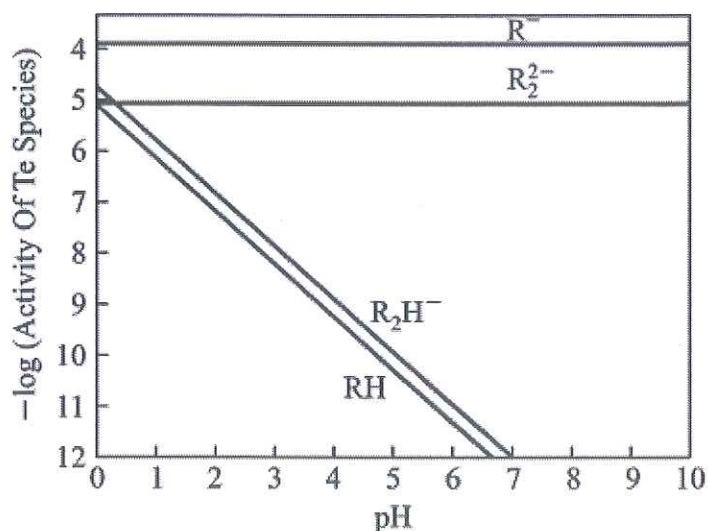
Figure 5. 4   Species Distribution Diagram of Sodium Dodecyl Sulfonate as a Function of pH [67].

The alkyl sulfonates (R^-) exist in ionized form in the entire pH range commonly used in flotation as they are strong electrolytes. This is of advantage in separation of oxide minerals which require neutral pH for optimum flotation. In contrast to the acid-soap molecule, the ionic dimer (R_2^{2-}) will have the two ionic heads as far apart as possible with maximum contact between the hydrocarbon chains.

In all pH range, the ionic (R^-) and dimer (R_2^{2-}) forms are predominant, but the concentration of ion molecule (R_2H^-) and molecular (RH) forms decrease with increasing pH. Therefore, in the acidic region, it should be considered that all species are active with almost same concentration. In neutral and basic region, the ionic and dimer forms (Figure 5.4) are constant at concentrations while the concentration of ion molecule and molecular forms decrease.

The electrokinetic potential values of the minerals, albite, biotite, muscovite, orthoclase, quartz and rutile (Figure 4.4, Figure 4.34, Figure 4.64, Figure 4.94, Figure 4.124 and Figure 4.154) decreased with increasing concentration of Aero 825. As it is seen in the figures given, no i.e.p. was observed for all minerals. This means that the charge reversal of the mineral surfaces was not occurred by interaction with ions of Aero 825. In other words, already present negative charges increased by interaction of positively charged surfaces with negatively charged sulfonate ions such as R^-, R_2^{2-}, R_2H^-.

5.1.4 The Effect of Acetone Washing on the Minerals Conditioned with the Collectors of Optimum Concentration and pH

The electrokinetic potential measurements conducted on the acetone-washed minerals which were previously conditioned in optimum flotation conditions showed that the zeta potential values of all the minerals (albite, biotite, muscovite, orthoclase, quartz and rutile) displayed similarities when compared to those of in distilled water.

In all minerals, when conditioned with Aero 704 and Aero 825 their zeta potential values became more negative and conditioned with Aero 3000C the zeta potential values increased to positive values up to a certain pH (about pH 11.0) and then decreased. Upon washing with acetone several times, their zeta potential values displayed almost the same as they were in distilled water. Therefore it may be possible to consider that all the collectors adsorbed weakly on the mineral surfaces. However, electrokinetic data alone do not explain the whole adsorption mechanism, it should be supported by the spectral results of the mineral samples before and after conditioning with the collectors.

5.2   Micro-Flotation Studies

A large number of micro-flotation experiments were performed on the mineral samples to investigate their flotation characteristics as a function of both concentration of the collectors, Aero 704, Aero 3000C and Aero 825, and pH.

5.2.1   The effect of Aero 704 on the Flotation Recovery of the Minerals

As Aero 704 loose its collecting power below pH 7.00, as shown in Figure 4.6, Figure 4.36, Figure 4.66, Figure 4.96, Figure 4.126 and Figure 4.156, where the neutral form of oleate, $RCOOH_{(aq)}$ is the predominant specie and the activities of the ionic oleate ($RCOO^-$) and the ionomolecular ($RCOOH \cdot RCOO^-$) species become less effective, all micro-flotation studies were conducted for all concentrations of Aero 704 above pH 7.0.

The flotation effectiveness of the Aero 704 on the mineral samples except for the quartz increases with increasing concentration and pH. In the more basic region, the activity of the ionic form ($RCOO^-$), the ionomolecular form ($RCOOH \cdot RCOO^-$) and the dimeric form $(RCOO)_2^{2-}$ of oleate are predominant. The maximum flotation recoveries of the minerals were obtained about pH 9.0 where the ionomolecular

(RCOOH • RCOO⁻) form of oleate reaches its maximum amount (Figure 5.2.) and from this point on its activity decreases through the more basic conditions. In addition to this, the activity of the ionic (RCOO⁻) and the dimer $(RCOO)_2^{2-}$ forms of oleate increase up to this pH, about pH 9.0, and from this point on their activity remain constant (Figure 5.2).

In the case of quartz, the flotation recoveries of the mineral were irrespective of both pH and concentration. Even in the presence of highest molarity of the Aero 704 tested, 5.0×10^{-4} M, the maximum flotation recovery did not exceed 10.0%. Although it gained more negative zeta potential values in the presence of Aero 704 compared to those in distilled water, the affinity of Aero 704 with the quartz surface could not be adequate to float the mineral particles and/or the adsorption on the mineral surface might be occurred mostly by the dimeric $(RCOO)_2^{2-}$ form of Aero 704 where their activity increases with increasing pH and reaches to its maximum activity at the point (about pH 9.0) where maximum flotation recovery is expected (Figure 5.2).

5.2.2 The effect of Aero 3000C on the Flotation Recovery of the Minerals

The micro-flotation studies performed with varying Aero 3000C concentrations showed that the flotation recoveries of the minerals increased proportionally to increasing concentration (Figure 4.7, Figure 4.37, Figure 4.67, Figure 4.97, Figure 4.127 and Figure 4.157). As seen from the figures given, Aero 3000C is effective in very wide range of pH (from highly acidic to highly basic conditions) and the maximum flotation recoveries were obtained for all the minerals between the pH range of 3.0 and 11.0. In acidic pH range, the dominant active species of Aero 3000C were the ionic, RNH_3^+, and the dimeric $(RNH_3)_2^{2+}$ forms. The concentrations of them remain almost constant up to about pH 11.0, then their concentrations decrease sharply towards the highly basic pH region. In addition, the concentration of the molecular (RNH_2) and the ionomolecular forms (RNH_2 • RNH_3^+) of Aero 3000C increase towards about pH 11.0. Then, the concentration of ionomolecular form decreases sharply while the concentration of molecular form remains constant. The

flotation recoveries of all the minerals decreased towards the highly basic conditions due to the decreasing activity of ionomolecular ($RNH_2 \bullet RNH_3^+$) and the ionic (RNH_3^+) forms of Aero 3000C (Figure 5.3). In fact, the concentration of the ionomolecular form decreases more rapidly when compared to the activity of the ionic (RNH_3^+) form. In addition to this decreasing activity of these species, the neutral molecule $RNH_2(aq)$ starts to precipitate above pH 10.0 which also has decreasing effect on the flotation recovery of the minerals. From this point on, the flotation recovery decreased sharply for all Aero 3000C concentrations with probably increasing precipitation as $RNH_2(s)$ (Figure 5.4).

5.2.3   The effect of Aero 825 on the Flotation Recovery of the Minerals

It is well known that sulfonates exist in ionized form and are predominantly anionic in the entire pH range (Figure 5.4). In this respect, the micro-flotation studies showed that the flotation recoveries of albite, biotite, muscovite, orthoclase and quartz samples were almost irrespective both Aero 825 concentration and pH. The interaction of Aero 825 with these minerals might be the reason of interaction of the ionic dimer (R_2^{2-}) which did not make the surface sufficiently hydrophobic. That is why the flotation recoveries of these minerals were limited to less than 20.0% even in the presence of highest Aero 825 concentration, $1.0x10^{-3}$ M. In the case of rutile, the flotation recoveries increased with increasing Aero 825 concentration between the pH range of slightly above and below its i.e.p. (pH 3.3 in distilled water) due to the interaction of anionic forms of Aero 825 (R^-, R_2H^-) with the charged rutile surface.

5.3   AFM and FTIR Analyses

The tapping mode AFM analyses and the FTIR analyses were conducted on the albite, biotite, muscovite, orthoclase, quartz and rutile samples in order to investigate the interaction of three different collectors, Aero 704, Aero 3000C and Aero 825,

with the mineral surfaces. The analyses were performed in the absence and presence of the collectors to provide easy comparison.

5.3.1   Determination of Interaction of the Collectors with the Mineral Surfaces by AFM

According to the tapping mode AFM 3D micro topographies and the corresponding histograms of the mineral samples in the absence and presence of Aero 704 results, the roughness values, the maximum peak values and the average height values of the Aero 704-treated mineral samples increased both for 100nm and 1µm scanning size ranges when compared to those of mineral samples. In addition, the height profiles of Aero 704-treated mineral samples increased when compared to the height profiles of mineral samples indicating the affinity of Aero 704 on the mineral samples.

The length of the oleate was calculated theoretically as 2.60nm by Chennakesavulu et al. [47]. The height profile of albite displayed variation between 1.00nm to 5.50nm for the scanned area (Figure 4.11). Aero 704-treated albite showed variation between 8.00nm to 12.50nm although at some points it decreased to 5.50nm. Those height profiles of albite and Aero704-treated albite coincide with monolayer and bilayer heights. The presence of concurrent monolayer and bilayer on the same surface clearly indicates that "normal–normal bonding of hydrocarbon chains takes place before the surface is completely covered with monolayer. This indicates that the oleate adsorption on mineral may proceed by admicelle hypothesis (adsorption of micelle) i.e. patches of bilayer could be seen even before the completion of monolayer coverage" [47]. The behavior of orthoclase in the presence of Aero 704 is similar to that of albite (Figure 4.101). The height profile differences of the remaining minerals (biotite, muscovite, quartz and rutile) are not clear enough to discuss the monolayer and bilayer adsorption of Aero 704 on their surfaces (Figure 4.41, Figure 4.71, Figure 4.131 and Figure 4.161).

The length of the hexadecylamine (it is considered to be similar to Aero 3000C) was calculated theoretically as 2.12nm by C.O'Dwyer et al., 2006 [80]. In the absence and presence of Aero 3000C, the AFM analyses results showed that the roughness values, the maximum peak values and the average height values of the Aero 3000C-treated mineral samples increased both for 100nm and 1μm scanning size ranges when compared to those of the mineral samples. Moreover, height profiles of Aero 3000C-treated mineral samples increased when compared to the height profiles of mineral samples in 1μm scanning size range indicating the affinity of Aero 3000C on the mineral samples. The height profiles of the biotite and muscovite and Aero3000C-treated of these minerals showed that, there might be monolayer adsorption (Figure 4.43 and Figure 4.73). In the case of the minerals, albite, orthoclase, quartz and rutile, the results indicated that "the concurrent monolayer and bilayer on the same surface clearly shows that normal–normal bonding of hydrocarbon chains takes place before the surface is completely covered with monolayer" indicating that the Aero 3000C adsorption on mineral may proceed by admicelle hypothesis (adsorption of micelle) [47].

The length of the petroleum sulfonate (it is considered to be similar to Aero 825 in structure) was calculated theoretically as 1.75nm by Zheng-Wu Wang et al., 2001, [81]. In the absence and presence of Aero 825, the AFM analyses results showed that the roughness values, the maximum peak values and the average height values of the Aero 825-treated mineral samples increased both for 100nm and 1μm scanning size ranges when compared to those of the mineral samples. Moreover, height profiles of Aero 825-treated mineral samples increased when compared to the height profiles of mineral samples in 1μm scanning size range indicating the affinity of Aero 825 on the mineral samples. The height profiles of the biotite and muscovite and Aero825-treated of these minerals showed that, there might be monolayer adsorption (Figure 4.45 and Figure 4.75). In the case of the albite, orthoclase, quartz and rutile, the results indicated that "the concurrent monolayer and bilayer on the same surface clearly shows that normal–normal bonding of hydrocarbon chains takes place before the surface is completely covered with monolayer" [47]. This indicates that the Aero 825 adsorption on mineral may proceed by admicelle hypothesis.

5.3.2 Determination of Interaction of the Collectors with the Mineral Surfaces by FTIR

The mechanism of oleic acid adsorption and oleate on oxide minerals were extensively studied by many researchers. Several authors published a comprehensive review on this subject, Vinagrow and Linnell (1971), Baes and Mesmer (1976), Israelachvili and Pashley (1985), Somadundaran and R. Ramachandran (1988) and Pugh and Rutland (1997) [82-86]. According to Somasundaran and Agar (1976) and Kulkarni and Somasundaran (1980) adsorption come about by electrostatic attraction as well as by chemisorption [87, 88]. As there was a measurable shift in the zeta potential over the entire range of pH, even at the low oleate concentration indicating a strong chemical interaction between calcite and oleate [89]. These results were in agreement with the results from spectroscopic investigations suggesting chemical interactions between calcite and the carboxyl group of adsorbed surfactants [90, 91].

In this study, the FTIR spectra showed that the Aero 704-treated mineral samples conditioned in optimum flotation conditions had additional bands at 2961 cm^{-1}, 2926 cm^{-1} and 2854 cm^{-1} assigned as CH_2 stretching vibrations when compared to the FTIR spectra of mineral samples [107-109]. As the intensity of these vibrations does not indicate the amount of adsorbed Aero 704 on the mineral surfaces quantitatively, these results clearly indicated the affinity of Aero 704 on the mineral samples and this affinity could not be removed completely by washing with large amount of distilled water. However, the FTIR spectrum of the albite, orthoclase, quartz and rutile samples conditioned with Aero 704 in optimum flotation conditions upon washing by acetone was altered, the bands at 2961 cm^{-1}, 2926 cm^{-1} and 2854 cm^{-1} disappeared upon washing indicating weak interaction. In the case of the FTIR spectrum of the biotite and muscovite, these additional bands (2961 cm^{-1}, 2926 cm^{-1} and 2854 cm^{-1}) upon washing several times with acetone was not altered indicating that the interaction was strong and irreversible which might be the reason of chemisorption of Aero 704 on their surfaces.

The flotation of silicates is invariably carried out with long-chain alkyl amines. These collectors are widely utilized in flotation processes due to their amphilitic feature and high solubility. There were a number of studies which were conducted mostly by indirect approaches like contact angel, zeta-potential, surface forces and recovery response on the adsorption of amines on silicate minerals carried out widely in the past [92-96]. The adsorption of surfactants on calcite in the literature display noteworthy varieties in different systems. For example, it has been suggested that amine type collectors are adsorbed due to electrostatic attraction on the negatively charged surface sites [97], while others considered the adsorption of amine as an ion exchange reaction [98]. "There is a general consensus that the mechanism of amine adsorption on silicate depends on pH. Within the pH 2.0–7.0 region, where the surface potential of silicate is negative, the literature is consistent with the Gaudin–Fuerstenau–Somasundaran model, where the ammonium ions undergo physisorption at the silicate–water interface much below the critical micelle concentration (CMC). They are electrostatically held in the Stern layer as individual counter ions behaving almost as an indifferent electrolyte" [43], [99, 100]. This model contends that amine cations are adsorbed, in the outer Stern layer, on the negatively charged surface sites owing to the electrostatic attraction.

The FTIR spectra showed that the mineral samples conditioned in optimum flotation conditions had additional bands at 2957 cm^{-1}, 2922 cm^{-1} and 2853 cm^{-1} (Figure 4.22, Figure 4.52, Figure 4.82, Figure 4.112, Figure 4.132 and Figure 4.152) which are known to represent C-H stretching vibrations respectively when compared to the FTIR spectra of mineral samples (Figure 3.3, Figure 3.6, Figure 3.9, Figure 3.12, Figure 3.15 and Figure 3.18). As the intensity of these vibrations does not indicate the amount of adsorbed Aero 3000C on the mineral surfaces quantitatively, these results clearly indicated the affinity of Aero 3000C on the mineral samples and these affinity could not be removed completely by washing with large amount of distilled water. However, the FTIR spectra of the albite, orthoclase, quartz and rutile samples conditioned with Aero 3000C in optimum flotation conditions upon washing several times with acetone was altered, the bands at 2957 cm^{-1}, 2922 cm^{-1} and 2853 cm^{-1} disappeared indicating weak interaction. In the case of the FTIR spectra of the biotite and muscovite, these additional bands upon washing with acetone was not altered

and the at 2957 cm^{-1}, 2922 cm^{-1} and 2853 cm^{-1} still exist indicating that the interaction was strong and irreversible which might be the reason of chemisorption of Aero 3000C on the surfaces of these minerals.

Previously, Somasundaran and Fuerstenau, (1966) studied the adsorption of sodium dodecyl sulfonate on alumina in aqueous media. It was proposed that sulfonate ions were adsorbed on the surface as counterions, as this adsorption occurred significantly below the zpc of alumina (pH 9.0). They also commented that at low concentrations of surfactants ($\leq 10^{-5}$ M) or at low surface potentials, the surfactant ions were adsorbed individually. This adsorption was due to the electrostatic forces occurred between the ions of surfactant and the charged solid surface. At greater concentrations, they proposed that surfactant aggregation at the surface through lateral interaction was onset between hydrocarbon chains which is referred to as hemimicelle formation. Such colloidal aggregates formed on the surface are referred to as surface colloids (solloids) in general, since many surface aggregates may have forms other than that characterized by half-micelles. "When sulfonate ions equivalent in number to the surface sites had been adsorbed, the contribution due to the electrostatic attraction disappeared, and the further increase in adsorption would be only due to association between the hydrocarbon chains" [101, 102].

J.B. Andersen et al. (1991), studied on the adsorption of anionic and cationic collectors on the pure calcite mineral through the electrophoretic measurements. They concluded that the adsorption of the anionic sodium dodecyl sulphate (SDS) took place on both positive and negative calcite surfaces at least partly by chemical interaction (at negative zeta potential) [103].

In another study, done by Siracusa, P.A. and Somasundaran, P. (1987), the dodecyl benzene sulfonate on kaolinite was investigated. It was found that below i.e.p. of kaolinite (pH 3.7), the dodecyl benzene sulfonate precipitation with cationic aluminum species, $\sim AlOH_2^+$, was significant and aluminum-sulfonate precipitates produced an abstraction (adsorption and precipitation) maximum. At the point or

close to PZC, a kind of decrease was observed in precipitation with the reduction in the concentration of cationic aluminum species [104].

In this study, the FTIR spectra showed that the Aero 825-treated mineral samples displayed additional bands at 2951 cm^{-1}, 2924 cm^{-1} and 2854 cm^{-1} except for muscovite and quartz. These bands are known to represent the stretching vibration of CH_2 group respectively. These results clearly indicated the affinity of Aero 825 on the mineral samples and this affinity could not be removed completely by washing with large amount of distilled water. These additional bands at 2951 cm^{-1}, 2924 cm^{-1} and 2854 cm^{-1} disappeared upon washing several times with acetone indicating weak interaction. In the case of muscovite, absence of the given additional bands indicated that Aero 825 interacted weakly with the muscovite and quartz surface and then easily removed by distilled water washing.

5.4 Overall Interpretation of the Results

This thesis is related with two types of minerals namely; two oxide minerals (quartz and rutile) and four silicate minerals (albite, biotite, muscovite, orthoclase). The electrokinetic potential measurements of the minerals in distilled water and 1.0×10^{-3} M KCl (indifferent electrolyte) solutions as a function of pH showed that while two of them, muscovite and rutile, displayed clear i.e.p. about pH 3.0 and 3.3 respectively, the other minerals (albite, biotite, orthoclase and quartz) displayed i.e.p. very close to pH 1.5. The negative charge on their surfaces may come from broken bond surfaces where silanol group (SiOH), AlOH group and TiOH group could be formed due to the interaction of surfaces with water. Dissociation and/or association of these groups results in the positive or negative charges on the surfaces (see Chapter 5.1 for reactions).

Based on the objective of the thesis, the highest purity of two feldspars, albite and orthoclase, and the highest purity of their associated minerals, biotite, muscovite,

quartz and rutile, were studied separately by using micro-flotation method in the presence of Aero 704, Aero 3000C and Aero 825 as a function of both concentration and pH. The purpose of the micro-flotation studies is to compare the flotation recoveries of the minerals in the two-staged acid circuit flotation (with Aero 3000C and Aero 825) with the single-stage alkaline circuit flotation (with Aero 704). For this purpose, the micro-flotation experiments were performed in wide range of pH starting from about pH 1.5 to 12.5 for Aero 3000C and Aero 825, in the case of Aero 704, the experiment pH were between neutral pH and 12.5 due to fact that the flotation recoveries of the minerals decreased with decreasing amount of oleate ionomolecular species below pH 7.0 considering the species distribution diagram of oleate (Figure 5.2). Besides the flotation responses of these minerals in the presence of these three different collectors, the other purpose of the study is to find out the interaction mechanisms of the collectors on the mineral surfaces by using convenient methods such as AFM and FTIR.

The results showed that the Aero 3000C was effective in the wide range of pH, from highly acidic to highly basic conditions for all minerals and the flotation recovery plots of them are almost bell shaped (Figure 4.7, Figure 4.37, Figure 4.67, Figure 4.97, Figure 4.127 and Figure 4.157). The maximum flotation recoveries of the minerals increased with increasing Aero 3000C concentration having the values of greater than 90.0%. In the acidic range, the concentrations of RNH_3^+ and $(RNH_3^{2+})_2^{2+}$ are predominant, so they interact with the negatively charged surface of the minerals. In addition to electrostatic interaction of Aero 3000C on the negatively charged minerals surfaces, it was also proposed previously that alkylamine group (RNH_2) may form hydrogen-bond (H-bond) with surface hydroxyl group [43]. The H-bond formation of amine can be given by the following equilibrium for silanol group on the surface as an example [44];

- $\sim SiOH + H_2N\text{-}R \quad \leftrightarrow \quad \sim SiO^- + H_3^+N\text{-}R$ ....(VIII).
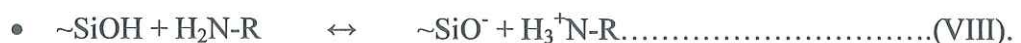
On the other hand, in neutral and basic range, the concentrations of RNH_3^+ and $(RNH_3^{2+})_2^{2+}$ stay almost constant while the concentrations of RNH_2 and inonomolecular forms increase. In highly basic region, the concentration of charged

231

amine species decrease sharply while RNH_2 stays constant at concentration which may precipitate/coagulate on the surface of the minerals. Overall results of the distribution of amine species in the solution result in maximum flotation recovery with in the certain pH range for the minerals under study. The strength of the interaction between Aero 3000C and the mineral surfaces was investigated by using FTIR spectra. According to the results of the FTIR analyses of Aero 3000C-treated minerals displayed additional bands at 2957 cm^{-1}, 2922 cm^{-1} and 2853 cm^{-1} (Figure 4.22, Figure 4.52, Figure 4.82, Figure 4.112, Figure 4.132 and Figure 4.152) which are known to represent C-H stretching vibrations coming from Aero 3000C. These additional bands were removed by acetone washing from the albite, orthoclase, quartz and rutile surfaces indicating weak interaction of Aero 3000C with mineral surfaces [62, 63]. On the other hand, the remaining minerals, biotite and muscovite showed strong interaction with Aero 3000C since these additional bands still exited after acetone washing. The weak interaction may correspond to the physical interaction while strong interaction corresponds to the chemical interaction including H-bonding at both ages and the faces of the biotite and muscovite.

It is known that sulfonate exist in ionized form and is predominantly anionic (R^-, R_2H^-, R_2^{2-}) in the entire pH range. In this respect, the micro-flotation studies with varying Aero 825 concentrations showed that the flotation recoveries of albite, biotite, muscovite, orthoclase and quartz samples were relatively low compared to the flotation of rutile (Figure 4.158). The flotation recoveries of the rutile increased with increasing concentration of Aero 825 between the pH range of slightly below and above its i.e.p. (pH 3.3 in distilled water). The interaction of Aero 825 with the rutile surface might be electrostatic which come from the anions of Aero 825 (R^-, R_2H^-, R_2^{2-}) and the positive charge of rutile surface as $\sim TiOH_2^+$. For the case of muscovite which has i.e.p. again about pH 3.0 in distilled water, the flotation recovery were limited as less than 20.0% even in the presence of highest Aero 825 concentration, 1.0×10^{-3} M. This may be due to the structure of muscovite. As mentioned before, muscovite has two types of charged surfaces namely, $\sim SiOH_2^+$, $\sim SiO^-$, $\sim AlOH_2^+$, $\sim AlO^-$. Interaction of the charged surfaces is not homogeneous and overall interaction of these oppositely charged surfaces result in less available positive charge than expected. Hence, the interaction of Aero 825 with the muscovite

surface becomes less than that of the rutile surface. As a result, less flotation recovery was observed.

The FTIR spectra showed that the Aero 825-treated mineral samples, except for muscovite and quartz, displayed additional bands at 2951 cm^{-1}, 2924 cm^{-1} and 2854 cm^{-1} which are known to represent the spectrum of unsymmetrical stretching and symmetrical stretching vibration of CH_2 group respectively. These results clearly indicated the affinity of Aero 825 on the mineral samples and these affinity could not be removed completely by washing with large amount of distilled water. Then after washing several times with acetone, the additional bands disappeared indicating weak interaction. In the case of muscovite and quartz, absence of the given additional bands indicated that Aero 825 adsorbed rather weakly on those mineral surfaces and then completely removed by distilled water washing. According to the results, the low flotation recovery of the minerals other than rutile may come from two reasons. Aero 825 may be interacted on the mineral surfaces with its dimer form which have adverse effect on flotation recovery. Aero 825 may be interacted with the positively charged sites of the mineral surfaces, but the degree of interaction is not enough to float the particles.

In the case of Aero 704, the results showed that the flotation recovery plots of the minerals are generally bell shaped and pH dependent. The maximum flotation recoveries were increased with increasing Aero 704 concentration and obtained between the pH range of 9.0 and 10.5 for all the minerals except for the quartz. The maximum flotation recoveries were $\geq 80.0\%$. However, the flotation of quartz was irrespective of both Aero 704 concentration and pH of the medium. In the pH region where the maximum flotation recoveries were obtained, the ionomolecular (RCOOH • RCOO$^-$) form of oleate reaches its maximum amount and from this point on its activity decreases through the more basic conditions while the concentration of the ionic (RCOO$^-$) and the dimeric forms $(RCOO)_2^{2-}$ of oleate remain constant. It is obvious that the flotation recoveries were mostly related with the ionomolecular and the ionic forms of Aero 704. The interaction of these species with the positively charged sites of the minerals might be one of the reason for the flotation recovery.

So; the flotation recovery of the minerals may decrease with decreasing of both positively charged surfaces on the minerals and the ionomolecular species. The other reason might be H-bonding formed between the OH groups on the mineral surfaces (~SiOH, ~AlOH, ~TiOH) and oxygens of carboxylate (O=C-O$^-$) group of Aero 704 species. According to the FTIR spectra of the minerals, the additional bands at 2961 cm^{-1}, 2926 cm^{-1} and 2854 cm^{-1} coming from Aero 704 disappeared after acetone washing for all Aero 704-treated minerals except for biotite and muscovite indicating weak interaction (reaction VIII).

According to the FTIR spectra of both biotite and muscovite in the presence of Aero 704 and Aero 3000C, the collector-treated mica minerals (biotite and muscovite) displayed additional bands which correspond to C-H vibrations even after acetone washing indicating rather strong interaction of Aero 704 and Aero 3000C with their surfaces. This strong interaction might occur between the ~SiOH and ~AlOH groups on the surface of tetrahedral and octahedral units. These groups produce ~SiOH$_2^+$, ~SiO$^-$, ~AlOH$_2^+$ and ~AlO$^-$ depending on the pH of the medium. Thus, interaction of those ions with the ions of the Aero 704 and Aero 3000C might be strong enough in addition to H-bonding which can not be removed by acetone washing. In the case of albite and orthoclase, ~SiOH (or ~AlOH) groups on the surface of only tetrahedral units are taken into account, so interaction of ~SiOH$_2^+$ and ~SiO$^-$ (or ~AlOH$_2^+$ and ~AlO$^-$) with the ions of Aero 704 and Aero 3000C may be relatively weak which can be removed easily. In quartz, only tetrahedral unit (which has less volume than octahedral unit) has silicon in the center and produce less amount of ~SiOH groups compared to other silicates. In addition, the attraction between the corner element oxygens and center element silicon is greater in tetrahedral unit. Thus the degree of silicon hydrolysis with water due to the broken bond surfaces becomes less. As mentioned before, ~SiOH dissociates into ~SiOH$_2^+$, ~SiO$^-$ depending on the pH of the medium. Interaction of these species with the ions of Aero 704 and Aero 3000C is relatively weak and can be easily removed by acetone washing. Rutile has hexagonal structure which may have comparable volume with the octahedral unit, and has titanium in the center which produce ~TiOH group. ~TiOH dissociates into ~TiOH$_2^+$, ~TiO$^-$ depending on the pH of the medium and the interaction of these

234

species with the ions of Aero 704 and Aero 3000C is weak and can be removed easily by acetone washing.

There is point to be clarified for AFM and FTIR results. The conditioning time for all the minerals with the collectors was kept constant as five minutes for the purpose of FTIR examination whereas in the case AFM analyses, the conditioning time was kept constant fifteen minutes. During this longer time, the possibility of settling of the collector molecules on the mineral surfaces may be the reason for differentiation between AFM and FTIR results. There was no additional peak due to interaction of Aero 825 with muscovite and quartz in the FTIR spectra whereas interaction of Aero 825 with muscovite and quartz was observed in AFM analyses.

There is another point for AFM analyses results to be mentioned; for the sheet like minerals such as muscovite and biotite which have two types surfaces, edge surface and face surface, as the AFM analysis was performed on the face surface, the obtained topographical image may not present information about the adsorption of the collector if it would occur between the edge surface groups and the collector ions.

In addition to these explanations, in general, the results of the electrokinetic potential measurements and the micro-flotation recovery values were not coincide with each other for some minerals. In electrokinetic potential measurements, the particle size was -10 micron whereas in micro-flotation particle size range was -212+38 microns. So the difference between the two experimental results may be due to the size difference of the minerals in the solution [105].

Separation of feldspar from quartz with the help of cationic collectors by using HF has proven to be the most suitable reagent scheme irrespective of the mechanism. In plant practice around the world, the use of HF has become a routine method till date. The use of HF creates corrosive chemical environment in the flotation cells in addition to its inherent cost. Besides, the growing consciousness of health and

environmental problems forces the industries to search for a new HF free reagent scheme. Although it has been under serious consideration for couple of decades, no considerable success has been achieved [10].

CHAPTER 6

CONCLUSIONS

In the study, the objective was to investigate the flotation characteristics of two different feldspars, albite and orthoclase, and the associated minerals, biotite, muscovite, quartz and rutile, in the presence of varying concentrations of Aero 704, Aero 3000C and Aero 825 flotation collectors. For this purpose the effects of the collectors were investigated as a function of their concentrations and pH of the medium. The experiments were carried out by laboratory micro-flotation on the highest purity minerals of albite, orthoclase, biotite, muscovite, quartz and rutile.

As well-known, the relationship established between floatability and the changes in the electrokinetic potential forms the basis for determining the interaction type of the collectors with the surface of minerals. Therefore, the zeta potential measurements were also conducted to determine the action of collectors on the mineral surfaces.

The interactions of the collectors with the mineral surfaces were followed by AFM and FTIR analyses. From the results of all studies, the following conclusions can be drawn;

1. The isoelectric point (i.e.p.) of albite, biotite, orthoclase and quartz were found to be similar and below pH 1.5 while the i.e.p. of muscovite and rutile were found to be about pH 3.0 in the presence of distilled water and 1.0×10^{-3} M KCl solution.

237

2. The electrokinetic potential values of the minerals decreased with increasing Aero 704 concentration and this decreasing effect was appreciable especially between the pH range of 8.5 and 10.0.

3. The i.e.p. of the minerals in distilled water shifted from acidic region towards the basic region, about pH 11.0, in the presence of Aero 3000C.

4. The i.e.p. of the minerals disappeared and their electrokinetic potential values decreased with increasing Aero 825 concentration.

5. The micro-flotation studies in the presence of all the concentrations of Aero 704 showed that the flotation recoveries of the minerals were pH dependent and effective between the pH range of 7.0 and 11.5.

6. In the case of flotation with Aero 3000C, the flotation recoveries of all the minerals increased with increasing concentration and pH. The recoveries reached up to 95.0% at certain concentrations and pH values and decreased sharply below pH 3.0 and above pH 9.5 for all the minerals tested.

7. The effect of Aero 825 on the flotation recovery of albite, biotite, muscovite, orthoclase and quartz mineral samples was not notable even in the presence of highest concentration tested, 1.0×10^{-3} M at any pH values.

8. The AFM method was found a useful tool to examine the collector adsorption on mineral surfaces as it provides the topographical presentation of the mineral surfaces after interacting them with the collectors.

9. The FTIR spectra of the minerals conditioned in optimum flotation conditions of Aero 704 showed additional bands at 2961 cm^{-1}, 2926 cm^{-1} and 2854 cm^{-1}, which are known to represent CH_2 stretching vibrations. These additional bands disappeared after washing with acetone indicating the weak interaction of Aero 704 with the albite, orthoclase, quartz and rutile. The biotite and muscovite had these additional bands even after washing with acetone indicating the strong interaction.

10. The FTIR spectra of the minerals conditioned in optimum flotation conditions of Aero 3000C displayed additional bands at 2957 cm^{-1}, 2922 cm^{-1} and 2853 cm^{-1} which represent C-H stretching vibrations. These additional bands disappeared after washing with acetone for albite, orthoclase, quartz and rutile mineral samples indicating the weak interaction. However in the case of biotite and muscovite samples, these additional bands still exist after washing with acetone indicating strong interaction.

11. The FTIR spectra of the minerals, except for muscovite and quartz, conditioned in optimum flotation conditions of Aero 825 displayed additional bands at 2951 cm^{-1}, 2922 cm^{-1} and 2853 cm^{-1} which represent stretching vibrations of CH_2 bands. These additional bands disappeared from the mineral surfaces indicating weak interaction.

12. In this study, it was shown that the removal of the associated minerals including biotite, muscovite and rutile from feldspars (albite and orthoclase) by flotation in single stage under alkaline conditions has been accomplished by the use of Aero 704.

13. In the well-known method for the separation of quartz from feldspar by flotation, hydrogen fluoride (HF) has been used. The use of HF suffers from the growing awareness of environmental and health problems, in addition to its corrosive

239

effect on the flotation cells. In the present study, the quartz did not respond to Aero 704 while feldspars (albite and orthoclase) responded in basic conditions without using HF.

REFERENCES

1. Wills, A.B. and Napier Munn, T., 2006, Mineral Processing Technology, An Introduction to the Practical Aspects of Ore Treatment and Mineral, Publisher: Elsevier Science & Technology Books, p. 268.

2. Shimoiizaka, J., Nakatsuka, T., and Katayanagi, T., 1976, Separation of Feldspar from Quartz by a New Flotation Process, World Mining and Metals Technology, Vol. 1, Baltimore, p. 423.

3. El Salmawy, M.S., Nakahiro, Y., Wakamatsu, T., 1993. The Role of Alkaline Earth Cations in Flotation Separation of Quartz from Feldspar. Minerals Engineering 6 (12), pp. 1231–1243.

4. Dana, J.D., 1855, Manual of Mineralogy Including Observation on Mines, Rocks, Reduction of Ores, Published by Durrie & Peck. p. 176.

5. Klein, C. and Hurlbut, C.S.jr., 1993, Manual of Mineralogy (21th Edition), Publisher: John Wiley & Sons, Inc., New York.

6. Geredeli, A., 1990, Flotation of Feldspar from Balıkesir District, M.Sc. Thesis, METU, Ankara.

7. Bayat, O., Arslan, V., Cebeci, Y., 2006, Combined Application of Different Collectors in the Flotation Concentration of Turkish Feldspars, Minerals Engineering, Volume 19, pp. 98-101.

8. Eurofel, European Association of Feldspar Producers, http://www.ima-europe.eu/fileadmin/downloads/publications/factsheets/ Feldspar_An-WEB-2011.pdf, last accessed on 10/03/2012.

9. Gülsoy, Ö., Bayraktar, İ., 2004, Manyetik Ayırma ve Flotasyonla Magmatik Kayaçlardan Feldspat Üretimi, Yerbilimleri, 30, pp. 49-61.

10. Vidyadhar, A., Rao, K.H., 2002, Adsorption of N-tallow 1.3-Propanediamine-Dioleate Collector of Albite and Quartz Minerals and Selective Flotation of Albite from Greek Stefania Feldspar Ore, J. Colloid Interface Sci.,248, pp. 19-29.

11. Orhan, E.C., Bayraktar, İ., 2005, Amine-Oleate Interactions in Feldspar Flotation, Minerals Engineering, Volume 19, Issue 1, pp. 48-55.

12. Bayraktar, İ., Gülsoy, Ö.Y., 2001, Feldspatların Zenginleştirilmesi, 4. End. Hammaddeler Sempozyumu, İzmir, pp. 97-105.

13. Bayraktar, I., Ersayın, S., Gulsoy, O.Y., 1997. Upgrading Titanium Bearing Na-Feldspar by Flotation Using Sulphonates, Succinamates and Soaps of Vegetable Oils. Minerals Engineering 1 (12), pp. 1363–1374.

14. The Industrial Minerals Association - North America (IMA-NA) http://ima-na.org/feldspar, last accessed on 10/03/2012.

15. Orhan, E.C., Bayraktar, I., 2005, Amine–Oleate Interactions in Feldspar Flotation, Minerals Engineering, 19, pp. 48–55.

16. Celik, M.S., Can, I., Eren, R.H., 1998, Removal of Titanium Impurities from Feldspar Ores by New Flotation Collectors, Minerals Engineering 11 (12), pp. 1201–1208.

17. Ozun S., Atalay U., Kadioglu, Y.K., 2009, Investigation on Possibility of Opaque Minerals Removal from Foid Bearing Rock, Mining and Geoengineering, Release Of Journals AGH, 33, z.4, pp. 269-276.

18. Sümer, G., Kaya, M., 1995, Aydın-Çine Feldspatlarının Flotasyon ile Zenginleştirilmesi, End. Hammaddeler Sempozyumu, pp. 59-69.

19. Katayanagi, T., 1973, Benefication of Feldspar without using Hydrofluoric Acid, Ceram. Jpn. 8, p. 58.

20. Malghan, S. G., 1976, Selective Flotation of Feldspar in Non-Fluoride Medium, Trans. SME-AIME Fall Meeting, Denver, CO, Preprint 76-H-331.

21. Malghan, S. G., 1981, Effect of Process Variables in Feldspar Flotation Using Non-HF System, Min. Eng. 33, pp. 1616-1622.

22. Bolin, N. J., 1983, A Study of Feldspar Flotation, Erzmetall 36, pp: 429-432.

23. Celik, M.S., Pehlivanoglu, B., Aslanbas, A., Asmatulu , R., 2001. Flotation of Colored Impurities from Feldspar Ores. Minerals & Metallurgical Processing 18 (2), pp. 101–105.

24. Seyrankaya, A., 2003, Removal of Mica and Heavy Minerals from Albite of Mugla-Milas District by Flotation, DEU, Mühendislik Fakültesi Fen ve Mühendislik Dergisi, 5, 3, pp. 171-180.

25. Sekulic, Z., Canic, N., Bartulovic, Z., Dakovic, A., 2004, Application of Different Collectors in the Flotation Concentration of Feldspar, Mica and Quartz Sand, Minerals Engineering 17, pp 77–80.

26. Gülsoy, Ö.Y., Can, N. M. and Bayraktar, I., 2005, Production of Potassium Feldspar Concentrate from a Low-Grade Pegmatitic Ore in Turkey, Mineral Processing and Extractive Metallurgy (Trans. Inst. Min. Metall. C), 114, pp. 80-86.

27. Kurcan I., Kaya E., Kececi I., Malayoglu U., Seyrankaya A., 1997, Removal of Mica and Iron Titanium Oxides from Feldspar Ores in Basic Conditions at One-Stage, (Mevlut K., Batar T., Kaya E. and Seyrankaya A., Eds.) Proceedings of 6th International Industrial Minerals Symposium, 01-03, February, Izmir, Turkey, pp. 156-163.

28. Eddy, W.H., Collins, E.W., Browning, J.S., Sullivan, G.V., 1972, Recovery of Feldspar and Glass Sand from South Carolina Waste Granite Fines, US Bureau of Mines, Report of Investigations 7651, Washington.

29. Manser, R.M., 1975. Handbook of Silicate Flotation. Warren Spring Laboratory, Stevanage, England, p. 206.

30. Crozier, R.D., 1990. Non-Metallic Mineral Flotation-Reagent Technology. Industrial Minerals, February, pp. 55–65.

31. Bayraktar, I., Ersayın, S., Gulsoy, O.Y., 1998. Magnetic Separation and Flotation of Biotite Ore. In: Atak, S., Onal, G., Celik, M.S., (Eds.), Proc. 7th International Mineral Processing Symposium, Turkey, pp. 315–318.

32. Baarson, R.E., Ray, C.L., Treweek, H.B., 1962, Plant Practice in Non-Metallic Flotation, Froth Flotation 50th Anniversary Volume, SME, AIMME, New York, pp. 427-446.

33. Giesekke, E.W., 1983, A Review of Spectroscopic Techniques Applied to the Study of Interactions Between Minerals and Reagents in Flotation Systems, International Journal of Mineral Processing, Volume 11, 1, pp. 19-56.

34. Marabini, A.M., Contini, G. and Cozza, C., 1993, Surface Spectroscopic Techniques Applied To The Study Of Mineral Processing, International Journal of Mineral Processing, 38, pp. 1-20.

35. ThermoNicolet, 2002, Nicolet's Introduction to FTIR, ThermoNicolet Instruments Corporation, Inc., http://mmrc.caltech.edu/FTIR/FTIRintro.pdf, last accessed on 10/03/2012.

36. Fuerstenau, D.W., Raghavan, S., 1980, The Crystal Chemistry, Surface Properties and Flotation Behaviour of Silicate Minerals, in "Proc. XII Int. Miner. Process.Congr," Vol. II, p. 368. D.N.P.M., Sao Paulo.

37. Termes, S.C., Richardson, P.E., 1996, Application of FTIR Spectroscopy For In Situ Studies of Sphalerite with Aqueous Solutions of Potassium Ethylxanthate and Diethyldixanthogen, International Journal of Mineral Processing, 18, pp. 167-178.

38. Smith, R.W., and Scott, J. L., 1990, Mechanisms of Dodecylamine Flotation of Quartz, Miner. Process. Ext.Metall. Rev. 7, p. 81.

39. Laskowski, J. S., 1989, in Challenges in Mineral Processing, (K. V. S. Sastry and M. C. Fuerstenau, Eds.), p. 15. SME, Littleton, CO.

40. Novich, B. E., and Ring, T. A., 1985, A Predictive Model for the Alkylamine-Quartz Flotation System, Langmuir 1, pp. 701-708.

41. Ince, D.E., Johnston C.T. and Moudgil, B.M., 1991, Fourier Transform Infrared Spectroscopic Study of Adsorption of Oleic Acid/Oleate on Surfaces of Apatite and Dolomite, Langmuir, 7, pp. 1453-1457.

42. Mielczarski, J.A., Cases, J.M., Bouquet, E., Barres, O. and Delon, J.F., 1993, Nature and Structure of Adsorption Layer on Apatite Contacted with Oleate Solution. 1. Adsorption and Fourier Transform Infrared Reflection Studies, Langmuir, 9, pp. 2370-2382.

43. Vidyadhar, A., Rao, K.H., Chernyshova, I.V., Pradip, and Forssberg, K.S.E., 2002, Mechanisms of Amine–Quartz Interaction in the Absence and Presence of Alcohols Studied by Spectroscopic Methods, Journal of Colloid and Interface Science 256, pp. 59–72.

44. Vidyadhar, A., Rao, K.H., Chernyshova, I.V., 2003, Mechanisms of Amine–Feldspar Interaction in the Absence and Presence of Alcohols Studied by Spectroscopic Methods, Colloids and Surfaces A: Physicochem. Eng. Aspects, 214, pp.127-142.

45. Vidyadhar, A., Rao, H.K., 2007, Adsorption Mechanism of Mixed Cationic/Anionic Collectors in Feldspar-Quartz Flotation System, Journal of Colloid and Interface Science 306, pp.195–204.

46. Labidi, N.S. and Iddou, A., 2007, Adsorption of Oleic Acid on Quartz/Water Interface, J. Saudi Chem. Soc., Vol. 11, No. 2; pp. 221-234.

47. Chennakesavulu, K., Raju, G.B., Prabhakar, S., Nair, C.M., Murthy, K.V.G.K., 2009, Adsorption of Oleate on Fuorite Surface as Revealed by Atomic Force Microscopy, Int. J. Miner. Process. 90, pp.101–104.

48. Paiva, P.R.P., Monte, M.B.M., Simão, R.A., Gaspar, J.C., 2011, In Situ AFM Study of Potassium Oleate Adsorption and Calcium Precipitate Formation on an Apatite Surface, Minerals Engineering 24, pp. 387–395.

49. The information about the minerals were obtained from internet sites of http://en.wikipedia.org, www.minerals.net, www.webmineral.com and www.biritannica.com, last accessed on 10/03/2012.

50. Mineral Powder Diffraction File Databook, Set 1-42, Published by the International Center for Diffraction Data (ICDD).

51. Iiishi, K., Tomisaka, T., Kato, T., and Umegakai, Y., 1971, Isomorphous Substitutions and Infrared and Far Infrared Spectra of the Feldspars. Neues Jahrbuch FTIR Mineralogie Abhandlungen, 115, pp. 98-119.

52. Couty, R. and Velde, B., 1986, Pressure-Induced Band Splitting in Infrared Spectra of Sanidine and Albite. American Mineralogist, Volume 71, pp. 99-104.

53. Matteson, A., Herron, M.M., 1993. End-Member Feldspar Concentrations Determined by FTIR Spectral Analysis, J. Sediment Petrol., 63, pp. 1144-1148.

54. Mohamed, M.M., Al-Esaimi, M.M., 2006, Characterization, Adsorption and Photocatalytic Activity of Vanadium-Doped TiO_2 and Sulfated TiO_2 (rutile) Catalysts: Degradation of Methylene Blue Dye, Volume 255, Issues 1–2, pp. 53–61.

55. Kim, H.M., Miyaji, F., Kokubo, T., 1997, Effect of Heat Treatment on Apatite-Forming Ability of Ti Metal Induced by Alkali Treatment, Journal of Materials Science: Materials in Medicine, Volume 8, Number 6, pp. 341-347.

56. Bulatovic, S.M., 2007, Handbook of Flotation Reagents, Chemistry, Theory and Practice: Flotation of Sulfide Ores, Publisher: Elsevier Science & Technology Books, pp.5-39.

57. Mining Chemicals, Handbook, Revised Edition, 2002, Cytec Industries Inc.

58. IR Spectroscopy Tutorial: Amines, http://orgchem.colorado.edu/Spectroscopy/irtutor/tutorial.html, last accessed on 10/03/2012.

59. Infrared Spectroscopy, Characteristic Peaks for Common Functional Groups, http://www.muhlenberg.edu/depts/chemistry/irexer/IRDATATB.htm, last accessed on 10/03/2012.

60. Chudacek, M.W., 1991, EMDEE Microflot Floatability Test, International Journal of Mineral Processing, Volume 33, Issues 1-4, pp. 383-396.

61. Paria, S., Khilar, K.C., 2004, A Review on Experimental Studies of Surfactant Adsorption at the Hydrophilic Solid–Water Interface, Advances in Colloid and Interface Science 110, pp. 75–95.

62. Hendrik A. Capelle, Leanne G. Britcher and Gayle E. Morris, 2003, Sodium Stearate Adsorption onto Titania Pigment, Journal of Colloid and Interface Science 268, pp.293–300.

63. Moon, K.S., Fuerstenau, D.W., 2003, Surface Crystal Chemistry in Selective Flotation of Spodumene [$LiAl(SiO_3)_2$] from Other Aluminosilicates, Int. J. Miner. Process. 72, pp.11–24.

64. Ribeiro R.C., Correia J.C.G., Seidl P.R., 2009, The Influence of Different Minerals on the Mechanical Resistance of Asphalt Mixtures, Journal of Petroleum Science and Engineering 65, pp.171–174.

65. Nosrati A., Addai-Mensah J., Skinner W., 2012, Rheological Behaviour of Muscovite Clay Slurries: Effect of Water Quality and Solution Speciation, Int.Journal of Mineral Processing, Volume 102-103, pp. 89-98.

66. Pugh R.J., 1974, Selective Coagulation in Quartz-Hematite and Quartz-Rutile Suspensions, Colloid & Polymer Sci., 252, pp. 400-406.

67. Somasundaran, P., Wang, D., 2006, Solution Chemistry: Minerals and Reagents, Developments in Mineral Processing, Printed by Elselvier Science, Volume 17, pp. 5-72.

68. Mohamed, A.M.O. and Antia, H.E., 1998, Geoenvironmental Engineering, Developments in Geotechnical Engineering, 82, Publisher: Elsevier Science, p.622.

69. Masliyah, J.H. and Bhattacharjee, S., 2006, Electrokinetic and Colloid Transport Phenomena, published by John Wiley & Sons, Inc. p.170.

70. James, R.O. and Parks, G.A., 1982, Characterization of Aqueous Colloids by Their Electrical Double-Layer and Intrinsic Surface Chemical Properties, Surface and Colloid Science, Vol. 12 (ed. E. Matijevic'), pp. 119–216. Plenum Press.

71. Davis, J.A. and Kent, D.B., 1990, Surface Complexation Modeling in Aqueous Geochemistry, Mineral–Water Interface Geochemistry, Vol. 23 (eds. M. F. Hochella Jr. and A. F. White), Mineralogical Society of America, pp. 177–259.

72. Casey, W.H., Westrich, H.R., Arnold G. W., 1988, The Surface Chemistry of Labradorite Feldspar Reacted with Aqueous Solutions at pH=2, 3, and 12. Geochim. Cosmochim. Acta 52, pp. 2795–2807.

73. Brady, P.V. and Walther, J.V., 1989, Controls on Silicate Dissolution Rates in Neutral and Basic Conditions at 25°C. Geochim. Cosmochim. Acta 53, pp. 2823–2830.

74. Blum, A.E. and Lasaga, A.C., 1988, Role Of Surface Speciation in the Low Temperature Dissolution of Minerals, Nature 331, pp. 431–433.

75. Hellmann, R., 1995, The Albite–Water System: Part II. The Time Evolution of the Stoichiometry of Albite Dissoltuion as a Function of pH at 100, 200, and 300°C. Geochim. Cosmochim. Acta 59, pp. 1669–1697.

76. Blum, A.E., and Lasaga, A.C., 1991, Role of Surface Speciation in the Dissolution of Albite, Geochim. Cosmochim. Acta, 55, pp. 2193–2201.

77. Koretsky, C.M., Sverjensky, D.A., Salisbury, J.W. And D'aria, D.M., 1997, Detection of Surface Hydroxyl Species on Quartz, γ-Alumina, and Feldspars Using Diffuse Reflectance Infrared Spectroscopy, Geochimica et Cosmochimica Acta, Vol. 61, No. 11, pp. 2193-2210.

78. Miller J.D., Misra M., 1984, The Hydrophobic Character of Semisoluble Salt Minerals with Oleate as Collector, Proceedings: MINTEK 50 International Conference on Recent Advances in Mineral Science and Technology, Johannesburg, South Africa, 1, pp. 259-267.

79. Somasundaran, P. and Zhang, L., 2006, Adsorption of Surfactants on Minerals for Wettability Control in Improved Oil Recovery Processes, Journal of Petroleum Science and Engineering, 52, pp. 198–212.

80. O'Dwyer, C., Navas, D., Lavayen, V., Benavente, E., Santa Ana, M.A., González, G., Newcomb, S.B., and Sotomayor Torres, C.M., 2006, Nano-Urchin: The Formation and Structure of High-Density Spherical Clusters of Vanadium Oxide Nanotubes, Chem. Mater., 18 (13), pp. 3016–3022.

81. Wang, Z., Yi, X., Li, G., Guan, D., Lou, A., 2001, A Functional Theoretical Approach to the Electrical Double Layer of a Spherical Colloid Particle, Chemical Physics, 274, pp. 57-69.

82. Vinnagradov, S.N. and Linnell, R.H., 1971, Hydrogen Bonding, Van Nostrand Reinhold Co.

83. Baes, C.F. and Mesmer, R.E., 1976, The Hydrolysis of Cations, John Wiley and Sons, Inc,, pp. 112-123.

84. Israelachvili, J.N. and Pashley, R.M., 1983, Molecular Layering of Water at Surfaces and Origin of Repulsive Hydration Forces, Nature, 306, pp.249-250.

85. Somasundaran, P. and Ramachandran, R., 1988, Surfactants in Flotation, Surfactants in Chemical/Process Engineering, Wasan, D.T., Ginn, M.E. and Shah, D.O. (Eds.), Marcel Dekker: New York, p. 195.

86. Pugh, R.J. and Rutland, M., 1997, Activation of Mica with Calcium Ions and Fatty Acid Flotation Collector. In: Hoberg, H., von Blottnitz, H. (Eds.), Proc. XX. IMPC, Aachen, Germany, vol. 3, pp. 583–592.

87. Hanna, H.S. and Somasundaran, P., 1976, in M.C. Fuerstenau (Ed.), Flotation, A.M. Gaudin Memorial Volume, Vol. 1, AIME, New York, pp. 197-272.

88. Kulkarni R.D., Somasundaran P., 1980, Flotation Chemistry of Hematite/Oleate System, Colloids and Surfaces, 1, pp. 387-405.

89. Andersen, J.B., El-Mofty, S.E. and Somasundaran, P., 1991, Using Electrophoresis for Determining the Mechanism of Amine, Sulfate and Oleate Adsorption on Calcite, Colloids and Surfaces, 55, pp.365-368.

90. Peck, A.S. and Wadsworth, M.E., 1965, in N. Arbiter (Ed.), 7th Int. Miner. Process. Congr., New York, Gordon and Breach, New York, pp. 259-267.

91. Fuerstenau, M.C. and Miller, J.D., 1967, The Role of the Hydrocarbon Chain in Anionic Flotation of Calcite, Trans. AIME, 238, pp.153-160.

92. Fuerstenau, D.W., and Raghavan, S., 1980, The Crystal Chemistry, Surface Properties and Flotation Behaviour of Silicate Minerals in Proc. XII Int. Miner. Process. Congr., Vol. II, p. 368. D.N.P.M., Sao Paulo.

93. Smith, R.W., and Scott, J.L., 1990, Mechanisms of Dodecylamine Flotation of Quartz, Miner. Process. Ext.Metall. Rev. 7, p. 81.

94. Laskowski, J.S., 1989, in "Challenges in Mineral Processing" (K. V. S. Sastry and M.C. Fuerstenau, Eds.), p. 15. SME, Littleton, CO.

95. Novich, B.E., and Ring, T.A., 1985, A Predictive Model for the Alkyamine-Quartz Flotation System, Langmuir 1, p. 701.

96. Cases, J.M., and Villieras, F., 1992, Thermodynamic Model of Ionic and Non Ionic Surfactant Adsorption-Abstraction on Heterogeneous Surfaces, Langmuir 8, p. 1251.

97. Dobias, B. and Spurny, J., 1960, Proc. 3rd Int. Congr. Surface Active Substances, Vol. 4, Köln, pp. 396-403.

98. Taggart, A. and Arbiter, N., 1944, The Chemistry of Collection of Non Metallic Minerals by Amine Type Collectors, AIME Tech. Pub. No 1685, Class B, No 157.

99. Gaudin, A.M., and Fuerstenau, D.W., 1955, Streaming Potential Studies. Quartz Flotation with Cationic Collectors, Trans. Soc. Min. Eng. AIME 202, pp. 958-962.

100. Somasundaran, P., Healy, Th.W., and Fuerstenau, D. W., 1964, Surfactant Adsorption at the Solid-Liquid Interface-Dependence of Mechanism on Chain Length, J. Phys. Chem. 68, pp. 3562-3566.

101. Somasundaran, P. and Fuerstenau, D.W., 1966, Mechanisms of Alkyl Sulfonate Adsorption at the Alumina-Water Interface, J. Phys. Chem., Volume 70 (1), pp 90–96.

102. Healy, T.W., Somasundaran, P., Fuerstenau, D.W., 2003, The Adsorption of Alkyl and Alkylbenzene Sulfonates at Mineral Oxide–Water Interfaces, Int. J. Miner. Process. 72, pp. 3–10.

103. Andersen, J.B., El-Mofty, S.E. and Somasundaran, P., 1991, Using Electrophoresis for Determining the Mechanism of Amine, Sulfate and Oleate Adsorption on Calcite, Colloids and Surfaces, 55, pp. 365-368.

104. Siracusa, P.A. and Somasundaran, P., 1987, The Role of Mineral Dissolution in the Adsorption of Dodecylbenzenesulfonate on Kaolinite and Alumina, Colloids and Surfaces, 26, pp.55-77.

105. Montes, S., Montes Atenas, G., and Valero, E., 2007, How Fine Particles on Haematite Mineral Ultimately Define the Mineral Surface Charge and the Overall Floatability Behaviour, The Journal of The Southern African Institute of Mining and Metallurgy, Volume 107, pp. 689-695.

106. Hauth, W.E., 1951, Crystal Chemistry in Ceramics, The Iowa State College Bulletin, Engineering Report No.7, pp. 1-8.

107. Kuznetsov, Yu. I., Andreeva, N.P., Sokolova N.P. and Bulgakova, R.A., 2003, Joint Adsorption of Oleic and Phenylanthranilic Acids at Passive Iron, Protection of Metals., Vol. 39, No. 5, pp. 462–467.

108. Kumar, V. and Raju, G.B., 2002, Adsorption of Oleic Acid at Sillimanite/Water Interface, Journal of Colloid and Interface Science, 247, pp. 275-281.

109. Suarez, D.L., Goldberg S. and Su, C., 1998, Evaluation of Oxyanion Adsorption Mechanisms on Oxides Using FTIR Spectroscopy and Electrophoretic Mobility, In Mineral–Water Interfacial Reactions Kinetics and Mechanisms (eds. D.L. Sparks and T.J. Grundl), ACS Symposium Series 715, pp.136–178.

CURRICULUM VITAE

PERSONAL INFORMATION

Surname, Name : ÖZÜN, Savaş

Nationality   : Turkish (T.C.)

Date and Place of Birth : 06 July 1976, Şarkikaraağaç/Isparta

E-mail   : savasozun@gmail.com

He received his B.S. degree from Mining Engineering Department of Eskisehir Osmangazi University in July 2001. He has been working as a research assistant in Mining Engineering Department, Middle East Technical University since January, 2002. In 2010, with a scholarship from Turkish Government, he worked at Chemistry Department of University of Illinois at Urbana-Champaign, USA for six months.

He is a member of Chambers of Mining Engineers of Turkey. He is married with a son.

PUBLICATIONS

1. Özün, S., Hiçyılmaz, C., 2005, The Effect of Comminution Type on Combustion Properties of Coal, Proceedings of the XIth Balkan Mineral Processing Congress, Mineral Processing in Sustainable Development (Edts. Fetahu, K., Peza, V., Zoga, P., Ahmataj, F., Bode A.), pp. 61-66, Tirana/Albania.

2. Özün, S., Hiçyılmaz, C., Altun, N.E., 2006, Rheological Properties of Asphaltite Water Slurries, Energy & Fuels , 20, pp. 2037-2045

3. Özün, S., Altun, N.E., Hiçyılmaz, C., 2008, A Study on the Rheological Behaviour of Asphaltite-Water Slurries, Proceedings of the International Conference 12th Conference on Environment and Mineral Processing & Exhibition, Ostrava, Czech Republic.

4. Altun, N.E., Özün, S., Hiçyılmaz, C., 2008, Investigation of the Rheological Behaviour of Asphaltite-Water Slurries: Possible Mechanisms and Their Impacts on Viscosity, Proceeding of the 11th International Mineral Processing Symposium, 21-23 October, Antalya, Turkey

5. Özün, S., Atalay, Ü., Kadıoğlu, Y.,K., 2009, Investigation on Possibility of Opaque Minerals Removal from Foid Bearing Rock, Mining and Geoengineering, Release of Journals AGH, 33, z.4, pp.269-276.